

## THESE de l'Université de Lyon

Délivrée par l'Ecole Centrale de Lyon

Spécialité : **Matériaux** de l'Ecole Doctorale **EDML**

en collaborations avec

**Tohoku University**  
**Total Marketing & Services**

Soutenue le 4 Février 2014 à Lyon

par

**Sophie LOEHLE**

---

# Understanding of adsorption mechanisms and tribological behaviors of C18 fatty acids on iron-based surfaces: a molecular simulation approach

---

*« Compréhension des mécanismes d'adsorption et des comportements tribologiques des acides gras C18 sur des surfaces à base de fer par la modélisation moléculaire »*

préparée au **Laboratoire de Tribologie et Dynamique des Systèmes**

Composition du jury :

MCF HDR	Nicolas FILLOT	LaMCoS Lyon	Rapporteur
D.R CNRS	Pierre MONTMITONNET	Cemef Sophia-Antipolis	Rapporteur
Prof.	Mitjan KALIN	Tint Ljubljana	Examineur
Prof.	Michael MOSELER	Fraunhofer Freiburg	Examineur
Dr.	Raphaele IOVINE	Total M&S Solaize	Membre Invité
Prof.	Akira MIYAMOTO	NICHe Sendai (Tohoku)	Co-Encadrant
MCF	Clotilde MINFRAY	LTDS Lyon	Co-Encadrante
Prof. Emérite	Jean-Michel MARTIN	LTDS Lyon	Directeur de Thèse



## RESUME

Les exigences actuelles en terme de lubrification automobile imposent des formulations extrêmement complexes. Parmi tous les additifs présents dans l'huile, on peut noter le dithiocarbamate de molybdène et le dithiophosphate de zinc, additifs à action tribologique à base de soufre et de phosphore. Pour des raisons environnementales, il est important de diminuer voir d'éliminer la présence de ces deux éléments dans les huiles. Les molécules organiques à base de carbone, oxygène et hydrogène semblent être de bons candidats. Le mécanisme de lubrification des acides gras (acides stéarique, oléique et linoléique) est revisité par une approche visant à combiner l'étude expérimentale et la modélisation moléculaire. Tout d'abord, les mécanismes d'adsorption des acides gras sur des surfaces à base de fer sont étudiés par couplage Chimie Quantique et Dynamique Moléculaire (UA-QCMD). L'adsorption des acides gras sur des surfaces à base de fer se fait par la fonction acide. Selon la nature du substrat, la densité du film et l'angle d'inclinaison de la molécule par rapport à la surface, différents mécanismes d'adsorption peuvent avoir lieu (physisorption et chimisorption). Les molécules d'acide stéarique forment une monocouche compacte et bien arrangée alors que les molécules insaturées en sont incapables à cause d'effet stériques induit par les doubles liaisons carbone-carbone. Le frottement favorise la formation de la fonction carboxylate. Ces résultats sont confirmés par des analyses de surface (XPS et PM-IRRAS). Les propriétés tribologiques des acides gras purs, dans la PAO 4 et en mélange dans la PAO 4 sont étudiées par simulation MD et par des tribotests. Un faible frottement et une absence d'usure visible ont été observés pour l'acide stéarique pur et dissous à 1% dans la PAO 4 à haute température. La présence de molécules insaturées inhibe les propriétés réductrices de frottement de l'acide stéarique, en particulier à 150 °C. Ceci est expliqué par la diffusion des acides gras insaturés bien supérieure à celle de l'acide stéarique dans la PAO 4 à toutes les températures étudiées.

**Mots clés :** acides gras C18, surfaces à base de fer, régime de lubrification mixte/limite, modélisation moléculaire, analyse de surface, mécanismes d'adsorption, tribochimie

## ABSTRACT

The current requirements in automotive lubrication impose complex formulation. Among all the additives present in oil, the presence of molybdenum dithiocarbamate and zinc dithiophosphate, both tribological additives containing sulfur and phosphorous is found. For environmental reasons, it is important to reduce or eliminate the presence of these two elements contained in oil. Organic molecules based on carbon, oxygen and hydrogen seems to be good candidate. The lubrication mechanism of fatty acids (e.g. stearic, oleic and linoleic acids) is revisited with a new approach combining experimental and computational chemistry studies. First, the adsorption mechanisms of fatty acids on iron-based surfaces are investigated by Ultra-Accelerated Quantum Chemistry Molecular Dynamics simulations. The adsorption of fatty acids on iron oxide surface occurred through the acid group. Depending on the nature of the substrate, on the density of the film and on the tilt angle between the molecule and the surface, different adsorption mechanisms (physisorption and chemisorption) can occur. Stearic acid molecules form a close-packed and well-arranged monolayer whereas unsaturation acids cannot because of steric effects induced by double carbon-carbon bonds. The friction process favors the formation of carboxylate function. Results are confirmed by surface analysis (XPS and PM-IRRAS). Tribological properties of pure fatty acids, blended in PAO 4 and mixture of saturated/unsaturated acids are studied by MD simulations and tribotests. Low friction coefficient with no visible wear is reported for pure stearic acid and single stearic acid blended in PAO 4 at 1%w at high temperature. This lubricating behavior is inhibited in the presence of unsaturated acids, especially at 150 °C. MD simulation results show a faster diffusion toward the surface for unsaturated fatty acids than for stearic acid at all studied temperature.

**Keywords:** C18 fatty acids, iron-based surfaces, mixed/boundary lubrication regimes, molecular simulations, surface analysis, adsorption mechanisms, tribochemistry.





---

Understanding of adsorption mechanisms and tribological behaviors of C18 fatty acids on iron-based surfaces: a molecular simulation approach

---

*« Compréhension des mécanismes d'adsorption et des comportements tribologiques des acides gras C18 sur des surfaces à base de fer par la modélisation moléculaire »*



# ACKNOWLEDGMENTS

This work is the fruit of collaborations between the Laboratory of Tribology and System Dynamics (LTDS) at Ecole Centrale of Lyon, Prof. Miyamoto's laboratory in Tohoku University in Japan and Total group in France. In addition, this thesis is the results of enriching works and meetings and I would like to thank all actors of this three flourishing years as a PhD student.

First, I would like to thank the members of the jury to accept to evaluate my work. Specific thanks to Pierre Montmitonnet and Nicolas Fillot to make me the honor of reading and reporting my PhD thesis during the Christmas holidays and to respect widely the timetable. Thank you for your comments, suggestions and discussions we had. Many thanks to Mitjan Kalin and Michael Moseler for their acceptance to evaluate my work with enthusiasm, the jury committee were therefore international. Thank you for all the discussions, especially fruitful talks I could have with Micheal during different conferences including the PhD defense.

This PhD work has been greatly supported by CNRS and Total group which I thank a lot. Moreover, I would like to thank the ELyT-Lab team to make the Japanese/French collaborations easier and I encourage them to continue such collaborations.

I would like to express my sincere gratitude to my supervisor, Jean-Michel Martin, for giving me the opportunity to make this original and international PhD and to welcome me in his team. I am grateful from your interest in my study and all the added value, the rich suggestions and the good advices you brought to me. Your scientific expertise on tribology and other fields helped me a lot. Thank you for giving me the opportunity to participate many conferences.

There are no words to express how thankful I am toward my co-supervisor Clotilde Minfray for your availability, your energy, your experimental expertise and your enthusiasm in this project. I enjoyed our rich discussion meetings and it was a real pleasure to work with you, always in a good atmosphere. I appreciate your kindness and the trust you gave to me.

I was very lucky to have the opportunity to work with Prof. Miyamoto and to spend nine months in his lab in Japan. I am very grateful for your computational chemistry expertise and your human qualities. I could learn a lot from you on how to become expert of molecular simulation. Thank you for your wonderful welcome and all the fantastic parties we shared together with other members. I extend my gratitude to all your secretaries that help me during my stay in Japan and I extend my gratitude to all your staff that have contributed to my formation and that helped me when I had problems with my models, especially Obara-san with whom I enjoyed to work very much.

What can I say about the contribution of Christine Matta? Thank you for all the work you have done: our team rocks! It was a pleasure to work with you and to share professional and

personal time. You have good human skills and the lab is definitely not the same without your 'Lebanese prestige'.

Many thanks to Raphaele Iovine for your support, your kindness and the trust you gave to me in the project. Always in a good mood, I appreciate how you follow this project with huge enthusiasm. I add Eric Lacroix and Dominique Faure which I thank with you for your interest in my work and everything you have done to make possible to this 'adventure' to continue.

I would like to thank the master of XPS, Thierry Le Mogne who has contributed greatly to this work with his expertise on XPS analysis but also his general knowledge. Thank you for your kindness and your advice.

I now would like to thank all members of LTDS. More specifically, I would like to thank Michel, Julien, Fabrice and Maria-Isabelle for all the good memories I kept from the conferences we went together but also all the nice discussions we had during my PhD. I cannot forget to thank my friends from the A9 office, which include the front office Anton!! Many thanks to the 'old' colleagues: Paulette, Imène, Sophia, Sam, Christine and Anton and also the 'new' ones: Paula, Catia and Modestino. I am happy to know that the office is in good hands. Thank you for the various parties we had to learn about our different culture, taste food from your country, for all the conferences we spend together (Aix-en-Provence, Lyon, Torino), all the bbq we had with Anton the bbq master (but also the car master and ... how many master do you have exactly?!), all the cake we had at the lab but mainly for all your smiles, kindness and availability that made every day wonderful in this lab, including when I had troubles with computer and hard disc! Many thanks to the coffee office with old members: Julian, Gaylord, Thib' Lafont (special dedication!), Fabou, Anton (again) and new members: Medard, Mr. Touche, Eloi and Julien. Thank you to my favorite Chinese girl Jiao for her kindness, dynamism and good mood! Thank you Simon for sharing common passion for Japan and lunch at EM with Didier also among other members. Thank you Hélène for our fashion talks. Thank you Mickael for your patience with Accelrys. Thank you Kèvin, Juliette, Medhi, Cyrielle, Olga, Cécile, Gaetan, Béa and everyone who has contributed to my daily flourishing. I wish good luck to the new members, especially Manuel, good luck with molecular simulation. May the force be with you ☺.

Finally, I would like to deeply thank my parents Armande and Guy for their support and their trust. Thank you to all my family in Alsace, especially my grandmother Gaby who was the first one to know about my project so I dedicate this work to her. Thank you to all my ENSIC truly friends who came from everywhere in France for my PhD defense and celebration but also for being here no matter what, this is friendship forever. Special dedication to Juju, Lulu and Chloé who 'enduce' the same future as me with choosing to do a PhD thesis: 'Rien ne vaut une belle thèse'. Thank you A-L, always here for important events. And to conclude with the best, thank you Anthony for your support and love, we did it together and we still have lots of good adventure waiting for us.

# Table of contents

<b>Notations.....</b>	<b>13</b>
<b>Abbreviation and acronyms .....</b>	<b>15</b>
<b>General introduction .....</b>	<b>17</b>
 <b>Chapter 1: Literature overview .....</b>	 <b>23</b>
1. Introduction .....	24
2. Generalities .....	25
2.1 Lubricant composition and function .....	25
2.1.1 Generalities .....	25
2.1.1.1 <i>Thermal engine lubrication</i> .....	25
2.1.1.2 <i>Friction reduction in a thermal engine</i> .....	26
2.1.2 Lubricant additives .....	27
2.1.2.1 <i>Lubricant composition</i> .....	27
2.1.3 Industrial restriction and new objectives.....	29
2.2 Organic friction modifiers .....	30
2.2.1 State of the art.....	30
2.2.1.1 <i>Chemistry of C18 fatty acids</i> .....	30
2.2.1.2 <i>Parameters influencing adsorption and friction reduction properties</i> .....	35
2.3 Contribution of computational chemistry .....	39
2.3.1 Limits of experimental approaches .....	39
2.3.2 Adsorption by density functional theory (DFT) calculation .....	39
2.3.3 MD simulation on monolayer.....	40
2.3.4 Other techniques .....	40
2.3.4.1 <i>First-principle MD simulation</i> .....	40
2.3.4.2 <i>Improved MD simulations</i> .....	41
3. Conclusion.....	41
4. References.....	43
5. Summary chapter 1 .....	48

<b>Chapter 2: Materials and methods</b>	<b>51</b>
1. Introduction	52
2. Computational techniques	53
2.1 Construction of OFMs, substrates and base oil	53
2.2 Molecular Dynamics simulation	55
2.2.1 Periodic boundary conditions	56
2.2.2 Inter and intra molecular potentials	56
2.2.2.1 Lennard-Jones potential	56
2.2.2.2 Morse potential	57
2.2.2.3 Angle potential	57
2.2.2.4 Torsion potential	58
2.2.2.5 Gilbert repulsive term	58
2.2.2.6 The Ewald method (Coulomb potential)	58
2.2.2.7 Potential function	59
2.2.3 The Verlet algorithm	59
2.2.4 Control of system temperature and pressure	60
2.2.5 Formation of adsorbed layer	60
2.2.6 Adsorbed film put under pressure and shear conditions	61
2.2.7 Evaluation of friction coefficient	63
2.2.8 Evaluation of diffusion coefficient	63
2.3 Quantum Chemistry methods	64
2.3.1 Density functional theory (DFT) method	64
2.3.2 Tight-binding quantum chemistry calculation	64
2.3.2.1 Quantum chemical method	64
2.3.2.2 First-principle parameterization	65
2.3.3 Models used for TB-QC calculations	66
2.3.4 Accuracy of our TB-QC method	67
2.4 Ultra Accelerated Quantum Chemistry Molecular Dynamics (UA-QCMD) simulation	68
2.4.1 UA-QCMD method	68
2.5. Summary	70
3. Experimental techniques	70

3.1 Materials.....	70
3.2 Experimental characterization techniques .....	70
3.2.1 X-ray photoelectron spectroscopy (XPS).....	70
3.2.2 Polarization modulation-infrared reflection-adsorption spectroscopy (PM-IRRAS)	73
3.3 Friction behavior measurements .....	76
3.3.1 Linear tribometer .....	76
3.4 Summary .....	77
4. Conclusion.....	77
5. References.....	79
6. Summary chapter 2.....	82
 <b>Chapter 3: Adsorption mechanism of pure C18 fatty acids.....</b>	<b>85</b>
1. Introduction .....	86
2. Adsorption mechanism: a computational study .....	87
2.1 Qualitative approach: MD simulation.....	87
2.1.1 “Random” model vs. SAM model.....	87
2.2 Quantitative approach: DFT, TB-QC, UA-QCMD simulations.....	89
2.2.1 Stearic acid: single molecule vs. single molecule included in SAM (50 °C, Fe <sub>2</sub> O <sub>3</sub> )...	89
2.2.1.1 <i>Adsorption mechanism of a single molecule</i> .....	89
2.2.1.2 <i>Adsorption mechanism of SAM</i> .....	90
2.2.1.3 <i>Influence of simulation time in the case of chemisorption</i> .....	92
2.2.1.4 <i>Discussion on molecular models</i> .....	93
2.2.2 Influence of orientation .....	94
2.2.3 Influence of the substrate .....	96
2.2.3.1 <i>Adsorption mechanism of a single molecule</i> .....	96
2.2.3.2 <i>Adsorption mechanism of SAM</i> .....	97
2.2.4 Influence of temperature.....	99
2.2.5 Influence of unsaturation.....	100
2.2.6 Influence of density of molecules in the SAM .....	102
2.2.7 Synthesis.....	105
3. Analytical characterization of adsorbed fatty acids on different type of surfaces by XPS and PM-IRRAS analysis .....	106

3.1 XPS analysis .....	106
3.1.1 Adsorption of stearic acid on iron oxide surface .....	106
3.1.2 Influence of the substrate .....	108
3.1.3 Influence of unsaturation.....	110
3.1.4 Combination of experimental study and molecular simulations .....	112
3.2 PM-IRRAS analysis.....	114
3.2.1 Characterization of adsorbed stearic acid film .....	114
3.2.2 Influence of unsaturation.....	116
3.2.3 Comparison XPS, PM-IRRAS analysis and UA-QCMD simulations.....	117
4. Conclusion.....	117
5. References.....	119
6. Summary chapter 3.....	121

## **Chapter 4: Tribological behavior of pure C18 fatty acids ..... 123**

1. Introduction .....	124
2. Friction between adsorbed layers by MD simulation .....	125
2.1 Generalities on friction behavior by MD .....	125
2.1.1 Tilt Angle .....	125
2.1.2 Sliding speed and temperature control .....	126
2.2 Influence of selected parameters .....	127
2.2.1 Influence of unsaturation degree and density .....	127
2.2.1.1 <i>Qualitative and quantitative study</i> .....	127
2.2.1.2 <i>Discussions</i> .....	130
2.2.2 Influence of oxidized/hydroxide layer on iron-based surface.....	132
2.2.2.1 <i>Qualitative and quantitative study</i> .....	132
2.2.2.2 <i>Discussions</i> .....	134
2.2.3 Influence of chain length.....	135
2.2.3.1 <i>Results</i> .....	135
2.2.3.2 <i>Discussions</i> .....	137
3. Evolution of adsorption films during sliding process by UA-QCMD .....	139
3.1 Effect of pressure and sliding: into the formation of carboxylate .....	139
4. Friction behavior of pure additives by experimental study.....	140



4.1 Effect of unsaturation and temperature .....	140
4.2 Analyzis of the tribofilm by PM-IRRAS .....	142
5. Comparison of experimental and numerical results.....	144
5.1 Considerations concerning MD calculations before comparison with experimental study .....	144
5.2 Effect of Parameters.....	145
5.2.1 Effect of unsaturation .....	145
5.2.2 Effect of the hydroxylation of the surface .....	145
5.2.3 Effect of sliding process on chemical reaction at the interface monolayer-substrate .....	145
6. Conclusion.....	146
7. References.....	147
8. Summary chapter 4.....	150
 <b>Chapter 5: Tribological behavior of C18 fatty acids blended in PAO 4.....</b>	<b>153</b>
1. Introduction .....	154
2. Friction behavior of C18 fatty acids in PAO 4 by experimental approach .....	154
2.1 Friction test experiments.....	154
2.1.1 Influence of unsaturation and temperature.....	155
2.1.2 Influence of concentration.....	158
2.3 Characterization of the tribofilm.....	159
2.2.1 PM-IRRAS analysis of the tribofilm.....	159
3. Competition of C18 fatty acids in PAO 4.....	162
3.1. Friction behavior of C18 fatty acids mixture in PAO 4 .....	162
3.2. Evaluation of diffusion coefficient of OFM in PAO 4 by MD simulation .....	163
3.2.1 C18 fatty acids blended at 1%w in PAO 4.....	163
3.2.2 C18 fatty acids 1%w in PAO 4 submitted to pressure and shearing .....	164
3.3 Discussions: coupling experimental results and MD simulations .....	166
4. Conclusion.....	166
5. References.....	168
6. Summary chapter 5.....	169

<b>Chapter 6 : Synthesis .....</b>	<b>171</b>
1. Main results.....	172
1.1 Adsorption mechanisms .....	172
1.2 Friction behavior .....	172
1.2.1 Pure additives.....	172
1.2.2 Additives in the solvent.....	173
1.2.3 Mixture of additives .....	173
2. Generalization to a real case application .....	173
2.1 Adsorption model.....	173
2.2 Friction model.....	174
 <b>General conclusion and perspectives .....</b>	 <b>175</b>
<b>Annex.....</b>	<b>183</b>

# Table des matières

<b>Notations.....</b>	<b>13</b>
<b>Abbréviations and acronymes .....</b>	<b>15</b>
<b>Introduction générale.....</b>	<b>17</b>
 <b>Chapitre 1 : Synthèse bibliographique .....</b>	 <b>23</b>
1. Introduction .....	24
2. Généralités.....	25
2.1 Composition et fonction d'un lubrifiant.....	25
2.1.1 Généralités.....	25
2.1.1.1 <i>Lubrification du moteur thermique</i> .....	25
2.1.1.2 <i>La diminution du frottement dans les moteurs</i> .....	26
2.1.2 Les additifs de lubrification .....	27
2.1.2.1 <i>Composition d'un lubrifiant</i> .....	27
2.1.3 Restrictions européennes et nouveaux objectifs .....	29
2.2 Les modificateurs de frottement organique .....	30
2.2.1 Etat de l'art.....	30
2.2.1.1 <i>La chimie des acides gras C18</i> .....	30
2.2.1.2 <i>Paramètres influencants l'adsorption et le comportement tribologique</i> .....	35
2.3 La contribution de la modélisation moléculaire.....	39
2.3.1 Les limites de l'approche expérimentale .....	39
2.3.2 L'adsorption par la méthode de la théorie de la fonctionnelle de la densité.....	39
2.3.3 La dynamique moléculaire pour les monocouches .....	40
2.3.4 Autres techniques.....	40
2.3.4.1 <i>Le premier principe couplé à la MD</i> .....	40
2.3.4.2 <i>La MD améliorée</i> .....	41
3. Conclusion.....	41
4. Références.....	43
5. Résumé chapitre 1 .....	48

<b>Chapter 2: Matériaux and méthodes .....</b>	<b>51</b>
1. Introduction .....	52
2. Les techniques de modélisation moléculaire.....	53
2.1 La construction des acides gras, surfaces, huile de base .....	53
2.2 La dynamique moléculaire.....	55
2.2.1 Conditions périodiques aux limites .....	56
2.2.2 Les potentiels intra et inter moléculaires .....	56
2.2.2.1 <i>Le potentiel de Lennard Jones</i> .....	56
2.2.2.2 <i>Le potentiel de Morse</i> .....	57
2.2.2.3 <i>Le potentiel pour les angles</i> .....	57
2.2.2.4 <i>Le potentiel pour les torsions</i> .....	58
2.2.2.5 <i>Le terme répulsif de Gilbert</i> .....	58
2.2.2.6 <i>La méthode d'Ewald (potentiel de Coulomb)</i> .....	58
2.2.2.7 <i>La fonction potentiel</i> .....	59
2.2.3 L'algorithme de Verlet .....	59
2.2.4 Contrôle de la température et de la pression .....	60
2.2.5 Formation d'une couche adsorbée.....	60
2.2.6 Adsorption du film sous pression et cisaillement .....	61
2.2.7 Evaluation du coefficient de frottement .....	63
2.2.8 Evaluation du coefficient de diffusion .....	63
2.3 La méthode de la chimie quantique (QC).....	64
2.3.1 La théorie de la fonctionnelle de la densité (DFT).....	64
2.3.2 La méthode chimie quantique (avec méthode CLOA) TB-QC.....	64
2.3.2.1 <i>La méthode QC</i> .....	64
2.3.1.2 <i>Le premier principe de paramétrisation</i> .....	65
2.3.3 Les modèles pour les calculs de TB-QC .....	66
2.3.4 Validité de la méthode TB-QC .....	67
2.4 Méthode de couplage MD/QC ultra-accélérée (UA-QCMD) .....	68
2.4.1 La méthode UA-QCMD .....	68
2.5. Résumé.....	70
3. Les techniques expérimentales.....	70
3.1 Matériels.....	70

3.2 Les techniques expérimentales de caractérisation .....	70
3.2.1 La spectroscopie à photo-electron (XPS) .....	70
3.2.2 La spectroscopie infrarouge de réflexion-absorption par modulation de polarisation (PM-IRRAS) .....	73
3.3 La mesure du frottement .....	76
3.3.1 Le tribomètre linéaire .....	76
3.4 Résumé.....	77
4. Conclusion.....	77
5. Références.....	79
6. Résumé chapitre 2.....	82

### **Chapter 3: Mécanismes d'adsorption des acides gras C18 purs..... 85**

1. Introduction .....	86
2. Les mécanismes d'adsorption par modélisation moléculaire .....	87
2.1 Une approche qualitative: la dynamique moléculaire .....	87
2.1.1 Le modèle aléatoire vs. le modèle SAM .....	87
2.2 Une approche quantitative: les simulations DFT, TB-QC, UA-QCMD .....	89
2.2.1 L'acide stéarique: une molécule vs. une molécule contenue dans une SAM (50 °C, Fe <sub>2</sub> O <sub>3</sub> ) .....	89
2.2.1.1 Mécanisme d'adsorption d'une molécule seule.....	89
2.2.1.2 Mécanisme d'adsorption d'une molécule contenu dans une SAM.....	90
2.2.1.3 Influence du temps de simulation .....	92
2.2.1.4 Discussion sur les modèles .....	93
2.2.2 Influence de l'orientation .....	94
2.2.3 Influence du substrat .....	96
2.2.3.1 Mécanisme d'adsorption d'une molécule seule.....	96
2.2.3.2 Mécanisme d'adsorption d'une molécule contenue dans une SAM .....	97
2.2.4 Influence de la température.....	99
2.2.5 Influence du degré d'insaturation.....	100
2.2.6 Influence de la densité de la monocouche .....	102
2.2.7 Synthèse.....	105
3. Caractérisation analytique des couches adsorbées sur différentes surfaces à base de fer: analyses XPS et PM-IRRAS .....	106

3.1 Analyses XPS.....	106
3.1.1 Adsorption de l'acide stéarique sur l'oxide de fer.....	106
3.1.2 Influence du substrat .....	108
3.1.3 Influence du degré d'insaturation.....	110
3.1.4 Combinaison de l'étude expérimentale et de la modélisation moléculaire .....	112
3.2 Analyse PM-IRRAS .....	114
3.2.1 Caractérisation des films adsorbés.....	114
3.2.2 Influence du degré d'insaturation.....	116
3.2.3 Comparaison des analyses XPS, PM-IRRAS et des simulations UA-QCMD .....	117
4. Conclusion.....	117
5. Références.....	119
6. Résumé chapitre 3.....	121
 <b>Chapter 4: Comportement tribologique des acides gras C18 purs .....</b>	<b>123</b>
1. Introduction .....	124
2. Comportement tribologique par MD .....	125
2.1 Généralités sur le comportement tribologique par MD .....	125
2.1.1 Angle d'inclinaison .....	125
2.1.2 Contrôle de la température et vitesse de cisaillement.....	126
2.2 Influence des paramètres.....	127
2.2.1 Influence du degré d'insaturation et de la densité.....	127
2.2.1.1 <i>Etudes qualitative et quantitative</i> .....	127
2.2.1.2 <i>Discussions</i> .....	130
2.2.2 Influence de la couche d'oxyde ou d'hydroxyde .....	132
2.2.2.1 <i>Etudes qualitative et quantitative</i> .....	132
2.2.2.2 <i>Discussions</i> .....	134
2.2.3 Influence de la longueur des chaînes alkyles .....	135
2.2.3.1 <i>Résultats</i> .....	135
2.2.3.2 <i>Discussions</i> .....	137
3. Evolution des films adsorbés pendant le processus de frottement par UA-QCMD.....	139
3.1 Effet de la pression et du cisaillement: vers la formation de la fonction carboxylate.....	139
4. Comportements tribologiques des additifs purs .....	140

4.1 Effets du degré d'insaturation et de la température.....	140
4.2 Analyse du tribofilm par PM-IRRAS.....	142
5. Comparaison des résultats numériques et expérimentaux.....	144
5.1 Considérations à prendre en compte pour les résultats de MD avant la comparaison avec l'étude expérimentale.....	144
5.2 Effets des paramètres .....	145
5.2.1 Effets du degré d'insaturation .....	145
5.2.2 Effets de la couche d'hydroxyde.....	145
5.2.3 Effets du frottement sur les réactions chimiques entre les monocouches et la surface.....	145
6. Conclusion.....	146
7. Références.....	147
8. Résumé chapitre 4.....	150

## **Chapter 5: Comportements tribologiques des acides gras C18 mélangés dans la PAO 4..... 153**

1. Introduction.....	154
2. Comportements tribologiques des acides gras dans la PAO 4 par approche expérimentale.....	154
2.1 Tests de frottement .....	154
2.1.1 Influence du degré d'insaturation et de la température.....	155
2.1.2 Influence de la concentration.....	158
2.3 Caractérisation des tribofilms obtenus .....	159
2.2.1 Analyses PM-IRRAS des tribofilms.....	159
3. Compétition des acides gras C18 dans la PAO 4 .....	162
3.1. Comportements tribologiques des mélanges d'acide gras dans la PAO 4.....	162
3.2. Evaluation du coefficient de diffusion des acides gras dans la PAO 4.....	163
3.2.1 Acides gras C18 1%w dans la PAO 4.....	163
3.2.2 Acides gras C18 1%w dans la PAO 4 soumis à une pression normale et du cisaillement.....	164
3.3 Discussions: couplage résultats expérimentaux et simulation MD .....	166
4. Conclusion.....	166
5. Références.....	168

6. Résumé chapitre 5.....	169
<b>Chapter 6 : Synthèses.....</b>	<b>171</b>
1. Résultats principaux .....	172
1.1 Les mécanismes d'adsorption .....	172
1.2 Les comportements en frottement.....	172
1.2.1 Additifs purs .....	172
1.2.2 Additifs dans le solvant .....	173
1.2.3 Mélanges d'additifs.....	173
2. Généralisation à un cas réel d'application .....	173
2.1 Modèle d'adsorption .....	173
2.2 Modèle de frottement .....	174
<b>Conclusion générale et perspectives.....</b>	<b>175</b>
<b>Annexe.....</b>	<b>183</b>



# Notations

$A_{ij}$ $B_{ij}$	Coefficient (Lennard-Jones potential (kcal.Å <sup>12</sup> /mol, kcal.Å <sup>6</sup> /mol))
$a, b$	Sum of size and stiffness of atoms (m)
$C$	Eigen vector matrix
$C^T$	Transformation matrix of the eigen vector matrix
$D$	Diffusion coefficient (m <sup>2</sup> /s)
$D_{ij}$	Coefficient (Morse potential (kcal/mol))
$e$	Elementary electric charge
$\varepsilon$	Eigen value
$f_0$	Constant for unit adjustment (Gilbert term (Å))
$F_x$	Frictional force in z (N)
$F_z$	Normal load (N)
$H$	Hamiltonian matrix
$H_{rr}, H_{ss}, H_{rs}$	Diagonal terms of Hamiltonian matrix
$h\nu$	Beam of X-rays (XPS)
$H_\theta$	Constant force (Angle potential)
$H_\varphi$	Constant force (Torsion potential)
$I$	Unit matrix
$K$	Distance dependent Wolfsberg Helmholtz constant
$k_b$	Boltzmann constant (1.38 10 <sup>-23</sup> J.K <sup>-1</sup> )
$m_i$	Mass of atom I (g)
$p$	Parallel polarized radiation
$R_{ij}$ $r_{ij}$	Distance between atom i and j (Å)
$s$	Perpendicular polarized radiation
$S, S_{rs}$	Overlap integral matrix
$r_0$	Bond length at minimum energy (Å)
$v_i$	Velocity of atom I (km/s)
$Z$	Charge
$\mu$	Friction coefficient

$b_{ij}$	Form factor ( $\text{\AA}^{-1}$ )
$\theta$	Bending angle
$\theta_0$	Bending angle at minimum energy
$\varphi$	Torsion angle
$\varphi_0$	Torsion angle at minimum energy
$\zeta$	Slater type atomic orbital

#### Conversion

$$1 \text{ Ha} = 27.2107 \text{ eV} = 627.503 \text{ kcal/mol}$$

$$1 \text{ eV} = 23.0609 \text{ kcal/mol}$$

## Abbreviation and acronyms

AFM	Atomic force microscopy
AO	Atomic orbital
AR-XPS	Angle resolved X ray photoelectron spectroscopy
BE	Binding energy (kcal/mol)
BL	Boundary lubrication
BOP	Bond order potential
BP	Bond population
CP	Car Parrinello
DFT	Density functional theory
DNP	Polarization function
ECR	Electrical contact resistance
EHL	Elastohydrodynamic lubrication
FM	Friction modifiers
FTIR	Fourier transformed infra-red
GGA	General gradient approximation
HD	Hydrodynamic lubrication
LA	Linoleic acid
LB	Langmuir-Blodgett
LCAO	Linear combination of atomic orbital
LDA	Local density approximation
LJ	Lennard Jones
MC	Monte Carlo
MD	Molecular dynamic
ML	Mixt lubrication
MM	Molecular mechanics
MO	Molecular orbital
MoDTC	Molybdenum dithiocarbamate
OA	Oleic acid
OFM	Organic friction modifier

PAO	Polyalphaolefin
PBC	Periodic bond conditions
PBE	Perdew-Burke-Ernzerhof
PM-IRRAS	Polarization Modulation-Infrared Reflection- Adsorption Spectroscopy
QC	Quantum chemistry
QCM	Quartz crystal microbalance
ReaxFF	Reactive force field
SA	Stearic acid
SAM	Self-assembled monolayer
SAPS	Sulfated ash, phosphorous and sulfur
TBA	Tight-binding approximation
TB-QC	Tight-binding quantum chemistry
UA-QCMD	Ultra-accelerated quantum chemistry molecular dynamic
VSIP	Valence state ionization potentials
VWN	Vosko-Wilk-Nusair
XAS	X-ray absorption spectroscopy
XPS	X-ray photoelectron spectroscopy
ZnDTP	Zinc dialkyl dithiophosphate

# **General introduction**

---

## **Introduction générale**

## General introduction

---

Because of the ecology and economy concerns, many rules appeared over the last few years and thus, in many different areas, including the field of automotive. In fact, exhaust gas from different types of vehicle are composed of NO<sub>x</sub>, CO, etc. and particles that are toxic for environment and need to be limited. Nowadays, many actions are done to limit these hazardous emissions. First of all, catalytic converters are used to “filter” gas refusals. Then, the limitation of vehicle fuel consumption presents some advantaged such as to reduce hazardous emissions and to preserve oil natural resources. In order to limit energy loss induced by friction, a lubricant, which is composed of a base oil and a package of additives, is used. The aim is to conceive a powerful lubricant, e. g. to extend oil and engine life expectancies and also to be respectful toward actual European environments requirements. Actual used friction modifiers and anti-wear additives (e.g. MoDTC and ZnDTP) contain sulfur and phosphorous compounds that damage catalytic converters. Therefore, the concentration of MoDTC and ZnDTP in base oils should be reduced as soon as possible.

Fatty acids which are organic friction modifiers seem to be good candidates to answer new lubricant requirements. In order to better understand the action mechanism of those molecules and to build adsorption model, the computational chemistry appears to be a pertinent tool. In fact, molecular simulation has come to an important development over the past two decades thanks to improvement in the informatics field. Different techniques such as Molecular Dynamics (MD) and Quantum Chemistry (QC) enable to study chemical molecular structures, their conformations, interactions and chemical reaction at a scale where experimental analysis sometimes reaches its limit. Its success is nowadays recognized and it is not surprising that the Nobel award 2013 on chemistry has been given to the pioneers of molecular simulation: Martin Karplus, Michael Levitt and Arich Warshel.

The PhD thesis is a collaboration work between Total M&S group, Professor Miyamoto’s laboratory in Tohoku University (Japan) and the Laboratory of Tribology and System Dynamics (LTDS) at Ecole Centrale of Lyon (France). In this PhD thesis, we wanted to revisit the study of adsorption mechanisms and tribological behavior of C18 fatty acids with an original approach, which consists in coupling molecular simulation and experimental work. The present work has been conducted in two steps: first of all, a study of molecules adsorption on surfaces followed by friction investigations. Software that are used in this work have been developed in Professor Miyamoto’s laboratory. Many travels were planned in order to learn how to use the different software and to improve the software for the field of tribology. Simultaneously, experimental study has been performed in LTDS by Dr. Christine Matta. The present work will be divided into 6 chapters.

The **first chapter** will focus on works that has been done in literature concerning organic friction modifiers, and more precisely C18 fatty acids. First, generalities on engine lubrication and lubricant composition will be presented. Then, the chemistry of fatty acids and parameters that might influence their tribological properties will be discussed. Finally, a review on molecular simulations applied on tribological issues will be done.

In the **second chapter** of this thesis, details concerning the different computational techniques used in this work will be explained: quantum chemistry (QC), molecular dynamics (MD) and the combination of both QC and MD called UA-QCMD. This last method is one million faster than classical MD *ab initio* method and, therefore, enables to work with a large complex system. The different models that have been built will be presented. Finally, surface characterization techniques, e.g. XPS and PM-IRRAS analysis and the tribometer for friction

measurements will be detailed. Additives, base oil and sample's preparation procedure will also be presented.

The **third chapter** of this thesis will focus on adsorption mechanisms of C18 fatty acids on iron-based surfaces. UA-QCMD technique has been applied to study the adsorption mechanism of one fatty acid molecule on iron oxide surface. Then, ideal model, e.g. the self-assembled monolayer (SAM) will be built for the three fatty acids: stearic, oleic and linoleic acids. Different parameters will be studied in order to understand their influence in the formation of the SAM: the nature of the substrate, the orientation of molecules, the density, the unsaturation degree and the temperature. This work will be completed by XPS *in-situ* and PM-IRRAS analysis of adsorbed films. Finally, correlations between experimental results and molecular simulation will be done.

In the **chapter four**, we focus on the friction behavior of pure fatty acids, e.g. without any solvent (stearic, oleic and linoleic acids). MD method will be applied to evaluate the friction coefficient and to follow the evolution of the adsorbed film during the friction process. The influence of the nature of the substrate, the unsaturation degree, the film density and the fatty acid chain length will be investigated. UA-QCMD method will be applied to investigate the chemical behavior of the adsorbed film when it is under pressure and shear stresses. Meanwhile, tribological behavior of fatty acids as a function of the temperature will be investigated with tribotests. Tribofilms will be analyzed by PM-IRRAS in order to validate our simulation results.

In the **chapter five**, the study is focused on the friction behavior of C18 fatty acids in presence of the PAO 4 base oil. Same approach as for chapter four, e.g. MD and experimental techniques, will be used for additives blended in PAO 4 at 1%w. In order to study the competition of additives and the presence of synergic or anti synergic effects, mixture of saturated and unsaturated fatty acids will be done and their tribological behavior will be presented. To complete this work, diffusion coefficient of each fatty acid in the PAO 4 will be calculated by MD simulation.

The **chapter six** is a chapter that summarizes the main results of the thesis and proposes a model that is close to a real application case.

# Introduction générale

---

Face aux enjeux écologique et économique, de nombreuses réglementations ont vu le jour au cours de ces dernières années dans divers secteurs industriels, et notamment dans le secteur des transports routiers. En effet, les gaz d'échappement émis par les différents types de véhicules sont composés de gaz (NO<sub>x</sub>, CO, etc ...) et de particules toxiques pour l'environnement qu'il convient de limiter. De nos jours, plusieurs actions sont mises en œuvre pour limiter ces émissions nocives. Tout d'abord, les pots catalytiques sont utilisés couramment afin de « filtrer » les gaz d'échappement. Ensuite, limiter à la base la consommation de carburant des véhicules présente différents avantages comme réduire les émissions nocives et préserver les ressources fossiles de pétrole. Afin de contribuer à limiter les pertes par frottement dans un moteur thermique, un lubrifiant constitué d'une huile de base et d'un mélange d'additifs est utilisé. L'objectif en terme de lubrification est de concevoir des huiles performantes, avec des durées de vie importante (espacement des vidanges) et ceci dans le respect des normes environnementales européennes en vigueur. Le problème des additifs actuellement utilisés en tant que modificateur de frottement et d'anti-usure (respectivement MoDTC et ZnDTP) est qu'ils contiennent des produits soufrés et phosphorés qui endommagent les pots catalytiques. De ce fait, la teneur en MoDTC et ZnDTP des huiles doit être réduite à court terme.

Les acides gras, modificateurs de frottement organiques, semblent être de bons candidats pour répondre aux nouvelles contraintes des lubrifiants. Afin d'obtenir des éléments de réponse sur la compréhension des mécanismes d'action de ces molécules et d'établir des modèles d'adsorption, la chimie computationnelle apparaît comme un outil pertinent. En effet, la modélisation moléculaire a connu un essor important ces deux dernières décennies grâce aux progrès de l'informatique. Différents outils comme la Dynamique Moléculaire et la Chimie Quantique vont permettre d'étudier les structures des molécules chimiques, leurs conformations, les interactions et réactions chimiques avec des surfaces à une échelle où l'analyse expérimentale atteint parfois ses limites. Son succès est reconnu aujourd'hui, preuve étant que le prix Nobel de chimie 2013 a été décerné aux pionniers de la modélisation moléculaire : Martin Karplus, Michael Levitt et Arich Warshel.

Dans le cadre de ce travail de thèse mené en collaboration avec le groupe Total M&S, le laboratoire du professeur Miyamoto à l'Université de Tohoku (Japon) et le Laboratoire de Tribologie et Dynamique des Systèmes (LTDS) à l'Ecole Centrale de Lyon (France), nous avons décidé de revisiter les mécanismes d'adsorption et le comportement tribologique des acides gras C18 avec une approche qui consiste à coupler la modélisation moléculaire à des techniques expérimentales. Ces travaux de thèse ont été menés en deux temps : tout d'abord une étude de l'adsorption des molécules sur les surfaces suivies par des études en frottement. Les logiciels utilisés ont été développés au laboratoire du professeur Miyamoto où de nombreux aller-retour ont été effectués dans le but d'apprendre à utiliser ces logiciels et à les améliorer pour répondre à nos problématiques. Simultanément, les expériences d'adsorption et de frottement ainsi que les analyses des surfaces ont été réalisées au LTDS par le Dr. Christine Matta. L'ensemble de l'étude est exposé sous forme de 6 chapitres.

Dans le **premier chapitre** de ce mémoire, nous nous intéresserons à l'état d'avancement des travaux concernant les modificateurs de frottement organiques, et plus particulièrement des acides gras C18. Nous aborderons les notions générales de la lubrification des moteurs et de la composition d'un lubrifiant. Puis, nous présenterons la chimie des acides gras et les paramètres pouvant influencer leurs propriétés tribologiques.



Enfin, nous ferons un état de l'art sur l'apport de la modélisation moléculaire par rapport aux études expérimentales.

Dans le **deuxième chapitre**, nous présenterons les différentes techniques de modélisation utilisées: la chimie quantique (QC), la dynamique moléculaire (MD) et enfin le couplage QC et MD appelé UA-QCMD, méthode un million de fois plus rapide que les méthodes de MD *ab initio* existantes. Cette méthode permet donc de travailler sur des systèmes complexes. Les différents modèles seront présentés également. Enfin, la démarche expérimentale sera présentée avec la description des additifs et des lubrifiants utilisés, la présentation des tribomètres ainsi que celle des techniques d'analyse de surface (XPS et PM-IRRAS) utilisées.

Le **troisième chapitre** porte sur l'adsorption des molécules d'acide gras sur les surfaces modèles. La méthode UA-QCMD a été appliquée, dans un premier temps, à l'étude de l'adsorption d'une simple molécule d'acide gras sur de l'oxyde de fer. Puis, le modèle « idéal » de la monocouche auto-assemblée (SAM) a été construit pour les trois acides gras considérés : acides stéarique, oléique et linoléique. L'influence de différents paramètres sur la formation du SAM ont été étudiés comme la nature de la surface, l'orientation des molécules sur la surface, leurs densités, leurs degrés d'insaturation, et la température. D'un point de vue expérimental, des expériences d'adsorption en environnement contrôlé ont été réalisées et suivies d'analyses XPS *in-situ* et PM-IRRAS des films adsorbés. Des corrélations entre résultats expérimentaux et simulation seront présentés.

Le **quatrième chapitre** porte sur l'étude du comportement en frottement des acides gras purs e.g. sans solvant (acide stéarique, oléique et linoléique). La méthode MD a été appliquée pour évaluer le coefficient de frottement, et suivre l'évolution de l'organisation des films adsorbés lors du frottement. L'influence de la nature du substrat, du degré d'insaturation, de la densité et de la longueur des chaînes alkyles, sur le comportement en frottement des films adsorbés sont discutés. La méthode UA-QCMD a également été utilisée pour compléter l'étude du comportement des films sous pression et cisaillement. En parallèle, les performances tribologiques des acides gras en fonction de la température ont été évaluées grâce à des tests de frottement expérimentaux. Les tribofilms obtenus sont analysés par PM-IRRAS afin de valider les résultats numériques.

Dans le **cinquième chapitre**, le comportement en frottement des acides gras C18 est également étudié, mais ici en présence de PAO. La même approche (couplage MD et techniques expérimentales) que dans le chapitre quatre est utilisée avec les additifs mélangés à 1% dans la PAO 4. Des mélanges d'acides saturés et insaturés seront réalisés et leur comportement tribologique sera présenté. Ceci, afin d'étudier d'éventuelles compétitions d'adsorption entre additifs ainsi que des effets synergique ou anti synergique. Pour compléter cette étude, La diffusion des acides gras dans la PAO 4 est étudiée par MD (calcul coefficient de diffusion).

Le **chapitre six** est un chapitre qui présente une synthèse des différents résultats obtenus et propose un modèle qui se rapproche du cas « réel » de l'application.



## **Chapter 1: Literature overview**

---

## **Chapitre 1: Synthèse bibliographique**

# Chapter 1: Literature overview

---

## Table of contents

1. Introduction .....	24
2. Generalities .....	25
2.1 Lubricant composition and function .....	25
2.1.2 Lubricant additives .....	27
2.1.3 Industrial restriction and new objectives .....	29
2.2 Organic friction modifiers .....	30
2.2.1 State of the art .....	30
2.3 Contribution of computational chemistry .....	39
2.3.1 Limits of experimental approaches .....	39
2.3.2 Adsorption by density functional theory (DFT) calculation .....	39
2.3.3 MD simulation on monolayer .....	40
2.3.4 Other techniques .....	40
3. Conclusion .....	41
4. References .....	43
5. Summary chapter 1 .....	48

## 1. Introduction

Nowadays, lubricant additives are continuously improved to provide better properties and performance to modern lubricants. Environmental legislations will drive changes of lubricant components and will constrain their future development.

The aim of chapter 1 is to expose the new industrial and scientific challenges concerning lubrication in the automotive industry. Moreover, the focus will be on automotive lubrication properties that can reduce friction and wear in the thermal engine. Generalities on lubricant composition and function will be described in the first section of this chapter. Then, the role of the different lubricant additives will be explained with a special focus on Organic Friction Modifiers (OFM). They have been studied for decades but the actual interest for them is still very important. In the second section, a literature review about lubricant properties of OFM additives will be described with a summary of the influence of different parameters (surface nature, temperature, density etc...) on their adsorption mechanism and wear properties. Finally, the knowledge of structural and dynamical aspects of organized system at atomic scale is very important to better understand functions of complex systems. In the last decades, computer science progress exploded and theoretical and modeling chemistry enabled to understand physical-chemical phenomena and consequences that cannot be interpreted by analytical tools at the atomic and electronic scales. This last section will be focused on the overview of computational chemistry tools that has been carried out to study adsorption mechanisms and friction behavior of such lubricant additives.

## 2. Generalities

### 2.1 Lubricant composition and function

#### 2.1.1 Generalities

##### 2.1.1.1 Thermal engine lubrication

Thermal combustion engines are made of different mechanical organs that are moving and generating metal to metal contacts (figure 1). Lubrication is thus needed and plays a key role in the life expectancy of an engine.

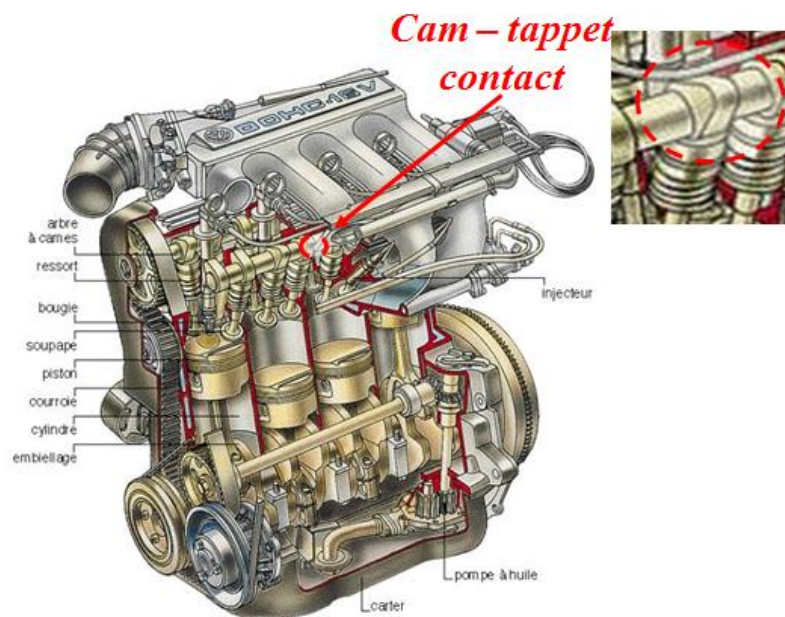


FIGURE 1: SCHEMATIC OF THERMAL COMBUSTION ENGINE AND ZOOM ON CAM-TAPPET CONTACT

Inside the engine, lubricant is pumped to various components such as the cam, bearings, piston, etc. All the mechanical devices are submitted to different contact conditions (pressure, temperature etc...) and the lubricant must be accurate for all cases.

Because of the variety of contact conditions in the different mechanical devices of the engine, the contact severity is not equal everywhere. Four lubrication regimes can be distinguished as shown on the Stribeck curve (figure 2) <sup>[1, 2]</sup>, which describes the friction coefficient variation as a function of a parameter defined by the product of sliding speed and lubricant viscosity divided by the applied pressure:

- ▶ The hydrodynamic lubrication (HD) <sup>[3]</sup>: the surfaces are completely separated by a thick lubricant film (thickness higher than the surface roughness). This prevents contact between substrate thanks to the lubricant load bearing capacity. The friction coefficient is dominated by the oil film shearing and is determined by the hydrodynamic theory.
- ▶ The elastohydrodynamic lubrication (EHL) <sup>[3]</sup>: the oil film thickness calculation takes into account the elastic deformation of surfaces and piezoviscous effects.
- ▶ The mixed lubrication (ML) <sup>[4]</sup>: the surfaces are separated by a thin lubricant film and some asperities from the two surfaces are in contact. The load is carried by the lubricant film and partial contacts between the surfaces. In this regime, the strict law of hydrodynamic lubrication is no longer fully accurate.

- The boundary lubrication (BL) [5]: as the lubricant film thickness is less than the composite surface roughness, the surface asperities come into contact under motion. The load is mainly supported by asperities in contact and the bulk fluid viscosity of the lubricant has little or no effect on friction and wear as no oil is found in the contact. The role of lubricant is so to dissipate the heating and to deliver surface additives to friction surfaces. BL conditions could result in high friction coefficient and high wear, which is influenced by the nature of the underlying surface as well as by the chemical composition of the lubricant.

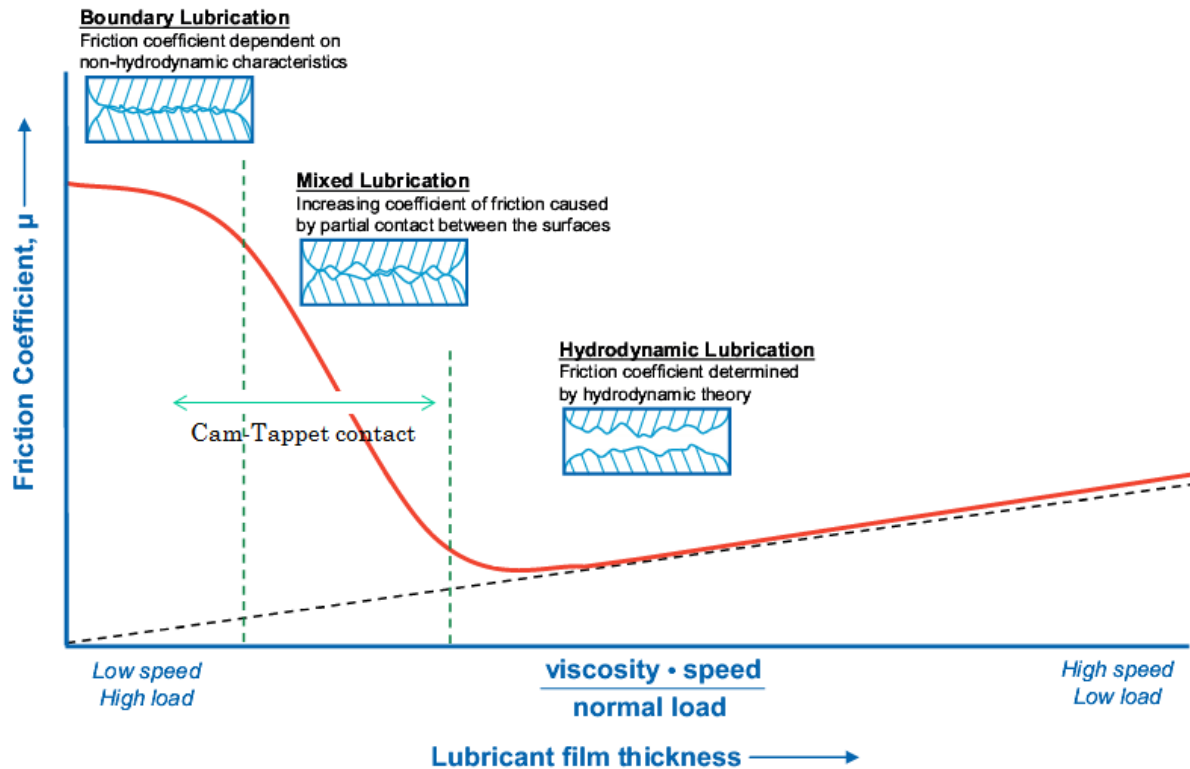


FIGURE 2: STRIBECK CURVE SHOWING DEPENDENCE OF FRICTION COEFFICIENT WITH LUBRICANT FILM THICKNESS, VISCOSITY, SPEED AND NORMAL LOAD [1]

Our study will be focused on the cam-tappet contact, which works under severe contact conditions, that is to say Boundary Lubrication or Mixed Lubrication regimes.

### 2.1.1.2 Friction reduction in a thermal engine

Reducing friction in engine has gained importance within the automotive industry in recent years. As there are different lubrication regimes in the thermal combustion engine, different ways to reduce friction must be considered.

In Hydrodynamic and Elastohydrodynamic regimes, the lubricant film ensures the separation of surfaces. The film thickness and the friction coefficient are viscosity dependent. A way to reduce friction is to decrease the lubricant viscosity. But if so, the film thickness in the contact will decrease. Therefore, there is a shift from HD regime to ML or BL regimes in the different contacts of the engine. This leads to an increased risk of wear phenomena.

Therefore, it is possible to optimize the surface, the lubricant formulation or both to better control friction and wear. Our study will be focused on the optimization of friction modifier additives for steel surfaces.

## 2.1.2 Lubricant additives

### 2.1.2.1 Lubricant composition

Main functions of a lubricant are the reduction of friction and wear, the cooling of components and the cleaning of contact surfaces. Formulated oils are products composed of a base oil and a package of additives designed for specific needed performance (figure 3). Additives range from 1% to 30% depending on the application <sup>[source: TOTAL MS]</sup> which includes 0% to 15% of polymers in order to improve the viscosity of the lubricant regarding temperature.

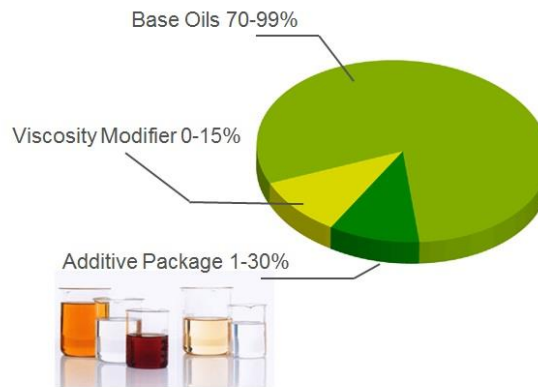


FIGURE 3: COMPOSITION OF AN ENGINE LUBRICANT [SOURCE: TOTAL MS]

#### *a. Base oil*

The base oil should full fill certain requirements <sup>[7]</sup>: it should be viscous enough to maintain a lubricant film in contact under operating conditions but not too much. It should also have the adequate calorific capacity to remove heat and be stable under thermal and oxidative stresses. Then, it should have the capacity to solubilize all additives. There are two types of base oil <sup>[7]</sup>:

- ▶ Mineral oils (obtained from crude oil) are composed of linear or branched carbon chains, aromatic or aliphatic rings. Differences between mineral oils, derived from different crude oil natures and refining processes, are mainly on viscosity, chemical structure, and sulfur content. Three main chemical structures of mineral oil are found depending of the crude oil nature:
  - ⊕ Paraffinic oil: linear or branched hydrocarbons chain;
  - ⊕ Naphthenic oil: hydrocarbons which contain cyclic saturated carbon molecules;
  - ⊕ Aromatic oil: hydrocarbons which contain benzene type compounds;

Mineral oils are classified regarding the proportion of these three chemical forms present. The sulfur content in oil varies with the source of crude oil. A small amount of sulfur enables to improve lubrication and oxidation properties and can also reduce wear. The viscosity degree depends on the refining process.

- ▶ Synthetic oils (obtained by chemical synthesis) can be designed to have specific properties. They are used in many applications but are more expensive than mineral oil. Synthetic oils can be classified in three basic types:
  - ⊕ Synthetic hydrocarbon lubricants (Poly- $\alpha$ -olefins, esters, polyglycols)
  - ⊕ Silicon derivates
  - ⊕ Organohalogens

The most used base oil in the automotive industry is the synthetic hydrocarbon lubricants and more specifically, the poly- $\alpha$ -olefins (PAO). PAO are synthesized from olefin monomers. These monomers consist of a linear carbon chain with unsaturated carbon at the end of the chain. The presence of unsaturated carbons enables oligomerization to form the oil. Most important characteristics of poly- $\alpha$ -olefins are their high viscosity, their low volatility and their good stability toward oxidation. Despite these characteristics, PAOs do not have double bonds or aromatic groups and, therefore, have low ability to dissolve additives. PAO acronym is always followed by a number which represents the kinematic viscosity ( $\text{mm}^2/\text{s}$  at  $100\text{ }^\circ\text{C}$ ): PAO4, PAO6, etc.

### *b. Additives*

Lubricant additives are added to the base oil to optimize its performance. Many additives are incorporated to the formulation with several functions in order to answer the constructor's requirements. The most commonly used additives are presented in the following [8, 9, 10]:

- ▶ **Antioxidants** delay the degradation of the base oil by oxidation and, therefore, extend the life expectancy of lubricant oil. In fact, high temperature and presence of air activate the oxidation process. Typical additives are aromatic amines, phenols, sulfur compounds and organo-molybdenum.
- ▶ **Detergents** ensure the cleanliness of some of the engine's components by preventing the formation of carbon-based deposit on the surfaces at high temperature. Detergents have a micellar structure, with a core made of alkaline compounds surrounded by surfactant chains. They could have a neutral or basic pH. Overbased detergents are used to neutralize acids compounds generated in operation.
- ▶ **Dispersants** enable to put solid impurities formed during the operating of the engine in suspension in the oil. They prevent agglomeration of solid residual that can form a deposit at low temperature (when the thermal engine is turned off). They are fully organic compound with polar head and hydrophobic tail. Succinimide is the most widely used dispersant.
- ▶ Several types of **Friction modifiers (FM)** are used. One group of FM is organic FM, which are amphiphiles molecules with polar head group such as alcohols, esters, fatty acids, etc. These additives are efficient at low loads and low temperature of about  $80\text{ }^\circ\text{C}$  –  $100\text{ }^\circ\text{C}$  (depending on the chain length). At high temperature, they desorb upon thermal activation. They are used to inhibit stick-slip by physical adsorption onto the surface. They adsorb onto the surface, prevent the direct contact of the surfaces and, therefore, contribute to reduce friction. Another group of FM is inorganic FM such as organomolybdenum compounds (MoDTC). Thanks to tribochemical reactions,  $\text{MoS}_2$  lamellar compound is generated in the contact and allow friction reduction.
- ▶ **Antiwear additives** are used to react with the surface and form a protective layer which ensures wear protection. They are mainly phosphorous based like zinc dialkyl dithiophosphate (ZnDTP) which is the most used in engine oil.
- ▶ **Extreme-pressure additives** work under very severe BL conditions. They react with the surface to prevent adhesive wear. These additives are sulfur based.
- ▶ **Corrosion inhibitors** protect the surface from reactive and oxidative species in the solution by adsorbing onto the surface via a high polar group and form continuous film. Amine succinate and alkaline earth sulfonates are typical materials to achieve this purpose.
- ▶ **Viscosity index improvers** are added to change the viscosity of the oil. They are high molecular weight polymers that increase the oil viscosity at high temperature by steric effect. Mainly, poly-alkyl-methacrylate (PMA) and olefin's copolymer are used.



- **Pour point depressant additives:** the pour point of a lubricant is the lowest temperature at which it can flow. PMA with small molecular weight are used to interfere with the crystallization process of paraffin contained in the oil.
- **Anti-foam additives** are used to correct the foaming caused by dispersants and detergents thanks to their low surface tension. Only few ppm are used in the formulation. They are mainly silicon-based with large molecular weight and are non-soluble in oil.

Important additives for tribological properties are friction modifiers and antiwear additives. In fact, in the BL regime, the asperities are in direct contact and high friction and wear can occur. To reduce these phenomena, protective film called tribofilm should be formed on the friction surfaces. In present formulation, molybdenum dithiocarbamate (MoDTC) and zinc dialkyldithiophosphate (ZnDTP) are the most famous and powerful additives used in terms of friction and wear reduction. In addition, ZnDTP is not only an excellent antiwear agent but also a good extreme-pressure additive and present effective anti-oxidation and corrosion inhibition properties. Nevertheless, their action modes in sensitive area of the engine are very complex and were studied for years <sup>[11, 12]</sup>. Despite the fact that MoDTC and ZnDTP are very powerful additives, they contain sulfur and phosphorus, which are at the origin of the deterioration of gas treatment system in cars and are pointed out by environmental norms. In the future, it will be needed to replace them by alternative additives that maintain the same efficiency in addition to be environmentally friendly.

### 2.1.3 Industrial restriction and new objectives

Global warming and generally speaking the fight against pollution lead to an automotive industry evolution. The new trend in engine conception is to optimize operations of the engine in order to be more powerful, to have less gas oil consumption and to respect restrictions. For example, European regulations are more and more severe as shown in table 1 <sup>[13]</sup> concerning NO<sub>x</sub>, CO and particles emissions.

TABLE 1: EVOLUTION OF EUROPEAN REGULATIONS FOR VEHICLE DIESEL ENGINE (MG/KM) <sup>[13]</sup>

Norms	Euro 1 1992	Euro 2 1996	Euro 3 2000	Euro 4 2005	Euro 5 2009	Euro 6 2014
Nitrogen oxide (NO <sub>x</sub> )	-	-	500	250	180	<b>80</b>
Carbon monoxide (CO)	2720	1000	640	500	500	<b>500</b>
Hydrocarbon (HC)	-	-	-	-	-	-
HC + NO <sub>x</sub>	970	900	560	300	230	<b>170</b>
Particles (PM)	140	100	50	25	5	<b>5</b>

To follow this objective, it is needed to develop new lubricants that can follow technological evolution, be more efficient in terms of friction and wear reduction and are respectful toward environment. In previous section, it was mentioned that ZnDTP and MoDTC are both very good additives in term of tribological properties. Nevertheless, their uses are reconsidered for two reasons:

- These molecules need an induction period to be thermally activated before being tribologically active.
- Their decompositions lead to the release of sulfur and phosphorous products, poisonous toward environment and damaging catalytic converters.

Evolution in emissions legislation is driving a fundamental change in lubricant formulation. The requirement mandates lower concentration of sulfated ash, phosphorous and sulfur (low SAPS) in the lubricant <sup>[14]</sup>. Two alternatives are proposed. The first one is to find new family of lubricant additives such as nanoparticle type additives <sup>[15]</sup>. Another alternative is to optimize the action of actual lubricant additives. For this approach, it is necessary to better understand the action mechanism of each additive in order to control their concentration, to fulfil environmental requirements.

In our study, we will focus on the study of organic friction modifiers and more precisely on model molecules such as C18 fatty acids. In fact, fatty acids do not contain SAPS and have already proved their efficiency as boundary additives but they won't be used in the thermal engine as their acid functions could generate corrosive wear or could neutralize over based detergent. Despite this, C18 fatty acids are kept as model molecules in this study. The next section will focus on the actual knowledge of OFM action mechanisms.

## 2.2 Organic friction modifiers

### 2.2.1 State of the art

OFM are generally long molecules with a linear hydrocarbon chain consisting of at least 10 carbon atoms and a polar group at the end of the alkyl chain. The hydrocarbon group must be long enough to be soluble in the oil. The polar group is the governing factor for the effectiveness of the molecule as a FM. Chemically, OFMs can be classified into different categories:

- ▶ Carboxylic acids or their derivatives
- ▶ Amides, amines, imides and their derivatives
- ▶ Phosphoric and phosphoric acid derivatives
- ▶ Organic polymers

The mechanism of friction reduction varies with the different categories. In the next section, further details about the lubrication properties of C18 fatty acid, e.g., stearic, oleic and linoleic acid will be developed.

#### 2.2.1.1 Chemistry of C18 fatty acids

##### *A bit of history*

Surprisingly, fatty acids have been already used as friction modifiers in fuels and lubricating oils for many years. Many studies have proved their efficiency under certain operating conditions and authors have proposed different lubrication models. In 1920, Well and Southcombe <sup>[16]</sup> have shown that the addition of a small amount of long chain carboxylic acids to mineral base oils improves the boundary lubricating properties of a liquid lubricant. Few years later, Hardy <sup>[16]</sup> has proposed that boundary lubrication is favored by the adsorption of a close-packed monolayer of brush-like polar molecules of fatty acids on metal surfaces. He has shown that the friction is not only influenced by the chemical nature and the length of the molecule but also by the nature of the underlying surface. Nevertheless, Hardy model of boundary lubrication is very idealistic as the surface is not infinitely flat in a real case.

In the 40's, Bowden and Tabor <sup>[17]</sup> have proposed a new model where contacts between asperities were considered. They have suggested that the normal load is supported by the contact between the surface asperities and that the generated pressure disrupted the adsorbed monolayer.

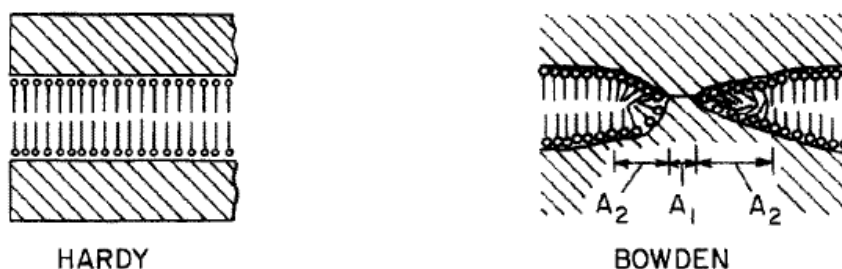


FIGURE 4: BOUNDARY LUBRICATION MODEL, HARDY: ADSORPTION OF MONOLAYER OF POLAR MOLECULES, BOWDEN: INTIMATE CONTACT OF SOLID SURFACES OCCURS [18]

In the 60's, Allen has opened the debate of thin films *versus* thick films when he presented the work of Needs and Fuks [18]. The formation of adsorbed layers occurs due to the polar nature of the fatty acids. First, the fatty acid is dissolved in the oil and attracted to the surface through long-range interactions. Once it reaches the surface, the polar head is adsorbed to the metal surface and van der Waals forces cause molecules to align themselves parallel to each other and form a self-assembled monolayer [18]. Finally, after the formation of the first monolayer, several hypotheses have been described and different models of liquids squeezed between two solid flats have been presented in the literature (monolayer versus multilayers) [18-20].

### *The ideal model: Self-Assembled Monolayer*

Self-assembled monolayers (SAM) consist of organic hydrocarbon-containing molecules such as fatty acids that are bound to a surface and spontaneously form ordered monolayers thanks to van der Waal's interactions between molecules. The natural formation of SAM follows several steps as shown in figure 5 [21, 22]. Molecules present in the base oil start to adsorb on the surface. Finally, molecules form a well-packed layer. The OFMs order in an upright manner with tilted angle that depends on the density of the molecules and due to variations in the substrate composition [22] which will be developed in the next section. The natural formation of SAM can take several hours [21].

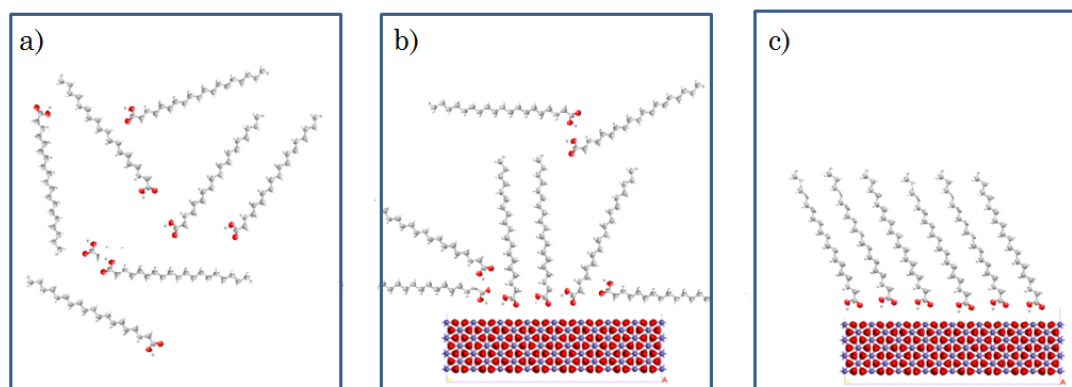


FIGURE 5: THE NATURAL FORMATION OF SAM. A) C18 FATTY ACIDS DISPERSED IN THE BASE OIL (NOT DRAWN FOR SIMPLIFICATION) B) THE SUBSTRATE IS EXPOSED TO THE LUBRICANT AND MOLECULES START TO ADSORB ON THE SURFACE, C) MOLECULES FORM WELL-PACKED LAYER WITH VAN DER WAAL INTERACTIONS BETWEEN THEM

Several techniques exist to form a self-assembled monolayer spontaneously. Langmuir-Blodgett (LB) technique is the most known technique for preparing SAMs films as it enables precise control of the monolayer thickness, density and monolayers can be deposited on many kinds of solid substrate [23]. The scheme of LB films deposition is presented in figure 6. The LB film balance can build highly organized SAMs. This is accomplished by dipping a solid substrate up and down through the monolayer while simultaneously keeping the surface

pressure constant by moving the barrier. Consequently, the floating monolayer is adsorbed to the solid substrate. Multilayers can be produced by this deposition process repeated several times.

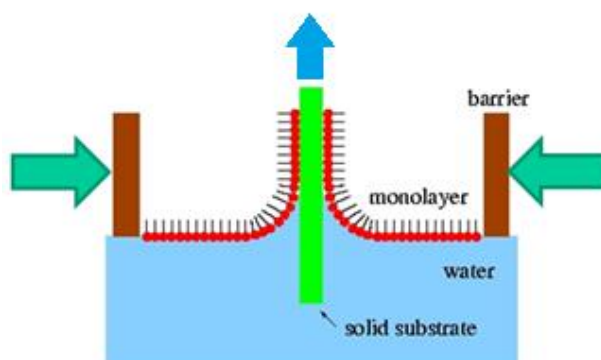


FIGURE 6: SCHEMATIC OF LANGMUIR-BLODGETT (LB) FILMS DEPOSITION PROCESS [22]

The most important indicator of the monolayer properties is given by the measurement of the surface pressure as a function of the area available for each molecule. It is possible to represent an isotherm (Figure 7) by compressing the film with the barriers and therefore have access to the density of the deposited film. Figure 7 shows that there are different regions in the isotherm. Depending on the density, the film can be what we call “solid-like”, “liquid-like” or “gas-like” film.

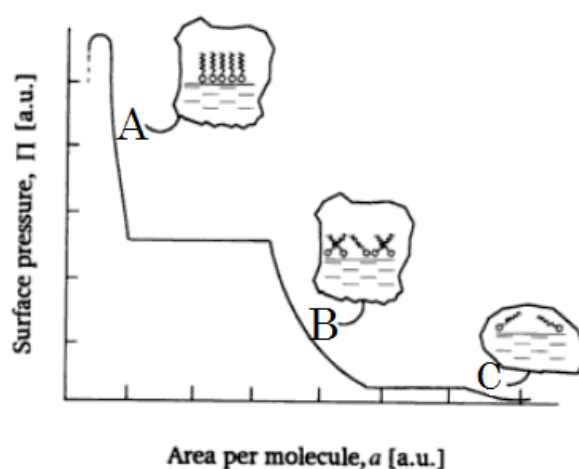


FIGURE 7: SURFACE PRESSURE VERSUS AREA PER MOLECULE ISOTHERM FOR A LONG CHAIN ORGANIC COMPOUND. A: SOLID LIKE FILM, B: LIQUID LIKE FILM, C: GAS LIKE FILM [24]

### *Adsorption and friction reduction mechanism of OFMs*

The friction reducing properties of OFMs come from the fact that the layers of molecules are difficult to compress but easy to shear at the tail interfaces. Adsorption on a metallic surface of organic polar molecules produces a low friction, mono-molecular layer on the surface as shown in figure 8 [21]. The polar head group is strongly attracted to the metallic surface which ensures that almost all available substrate sites are occupied by the fatty acid to produce a dense and robust film. The repulsion between the contacting alkyl groups ensures that the shear strength of the interface is relatively low. This repulsion force can be produced

by entropic effects which may balance the attractive van der Waals forces and prevent molecules from interdigitation [25].

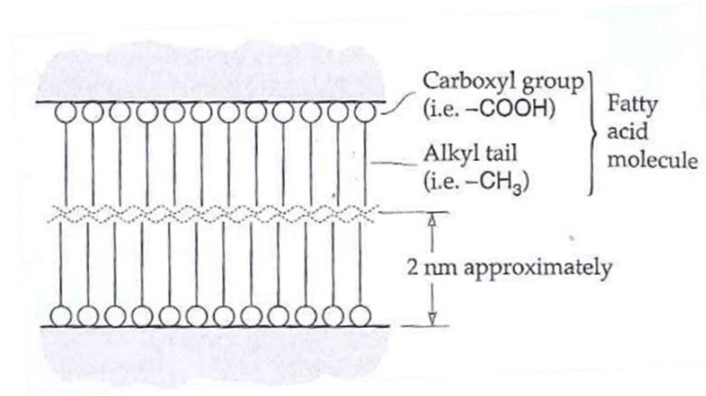


FIGURE 8: ADSORBED ORGANIC POLAR MOLECULES ON METALLIC SURFACES [21]

Fatty acids are able to reduce friction in a wide range of temperature. In fact, the coefficient of friction is quite low below a critical temperature where molecules desorb, resulting in a sharp increase of friction coefficient as shown in figure 9.

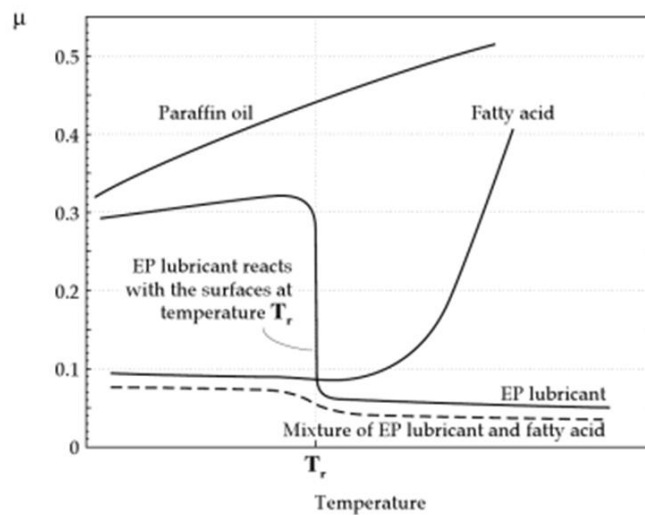


FIGURE 9: EFFECT OF TEMPERATURE ON THE FRICTION COEFFICIENT OF DIFFERENT LUBRICANT: EXTREME PRESSURE LUBRICANT, FATTY ACID, MIXTURE OF EP LUBRICANT AND FATTY ACID, PARAFFIN OIL [21]

Adsorption can be divided into two main categories: physisorption and chemisorption.

The first possible adsorption mechanism is **physisorption**. Physisorption occurs when binding interactions are less than 40 kJ/mol [26]. No specific chemical function are needed for physisorption so all the lubricants have some potential to form such boundary films. Physical adsorption involves intermolecular forces like van der Waals or hydrogen bonds.

The second possible adsorption mechanism is **chemisorption**. With chemisorption, the binding energy is much higher than for physisorption as the binding interactions are more than 40 kJ/mol [26]. Ku [27] has highlighted that fatty acids can react with metals to form metal soaps. Figure 10 shows stearic acid molecules adhering on an iron or iron oxide surface and bind to the iron to form iron carboxylate. Chemical adsorption involves that valence electrons are shared by both the molecule and the substrate. The chemisorption can be symmetric (through the two oxygens) or asymmetric (through one oxygen) when the hydrogen is not dissociated from the hydroxyl group.

At this step, it is shown in literature that fatty acids react with the surface to form a carboxylate that can be either mono-dentate, bi-dentate or bridging. Crowell *et al.* have defined mono-dentate, bridging and bi-dentate adsorption for aluminum substrate [28, 29]. Mono-dentate adsorption is through one oxygen atom, bi-dentate adsorption is through the two oxygens of the acid group on the same surface atom, bridging adsorption is through the two oxygen of the acid group on two different surface atoms. This definition is mainly used when a carboxylate is formed even though it is not always clear whether the hydrogen is dissociated or not from the hydroxyl group. The hydrogen dissociation from the hydroxyl group seems to be favored by friction. Kajdas proposed that this dissociation is due to the ionization of the polar group by low energy electron emitted from the metal surface during rubbing. Then, the carboxylic anions bond to the surface iron atoms while the hydrogen radicals recombine and form dihydrogen molecules [30, 31]. More recently, Simič and Kalin summarize the different adsorption mechanisms that can occur on the steel surfaces [32]. In fact, the steel surface is partially covered by oxides and hydroxides and, therefore, different adsorption mechanism can occur regarding the type of oxides: physisorption and chemisorption. He also pointed out that the formation of stearate is induced by rubbing. In the literature, it is not clear whether or not the formation of carboxylate can be formed during the adsorption of the thermal film or only during friction so clarification of the adsorption mechanism will be one key point of the present study.

The most effective fatty acid is the one that can combine a chemical reaction with the surface and cohesive interactions between the alkyl chains to maintain the monolayer. Stearic acid seems to be the preferred OFM to achieve this objective. In the case of multilayers films, the first film is chemisorbed and then other films are physisorbed. Physisorbed layers are less durable than chemisorbed layers.

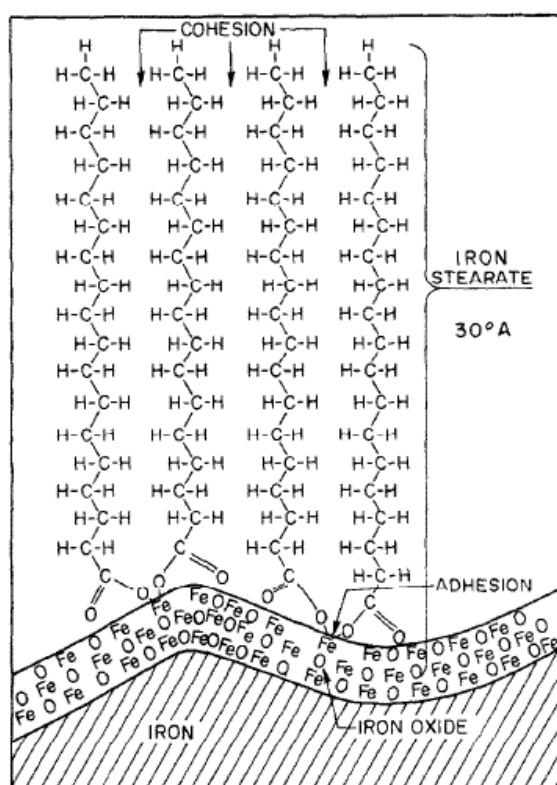


FIGURE 10: CHEMISORPTION OF STEARIC ACID MONOLAYER ON IRON OXIDE SURFACE [27]

Through the years, several authors have used different techniques and methods to validate their models by studying different parameters. They have studied for example the

influence of the substrate (nature of the oxide layer), of the fatty acid chain length, of the unsaturation degree and of the humidity.

### 2.2.1.2 Parameters influencing adsorption and friction reduction properties

#### *Effect of substrate*

Boundary lubrication mechanism of fatty acids has been studied on different substrate such as iron-based, aluminum-based and copper-based. Then, depending on the working environment, different oxide layers can cover the substrate and lead to various adsorption mechanisms. Different examples are developed in the following.

Adsorption mechanism of stearic acid SAMs on different aluminum oxide has been studied [22, 33]. Several interactions between the carboxylic acid head group and the aluminum oxide surfaces can occur as shown in figure 11. X-ray Photoelectron Spectroscopy (XPS) can confirm the presence of aliphatic and carboxylic carbons but is not sensitive enough to reveal the type of chemisorption (symmetric, asymmetric or formation of carboxylate). But Infra-Red spectroscopy (IR) can distinguish the different type of adsorption such as monodentate binding mode (figure 11 A) or bidentate binding mode (figure 11 D). Finally on alumina surface, binding modes are a mixture of A, B, C and D represented in figure 9 whereas with single crystalline sapphire, a single adsorption type that is bidentate bonding mode of carboxylate occurs [33]. It is difficult to quantify the proportion of each different binding mode. The differences can be related to binding geometry or strength, to the number of adsorption site that can provide different degree of affinity among other factors. This study clearly shows the importance of combining at least two techniques to understand the adsorption mechanism.

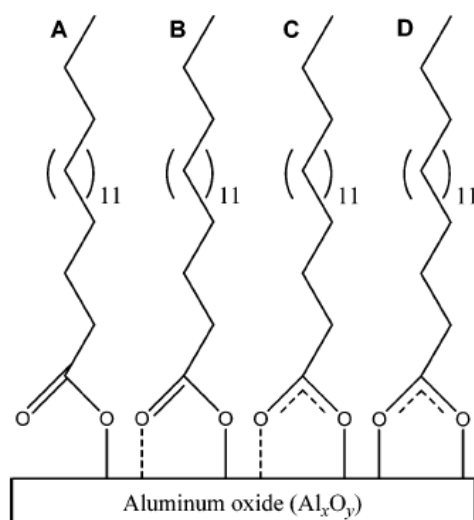


FIGURE 11: POSSIBLE INTERACTIONS BETWEEN THE CARBOXYLIC ACID HEAD GROUP AND THE SURFACES (EXAMPLE OF ALUMINUM OXIDE), A: MONODENTATE BINDING MODE B AND C: ASYMMETRIC DOUBLET, WEAKENING OF THE CARBOXYLATE DOUBLE BOND, TWO DIFFERENT BINDING MODES, D: BIDENTATE BINDING MODE OF CARBOXYLATE GROUP [33].

Concerning polycrystalline copper surfaces, one LB monolayer of stearic acid could bond to the surface both symmetrically and asymmetrically through the acid group with a tilt angle from 39° to 49° [34]. The role of the copper oxide layer on the boundary lubrication properties of fatty acids has been studied by electrochemical and surface analysis techniques [35]. A minimum oxide thickness of 4 nm is needed to have chemical reaction between fatty acid and Cu<sub>2</sub>O.



On steel surfaces, some investigations have also been done but it is difficult to compare all results because information concerning the type of iron oxide layers is sometimes missing. Nevertheless, different adsorption mechanisms have been found for fatty acid on iron oxide surface. XPS study <sup>[36]</sup> shows the adsorption of a 20 Å monolayer of stearic acid in which the presence of COOH peak suggests that the adsorption mechanism is either physisorption or symmetric/asymmetric chemisorption. On the other hand, analyzes of the wear track obtained after a tribotest with a solution of hexadecane containing fatty acids show that the acids are covalently bound to the surface under carboxylate forms in a bidentate manner <sup>[37]</sup>. This result is nuanced by Kalin <sup>[32]</sup> which suggest that the formation of carboxylate is favored by friction but both in a monodentate and bidentate manner on steel surface. Recently, it was shown that a textured steel surface obtained by piranha solution etching and then covered by stearic acid film gives very good friction-reducing performances <sup>[38]</sup>. The roughness and the nature of the oxide layers are therefore key factors concerning the boundary lubrication behavior of C18 fatty acids.

In different metal substrate types which include steel, silver, aluminum, copper based surfaces, defects are important to consider as they enable different adsorption sites and lead to different density of fatty acids monolayer. In addition, the adsorption mechanism is controlled by the presence of oxygen and/or water that will define the oxide layer.

#### *Effect of humidity*

It has been pointed out that moisture has a very pronounced effect on metallic compounds formation rate <sup>[39]</sup>. In fact, Ratoi *et al.* <sup>[40]</sup> have used ultrathin film interferometry to measure the boundary film-forming behavior of long chain carboxylic acid oiliness additives. They have shown that under dry conditions, these acids form very thin film of 2-3 nm thick which corresponds to one monolayer, while in presence of water, some acids form significantly thicker films (up to 10 nm). Another study has shown that under dry air, hydrocarbons, fatty acids and their mixture lead only to physisorption <sup>[39]</sup>. It has been shown that oxygen and reactive metal are needed to have effective lubrication in boundary regime as they induce the formation of a strongly adsorbed surface film of polar molecules <sup>[35, 39, 40]</sup>.

#### *Effect of unsaturation and density*

Organic friction modifiers and more precisely C18 fatty acids can be saturated like stearic acid, or unsaturated, e.g., which contain one or more double carbon bonds, like oleic and linoleic acid.

Some work has been done on the adsorption of saturated fatty acids on steel surfaces. It has been shown that the chemisorbed amount of matter on the surface is not influenced by the saturated or unsaturated alkyl chain of the fatty acids but is only dependent on the interactions between the head group of fatty acids and the substrate. Nevertheless, physisorbed amount (layers above the chemisorbed layer) increases with the number of unsaturation in fatty acids <sup>[41]</sup>. It has been shown that friction increases with increasing the unsaturation degree of fatty acid <sup>[42, 43]</sup>. This is related to steric effect that inhibits the formation of a close-packed monolayer.

The difference in the formation of the boundary film structures has different response to sliding speed and temperature effects. Stearic acid friction coefficient increases from 0.04 to 0.07 with increasing the sliding speed from  $1 \cdot 10^{-7}$  m/s to  $1 \cdot 10^{-2}$  m/s whereas oleic acid friction coefficient remains constant and equal to about 0.11 <sup>[44]</sup>. Moreover, friction of saturated fatty acids decreases with increasing the temperature from 35 °C to 100 °C (from 0.06 to 0.04 for



stearic acid 0.01M blended in hexadecane at a sliding speed of  $1.10^{-5}$  m/s as an example) whereas no effect is observed for unsaturated fatty acids [44, 45].

Quartz Crystal Microbalance (QCM) study was performed to investigate the adsorption of stearic and oleic solutions on steel surface [41]. It allows studying the adsorbed mass and the film thickness of fatty acid onto a substrate. QCM is sensitive to nanogram quantities of the adsorbed material [46, 47]. The use of QCM has confirmed that saturated fatty acid can form close-packed monolayers where unsaturated fatty acids cannot. In fact, depending on the orientation of the molecule, it requires a surface area as summarized in table 2 [48]. The area per molecule increases with increasing unsaturation, which is due to steric effect induced by the double bond.

TABLE 2: THE SURFACE AREA NEEDED FOR DIFFERENT ARRANGEMENTS AT THE SURFACE AS ESTIMATED WITH MOLECULAR MODELS [48]

	Perpendicular arrangement at the surface ( $\text{\AA}^2$ )	Parallel arrangement at the surface ( $\text{\AA}^2$ )
Stearic acid	20	110
Oleic acid	25	130
Linoleic acid	25	143

Finally, the friction increases when the degree of unsaturation increases. It is suggested that the reason of this result is that the layer is less well ordered with unsaturated molecules which increase entanglement between the molecules in the opposing layers [49].

### *Effect of the chain length*

Another important parameter is the chain length of the fatty acid. When chain length of carboxylic acid increases, it has been shown that a closer molecules packing is found with a stronger adsorbed film and with higher lateral cohesive forces. This exhibits lower friction coefficient [50, 51]. Depending on the deposition technique and the friction conditions, the friction coefficient can linearly decrease when chain length of fatty acids increases. When a certain number of carbon atoms in the molecule is reached (around 10 to 14 carbons) the friction coefficient remains constant as shown in figure 12.

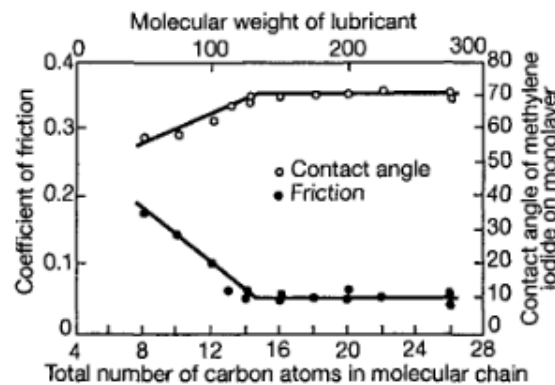


FIGURE 12: EFFECT OF CHAIN LENGTH ON THE EFFECTIVENESS OF A BOUNDARY LUBRICANT. FRICTION COEFFICIENT AS A FUNCTION OF CHAIN LENGTH [51]

Nevertheless, the solvent in which the fatty acids are blended has an impact on the effect of the alkyl chain length toward friction coefficient. In some solvents, the friction

decreases linearly with increasing the chain length whereas in some other solvents, the behavior is as mentioned above in figure 13 [18].

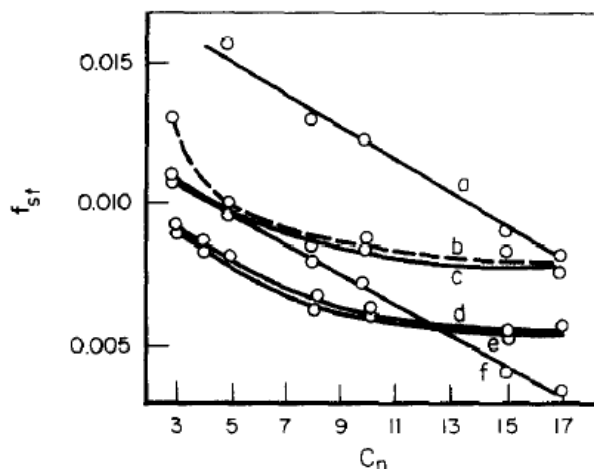


FIGURE 13: STATIC COEFFICIENT OF FRICTION AS A FUNCTION OF FATTY ACID CHAIN LENGTH: A) NORMAL STRESS (NS) 22 KG/CM<sup>2</sup> 0.05% FATTY ACID IN BENZENE, B) NS 22 KG/CM<sup>2</sup> 0.1% FATTY ACID IN PPF, C) NS 14 KG/CM<sup>2</sup> 0.1% FATTY ACID IN PPF, D) NS 4 KG/CM<sup>2</sup> 0.1% FATTY ACID IN PPF, E) NS 6 KG/CM<sup>2</sup> 0.1% FATTY ACID IN PPF, F) NS 4 KG/CM<sup>2</sup> 0.1% FATTY ACID IN ISO-OCTANE [18]

### *Effect of film thickness*

Depending on the experimental procedure [16], it has been reported that it is possible to form only one monolayer of fatty acid or a thick film that can reach a thickness of 15 nm. Bowden and Tabor have studied the effect of the number of stearic acid layers on stainless steel surfaces. They have compared the results to the unlubricated case. As shown in figure 14, the lubrication effectiveness increases with increasing the number of films [52].

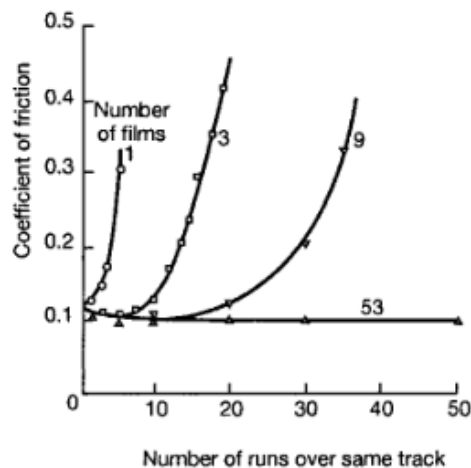


FIGURE 14: EFFECT OF THE NUMBER OF FATTY ACIDS LAYERS ON FRICTION FOR LANGMUIR-BLODGETT FILMS [52]

Despite all these experimental studies, the precise nature of the chemical interactions is still a subject of controversy [53]. To overcome these difficulties, theoretical analysis has been done recently to improve the fundamental understanding of organic friction modifiers mechanism on iron oxide surfaces.

## 2.3 Contribution of computational chemistry

### 2.3.1 Limits of experimental approaches

In order to study friction properties of OFM, researchers have access to a variety of experimental tools such as X-Ray Photoelectron Spectroscopy (XPS), Infrared (IR) Spectroscopy, Quartz Crystal Microbalance (QCM), atomic force microscope (AFM) etc. Some of these methods will be explained with more details in chapter 2.

Combining different experimental techniques can enable to have a good understanding of the adsorbed film and on the friction behavior of the system under friction. But, it is very difficult to have information about the formation of the thermal film and to follow *in-vivo* the behavior of those molecules during friction. Then, experimental analyses are expensive to screen potential of new additives. This highlights the fact that it is needed to use computational and theoretical approaches to develop models useful for understanding and controlling tribological processes. In the following, an overview of computational chemistry work related to friction behavior of fatty acids is reported to show the potential of these approaches for the study of tribochemical systems.

### 2.3.2 Adsorption by density functional theory (DFT) calculation

DFT calculation enables to make electronic analysis such as calculation of binding energy, density of state, charge, equilibrium geometry and so on. It is also possible to investigate the vibrational spectroscopy of molecules and compare this calculated spectrum with experimental Infra-Red and Raman spectroscopies [54].

First of all, DFT can be used to study lubricant additives adsorption on substrate. For example, the adsorption of carboxylic acids on Zn-terminated ZnO surface was studied by DFT calculations in which different adsorption pathways are considered and the most stable in terms of energy is the most likely to occur. The most likely mechanism for carboxylic acid on Zn-terminated ZnO (0 0 0 1) surface is dissociative bridging adsorption with the carboxylate group attached to two Zn atoms and the proton is transferred to a neighboring Zn atom in order to form Zn-H bond. The next step is to study the formation of the Self-Assembled Monolayer. DFT calculations can treat only few atoms so the chain length that has been studied by DFT is no longer than 9 carbons. It was shown that there is a transition between perpendicular and tilted orientation on the zinc-based surface for carboxylic acid larger than 5 carbons due to intermolecular van der Waals interactions. The SAM formed has a tilt angle of about 35 ° to the surface [55]. The presence of tilt angle in the organization of SAM has already been observed experimentally [34]. In fact, Ulman shows that the optimized distance between two acid groups in a SAM is between 4.45 and 4.6 Å [56]. If the distance is larger, a tilt of the chains to the surface is needed to optimize lateral interactions between the alkyl chains.

Recently, the trend is to couple experimental studies with computational work. As an example, the adsorption of sodium laurate on ferric (hydr)oxide is measured under different conditions by vibrational spectra and is completed by X-ray photoelectron spectroscopy analysis as well as DFT simulations [57] which help greatly the current understanding of the oxide-carboxylate interactions.

As it was just presented, in case of tribochemical systems, DFT calculations are used to study the adsorption mechanism of additives on metal-based surfaces and can simulate IR spectra of the system. But the simulations are only static. Another computational technique used to study tribological contacts is the molecular dynamic (MD) simulation. This technique gives qualitative information but has advantage to be fast and allow molecules movement. MD simulations have been applied mainly for SAM model of organic friction modifiers.

### 2.3.3 MD simulation on monolayer

Molecular Dynamics (MD) simulations (principle of the technique will be explained in chapter 2) have been applied for a variety of surfactant type molecule/surface systems [58]. Particularly, MD simulations have been applied for stearic acid on gold, silicon or carbon using the self-assembled monolayer (SAM) model [59, 60, 61]. Well organized SAM exhibits lower friction than less densely packed or disordered monolayers which possess some defects and exhibit higher friction [61, 62]. Greenfield and Ohtani [59] have highlighted that in presence of a mixture of friction modifiers in a solvent, there is a possibility of having a mixture of ordered chains lying perpendicular and parallel to the surface at the same time.

Moreover, it has been observed that the SAM tilt angle varied regularly with the sliding direction as well as with frictional stage [60]. These works as well as Mikulski and Harrison's works [59, 63, 64] confirm that Molecular Dynamics simulations can provide unique atomic-scale insights of processes that occur at the sliding interfaces such as the frictional response of SAMs.

In addition to experimental study, the effect of alkyl chain length on friction was also studied by MD simulation of different n-alkanes. It was shown that, as in experimental analyses, longer chains reduce the friction significantly compared to shorter alkyl chain [65].

Other parameters can be treated quantitatively by MD simulation such as atom's velocity, mean square displacement, density distribution, surface coverage, etc.

In the tribochemistry field, it is needed to follow the motion of atoms in addition to electron-electron interactions. Therefore, other techniques have been developed to achieve this objective and consist more or less in a coupling of QC and MD.

### 2.3.4 Other techniques

#### 2.3.4.1 First-principle MD simulation

First principle MD simulations have been developed by Car and Parrinello (CP) in order to treat chemical reactions in addition to the equation of motion [66] and are then used and improved by researchers in the field of tribology. Mosey and Müser [67] are using CP-MD simulations to study anti-wear properties of zinc phosphate materials, which are found in protective films formed in automotive engine in presence of ZnDTP additives. Righi has also used both DFT calculations and *ab initio* MD simulations to elucidate atomistic mechanisms in lubrication [68] for organo-phosphorous and sulphur additives [69]. Finally, combining *ab initio* and classical MD simulations is a powerful tool to study tribological properties of material and additives but this technique is very expensive in term of simulation time and is, therefore, limited to very small systems of few hundreds of atoms.

Table 3 summarizes advantages and disadvantages of classical MD and first principles MD simulations.

TABLE 3: COMPARISON OF CLASSICAL AND FIRST PRINCIPLE MD SIMULATIONS

Classical MD	First Principle MD
- Phenomenological potential	+ Potential energy surface calculated from the Schrödinger equation
+ Atom-atom interactions + motion + velocity	+ Electron-electron interactions + motion + velocity
- Cannot describe bond breaking/making	+ Describe bond breaking/making
- Electronic properties are not available	+ Electronic spectra included in calculation
+ Can do millions of particles with reasonable time	- Limited to few hundreds of atoms with long calculation time

In professor Miyamoto's laboratory, a software which couple QC and MD simulations is developed and, by using some approximations, can treat large complex system at 1 000 000 times faster than the first principle MD simulations. This method will be developed in Chapter 2.

#### 2.3.4.2 Improved MD simulations

Another technique to make the bridge between quantum chemistry and molecular dynamic is the use of reactive potential to simulate reactions between molecules and surface by employing the concept of bond-order. This ensures smooth transition of bond formation and dissociation. MD simulations using reactive force fields (ReaxFF) has been developed by Van Duin and Goddard <sup>[70]</sup>. It is an empirical approach which derives its parameters from QC calculations and can be run at a larger time scale (ns) and larger number of atoms (1 000 – 1 000 000 atoms) than first-principle MD. Applications using ReaxFF for studying reactive processes have been reported for many systems including tribology of additives on diamond-like carbon (DLC) coating <sup>[71]</sup>.

In the same way, Moseler's group have developed bond order potentials (BOP) such as Brenner BOP <sup>[72]</sup>, Coulson BOP <sup>[73]</sup> and other BOP <sup>[74]</sup> to study the atomic scale process that cause the wear of solid films, e.g. metallic tribosystem and covalent materials.

Computational work is becoming sources of practical tools that are more and more adopted by both physicists and chemists in order to explore the atomic or molecular nature of tribological events.

### 3. Conclusion

Fatty acids adsorption on steel surfaces and their friction behavior have been studied for decades. The effect of various parameters such as the impact of surface nature, the number of unsaturation in alkyl chains on both adsorption and friction has also been investigated. Some questions still remain and need further investigations:

- Concerning the effect of surface nature, it has been understood that different surface compositions lead to different adsorption mechanisms (physisorption or chemisorption). It will be interesting to deeply investigate the exact nature of the surface in a real contact and to study its impact on adsorption of fatty acids and then on friction behavior.

- In addition, it was reported in litterature that carboxylate functions are found after adsorption of fatty acids on steel and after friction. But it was not well proved if the carboxylate function is created during the formation of the thermal film or is only induced by friction.

- Moreover, increasing number of unsaturations in the fatty acid has no impact on the adsorption mechanism (physisorption and chemisorption) but it induces an increase of the friction coefficient. It is said that it is due to steric effect but the organization of the different films has not been investigated in details. It will be interesting to study the organization of the thermal film during adsorption and during friction processes.

Then, to investigate deeply the adsorption mechanism and the friction behavior of fatty acids on iron based surfaces, different experimental techniques are available. But, coupling different techniques is expensive and the *in vivo* information is poor. In fact, it is difficult to measure experimentally the atomistic processes involved during friction. To overcome this difficulty, the use of computational chemistry can be useful. QC such as DFT has been widely used for understanding the mechanism of chemical reactions but is limited to small systems. On the other hand, MD simulation can work with large systems but the mechanism is studied

qualitatively. This is why new computational techniques are developed and consist in coupling QC calculations with MD simulations. In this work, we propose to revisit the adsorption mechanism of some fatty acids and their tribological behaviors on some iron-based surfaces by coupling experimental analysis and computational chemistry.

## 4. References

- [1] Hutchings I M, Tribology friction and wear of engineering materials, *London: Elsevier Butterworth Heinemann Ltd*, **1992**
- [2] Woydt M, Wäsch R, The history of the Stribeck curve and ball bearing steels: the role of Adolf Martens, *Wear* 268 (**2010**) 1542-1546
- [3] Zhu D, Wang Q J, Elastohydrodynamic lubrication: a gateway to interfacial mechanics – review and prospect, *Journal of Tribology* 133 4 (**2011**)
- [4] Spikes H A, Mixed lubrication – an overview, *Lubrication Science* 9 3 (**1997**) 221-253
- [5] Spikes H A, Boundary lubrication and boundary films, *Tribology Series* 25 (**1993**) 331-346
- [6] Erdemir A, Donnet C, Tribology of diamond-like carbon films: recent progress and future prospects, *Journal of Applied Physics* 39 (**2006**) 311-327
- [7] Ayel J, Lubrifiants: constitution, *Technique de l'ingénieur* bm5341 **2003**
- [8] Ayel J, Lubrifiants : additifs à action chimique, *Technique de l'ingénieur* bm5343 **2003**
- [9] Ayel J, Lubrifiants : additifs à action physique ou physiologique, *Technique de l'ingénieur* bm5344 **2003**
- [10] Ahmed S A, Nassar A M, Tribology – Lubricant and lubrications, Chapter 10: Lubricating oil additives, *INTECH*, **2011**
- [11] Martin J M, Antiwear mechanisms of zinc dithiophosphate: a chemical hardness approach, *Tribology Letters*, 6 (**1999**) 1-8
- [12] De Barros Bouchet M I et al, Mechanism of MoS<sub>2</sub> formation by MoDTC in presence of ZnDTP: effect of oxidative degradation, *Wear* 258 (**2005**) 1643-1650
- [13] <http://eurlex.europa.eu/LexUriServ/LexUriServ.do?uri=OJ:L:2007:171:0001:01:FR:PDF>  
Official Journal L171/12, 24.6.2011
- [14] Mortier R M, Fox M F, Orszulik S T, Chemistry and technology of lubricants, part III, *3rd edition Springer*, **2010**
- [15] Lahouij I, Mécanisme de lubrification des nanoparticules à structure Fullerène. Approche multi-échelle, *Thèse LTDS*, **2012**
- [16] Anghel V, Cann P M, Spikes H A, Direct measurement of boundary lubricating films, *Tribology Series* 32 (**1996**) 459-466.
- [17] Bowden F P, Tabor D, The Friction and Lubrication of Solids, *Oxford Classic Texts in the Physical Science*, Chapter X, **2001**.
- [18] Allen C M, Drauglis E, Boundary layer lubrication: monolayer or multilayer, *Wear* 1 4 (**1969**) 363-384.
- [19] Russel J A, Campbell W E, Burton R A, Ku P M, Boundary lubrication behavior of organic films at low temperature, *ASLE Transactions* 8 (**1965**) 48-58
- [20] Stachowiak G W, Batchelor A W, Engineering Tribology, 3<sup>rd</sup> edition, *Elsevier*, Chapter VIII, **2005**.

- [21] Schwartz D K, Mechanisms and kinetics of self-assembled monolayer formation, *Annual Review of Physical Chemistry*, 52 (2001) 107-137.
- [22] Ulman A, Formation and structure of self-assembled monolayer, *Chemistry Review*. 96 4 (1996).
- [23] Hussain S A, Langmuir-Blodgett films: a unique tool for molecular electronics, *Langmuir-Blodgett films*, GRIN edition, 2010.
- [24] Petty M C, Langmuir-Blodgett films: an introduction, Chapter II, *Cambridge university press*, 1996.
- [25] Tabor D, Gases, liquids and solids and other states of matter, Chapter 12 The colloidal state of matter, 3<sup>rd</sup> edition, Cambridge (1991).
- [26] Buckley D H, Surface effects in adhesion, friction, wear and lubrication, *Tribology Series* 5, 1981.
- [27] Ku P M, Interdisciplinary approach to the lubrication of concentrated contacts, *NASA* (1970).
- [28] Przedlacki M and Kajdas C, Tribochemistry of fluorinated fluids hydroxyl groups on steel and aluminum surfaces, *Tribology Transactions*, 49 (2006) 202-214.
- [29] Crowel J E, Chen J G, Yates Jr J T, A vibrational study of the adsorption and decomposition of formic acid and surface formate on Al(111), *Journal Chemical Physics* 85 (1986) 3111-3122.
- [30] Kajdas C, Importance of the triboemission process for tribochemical reaction, *Tribology International* 38 (2005) 337-353.
- [31] Majzner M, Kajdas C, Reactions of carboxylic acids under boundary friction conditions, *Tribologia* 34 (2003) 63-80.
- [32] Simić R, Kalin M, Adsorption mechanisms for fatty acids on DLC and steel studied by AFM and tribological experiments, *Applied Surface Science* 283 (2013) 460-470.
- [33] Lim M S et al., Adsorption and desorption of stearic self-assembled monolayers on aluminum oxide, *Langmuir* 23 (2007) 2444-2452.
- [34] Fischer D A, Hu Z S, Hsu S M, Molecular orientation and bonding of monolayer stearic acid on a copper surface prepared in air, *Tribology Letters* 3 (1997) 41-45.
- [35] Yea Yang Su, Electrochemical study of the interaction between fatty acid and oxidized copper, *Tribology International* 30 (1997) 423-428.
- [36] Johansson E, Nyborg L, XPS study of carboxylic acid layers on oxidezed metals with reference to particulate materials, *Surface Interface Analysis*, 35 (2003) 375-381.
- [37] Sahoo R R, Biswas S K, Frictional response of fatty acids on steel, *Journal of Colloid and Interface Science*, 333 (2009) 707-718.
- [38] Dong Z, Wan Y, Yang S, Zhang J, Enhanced friction-reducing behavior of stearic acid film on textured steel, *Tribology Letters* DOI 10.1007/s11249-013-0124-z (2013).
- [39] Russel J A, Campbell W E, Burton R A, Ku P M, Boundary lubrication behavior of organic films at low temperature, *ASLE Transactions* 8 (1965) 48-58



- [40] Ratoi M, Anghel V, Bonvington C, Spikes H A, Mechanism of oiliness additives, *Tribology International* 33 (2000) 241-247.
- [41] Lundgren S M et al., Unsaturated fatty acids in alkane solution: adsorption to steel surfaces, *Langmuir* 23 (2007) 10598-10602.
- [42] Lundgren S M, Ruths M, Danerlöv K, Persson K, Effects of unsaturation on film structure and friction of fatty acids in a model, *Journal of Colloid Interface Science* 326 (2008) 530-536.
- [43] Ruths M, Lungdren S, Danerlov K, Persson K, Friction of fatty acids in nanometer- sized contacts of different adhesive strength, *Langmuir* 24 (2008) 1509-1516.
- [44] Campen S et al., On the increase in boundary friction with sliding speed, *Tribology Letters*, DOI 10.1007/s11249-012-0019-4 (2012).
- [45] Briscoe B J; Evans D C B, The shear properties of Langmuir-Blodgett layers, *Proceeding of the Royal Society London A* 380 (1982) 389-407.
- [46] Lundgren S M, Persson K, Kronberg B, Claesson P M, Adsorption of fatty acids from alkane solution studied with quartz crystal microbalance, *Tribology Letters* 22 (2006) 15-20.
- [47] Evans K O, Biresaw G, Quartz crystal microbalance investigation of the structure of adsorbed soybean oil and methyl oleate onto steel surface, *Thin solid film* 519 (2010) 900-905.
- [48] Wheeler D H, Potente D, Wittcoff H, Adsorption of dimer, trimer, stearic, oleic, linoleic, nonanoic and azelaic acids on ferric oxide, *Journal American Oil Chemistry Society* 48(1971) 125.
- [49] Lungdren S M, Unsaturated fatty acids in alkane solution: adsorption and tribological properties, *PhD Thesis* 2008.
- [50] Jahnamir S et al., Chain length effects in boundary lubrication, *Wear* 102 (1985) 331-349.
- [51] Zisman W A, Durability and wettability properties of monomolecular films on solids, Friction and Wear, *Elsevier* (1959) 110-148.
- [52] Bowden F P, Tabor D, The Friction and Lubrication of Solids, Part I, *Oxford Clarendon Press*, 1950.
- [53] Hsu S M, Zhang J, Yin Z F, The nature and origin of tribochemistry, *Tribology Letters* 13 (2002) 131-139.
- [54] Mishra S, Chaturvedi D, Kumar N, Tandon P, Siesler H W, An ab initio DFT study of structure and vibrational spectra of  $\gamma$  form of Oleic acid: comparison to experimental data, *Chemistry and Physics of Lipids* 163 (2010) 207-217.
- [55] Islam M M, Diawara B, Marcus P, Costa D, Synergy between iono-covalent bonds and van der Waals interactions in SAMs formation: a first principles study of adsorption of carboxylic acids on the Zn-ZnO(0 0 0 1) surface, *Catalysis Today* 177 (2011) 39-49.
- [56] Ulman A, Formation and structure of self-assembled monolayer, *Chemical Review* 96 (1996) 1533.
- [57] Chernyshova I V, Ponnurangam S, Somasundaran P, Adsorption of fatty acids on iron hydroxides from aqueous solutions, *Langmuir* 27 (2011) 10007-10018.

- [58] Greenfield M L, Ohtani H, Molecular dynamics simulation study of model friction modifier additives confined between two surfaces, *Tribology Letters* 7 (1999) 137-145.
- [59] Mikulski P T, Van Workum K, Chateauneuf G M, Gao G, David Schall J, Harrison J A, The effects of interface structure and polymerization on the friction of model self-assembled monolayers, *Tribology Letters* 42 (2011) 37-49.
- [60] Wu C D, Lin J F, Fang T H, Molecular dynamic simulation and characterization of self-assembled monolayer under sliding friction, *Computational Materials Science* 39 (2007) 808-816.
- [61] Cheng H, Hu Y, Influence of chain ordering frictional properties of self-assembled monolayers (SAMs) in nano-lubrication, *Advances in Colloid and Interface Sci.*, 171- 172 (2012) 53-65.
- [62] Davidson J E, Hinchley S L, Harris S G, Parkin A, Parsons S, Tasker P A, Molecular dynamics simulations to aid the rational design of organic friction modifiers, *Journal of Molecular Graphics and Modelling* 25 (2006) 495-506.
- [63] Harrison J A, Gao G, Schall J D, Knippenberg M T, Mikulski P T, *Friction between solids, Philosophy Transaction Royal Society A*, 366 (2008) 1469-1495.
- [64] Harrison J A, Schall J D, Knippenberg M T, Gao G, Mikulski P T, Elucidating atomic-scale friction using molecular dynamics and specialized analysis techniques, *Journal of Physics: Condensed Matter*, 20 (2008) 354009.
- [65] Zheng X, Zhu H, Kosasih B, Tieu A K, A molecular dynamics simulation of boundary lubrication: the effect of n-alkanes chain length and normal load, *Wear* 301 (2013) 62-69.
- [66] Car R, Parrinello M, Unified approach for molecular dynamics and DFT, *Physical Review Letters* 55 (1985) 2471.
- [67] Mosey N J, Muser M H, Woo T K, Molecular mechanisms for the functionality of lubricant additives, *Science* 307 (2005) 1612-1615.
- [68] Righi MC, Combined ab initio and classical molecular dynamics simulations of the tribological properties of rare gas monolayer sliding on metal surface, *APS vol 53 n° 2* (2008).
- [69] Righi MC et al, Ab initio investigation of atomistic mechanism in solid and boundary lubrication, *TriboLyon* 2013
- [70] Van Duin A C T, Dasgupta S, Lorant F, Goddard III W A, ReaxFF: a reactive force field for hydrocarbons, *Journal Physical Chemistry A* 105 (2001) 9396-9409
- [71] Goddard III W A, Structure and tribology of diamond-like carbon from first principles theory and simulation comparison to experiment, *Frontiers in Boundary Lubricating Films* 2005.
- [72] Pastewka L, Pou P, Pérez R, Gumbsch P, Moseler M, Describing bond-breaking processes by reactive potentials: importance of an environment dependent interaction range, *Physical Review B* 78 (2008)
- [73] Pastewka L, Mrover M, Moseler M, Gumbsch P, Bond order potentials for fracture, wear and plasticity, *MRS Bulletin* 37 (2012) 493-503

- [74] Pastewka L, Klemenz A, Gumbsch P, Moseler M, Screened empirical bond-order potentials for Si-C, *Physical Review B Condensed Matter and Materials Physics* 87 (**2013**)

## 5. Summary chapter 1

Respecting new environmental restrictions and improving thermal engine performances represent a real challenge in the development of new lubricant. In fact, the progressive reduction of product containing sulfur and phosphorous compounds leads to reformulate engine oil. To complete this objective, we have decided to revisit the adsorption mechanisms and the tribological behavior of fatty acids which are organic friction modifiers and which are representing a good alternative to actual friction modifiers.

After a summary on the evolution of lubricant for thermal engine, a state of the art over the last decades on action mechanisms of C18 fatty acids is presented. Different adsorption mechanisms through the acid group on iron-based surfaces are listed. Both physisorption and chemisorption of molecules on substrates are possible, which can be classified as symmetric, asymmetric, mono-dentate, bi-dentate or bridging depending on the nature of the surface and the applied tribological constraints. The influence of several parameters on the formation of the Self-Assembled Monolayer (SAM) and their behavior under tribological conditions are also studied. Nevertheless, some points need clarifications. For example, it has been shown that increasing the unsaturation degree increased the friction. This behavior seems not to be caused by adsorption mechanism but to be due to steric effects induced by double carbon-carbon bonds which inhibit the formation of a well-arranged monolayer. It would be interesting to check this behavior by studying different unsaturation degrees but also different film densities. Then, those additives are efficient until a critical temperature where the good tribological behaviors of fatty acids are lost. It will be interesting to check their efficiency over the temperature range that reaches the lubricant in the distribution area of the thermal engine, e.g. from 50 °C to 150 °C. The formation of carboxylate function with the dissociation of the hydroxyl group's hydrogen has been proposed on the literature. A particular attention will be paid on this chemical reaction which seems to be favored by mechanical constraints.

Finally, a state of the art on different molecular simulation techniques used to deal with tribological issues is presented. Three techniques are identified as being interesting: Quantum Chemistry, Molecular Dynamic and the coupling of the two methods. In fact, quantum chemistry calculations are widely used to understand chemical reactions but the technique is limited to small system and static studies. On the other hand, molecular dynamics simulations enable to study the motion of atoms with much bigger system than with quantum chemistry method but the chemical reaction study is remained qualitative. This is why the coupling of the two methods represents a powerful tool to study the formation of adsorbed layer and its behavior under severe conditions.

Therefore, it is propose in this thesis to revisit adsorption mechanisms and tribological behavior of fatty acids on iron-based surfaces by coupling two different approaches: experimental approach and molecular simulation approach.

## 5. Résumé chapitre 1

Respecter les nouvelles contraintes environnementales et améliorer les performances des moteurs thermiques représentent un vrai challenge dans le développement de nouveaux lubrifiants. En effet, la réduction progressive des produits soufrés et phosphorés amène à revoir la formulation des huiles pour moteur. C'est dans cette optique que nous avons décidé de revisiter les mécanismes d'adsorption et le comportement tribologique des acides gras, modificateurs de frottement organiques, représentant une alternative attractive aux modificateurs de frottement inorganiques utilisés actuellement.

Après un rappel concernant le contexte d'évolution des lubrifiants pour moteurs thermiques, une étude bibliographique synthétisant les mécanismes d'action des acides gras C18 étudiés durant des décennies est présentée. Les différents mécanismes d'adsorption par la fonction acide sur les surfaces métalliques sont répertoriés. On note les possibilités de physisorption ou de chimisorption des molécules sur les surfaces, pouvant être symétrique, asymétrique, mono-dentate, bi-dentate ou pontée en fonction de la nature de la surface et des contraintes tribologiques appliquées. L'influence de différents paramètres sur la formation de couches auto-assemblée (Self-Assembled-Monolayer) et sur leur comportement en frottement a également été étudiée. Certains points restent à clarifier. Par exemple, il a été montré qu'augmenter le degré d'insaturation des acides gras augmentait le frottement. Ceci ne serait non pas dû au mécanisme d'adsorption mais à l'organisation du film rendu difficile à cause des gênes stériques engendrées par les doubles liaisons carbone-carbone. Il serait donc intéressant de vérifier ce phénomène en jouant sur le degré d'insaturation mais également sur la densité des films adsorbés. Ensuite, ces additifs sont efficaces jusqu'à une température critique où les propriétés tribologiques des acides gras sont perdues. Il serait intéressant de vérifier leur efficacité dans la gamme de température qu'atteint une huile au niveau de la distribution dans le moteur thermique, c'est-à-dire entre 50 °C et 150 °C environ. La formation de carboxylates pendant le frottement, par dissociation de l'hydrogène du groupement hydroxyle de la fonction acide, a été proposée dans la littérature. Une attention particulière sera portée sur cette réaction chimique *a priori* favorisée par l'apport de contraintes mécaniques.

Enfin, un état des lieux des différentes techniques utilisées en modélisation moléculaire pour aborder un problème de frottement est présenté. Trois techniques sont identifiées comme intéressantes : la Chimie Quantique, la Dynamique Moléculaire et le couplage des deux méthodes. En effet, la Chimie Quantique est largement utilisée pour comprendre les mécanismes réactionnels mais reste limitée à des petits systèmes et à une étude statique. En revanche, la Dynamique Moléculaire permet comme son nom l'indique, d'avoir de la « dynamique », de travailler sur des systèmes plus grands qu'en chimie quantique mais l'étude des mécanismes réactionnels reste qualitative. C'est pourquoi le couplage des deux méthodes représente un outil intéressant pour étudier la formation des films thermiques et de leur comportement lorsqu'ils sont soumis à des contraintes tribologiques.

Il est donc proposé dans cette thèse de revisiter les mécanismes d'adsorption et le comportement tribologique des acides gras sur des surfaces à base d'acier, en couplant deux types d'approches méthodologiques : une approche expérimentale et une autre numérique.



# **Chapter 2: Materials and methods**

---

# **Chapitre 2: Matériaux et méthodes**

## Chapter 2: Materials and methods

---

### Table of contents

1. Introduction .....	52
2. Computational techniques .....	53
2.1 Construction of OFMs, substrates and base oil .....	53
2.2 Molecular Dynamics simulations.....	55
2.3 Quantum Chemistry method .....	64
2.4 Ultra Accelerated Quantum Chemistry Molecular Dynamics (UA-QCMD) simulation .....	68
2.5. Summary .....	70
3. Experimental techniques .....	70
3.1 Materials.....	70
3.2 Experimental characterization techniques .....	70
3.3 Friction behavior measurements .....	76
3.4 Summary .....	77
4. Conclusion.....	77
5. References.....	79
6. Summary chapter 2.....	82

### 1. Introduction

Rapid advances in computer technology open many opportunities in materials science research. Even if the development of experimental techniques has enabled to obtain highly accurate information on materials, details in the atomistic and electronic level have to be investigated. The computational chemistry combines all numerical methods based on quantum chemistry (QC), molecular dynamics (MD), Monte Carlo (MC) as well as molecular mechanics (MM) in order to predict the structure and electronic properties of materials <sup>[1-2]</sup> in different time and size scales as shown in figure 1. Computer simulation is a powerful and modern tool to solve scientific problems as it can be performed on new materials without synthesizing them.

The main aim for using computer simulation is to reproduce experiment for explaining nanoscopic details. This work is dedicated to perform simultaneously computer simulation and experimental analyses in order to understand the adsorption mechanism of OFM on iron based surfaces and their tribological behavior.

In this chapter, both computational and experimental techniques are described. Numerically, MD simulations as well as Density Functional Theory (DFT), Tight-Binding QC (TB-QC) and combination of MD and TB-QC are applied. Experimentally, characterization of materials by X-ray Photoelectron Spectroscopy (XPS) and Polarization-Modulation-Infra Red



Reflection Absorption Spectroscopy (PM-IRRAS) analyses are performed and the tribological behavior of OFMs is investigated by friction tests.

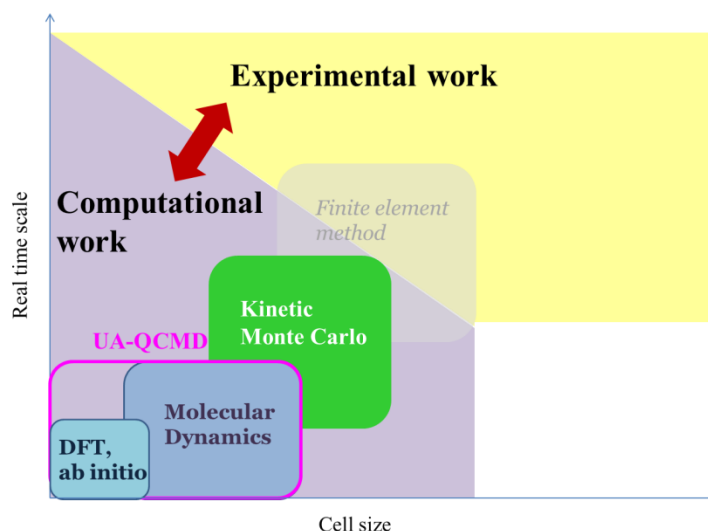


FIGURE 1: DIFFERENT SIMULATION TECHNIQUES AS A FUNCTION OF CELL SIZE AND REAL TIME SCALE

## 2. Computational techniques

In this part, different computational techniques are described. First the different models should be designed by varying different parameters depending on the purpose: cell size, positions of molecules, type of substrates, etc. Then, MD simulations as well as DFT calculations, TB-QC and Ultra-Accelerated QCMD are applied in order to evaluate the friction coefficient, the adsorption mechanism, the diffusion coefficient, the organization of molecules etc.

### 2.1 Construction of OFMs, substrates and base oil

All models are designed with Material Studio® V6. Figure 2 shows the three selected C18 fatty acids molecules models for the study: stearic acid ( $C_{18}H_{36}O_2$ ) which is a saturated molecule, cis-9-oleic acid ( $C_{18}H_{34}O_2$ ), cis-9-cis-12-linoleic acid ( $C_{18}H_{32}O_2$ ) which are both unsaturated molecules. The PAO 4 ( $C_{24}H_{50}$ ) molecule model is built on the basis of Total's information as shown in table 1 and figure 3. The geometry optimization of these molecules is performed with DMol3<sup>[3]</sup> by using the Vosko, Wilk and Nusair as the local density approximation functional<sup>[4]</sup> (see section DFT).

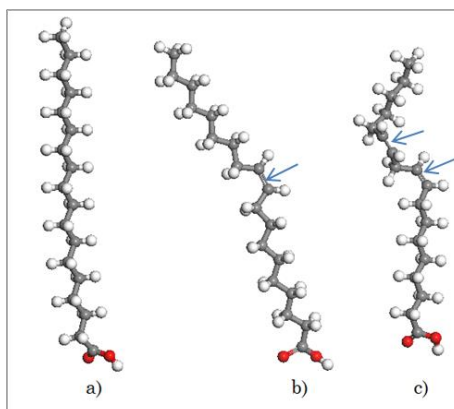
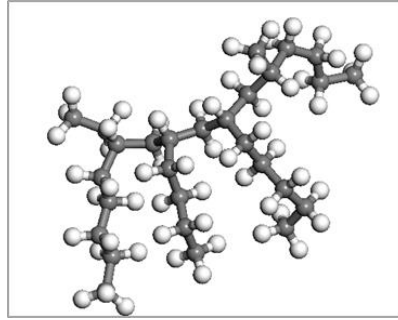


FIGURE 2: MODEL MOLECULES USED IN THE SIMULATION: A) STEARIC ACID ( $C_{18}H_{36}O_2$ ), B) CIS-OLEIC ACID ( $C_{18}H_{34}O_2$ ), C) CIS-CIS-LINOLEIC ACID ( $C_{18}H_{32}O_2$ ), DOUBLE CARBON BONDS ARE INDICATED BY BLUE ARROWS

TABLE 1: SOME PROPERTIES OF PAO 4 MODELS

Properties	PAO 4
Molecular weight (g/mol)	392
Density (g/cm <sup>3</sup> )	0.819
Principal chain number of carbon	10
Number of ramification	4
Ramification length	4 or 5 carbons

FIGURE 3: MODEL MOLECULE USED AS BASE OIL IN THE SIMULATION: PAO 4 (C<sub>24</sub>H<sub>50</sub>)

Depending on the studied environment, the pure iron surface is covered by iron oxides or hydroxides in addition to contaminations (Figure 4). An XPS depth composition profile of a native steel sample has been studied elsewhere [5] and has guided us in the choice of iron-based model surfaces.

Figure 5 shows the three chosen substrates systems that have a size of 23x23x100 Å<sup>3</sup> for pure iron, 27x21x100 Å<sup>3</sup> for iron oxide and hydroxide. The cell size has been chosen in order to have a compromise between a cell big enough to be representative of the system and a cell small enough for reasonable calculation time. Z direction includes vacuum, not only substrate's atoms. The pure iron substrate is composed of 576 atoms, the iron oxide surface Fe<sub>2</sub>O<sub>3</sub> is composed of 560 atoms (336 oxygen atoms and 224 iron ones) and the iron hydroxide FeOOH substrate is composed of 656 atoms (368 oxygen atoms, 64 hydrogen atoms and 224 iron ones). The last surface is called FeOOH by misuse of language: it is actually iron oxide surface Fe<sub>2</sub>O<sub>3</sub> that has been fully covered by hydrogen as shown in figure 5.

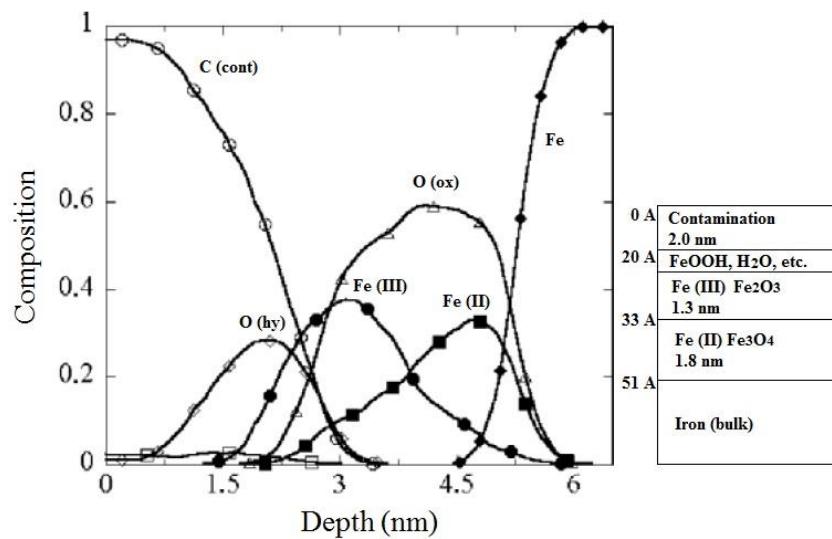


FIGURE 4: IN-DEPTH COMPOSITION PROFILE OF IRON SAMPLE [5]

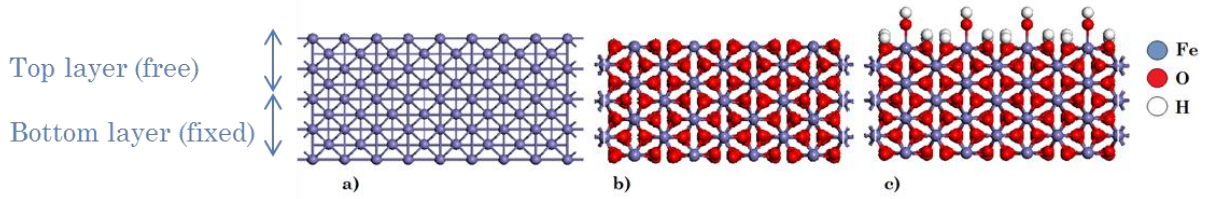


FIGURE 5: SUBSTRATE MODELS SYSTEM: A) FE  $(-1\ 0\ 0)$ , B)  $\text{Fe}_2\text{O}_3$   $(-1\ 1\ 0)$ , C)  $\text{FEOOH}$  ( $\text{Fe}_2\text{O}_3$   $(-1\ 1\ 0)$  TERMINATED BY HYDROGEN)

Each surface is divided into two parts: the first part (bottom) is fixed in order to prevent the movement of the whole system whereas a second substrate is subjected to pressure and shear and the second part (top) is free to move and interact with molecules.

## 2.2 Molecular Dynamics simulation

Molecular dynamics simulation is the most detailed molecular simulation method which computes the motion of atoms and molecules by applying the classical Newton mechanics [2]. It was introduced by Alder and Wainwright in the late fifties' [6, 7] in order to study the interactions of hard spheres. Later, Rahman carried out the first simulation using a realistic potential for liquid argon [8]. The first molecular dynamics simulation of a realistic system was done by Rahman and Stillinger in their simulation of liquid water in 1974 [9]. In the last few years, computer capacity increases widely and, so does the use of MD.

In the present study, in house code (developed in Prof. Miyamoto's laboratory) called "RYUDO" [10] is used to carry out MD simulations. MD simulation is based on the integration of the Newton's equation. It enables the study of atom-atom's interactions and to have access to every atom's position as a function of time. Nevertheless, it does not take into consideration electron-electron interactions and cannot be used to study chemical reactions. The procedure followed by "RYUDO" code is presented in figure 6.

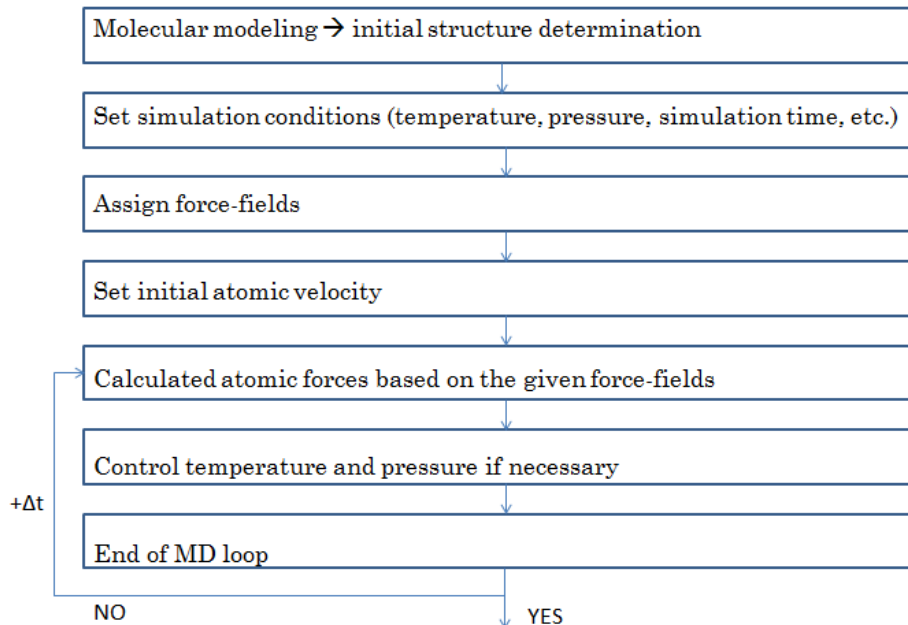


FIGURE 6: PROCEDURE OF MD SIMULATION

When running MD simulations, it is important to choose adequate force-fields potentials for molecules as well as for substrates.

### 2.2.1 Periodic boundary conditions

In simulation, it is difficult and too expensive in terms of calculation time to represent the real number of atoms. Therefore, a simulation box which represents a sample of a real case is created and the periodic boundary condition (PBC) is applied to simulate the bulk material. If 1000 atoms in a 10x10x10 arbitrary unit cube are arranged, nearly half of them are on the outer faces and have an effect on the measured properties. Surrounding this cube with replicates of itself can solve the problem. If an atom leaves the simulation box, its image atom comes simultaneously to replace it through the opposite face as shown in figure 7. In calculating atom interactions with the cutoff range, both real and image neighbors are included.

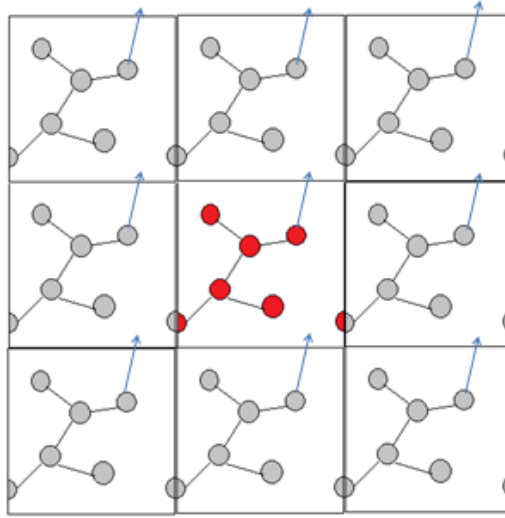


FIGURE 7: PERIODIC BOUNDARY CONDITIONS: WHEN AN ATOM MOVES OUT OF THE SIMULATION BOX, AN IMAGE ATOM MOVES IN TO REPLACE IT.

### 2.2.2 Inter and intra molecular potentials

#### 2.2.2.1 Lennard-Jones potential

The interatomic potential function described by Lennard-Jones type potential is presented (equation 1):

$$E_{ij} = \frac{A_{ij}}{r_{ij}^{12}} - \frac{B_{ij}}{r_{ij}^6} \quad (1)$$

where  $A_{ij} = (A_i A_j)^{1/2}$ ,  $B_{ij} = (B_i B_j)^{1/2}$ ,  $r_{ij}$  = distance between atom i and atom j.

Table 2 gathered A and B coefficient for each atom type of our system. The term with the power 6 is the attractive term that is predominant at long distance and is named van der Waals interactions. The term with the power 12 is the repulsive term and is based on the Pauli principle of exclusion.

TABLE 2: COEFFICIENTS A AND B FOR DIFFERENT TYPES OF FORCE FIELD ATOMS USED IN THE STUDY

Force field type	A (kcal.Å <sup>12</sup> /mol)	B (kcal.Å <sup>6</sup> /mol)
<b>Molecules</b>		
COOH, C=	29.7x10 <sup>5</sup>	13.3x10 <sup>2</sup>
CH <sub>2</sub> , CH <sub>3</sub> , CH	17.9x10 <sup>5</sup>	528
OH, O=	27.3x10 <sup>4</sup>	499
H	71.1x10 <sup>2</sup>	32.9
HO	1.0x10 <sup>-8</sup>	1.0x10 <sup>-8</sup>
<b>Substrate</b>		
Fe	11.9x10 <sup>5</sup>	75.9x10 <sup>2</sup>
O	27.3x10 <sup>4</sup>	499

### 2.2.2.3 Morse potential

The function of Morse potential energy between atoms  $i$  and  $j$  is presented by equation 2:

$$E_{ij} = D_{ij}[\exp\{-2\beta_{ij}(r_{ij}-r_0)\} - 2\exp\{-\beta_{ij}(r_{ij}-r_0)\}] \quad (2)$$

Where  $D_{ij}$ = bond energy,  $\beta_{ij}$ = form factor,  $r_0$ = bond length at minimum energy.

The Morse potential can deal with covalent bond or other short-range interactions and is generally used for intra molecular interaction in organic compounds and metallic materials.

TABLE 3: BOND ENERGY AND SHAPE FACTOR FOR DIFFERENT PAIRS USED IN THE STUDY

Force field type i	Force field type j	$D_{ij}$ (kcal/mol)	$\beta_{ij}$ (1/Å)
COOH	OH	100	2.00
COOH	O=	145	2.06
COOH	CH <sub>2</sub>	76	1.93
CH <sub>2</sub>	CH <sub>2</sub>	88	1.915
CH <sub>2</sub>	H	108.6	1.771
CH <sub>2</sub>	CH <sub>3</sub>	88	1.915
CH <sub>2</sub>	C=	108.6	1.771
CH <sub>3</sub>	H	108.6	1.771
C=	H	90.4	2.00
C=	C=	163.6	2.00
OH	HO	104	2.28
Fe	O	76	2.00

### 2.2.2.3 Angle potential

The function of angle potential energy is presented by equation 3:

$$E_{ijk} = H_{\theta}(\theta_{ijk} - \theta_0)^2 \quad (3)$$

Where  $H_{\theta}$ = force constant,  $\theta_{ijk}$ = bending angle and  $\theta_0$ = bending angle at minimum energy.

Angle potential represents equilibrium angle among neighboring three atoms.

### 2.2.2.4 Torsion potential

The function of torsion potential energy is presented by equation 4:

$$E_{ijkl} = H\varphi[1 + \cos(n\varphi_{ijkl} - \varphi_0)] \quad (4)$$

Where  $H_\varphi$  = force constant,  $n$  = order of rotation axis,  $\varphi$  = torsion angle and  $\varphi_0$  = torsion angle at minimum energy.

Torsion potential represents dihedral made by neighboring four atoms.

Figure 8 summarizes the three considered intra molecular interaction with a scheme of possible pair, trio or quadric movement. All forcefields are gathered in annex 1.

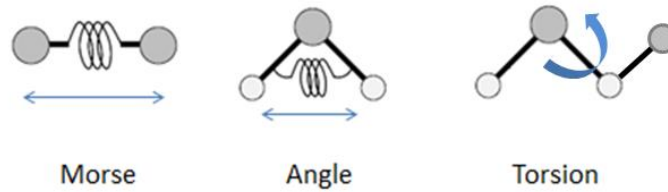


FIGURE 8: INTRA MOLECULAR POTENTIAL FOR PAIR (MORSE), TRIO (ANGLE) AND QUADRIC (TORSION) WITH POSSIBLE MOVEMENT

### 2.2.2.5 Gilbert repulsive term

This term is a short-range repulsion exchange potential. This term is used in order to keep the crystal structure stable. The potential function of Gilbert is defined as equation 5:

$$E_{ij} = f_0(b_i + b_j) \exp[(a_i + a_j - r_{ij}) / (b_i + b_j)] \quad (5)$$

Where  $f_0$  = constant for unit adjustment,  $a$  = size of the surface,  $b$  = stiffness of the surface

This term is used in presence of iron oxide substrate with  $f_0$  of oxygen = 1.520 Å and  $f_0$  of iron = 1.280 Å [11].

### 2.2.2.6 The Ewald method (Coulomb potential)

Long-range Coulombic interaction decreases inversely proportionally to interatomic distance. In the construction of model, the introduction of a cutoff enables to delete interactions after a certain distance which is usually set as half length of the smallest cell edge [12]. In order to take into account long-range Coulombic interactions more precisely, the Ewald method is also used [2, 13]. The Ewald method divides Coulombic energy into two terms: short-range and remaining longer range contributions. The later one is expressed by the arithmetical series in reciprocal lattice space and, therefore, the contributions from far atoms to Coulombic interaction are considered without finite cutoff. The method calculates the energy and force of a charged particle, which acted by atoms in original and image cells (see section 2.2.1). Coulombic energy of an atom  $i$  is computed by the following equation [13]:

$$E_i = E_{1i} + E_{2i} - E_{3i} \quad (6)$$

With:

$$E_{1i} = Z_i e^2 \sum_j Z_j \frac{\text{erfc}(\alpha |r_{ij}|)}{r_{ij}} \quad (7)$$

$$E_{2i} = \frac{Z_i e^2}{\pi V} \sum_j \left[ \exp\left(\frac{-\pi^2 |n'|^2}{\alpha^2}\right) \frac{1}{|n'|^2} \cos(2\pi n' r'_{ij}) \right] \quad (8)$$

$$E_{3i} = \frac{Z_i e^2 \alpha}{\sqrt{\pi}} \quad (9)$$

Where  $Z$ =charge,  $e$ =elementary electric charge,  $r_{ij}$ =position vector of  $i$  to  $j$ ,  $V$ =cell volume,  $\text{erfc}$ =complement of error function,  $n$  and  $n'$ =reciprocal lattice vector,  $\alpha$ =convergence factor.

This method evaluates interactions of a molecule with all other molecules located in the cell and all neighboring cells. It increases considerably the cost of calculation but it is necessary for long range interactions, especially in presence of ionic species.

Charges are initially set up by *cvff* function <sup>[14]</sup> available on Material Studio© software. For each model, TB-QC is first run in order to set up charges to the different force field type of atoms in order to be more accurate than the mean value that is initially set.

### 2.2.2.7 Potential function

The potential function is equal to the sum of all mentioned potentials which consider the van der Waals, ionic and covalent interactions among atoms as shown on equation 10.

$$U = \sum_i \sum_{j>i} \left[ \frac{Z_i Z_j e^2}{r_{ij}} + f_0(b_i + b_j) \exp\left(\frac{a_i + a_j - r_{ij}}{b_i + b_j}\right) + \frac{A_{ij}}{r_{ij}^{12}} - \frac{B_{ij}}{r_{ij}^6} \right] +$$

$$\sum_i \sum_{j>i} D_{ij} \{ \exp[-2\beta_{ij}(r_{ij} - r_0)] - 2 \exp[-\beta_{ij}(r_{ij} - r_0)] \} +$$

$$\sum_\theta H_\theta (\theta - \theta_0)^2 + \sum_\varphi H_\varphi [1 + \cos(n\varphi - \varphi_0)] \quad (10)$$

The force that will be used to solve the equation of motion in the following section is calculated by derivating this potential  $U$ .

### 2.2.3 The Verlet algorithm

In MD method, Verlet integration is a numerical method used to integrate Newton's equations of motion <sup>[15]</sup>:

$$m_i \frac{d^2 r_i}{dt^2} = F_i \quad (11)$$

The Verlet integration is using the central difference approximation to the second derivative of equation 11  $\left(\frac{dr^2}{dt^2}\right)$  <sup>[15]</sup>. Therefore, the following equation is obtained for position and velocity of atoms  $i$ :

$$r_i(t+\Delta t)=2r_i(t)-r_i(t-\Delta t)+(\Delta t)^2\frac{F_i(t)}{2m_i} \quad (12)$$

$$v_i=\frac{r_i(t+\Delta t)-r_i(t)}{\Delta t} \quad (13)$$

The calculation time is directly linked to the integration time  $\Delta t$ . The larger  $\Delta t$  is, the shorter calculation time is. Meanwhile, integration time should not be too small in comparison with the vibration of the lighter system which is generally hydrogen (O-H). When hydrogen is present in the system, which is the case in our study, the chosen integration time is  $10^{-15}$  seconds. Actually, for stable calculation, it is necessary to choose the time step approximately less than one-tenth of the vibration period. Initially, position and velocity are defined. Position of atoms is set up by the model designed with Material Studio©. Velocity is set up in order to respect the Boltzmann distribution. At each step, position and velocity are updated until the end of the simulation.

#### 2.2.4 Control of system temperature and pressure

The system temperature appears by kinetic energy of atoms which build molecules or substrates. Temperature rises with increasing kinetic energy and drops with decreasing kinetic energy. The relationship between atomic velocity and temperature is expressed by the following equation:

$$\frac{1}{2}\sum_{i=1}^N m_i v_i^2 = \frac{3}{2} N k_b T \quad (14)$$

Where  $N$ = total number of atoms in the particle system,  $k_b$ = Boltzmann constant,  $T$ = temperature

In our code, the pressure is computed from Virial theorem <sup>[15]</sup> of all atoms, which is based on the following equation:

$$P=\frac{Nk_bT}{V} - \frac{1}{3V}\sum_i \sum_{j>i} F_{ij}r_{ij} \quad (15)$$

Cell lengths of x, y and z axes are scaled in order to maintain system pressure as well as velocity algorithm.

#### 2.2.5 Formation of adsorbed layer

The first step to understand tribological behavior of C18 fatty acids on iron based surfaces is to study the generation of an adsorbed layer. Two models were considered as shown in figure 9. The first model consists in placing initially molecules in random position so they will reach the surface one after the other with random orientation toward the surface. The second model is an ideal model, the Self-Assembled Monolayer (SAM) model <sup>[17]</sup>.



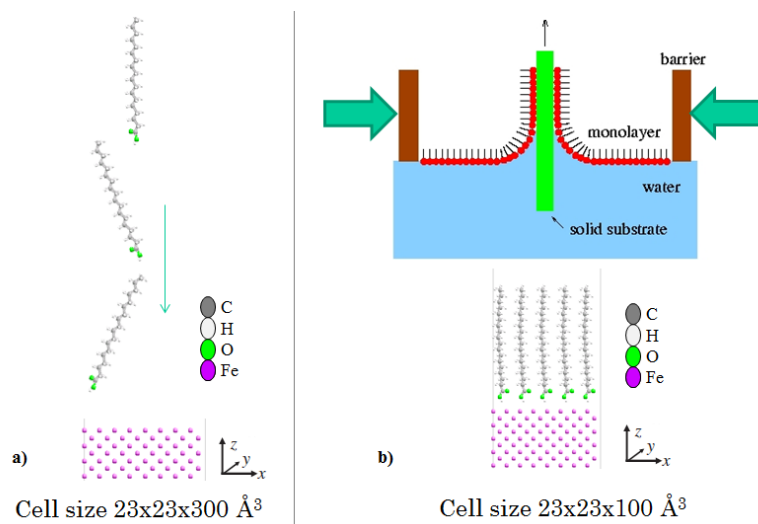


FIGURE 9: ADSORPTION MODEL: A) RANDOM MODEL: MOLECULE ARRIVE TO THE SURFACE ONE AFTER THE OTHER WITH RANDOM ORIENTATION, B) SELF-ASSEMBLED MONOLAYER (SAM)[16]: IDEAL MODEL PREPARED EXPERIMENTALLY WITH THE LANGMUIR BLODGETT METHOD

This two models were applied for stearic, oleic and linoleic acid on pure iron and iron oxide surface  $\text{Fe}_2\text{O}_3$  at 50 °C, 100 °C and 150 °C at different densities (15 molecules ‘gas’ like system and 24 molecules ‘liquid’ like system). An example of constructed initial model is given in figure 10. It represents SAM of 15 saturated and unsaturated fatty acids molecules respectively (‘liquid’ like) on iron oxide surfaces. The SAM is placed  $\sim 6$  Å above the surface. For each model, MD simulation is run for 1 ns (10 000 000 steps with 0,1 fs/step).

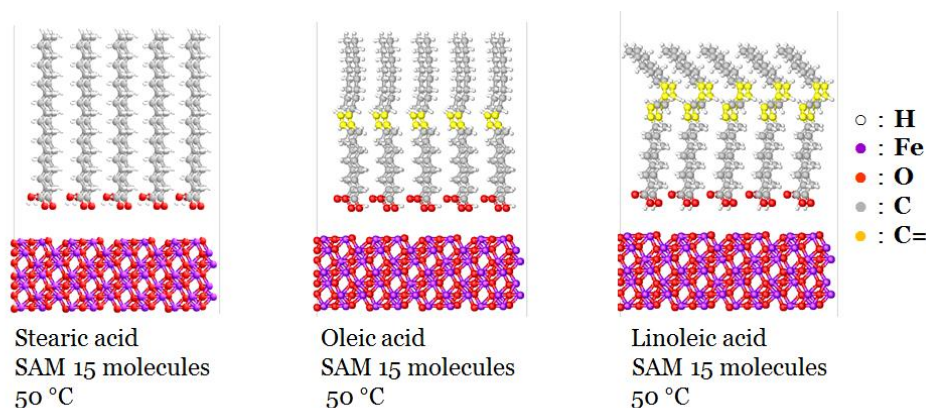


FIGURE 10: INITIAL STATE: SAM MODEL OF 15 MOLECULES OF STEARIC ACID, OLEIC ACID AND LINOLEIC ACID RESPECTIVELY ON IRON OXIDE SURFACE AT 50 °C.

## 2.2.6 Adsorbed film put under pressure and shear conditions

After the formation of an adsorbed layer, the two SAM are placed between two iron-based surfaces and then, pressure and shear are applied following different steps as shown in figure 11. First, surfaces are relaxed. Then, molecules contained in the SAM are relaxed too. After these two steps, a pressure of 300 MPa is applied on the top substrate. This step is renewed until there are no more oscillations observed on the top substrate which means that the system is at equilibrium state under 300 MPa. The last step is to maintain the pressure of 300 MPa on the top substrate and simultaneously to apply a sliding speed of 100 m/s on the top surface (green square in figure 12) for 1 ns (10 000 000 steps, 0,1 fs/step). This speed is voluntary high to get reasonable simulation costs. At this speed, the heat increase generated in the calculation is not representative of heat increase in the experiments (experimental

sliding speeds around 70 mm/s). To work close to experimental conditions with reasonable computational time, a thermostat is used to keep the temperature constant during the simulation.

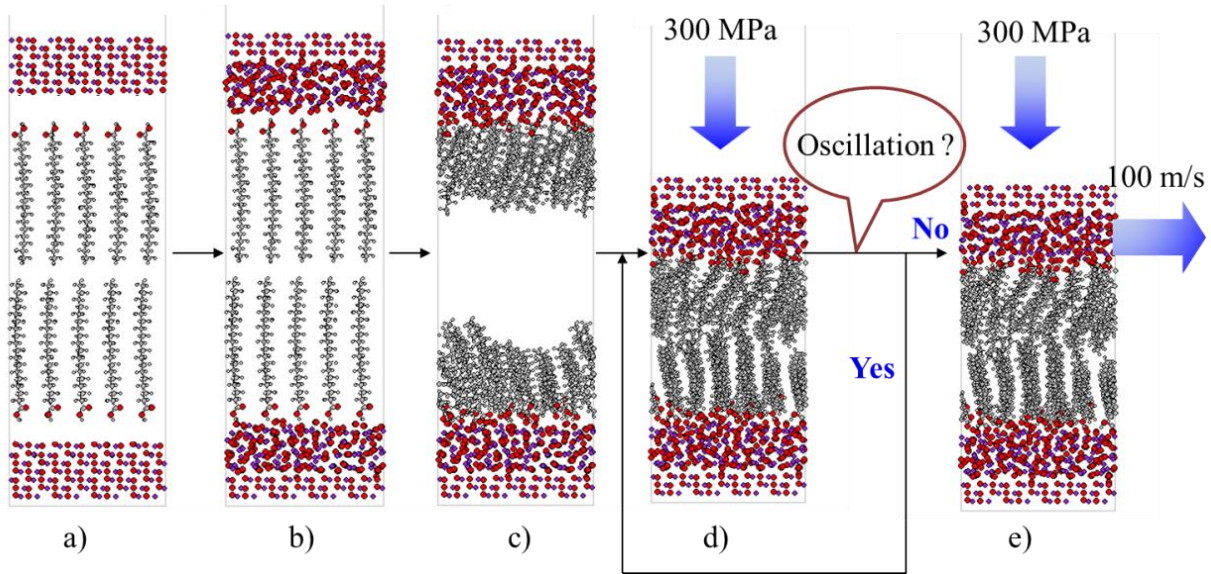


FIGURE 11: MD SIMULATIONS UNDER PRESSURE AND SHEAR CONDITIONS: A) INITIAL MODEL DESIGN WITH MATERIAL STUDIO V6, B) SURFACES ARE RELAXED, C) MOLECULES ARE RELAXED, D) PRESSURE OF 300 MPa IS APPLIED ON THE UPPER SUBSTRATE, E) PRESSURE OF 300 MPa AND SHEAR OF 100 M/S ARE APPLIED ON THE UPPER SUBSTRATE

For this reason, we input a thermostat in the model by scaling the velocity. The most famous and used thermostat for MD simulations is the Nosé Hoover thermostat but several constant temperature MD methods have been proposed <sup>[18]</sup>. The earliest method is a momentum scaling procedure in which velocities of atoms are scaled at each time step to maintain the total kinetic energy at a constant value. The temperature scaling method implemented in the system is similar to the Woodcock algorithm <sup>[16]</sup>. Every 100 steps, which are equivalent to 10 fs, the temperature come back to the defined temperature. With the exception of fixed surface, the other atoms (molecules and substrate which are included in the blue square in figure 12) have free temperature from step 0 to 99. The heating generated by high sliding speed is removed from the substrate every 100 steps as represented in figure 12 (blue arrow). Following each atom's type as a function of time show constant temperature around the temperature that is setting up (this will be shown in *chapter 4 § 2.1.2*).

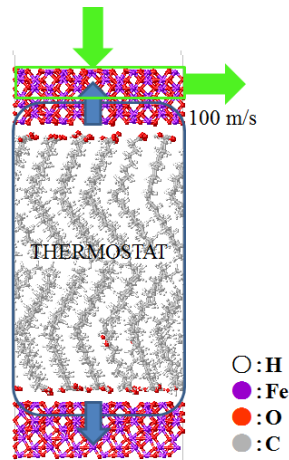


FIGURE 12: THERMOSTAT APPLIED IN THE CELL BY SCALING THE VELOCITY OF ATOMS IN CONTACT (BLUE RECTANGLE)- THE HEAT GENERATED BY HIGH SLIDING SPEED IS REMOVED EVERY 100 STEPS FROM THE FIXED SUBSTRATE

### 2.2.7 Evaluation of friction coefficient

The frictional force  $F_x$  is defined as the force acting on the upper substrate in the sliding direction (see green square in figure 12). The frictional force  $F_x$  was summed every 100 fs and accumulated in the simulations. The time step and number of calculation steps were 0.1 fs and 10,000,000 respectively. It is then possible to evaluate the friction coefficient by divided the frictional force  $F_x$  with the normal load  $F_z$ . This friction coefficient cannot be compared quantitatively with friction coefficient obtained by experimental study (see §3.3.1 tribometer) as the time and space scale are completely different. It is proposed to compare the trend between experimental and MD simulation tribological results. The friction coefficient has been evaluated for stearic, oleic and linoleic acid on iron oxide and iron hydroxide at 50 °C and with two different densities: 15 molecules ('liquid' like) and 24 molecules ('solid' like). In addition, the effect of chain length is studied. Different saturated fatty acids models (from C6 to C18 fatty acids) are built by following the same procedure, and their friction behavior when adsorbed on an iron oxide surface is then studied.

### 2.2.8 Evaluation of diffusion coefficient

One molecule of C18 fatty acid is placed in 42 molecules of PAO 4 in order to reach a concentration of 1%w of additives in the base oil. The model is presented on figure 13. The cell size is 27.4x40.3x35.3 Å<sup>3</sup> so the density of the PAO 4 is equal to 0.819 g/cm<sup>3</sup> (cf. Table 1). Periodic boundaries conditions are imposed in all directions. To reduce the time-scale and length-scale gap between experimental and computational work, unit atom (coarse-graining) method is used [19]. Instead of representing every atoms of the system, we use 'pseudo-atoms' to represent CH, CH<sub>2</sub> and CH<sub>3</sub> group of atoms for PAO 4. The diffusion is carried out under atmospheric pressure. The time step and number of calculation steps were 0.1 fs and 10,000,000 respectively. Simulations are carried out under a constant volume and a temperature of 50, 100 and 150 °C for each fatty acid in the PAO 4. MD simulations can output mean square displacement of each atom in x, y and z directions. The mean square displacement function is defined as:

$$\langle \Delta r^2 \rangle = \frac{1}{N} \sum_{i=1}^N (r_i(t) - r_i(t=0))^2 \quad (16)$$

The diffusivity in liquids can be calculated as:

$$D = \frac{1}{2d} \lim_{t \rightarrow \infty} \frac{d\langle \Delta r^2 \rangle}{dt} \quad (17)$$

Where d describes the dimensionality (d = 3 in 3D).

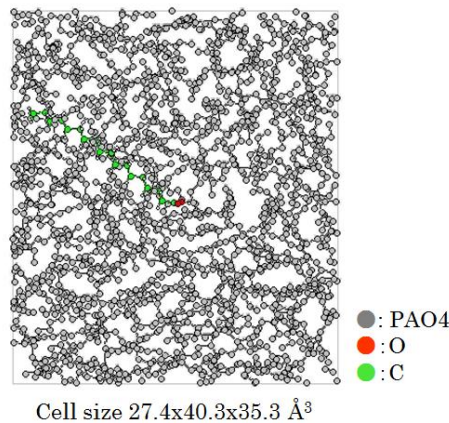


FIGURE 13: MD SIMULATION MODEL 1%W STEARIC ACID IN PAO4 (UNIT ATOM METHOD)

Other models are proposed with the presence of substrate and shearing.

As MD simulation can only treat atom-atom interactions, additional methods are used in the study to treat with electron-electron interactions and, therefore, eventual chemical reactions.

## 2.3 Quantum Chemistry methods

Different quantum chemistry methods exist depending on the approximation that is used to solve the Schrödinger equation. Among them, the DFT method is the most used quantum chemistry technique and will be used to confirm the accuracy of our method. The QC method that is used in this study is the Tight-Binding QC (TB-QC).

### 2.3.1 Density functional theory (DFT) method

In order to validate the accuracy of our TB-QC method (see next section), DFT calculations are performed. The DMol3 code <sup>[20]</sup> available in Material Studio© software is applied on the same system and double numerical basis sets with polarization functions (DNP) are employed. The geometry optimization is performed by using the Vosko, Wilk, and Nusair (VWN) as the local density approximation functional <sup>[21]</sup>. Energies are calculated by using the generalized gradient approximation (GGA) with Perdew, Burke, and Ernzerhof (PBE) exchange-correlation function <sup>[22]</sup>. The charge population is analyzed by Hirshfeld method <sup>[23]</sup>. Charge and binding energy are calculated by TB-QC and DFT and results from the two methods are compared. The geometrically optimized substrate and stearic or oleic or linoleic acids are used to construct different adsorption models for TB-QC calculations and for MD simulations as presented previously.

### 2.3.2 Tight-binding quantum chemistry calculation

#### 2.3.2.1 Quantum chemical method

The quantum chemical program “COLORS” is based on Tight-Binding (TB) approximation, designed in Prof. Miyamoto’s laboratory <sup>[24-27]</sup>. In “COLORS”, the total energy  $E$  and force  $F_i$  for each atom are expressed by equations 18 and 19 respectively:

$$E = \sum_{i=1}^n \frac{1}{2} m_i v_i^2 + \sum_k^{\text{occ}} \varepsilon_k + \sum_{i=1}^n \sum_{j=i+1}^n \frac{Z_i Z_j e^2}{R_{ij}} + \sum_{i=1}^n \sum_{j=i+1}^n E_{ij}^{\text{repul}}(R_{ij}) \quad (18)$$

Where terms on the right side refer to the kinetic energy ( $m$ = the atomic mass,  $v$  = velocity of atom), the molecular orbitals energy ( $\varepsilon_k$ =  $k$ -th eigen value,  $n_k$  = number of electrons occupied in  $k$ -th molecular orbital, “occ” means summation for all occupied molecular orbitals), the long-range Coulombic interaction energy ( $Z$ =charge,  $e$ =elementary electric charge) and the exchange-repulsion energy ( $R_{ij}$ = interatomic distance) respectively.

$$F_i = \sum_{j \neq i}^n \sum_{k=1}^{\text{occ}} C_k^T \left( \frac{\partial H}{\partial R_{ij}} \right) C_k + \sum_{j \neq i}^n \sum_{k=1}^{\text{occ}} C_k^T \left( \frac{\partial S}{\partial R_{ij}} \right) C_k - \sum_{j \neq i} Z_i Z_j \frac{e^2}{R_{ij}^2} + \sum_{j \neq i} \frac{\partial E_{\text{repul}}(R_{ij})}{\partial R_{ij}} \quad (19)$$

Where  $H$ = Hamiltonian matrix,  $C$  = eigenvector matrix,  $C^T$  = transposed matrix of the eigenvector matrix,  $S$  = overlap integral matrix.

The short-range repulsion term  $E_{\text{rep}}(R_{ij})$  is represented by equation 20:

$$E_{rep}(R_{ij}) = b_{ij} \exp \frac{a_{ij} - b_{ij}}{b_{ij}} \quad (20)$$

Where  $a$  and  $b$  = sum of the size and stiffness of atoms  $i$  and  $j$  respectively.

Each energy term can be divided to the sum of mono-atomic contribution and di-atomic contribution to the binding energy as shown in equation 21 for molecular orbitals energy:

$$\sum_{k=1}^{occ} n_k \varepsilon_k = \sum_{k=1}^{occ} \sum_r n_k (C_{kr})^2 \mathbf{H}_{rr} + \sum_{k=1}^{occ} \sum_r \sum_s n_k C_{kr} C_{ks} \mathbf{H}_{rs} \quad (21)$$

Where  $\varepsilon$  = eigen value.

In the TB-QC, the electronic structure calculation is performed by solving the Schrödinger equation with diagonalization condition as follows [28]:

$$HC = \varepsilon SC, \quad (22)$$

$$C^T SC = I. \quad (23)$$

Where  $I$  = unit matrix.

In TB-QC, the double Slater type basis set is employed and the Ewald method [29] is used in order to compute long-range Coulombic interactions. To determine the off-diagonal elements of  $\mathbf{H}$ , denoted  $\mathbf{H}_{rs}$ , the corrected distance-dependent Wolfsberg-Helmholtz (W-H) [30] is used as shown in equation 24:

$$H_{rs} = \frac{K}{2} S_{rs} (H_{rr} + H_{ss}) \quad (24)$$

Where  $K$  = distance-dependent W-H constant,  $S_{rs}$  = integral overlap matrix,  $H_{rr}$ ,  $H_{ss}$  = diagonal terms of Hamiltonian matrix.

Tight-Binding Approximation (TBA) performs parameterization using atomic orbital function of valence band on the basis of extended Hückel method named LCAO (Linear Combination of Atomic Orbital) [31]. There are various Hamiltonians for TBA and we are using the first principles parameterization.

### 2.3.1.2 First-principle parameterization

$\mathbf{H}$  and  $\mathbf{S}$  in our TB-QC simulator need to be set by evaluating exponents of a Slater-type  $\zeta_r$  atomic orbital (AO) and valence-state ionization potentials (VSIP) for the valence shell of an AO of C, O, H and Fe atoms.  $\zeta_r$  is used to calculate the  $\mathbf{S}$  matrix and  $\mathbf{H}_{rs}$  in equation 24. The VSIP parameter of AO number  $r$  and atom number  $i$ , denoted  $I_r^i$  is linked to  $H_{rr}$  by equation 25:

$$H_{rr} = -I_r^i \quad (25)$$

This parameter is used to determine the diagonal element of  $\mathbf{H}$  in equation 24.  $\zeta_r$  and  $H_{rr}$  are calculated by the polynomial function of atomic charges as described in equation 26 and 27.

$$\zeta_r = a_0 + \sum_{k=1}^5 a_k (Z_i)^k \quad (26)$$

$$H_{rr} = b_0 + \sum_{k=1}^5 b_k (Z_i)^k \quad (27)$$

Where  $Z_i$  = atomic charge of atom  $i$ .

All parameters ( $a_0, \dots, a_5, b_0, \dots, b_5$ ) of AO s, p and d are adjusted to reproduce the binding energies and electronic structures of each reactant calculated by the first-principle parameterization and are gathered in Table 4 and Table 5.

TABLE 4: DETERMINED COEFFICIENTS FOR SINGLE ZETA PARAMETER  $\zeta_r$  IN SLATER-TYPE ATOMIC ORBITAL

Element	AO	$a_0$	$a_1$	$a_2$	$a_3$	$a_4$	$a_5$
H	S	1.71	3.97	0.00	0.00	0.00	0.00
C	S	1.91	1.01	0.41	0.00	0.00	0.00
	P	1.81	1.21	0.71	0.00	0.00	0.00
O	S	2.81	2.08	0.02	0.00	0.00	0.00
	P	2.40	1.83	0.68	0.00	0.00	0.00
FE	S	2.09	1.06	0.17	0.00	0.00	0.00
	P	1.39	0.61	0.10	0.00	0.00	0.00
	D	2.66	1.91	0.002	0.00	0.00	0.00

TABLE 5: DETERMINED COEFFICIENTS FOR  $HRR$  PARAMETER

Element	AO	$b_0$	$b_1$	$b_2$	$b_3$	$b_4$	$b_5$
H	S	-8.94	-3.38	0.00	0.00	0.00	0.00
C	S	-10.7	-3.21	-1.40	0.032	0.00	0.00
	P	-6.96	-3.39	-1.59	-0.065	0.00	0.00
O	S	-18.7	-8.43	-1.45	0.00	0.00	0.00
	P	-10.5	-8.82	-1.62	0.00	0.00	0.00
FE	S	-4.47	-4.95	-1.45	0.00	0.00	0.00
	P	-3.53	-1.69	-0.22	0.00	0.00	0.00
	D	-6.05	-10.8	-1.09	0.00	0.00	0.00

### 2.3.3 Models used for TB-QC calculations

TB-QC simulations can be run for static study and, therefore, compared with DFT simulations. It has also been used to evaluate atom charge for MD simulations. TB-QC simulations are run for all MD models at initial and final steps: single molecules, SAM, additives under pressure and shear, etc. In addition, the influence of additives position toward the surface has been studied by TB-QC simulations. Different angles between the substrate (iron, iron oxide or iron hydroxide) and the alkyl chain have been imposed. Moreover, the position of acid group (rotation) toward the surface has also been studied. Finally, TB-QC simulations were run for partial density of state study and to help at XPS chemical shift interpretation. All models are designed using Material Studio© V6.



### 2.3.4 Accuracy of our TB-QC method

Preliminary calculations on the Fe and Fe<sub>2</sub>O<sub>3</sub> bulk model presented in figure 14 and on a single molecule of stearic, oleic and linoleic acids respectively are performed to validate the parameters shown in tables 4 and 5. Atomic charges and atomic orbital populations in the Fe<sub>2</sub>O<sub>3</sub> and Fe bulks are calculated by TB-QC and DFT as shown in table 6. Binding energies in the Fe<sub>2</sub>O<sub>3</sub> bulk, Fe bulk and stearic, oleic, linoleic acids are also calculated by TB-QC and DFT and the results are shown in tables 7 and 8. In addition, binding energy of pure iron and iron oxide surfaces are compared with those recorded in the chemical Handbook (CRC) [32]. The bulk model obtained by DFT as well as by TB-QC show good agreement in terms of charges, atomic orbital population and total binding energy for both iron oxide and pure iron. Errors between the DFT and TB-QC of total binding energy calculation are from 0.2 % to 4.3 % for fatty acids and bulk substrate as shown in tables 7 and 8. A fairly good agreement between the results calculated by DFT and TB-QC methods can be seen. Error between the CRC and TB-QC of total binding energy calculation is 9.1 % and 4.5% for pure iron and iron oxide surface respectively which is considered as accurate.

We can thus confirm that the ‘COLORS’ program with our first-principles parameterization reproduces well the results obtained by the DFT method.

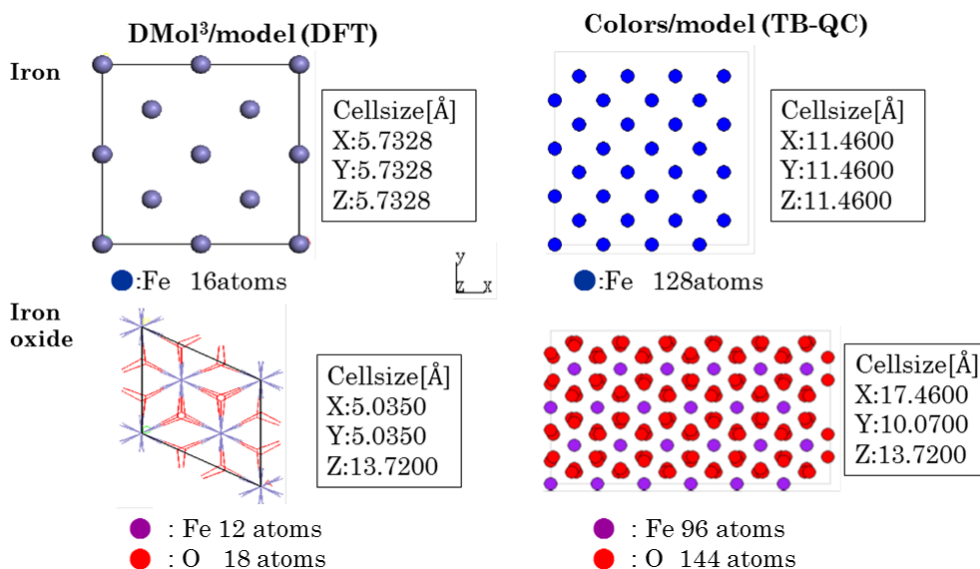


FIGURE 14: BULK FE AND BULK FE<sub>2</sub>O<sub>3</sub> MODELS FOR DFT CALCULATIONS AND TB-QC CALCULATIONS TO VALIDATE THE ACCURACY OF OUR METHOD

TABLE 6: CHARGE DISTRIBUTION OF FE AND Fe<sub>2</sub>O<sub>3</sub> MODELS CALCULATED BY DFT AND TB-QC METHODS

		Charge	s	p	d	s(%)	p(%)	d(%)
<b>Fe</b>								
	DFT	0.00	0.64	0.67	6.69	8.00	8.38	83.63
	TB-QC	0.00	0.43	0.56	7.00	5.39	7.05	87.56
<b>Fe<sub>2</sub>O<sub>3</sub></b>								
<b>Fe</b>								
	DFT	0.31	0.32	0.43	6.94	4.20	5.60	90.20
	TB-QC	0.25	0.28	0.59	6.88	3.60	7.63	88.77
<b>O</b>								
	DFT	-0.21	1.77	4.44	-	28.46	71.54	-
	TB-QC	-0.17	1.81	4.36	-	29.36	70.64	-

TABLE 7: TOTAL BINDING ENERGY OF FE AND  $\text{Fe}_2\text{O}_3$  CALCULATED BY DFT, TB-QC AND FROM CHEMICAL HANDBOOK

	Binding energy [kcal/mol]				
	CRC	DFT	TB-QC	Error %(CRC)	Error %(DFT)
Colors Fe	-12735	-11592	-11573	9.1%	0.2%
Colors Fe <sub>2</sub> O <sub>3</sub>	-27791	-28855	-29051	4.5%	0.7%

TABLE 8: TOTAL BINDING ENERGY OF STEARIC, OLEIC AND LINOLEIC ACID CALCULATED BY DFT AND TB-QC METHOD

	Binding energy [kcal/mol]		
	DFT	TB-QC	Error %
Stearic Acid	-6379	-6569	2.9
Oleic Acid	-6227	-6466	3,7
Linoleic Acid	-6090	-6366	4,3

## 2.4 Ultra Accelerated Quantum Chemistry Molecular Dynamics (UA-QCMD) simulation

### 2.4.1 UA-QCMD method

To investigate the atomic interaction between stearic acid and iron oxide surface during friction, the in house code UA-QCMD is used. The program is based on a Tight-Binding Quantum Chemistry (TB-QC) calculation program named “COLORS” and a classical molecular dynamics (MD) program named “RYUDO”, which were described previously. In the UA-QCMD program, charges, potentials, and binding energies, etc. are calculated by COLORS program while positions and velocities of atoms are calculated by RYUDO program. Figure 15 describes the different steps that occur during an UA-QCMD calculation. First the model is constructed by using Material Studio© V6 software. Selected models are the same as models used for MD simulations: single fatty acid on iron based surface, SAM of fatty acids on iron based surface and two adsorbed films under pressure and shear stress. Once the model is designed, TB-QC calculation is run. Output from TB-QC calculation becomes input information for MD calculation. At this step, parameters fitting are made.

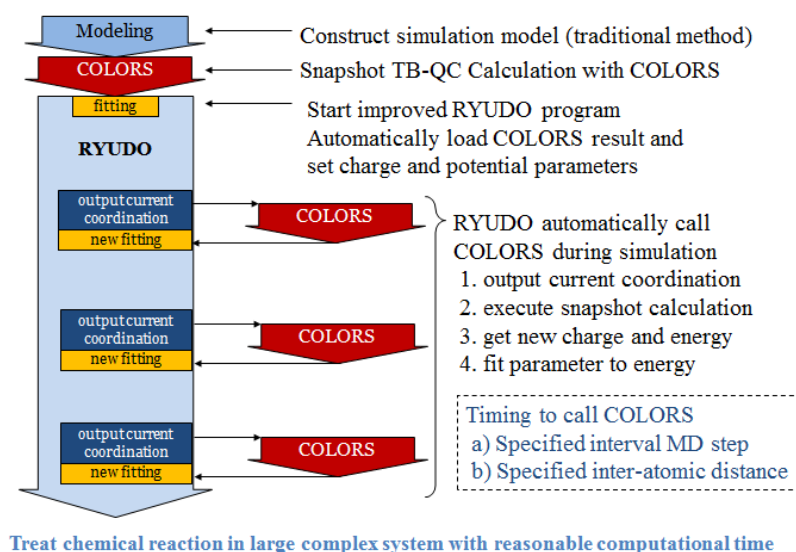


FIGURE 15: PROCEDURE SCHEMATIC OF THE UA-QCMD METHOD



If the total energy calculated by TB-QC is negative, it is mainly due to Morse potential and, therefore, interactions in the considered pair of atoms. In this case, the fitting is done on Morse potential as shown in figure 16. The potential curve calculated by TB-QC is a bit different from the curve initially calculated by MD simulation.  $D_{ij}$  is then chosen in order to fit with the TB-QC curve and the new Morse potential energy is input in the equation of motion during MD simulation.

### Morse potential ( $E < 0$ )

*Between two atoms:*

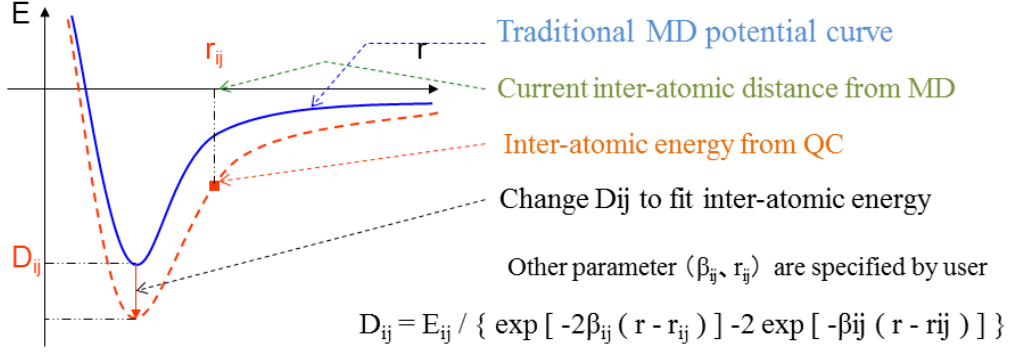


FIGURE 16: PARAMETER FITTING FOR NEGATIVE ENERGY

On the other hand, if the total energy calculated by TB-QC is positive, repulsion occurred and the main potential is the Gilbert repulsive term. In the same way, parameter is modified to fit with TB-QC curve as shown in figure 17.

Ionic bond interactions are calculated by coulomb potential with the charge of each atom and Ewald method in RYUDO software.

### Repulsion ( $E > 0$ )

*Between two atoms:*

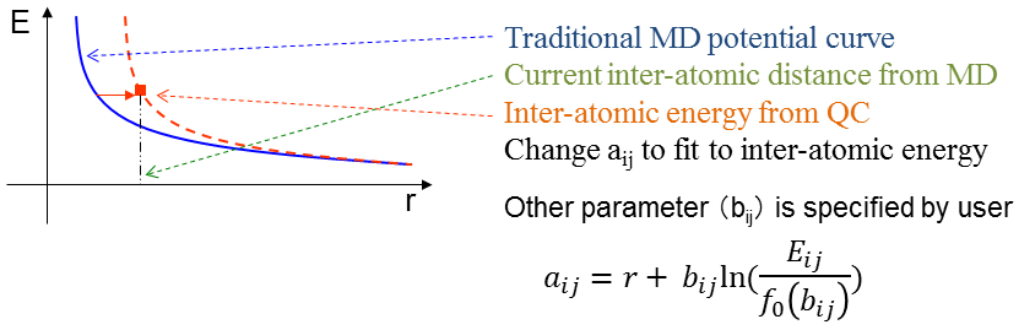


FIGURE 17: PARAMETER FITTING FOR POSITIVE ENERGY

MD simulation with new parameter is running in order to output new positions for TB-QC calculation. We 'go' from 'COLORS' to 'RYUDO' with a specific interval MD step depending on the size of the cell as well as on the information that is needed. In our study, Molecular Dynamic simulation is running and 'COLORS' is called every 1000 steps. The time step and number of calculation step were 0.1 fs and 150,000 respectively. Nevertheless, the number of calculation step is tested from 150,000 to 500,000 to check the equilibrium state of the system which is equivalent of 15 to 50 ps. Simulations are carried out under a constant volume and temperature of 50, 100 and 150 °C for each adsorption model.

## 2.5. Summary

TABLE 9: COMPUTATIONAL TECHNIQUES USED IN THE STUDY

Techniques	Principle	Scale (size-time)	Main information
MD	Newton's equation	Thousands of atoms Up to few ns	Position Motion of atoms
DFT	Schrödinger equation	Hundreds of atoms Static	Binding energy Charge
TB-QC	Schrödinger equation	Thousands of atoms Static	Binding energy Charge
UA-QCMD	Combination of MD and TB-QC	Thousands of atoms Up to few ns	Position, motion, binding energy

## 3. Experimental techniques

To validate our computational chemistry approach, it is necessary to perform some experimental analysis simultaneously. Experimental study was performed by Dr. Matta, a scientific researcher in LTDS.

### 3.1 Materials

The material used in the experimental study is AISI 52100 steel for both cylinder and flat samples. The lubricant used is poly-alpha-olefin base oil (PAO 4 supplied by TOTAL). Information about PAO4 kinematic viscosity is available in table 10. Three pure fatty acids from Sigma-Aldrich containing 18 carbon atoms are studied: stearic acid (C18:0), oleic acid (C18:1) and linoleic acid (C18:2).

TABLE 10: KINEMATIC VISCOSITY OF PAO 4 AT 40, 100 AND 150 °C

Temperature (°C)	Kinematic viscosity (cSt)
40	17.56
100	4.00
150	1.98

### 3.2 Experimental characterization techniques

In order to study the adsorption mechanism of C18 fatty acids on iron-based surfaces, sensitive surface analyses techniques are used: XPS and PM-IRRAS as the adsorbed films are thin. Then, the tribological properties of the different additives are evaluated by friction tests and films are analyzed by PM-IRRAS.

#### 3.2.1 X-ray Photoelectron Spectroscopy (XPS)

X-ray Photoelectron Spectroscopy (XPS) is a surface-sensitive spectroscopic technique that allows to measure the elemental composition, chemical state and electronic state of the elements present within a material. It is based on the principle of photo-electron emission <sup>[33]</sup>.

XPS spectra are obtained by irradiating a material with a beam of X-rays ( $h\nu$ ) while simultaneously measuring the kinetic energy and the number of electrons that escape (see figure 18 left) from less than 10 nm of material surface regarding the mean free path of emitted photoelectrons.

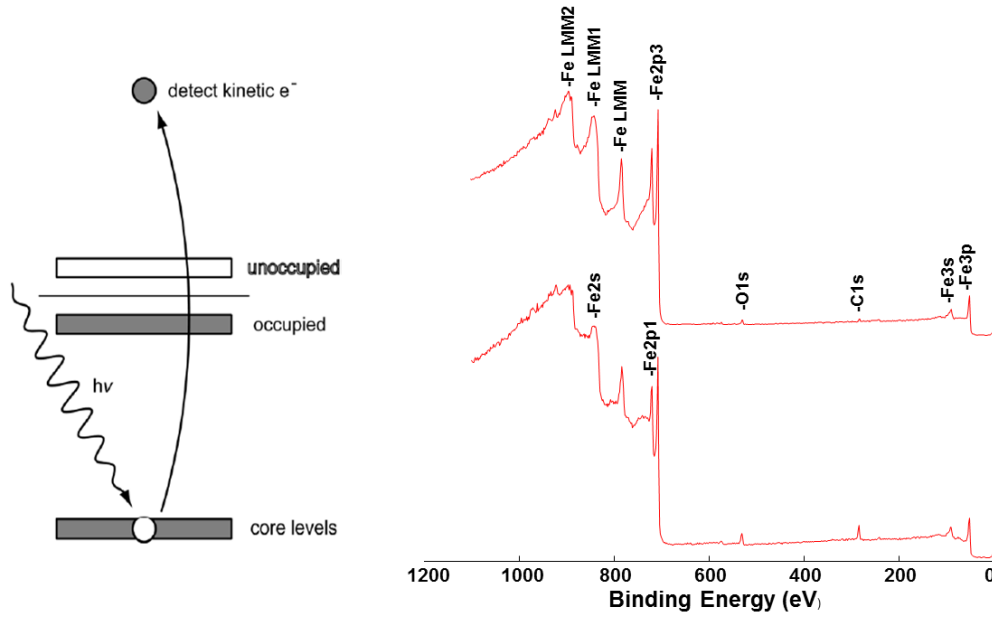


FIGURE 18: LEFT: SIMPLIFIED ENERGY LEVEL DIAGRAM OF X-RAY PHOTOELECTRON SPECTROSCOPY OR PHOTOEMISSION, RIGHT: EXAMPLE OF GENERAL XPS SPECTRA

XPS spectra are presented as the intensity of electrons as a function of electron binding energy <sup>[32]</sup>. This binding energy is related to the kinetic energy by:

$$E_{binding} = h\nu - E_{kinetic} \quad (28)$$

One of the most powerful aspects of XPS for this work is to identify elements that constitute the adsorbed surface as well as their chemical nature adsorbed to the surface to therefore investigate the adsorption mechanism.

XPS analysis measurements are made on the thermal film formed *in situ* on the surface and on the tribofilm after friction tests. Any residual oil or contaminants are removed by cleaning the samples after tribotests in n-heptane for 10 minutes prior to the XPS analysis. Surface analyses are performed under a pressure of  $10^{-7}$  hPa in the analytical chamber. The XPS study has been carried out on a PHI 5000 VersaProbe apparatus using monochromatic AlK $\alpha$  X-ray source. The analyzed size area was  $100 \times 100 \mu\text{m}^2$ . The experimental device, which includes many chambers: sample's preparation, adsorption, friction chamber in controlled environment and then analytical chamber, is schematically presented in figure 19. XPS spectrums are analyzed with the PHI Multipak© software. For quantification, the area under peak is determined after subtraction of the 'Shirley-type' background.

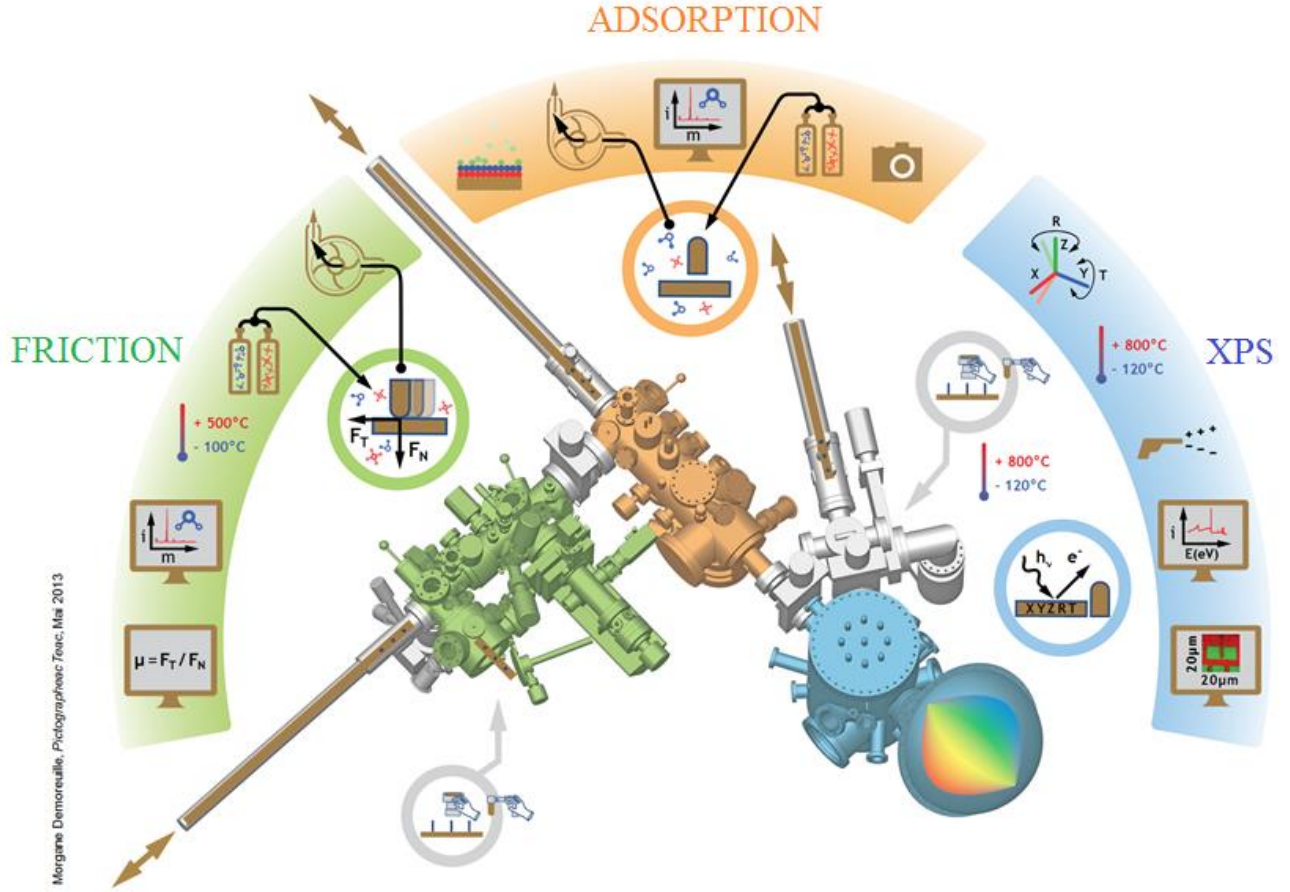


FIGURE 19: EXPERIMENTAL DEVICE USED FOR IN-SITU ADSORPTION EXPERIMENTS

First, a survey scan is carried out to identify each element present in the sample.

Then, high-resolution spectra of the selected peaks are performed. The deconvolution of the peaks allowed the identification of chemical species. Chemical species corresponding to each binding energy have been found using a handbook <sup>[34]</sup>.

Acquisition conditions for the general spectra and parameters for high-resolution spectra are gathered in table 11.

TABLE 11: ACQUISITION CONDITIONS OF XPS SPECTRA

Spectra	Pass energy (eV)	Integration step (eV)	Dwell time (ms)	Range
General	187.85	1.6	500	0→1100 eV
C1s	23.5	0.1	500	274→294 eV
O1s	23.5	0.1	500	524→540 eV
Fe2p	23.5	0.1	500	700→720 eV
Au4f	23.5	0.1	500	79→99 eV

To begin, the different substrates are analyzed without additives as references. Steel 100C6 (AISI 52100) is used. The steel surface is subject to 2x2 mm<sup>2</sup> of argon ion etching in order to remove the hydrocarbon and the different oxide layers. Figure 20 shows the preparation procedure of substrates. Therefore, three substrates are analyzed by XPS: steel as received, iron oxide (after 10 second of Argon ion (Ar<sup>+</sup>) etching) and metallic iron (after 2 minutes of Ar<sup>+</sup> etching).

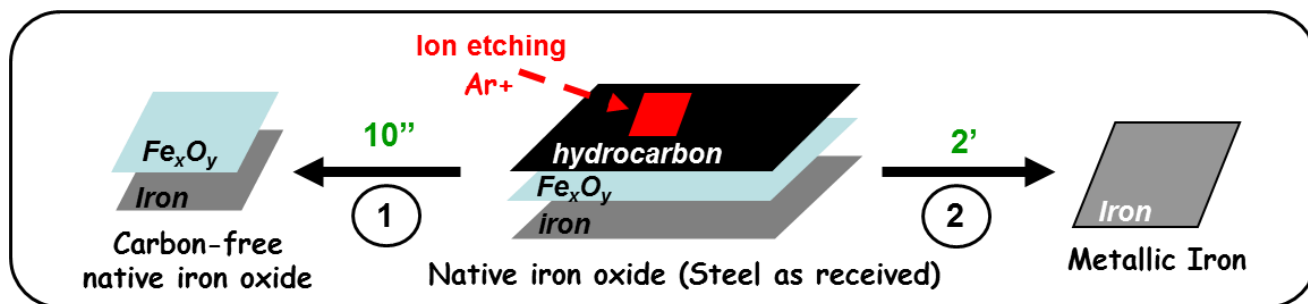


FIGURE 20: PREPARATION PROCEDURE OF SUBSTRATES

Then, stearic, oleic or linoleic acid are evaporated in the chamber separately by heating solutions at 95 °C for oleic acid, 85 °C for linoleic acid, and 120 °C for stearic acid as it is a powder at room temperature. Thus *in situ* adsorption was performed. Minimum temperature to evaporate the fatty acid in the chamber is used in order to prevent deterioration of fatty acids by temperature increase. Different adsorption time has been chosen: 10', 30' and 2h. The pressure in the adsorption chamber was  $10^{-4}$  hPa after the introduction of the fatty acid vapor. Then, the excess of vapor is pumped until pressure of  $10^{-7}$ hPa is reached and finally, samples are transferred *in situ* to the XPS analytical chamber. The adsorption procedure is presented in figure 21.

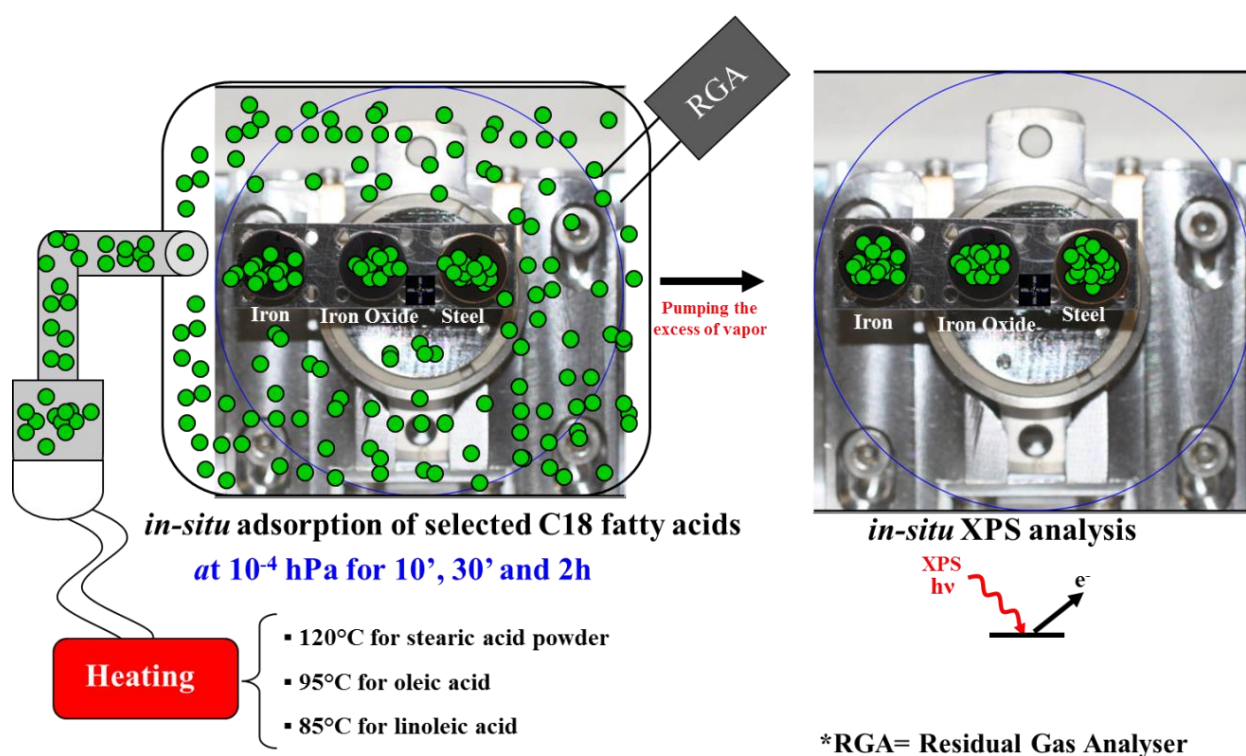


FIGURE 21: ADSORPTION PROCEDURE

### 3.2.2 Polarization modulation-infrared reflection-adsorption spectroscopy (PM-IRRAS)

Infrared Fourier transform spectroscopy (FTIR) is a technique for physicochemical analysis. This method allows direct access to molecular and chemical information, conformational organization and structural information of the analyzed sample.

The vibrational method is non-destructive, qualitative and quantitative. The wave numbers ( $\text{cm}^{-1}$ ) and the attenuation of the radiation energy that the sample absorbs are measured enabling identification of chemical groups and an assessment of their concentration.

The wide variety of experimental setups allows the characterization of any type of sample regarding their thickness or surface nature. However, in the case of less than  $500 \text{ \AA}$  thick layers, the conventional FTIR spectroscopy reached its limit of sensitivity and detection. A method based on differential reflectivity and fast modulation of the polarization of the electromagnetic wave is used (PM-IRRAS) [35]. The technique favors polarized surface absorption rather than the one coming from the environment.

With this technique, a molecule that is parallel to the surface is hard to detect or analyze because the net amplitude of IR radiation parallel to the surface is zero [36]. In contrast, molecule that is perpendicular to the surface can be analyzed very clearly.

In our study, this technique is used to identify the thickness, composition and molecular structure of the adsorbed surfaces and tribofilms studied.

PM-IRRAS device consists of the IR-TF spectrometer Nicolet 850 combined with an optical set of the polarization modulation that is external to the spectrometer as shown on figure 22. The ISM laboratory (Molecular Spectroscopy Group) in University of Bordeaux 1 are performing all PM-IRRAS analysis so further information about the procedure are not available.

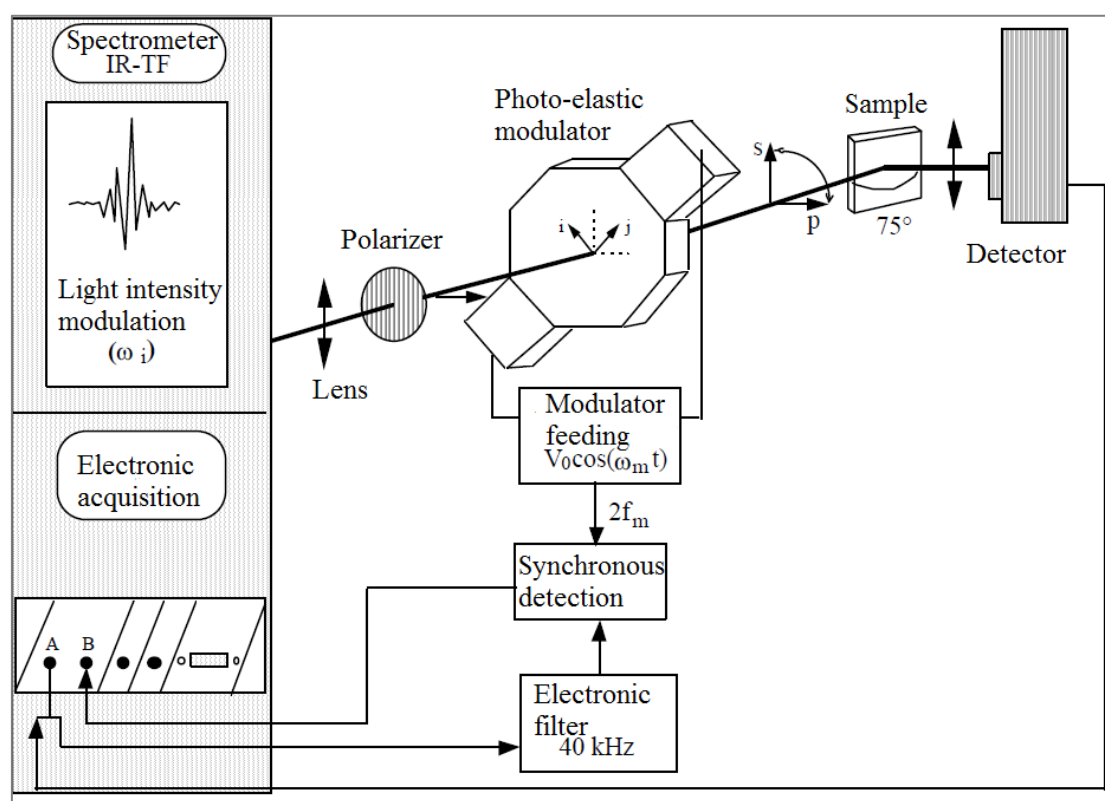


FIGURE 22: OPTICAL SET OF THE POLARIZATION MODULATION [35]

Sensitivity of PM-IRRAS technique favors the qualitative analysis of ultra-thin film. It enables the identification of the surface chemical layer by comparing with well-known spectrum or with the detection of specific group that characterize a compound by functional analysis. With the intensity of the peak, it is also possible to study the orientation, the organization and the conformation of a molecule or a monolayer on a surface. Nevertheless,



the quantitative analysis of the observed peak's intensity is not direct because of the small effect of *s*-polarized radiation.

First, thermal film of OFM is analyzed by PM-IRRAS in order to determine the thickness of the layer, the composition and the molecular structure of the adsorbed surfaces. Adsorbed surfaces samples are prepared as shown in figure 23. The AISI 52100 Steel surface is immersed in a solution containing PAO 4 and 1%w of stearic, oleic and linoleic acid respectively. The adsorption takes place under room temperature except for stearic acid that is heated up to 80 °C in order to have a liquid. After adsorptions, samples are sent to the ISM laboratory where they have performed PM-IRRAS analyses after washing sample with n-heptane to remove the excess of additives on each sample.

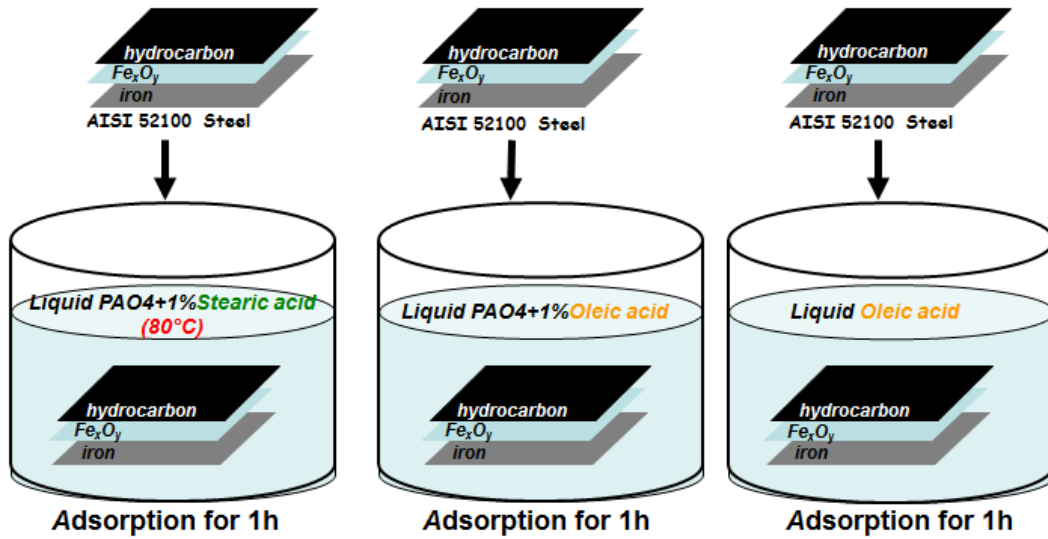


FIGURE 23: ADSORBED SURFACES PREPARATION BEFORE PM-IRRAS ANALYSIS

After some friction tests (see § 3.3.1), some samples (see figure 24) are also sent for PM-IRRAS analysis to study the thickness, composition and molecular structure of tribofilms. Like adsorbed surfaces, samples are washed with n-heptane before analysis. Because of the small size of the plane, it was not possible to analyze only the inside of the track so the analysis take into account signal from both inside and outside the track.

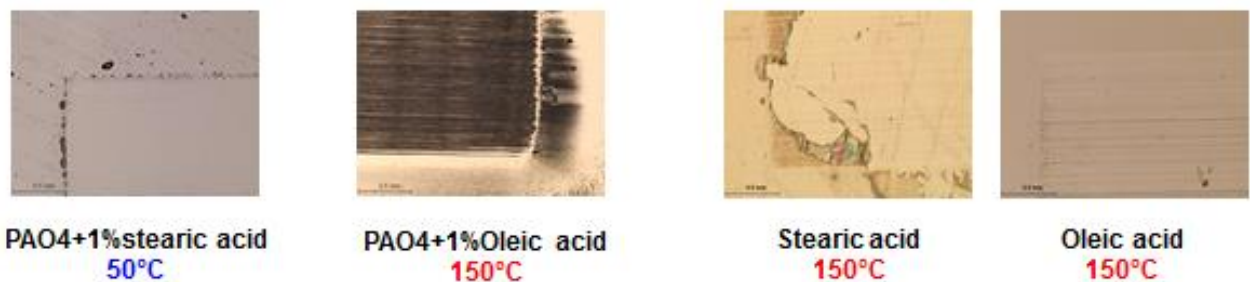


FIGURE 24: PLAN AFTER FRICTION TEST FOR PM-IRRAS ANALYSIS

For all samples, spectra are mean values of 3 to 5 spectra. Spectra have been corrected by taking into consideration the steel surface without adsorbed layer and all spectra are presented with IRRAS intensity.

### 3.3 Friction behavior measurements

#### 3.3.1 Linear tribometer

The linear tribometer enables to work in conditions not far from the cam-tappet contact inside the thermal combustion engine and is used to determine the tribological performance of the studied system. It is therefore possible to quantify the potential of studied friction modifiers additives for the cam-tappet area. Table 12 represents the principal characteristics of the tribometer and main parameters that are chosen in our study. The schematic and the picture of the tribometer of our experimental device is presented in figure 25. The flat is fixed in a tank full of lubricant which can be heated or cooled.

TABLE 12: CHARACTERISTICS OF THE LINEAR TRIBOMETER AND PARAMETERS CHOSEN IN THE STUDY OF TRIBOLOGICAL BEHAVIOR OF ORGANIC FRICTION MODIFIERS

Characteristics	Possibilities	In our study
Contact	flat/flat, pin/ball, cylinder/ flat	Cylinder ( $\varnothing$ 10 mm, H = 3 mm) / flat ( $\varnothing$ 7 mm, L= 7 mm)
Load	1 $\rightarrow$ 1000 N	50 N
Temperature	-100 °C $\rightarrow$ 500 °C	50 °C, 100 °C, 150 °C
Speed	0.1 mm/s $\rightarrow$ 1 m/s	56 mm/s
Amplitude	0.1 mm $\rightarrow$ 4 mm	4 mm
Kinematic	Reciprocating linear or sinusoidal	Alternate
Frequency		7 Hertz
Maximum Hertzian pressure		320 MPa
Number of cycles		4000
Immersion volume		80 mL

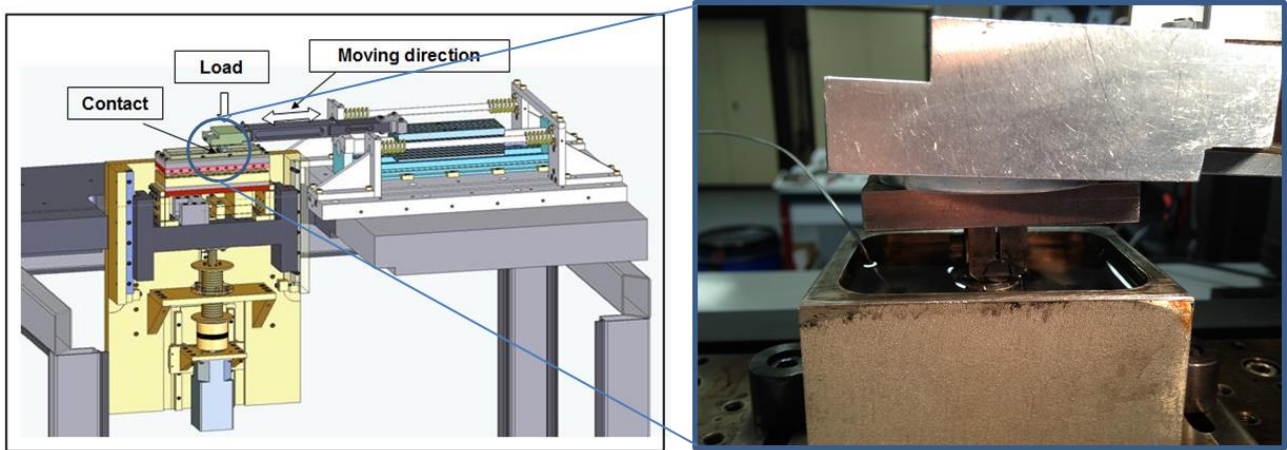


FIGURE 26: GENERAL VIEW OF THE LINEAR TRIBOMETER AND EXPERIMENTAL ASSEMBLY

Tribological tests are performed using a reciprocating cylinder-on-flat tribometer to have friction area that is big enough to make surface characterization as described in previous sections. The cylinder and flat are made of AISI 52100 steel with a mirror surface finish ( $R_a$  equal to 2 nm).

The friction counterparts are completely immersed in a solution of lubricant (or liquid fatty acids) prior to the friction test. The lubricant used is a Poly-Alpha-Olefin base oil (PAO 4

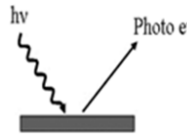
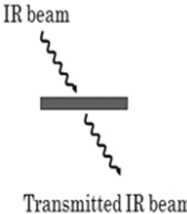


supplied by TOTAL) additivated with 0,5%w, 1%w and 2%w of a single fatty acid respectively or with 2%w (1:1) of a mixture of saturated and unsaturated fatty acids. Three pure fatty acids from Sigma-Aldrich containing 18 carbon atoms are studied: stearic acid (C18:0), oleic acid (C18:1) and linoleic acid (C18:2). First, the tribological behavior of steel samples in presence of pure additives and then in presence of PAO 4+1%w of each single fatty acid are studied. Afterwards, the effect of concentration is studied by varying from 0.5 to 2%w of C18 fatty acid in PAO 4. Finally, the synergetic or anti-synergetic effect of two mixtures: stearic and oleic acids and stearic and linoleic acids blended in PAO 4 are investigated.

The experiments are run for 4000 cycles respectively at 50 °C, 100 °C and 150 °C with a stroke length of 4 mm at 7 Hz corresponding to a sinusoidal movement (the maximum sliding speed was 56 mm/s at the middle of the stroke). The applied normal load is 50 N resulting in a maximum Hertzian pressure of 320 MPa. All tests are repeated three times to check their reproducibility. Considering the test conditions the lubrication regime used in this study is mostly the mixed regime.

### 3.4 Summary

TABLE 13: SURFACE ANALYTICAL TECHNIQUE USED IN THE STUDY

Techniques	Principle	Information obtained	Analyzed thickness	Analyzed size area
XPS		Elementary chemistry, element's chemical environment (Sensitivity 1%)	10 nm	100x100 $\mu\text{m}^2$
IR PM-IRRAS		Film thickness, composition, molecular structure (Sensitivity 1-5% weight)	< 500 Å	10x10 mm <sup>2</sup>

## 4. Conclusion

Computational study enables to study tribological and chemical behavior at different scales but most importantly at the nanoscale. Combining both experimental and computational work enables to make multi-scales work.

In this study, the adsorption mechanism and tribological behavior of some fatty acids on iron-based surfaces will be investigated.

The present research work is divided into three parts:

First, the work will be focused on the formation of the thermal film. Therefore, the adsorption mechanism of stearic, oleic and linoleic acid on iron-based surfaces will be investigated. Different parameters will be varied to evaluate their impact: temperature, density, unsaturation, oxide layer, etc. (Chapter 3)

Then, the friction behavior of this fatty acid on some iron based surfaces will be evaluated. (Chapter 4)

Finally, the behavior of these fatty acids in presence of solvent will be studied with PAO 4 as base oil. (Chapter 5)

For each part, both experimental and numerical study will be done as shown in table 14.

TABLE 14: DIFFERENT TECHNIQUES USED IN THE STUDY: COMPUTATIONAL AND EXPERIMENTAL TECHNIQUES

<b>Parts</b>	<b>Computational simulation</b>	<b>Experimental analyses</b>
Adsorption	TB-QC and DFT: adsorption energy, energetic barrier, IR spectra	XPS: sensitive surface analysis, change in chemical function
	UA-QCMD: adsorption kinetic, adsorption energy	PM-IRRAS: sensitive surface analysis, adapted to carbon, can dissociate steel and fatty acid
Friction	MD: qualitative organization of films, evaluation of friction coefficient, speed profile	Tests on linear tribometer: friction coefficient, qualitative presence/absence of wear
	UA-QCMD: chemical reaction during friction process	Analysis of the tribofilm: XPS and PM-IRRAS

## 5. References

- [1] Toulhoat H, Modélisation moléculaire: bases théoriques (partie 1 et 2), *Technique de l'ingénieur J 1 011 et 012* (2007).
- [2] Allen M P, Tildesley D J, Computer simulation of liquids, *Clarendon press*, Oxford (1987).
- [3] Delley B J, From molecules to solids with the DMol<sup>3</sup> approach, *Journal of Chemical Physics* 113 (2000) 7756.
- [4] Vosko SH, Wilk L, Nusair M, Accurate spin-dependent electron liquid correlation energies for local spin density calculations: a critical analysis, *Canadian Journal of Physics* 58 (1980) 1200.
- [5] Olla M, Navarra G, Elsener B, Rossi A, Nondestructive in-depth composition profile of oxy-hydroxide nanolayer on iron surfaces from ARXPS measurement, *Surface and Interface Analysis*, 38 (2006) 964-974.
- [6] Alder B J, Wainwright T E, Phase transition for a hard sphere system, *Journal Chemical Physics* 27 (1957) 1208.
- [7] Alder B J, Wainwright T E, Studies in molecular dynamics I. General method, *Journal Chemical Physics* 31 (1959) 459.
- [8] Rahman A, Correlation in the motion of atoms in liquid argon, *Physical Review A* 136 (1964) 405.
- [9] Stillinger F H, Rahman A, Improved simulation of liquid water by molecular dynamics, *Journal Chemical Physics* 60 (1974) 1545.
- [10] Onodera T et al., Influence of film deposition condition on friction of diamond like carbon film: a theoretical investigation, *Tribology Online* 5 3 (2010) 173.
- [11] Minfray C et al., Experimental and molecular dynamics simulations of tribochemical reactions with ZDDP:Zinc Phosphate-Iron Oxide Reaction, *Tribology transactions* 51 (2008) 589-601.
- [12] Chipot C, Les méthodes numériques de la dynamique moléculaire, *Cours Université Henri Poincaré Nancy* (2002).
- [13] Ewald P P, The calculation of optical and electrostatic grid potential, *Annals of Physics*. 64 (1921) 253-287.
- [14] Dauber-Osguthorpe P, Roberts V. A., Osguthorpe D. J., Wolff J., Genest M., Hagler A. T., 'Structure and energetics of ligand binding to proteins: E. coli dihydrofolate reductase-trimethoprim, a drug-receptor system', *Proteins: Structure, Function and Genetics*, 4, 31-47 (1988).
- [15] Buehler M J, Atomistic Modeling of Materials Failure – Chapter 2, *Springer* (2008) 38-40.
- [16] Woodcock L V, Isothermal molecular dynamics calculations for liquid salts, *Chemical Physics Letters* 10 (1971) 257.
- [17] Hussain S A, Langmuir-Blodgett films: a unique tool for molecular electronics, *Langmuir-Blodgett films*, GRIN edition, 2010.

- [18] Nosé S, A unified formulation of the constant temperature molecular dynamics methods, *Journal of Chemical Physics* 81 (1984) 511-519.
- [19] Saunders M G, Voth G A, Coarse-Graining Method for Computational Biology, *Annual Review of Biophysics* 42 (2013) 73-93
- [20] Delley B J, From molecules to solids with the Dmol3 approach, *Journal of Chemical Physics* 113 (2000) 7756.
- [21] Vosko S H, Wilk L, Nusair M, Accurate spin dependent electron liquid correlation energies for local spin density calculations: a critical analysis, *Canadian Journal of Physics* 58 (1980) 1200.
- [22] Perdew J P, Burke K, Ernzerhof M, Generalized gradient approximation made simple, *Physics Review Letters* 77 (1996) 3865.
- [23] Hirshfeld F L, Bonded-atom fragments for describing molecular charge densities, *Theoretical Chemistry Acta* 44 (1977) 129-138.
- [24] Alam M K et al., Study of carbon monoxide oxidation on CeO<sub>2</sub>(111) using ultra accelerated quantum chemical molecular dynamics, *Journal Physical Chemistry C* 113 (2009) 7723.
- [25] Alam M K et al., Modeling of Hydrogen Vacancy for Dissociative Adsorption of H<sub>2</sub> on Pd(111) Surface by a Quantum Chemical Molecular Dynamics, *Catalysis Today* 164 (2011) 9.
- [26] Ahmed F et al., Dynamics of hydrogen spillover on Pt/γ-Al<sub>2</sub>O<sub>3</sub> catalyst surface: a quantum chemical molecular dynamics study, *Journal Physical Chemistry C* 113 (2009) 15676.
- [27] Onodera T et al., A Computational Chemistry Study on Friction of h-MoS<sub>2</sub>. Part I: Mechanism of Single Sheet Lubrication, *Journal of Physical Chemistry B* 113 (2009) 16526.
- [28] Onodera T et al., Development of a quantum chemical molecular dynamics tribochemical simulator and its application to tribochemical reaction dynamics of lubricant additives, *Modelling Simulation Material Science Engineering* 18 (2010) 034009.
- [29] Ewald P P, Die berechnung optischer und elektrostatischer Gitterpotentiale, *Annalen der Physik* 64 (1921) 253-287.
- [30] Carzaferri G, Forss L, Kamber I, Molecular geometries by the extended Hückel molecular orbital method, *Journal Physical Chemistry* 93 (1989) 5366-5371.
- [31] Kubo M et al., Development of tight-binding chemical reaction dynamics simulator for combinatorial computational chemistry, *Applied Surface Science* 223 (2004) 188-195.
- [32] CRC Handbook of Chemistry and Physics. 91st Edition. Edited by W. M. Haynes CRC Press, 2010-2011.
- [33] Fadley C S, Basic concepts of X-ray photoelectron spectroscopy, chapter Electron Spectroscopy, Theory, Techniques and Applications, *Pergamon press* (1978)
- [34] Handbook of the elements and native oxides, 1999 *XPS International, Inc.*
- [35] Buffeteau T, Desbat B, Turlet J M, Polarization Modulation FT-IR spectroscopy of surface and ultra-thin films : experimental procedure and quantitative analysis, *Applied Spectroscopy*, 45 3 (1991) 380.

[36] Ferraro J R, Basile L J, in « Fourier Transform Infrared Spectroscopy » Vol 3, Chap 3, *Edition L. A Nafie and D. W Vidrine, (1993).*

## 6. Summary chapter 2

The drastic improvement in the informatics field over the past decades coupled with the development of new algorithms based on theoretical chemistry enable to study physicochemical phenomenon at the atomistic or the electronic scales more and more precisely. In the present study, we have performed experimental analyses and molecular simulations simultaneously. In fact, the two approaches are complementary so molecular simulations can help the comprehension of experimental results.

This chapter will first present simulation models that have been built in addition to computational techniques, e.g. Molecular Dynamic (MD) simulation, Quantum Chemistry (QC) calculation, and the coupling QC/MD method. Molecular dynamic simulation is based on the resolution of Newton's equation of motion. It enables to study atom-atom interactions for a large complex system composed of thousands of atoms and to follow the motion of those atoms with respect to time up to few nanoseconds. This technique is employed for the qualitative study on the organization of adsorbed films, the evaluation of friction coefficient of studied systems and the evaluation of diffusion coefficient of fatty acids molecules in PAO 4 base oil. Quantum chemistry calculation is based on the resolution of the Schrödinger equation. According to employed approximations, the technique enables to perform quantitative study of electrons-electrons interactions for a system composed of hundreds of atoms (DFT method) or thousands of atoms (TB-QC method) but it is a static method. This method is used to determine atom's charge for MD simulations but also to validate our models by comparing binding energies obtained by DFT and TB-QC. The coupling of MD and TB-QC methods called UA-QCMD is the innovative method used in the present work to follow adsorption mechanisms of C18 fatty acid on iron-based surfaces with respect of time and with respect of different parameters. Moreover, this technique enables to follow the evolution of the adsorbed film during the friction process.

Secondly, experimental approach is presented. Different organic friction modifiers additives and base oil used in the present study, characterization techniques and used tribometer are described. The X-Ray Photoelectron Spectroscopy (XPS) is a surface sensitive technique. It enables an elemental chemical and quantitative analysis of the surface and is used to characterize substrates with adsorbed stearic, oleic and linoleic acids. With even higher sensitivity, the Polarization Modulation-Infrared Reflection-Adsorption Spectroscopy (PM-IRRAS) is used in order to evaluate the film thickness, the composition and molecular structure of substrate with adsorbed layer and with tribofilm (e.g. after friction). Finally, friction tests with a linear reciprocating tribometer enable to determine tribological performance of studied systems in conditions that are close to the cam-tappet contact in the distribution area of the thermal engine.

## 6. Résumé chapitre 2

L'explosion des moyens informatiques, amorcée depuis une vingtaine d'année, et le développement d'algorithmes performants basés sur la chimie théorique, permettent d'étudier des phénomènes physico-chimiques à l'échelle de l'atome et de l'électron de plus en plus précisément. Dans cette étude, nous avons effectué simultanément des analyses expérimentales et des simulations moléculaires. Les simulations pouvant aider à la compréhension des résultats expérimentaux.

Ce chapitre présente dans un premier temps les modèles de surfaces et de molécules qui ont été construits, ainsi que les techniques de dynamique moléculaire (MD), de chimie quantique (QC) et du couplage QC/MD. La dynamique moléculaire est basée sur la résolution de l'équation du mouvement de Newton. Elle permet d'étudier les interactions atomes-atomes d'un système comportant des milliers d'atomes et de suivre le mouvement de ces atomes sur une période allant jusqu'à quelques nanosecondes. Cette technique est employée pour l'étude qualitative de l'organisation des films formés, l'évaluation du coefficient de frottement du système étudié et du coefficient de diffusion des molécules d'acide gras dans la PAO. La chimie quantique est basée sur la résolution de l'équation de Schrödinger. Selon les approximations employées, la technique permet l'étude quantitative des interactions électrons-électrons de systèmes comportant quelques centaines d'atomes (DFT) ou quelques milliers d'atomes (TB-QC) mais reste une méthode statique. Elle est employée dans la détermination des charges pour les simulations MD ainsi que pour la validation des modèles par comparaison des énergies de liaison obtenus par DFT et TB-QC. Le couplage des deux méthodes MD et TB-QC appelée UA-QCMD est la méthode innovante utilisée dans cette étude pour suivre les mécanismes d'adsorption des acides gras C18 sur des surfaces à base de fer au cours du temps en jouant sur divers paramètres. Elle permet également de suivre l'évolution des interactions chimiques durant le processus de frottement.

Dans un deuxième temps, la méthodologie expérimentale est présentée. Les divers additifs organiques modificateurs de frottement et huile de base utilisés, les techniques de caractérisation chimique employées, le tribomètre utilisé sont décrits. La spectroscopie des photoélectrons (XPS) est une technique adaptée à la caractérisation de l'extrême surface des échantillons. Elle permet une analyse chimique élémentaire et quantitative de la surface du matériau et est utilisée dans la caractérisation des surfaces adsorbées par l'acide stéarique, oléique ou linoléique. Avec une plus grande sensibilité, la spectroscopie infrarouge de réflexion-absorption par modulation de polarisation (PM-IRRAS) a également été utilisée dans le but d'identifier l'épaisseur, la composition et la structure moléculaire des surfaces adsorbées et des surfaces frottées. Enfin, des expériences sur le tribomètre linéaire ont été réalisées afin de déterminer les performances tribologiques du système étudiés dans des conditions proches de celle de la région came-poussoir au niveau de la distribution d'un moteur thermique.





## **Chapter 3: Adsorption mechanism of pure C18 fatty acids**

---

## **Chapitre 3: Mécanisme d'adsorption des acides gras C18**

## Chapter 3: Adsorption mechanisms

---

### Table of contents

1. Introduction .....	86
2. Adsorption mechanism: a computational study .....	87
2.1 Qualitative approach: MD simulation .....	87
2.2 Quantitative approach: DFT, TB-QC, UA-QCMD simulations .....	89
3. Analytical characterization of adsorbed fatty acids on different type of surfaces by XPS and PM-IRRAS analysis .....	106
3.1 XPS analysis .....	106
3.2 PM-IRRAS analysis .....	114
4. Conclusion .....	117
5. References .....	119
6. Summary chapter 3 .....	121

### 1. Introduction

The first step in order to understand the tribological behavior of C18 fatty acid on iron-based surfaces is to study the adsorption mechanism (that occurs during the formation of the thermal film). Until now, different kinds of experimental analyses as well as MD or static QC simulations have been applied to study the adsorption of stearic, oleic and linoleic acids onto steel surfaces but the complete understanding of the action mechanism is still unclear.

In this thesis, a novel method based on the coupling of MD simulations with QC simulations and an ultra-accelerated method (UA-QCMD) is used in order to understand how molecules interact with the surface and to identify the adsorption mechanism of C18 fatty acids on iron-based model surfaces.

In the present study, the computational work is done with no solvent, e.g. only fatty acids molecule in vacuum, which is not representative of the reality. In fact, the lubrication of thermal engine is in a liquid phase (additives in base oil). Models presented in this part are therefore simplified models.

After a preliminary qualitative analysis by MD simulations, UA-QCMD calculations will be applied considering two models: the adsorption mechanism on iron oxide surface of: 1) a single molecule of stearic acid (called random model) and 2) a self-assembled monolayer (SAM) of stearic acid. The effect of different parameters will be studied: the simulation time, the temperature, the surface composition (iron oxide or hydroxide surface), the number of unsaturations in the fatty acid molecule, the density of molecules in the SAM, and the orientation of molecules with the surface.

In parallel, experimental analyses are made in order to validate the adsorption model obtained by computational work. XPS analyses are performed with the three mentioned fatty acids (stearic, oleic and linoleic acids) on pure iron, iron oxide and native iron oxide,

respectively. In addition, PM-IRRAS analyses are performed on the adsorbed thermal film and compared with XPS results.

## 2. Adsorption mechanism: a computational study

### 2.1 Qualitative approach: MD simulation

#### 2.1.1 “Random” model vs. SAM model

Before performing any quantum chemistry calculations, it is interesting to run some MD simulations in order to better choose between available adsorption models. In the literature, the SAM model is always used as an ideal one and will be used in this study as a reference model (model b in figure 2) for the investigation of the adsorption mechanism. However, in practice, molecules of additives do not reach the surface simultaneously but arrive one after the other and then they arrange themselves. This is why we ran MD simulations where a molecule arrives randomly one after the other (model a) in figure 2), on iron oxide and pure iron surfaces respectively. After 1 ns of MD simulation, some snapshots are taken as shown in figures 1 and 2.

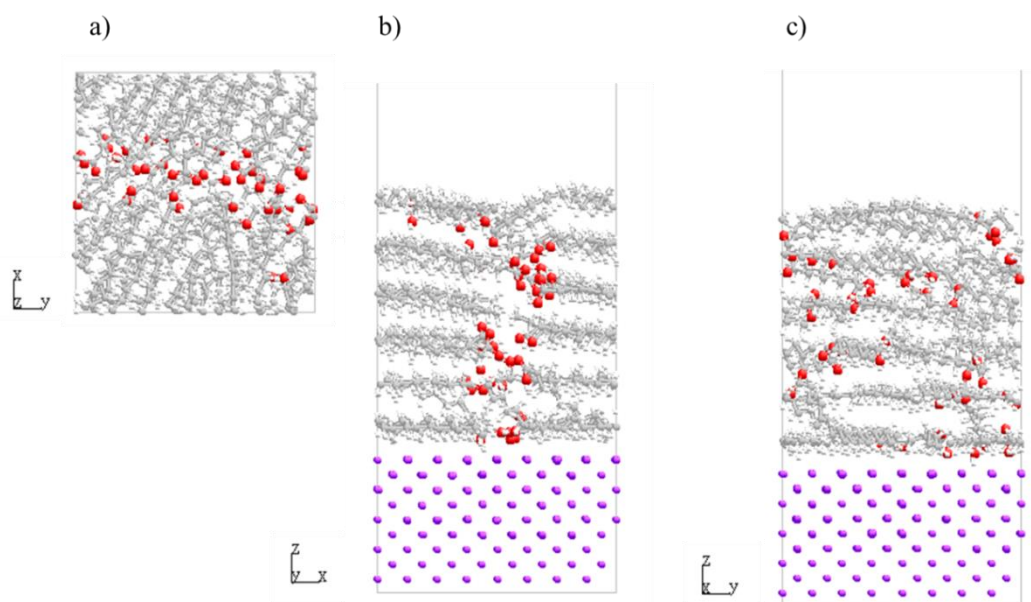


FIGURE 1: SNAPSHOTS IN DIFFERENT DIRECTIONS ( A) (XY), B) (ZX), C) (ZY)) AFTER 1 NS OF MD SIMULATIONS, MODEL A: 24 MOLECULES OF STEARIC ACID ARRIVE RANDOMLY ON THE PURE IRON SURFACE

On pure iron, the first stearic acid molecule arrives on the surface and lays down with the backbone parallel to the surface. Once the surface is fully covered by stearic acid molecules laying on the surface, a second horizontal layering is formed and so on. The configuration after 1 ns of MD simulation is not a SAM at all and is even the opposite. To have the formation of a SAM afterwards, much longer time is probably necessary for the molecules to re-arrange in the SAM structure (typically 12 and 24 hours in case of adsorption experiments) <sup>[1,2]</sup>.

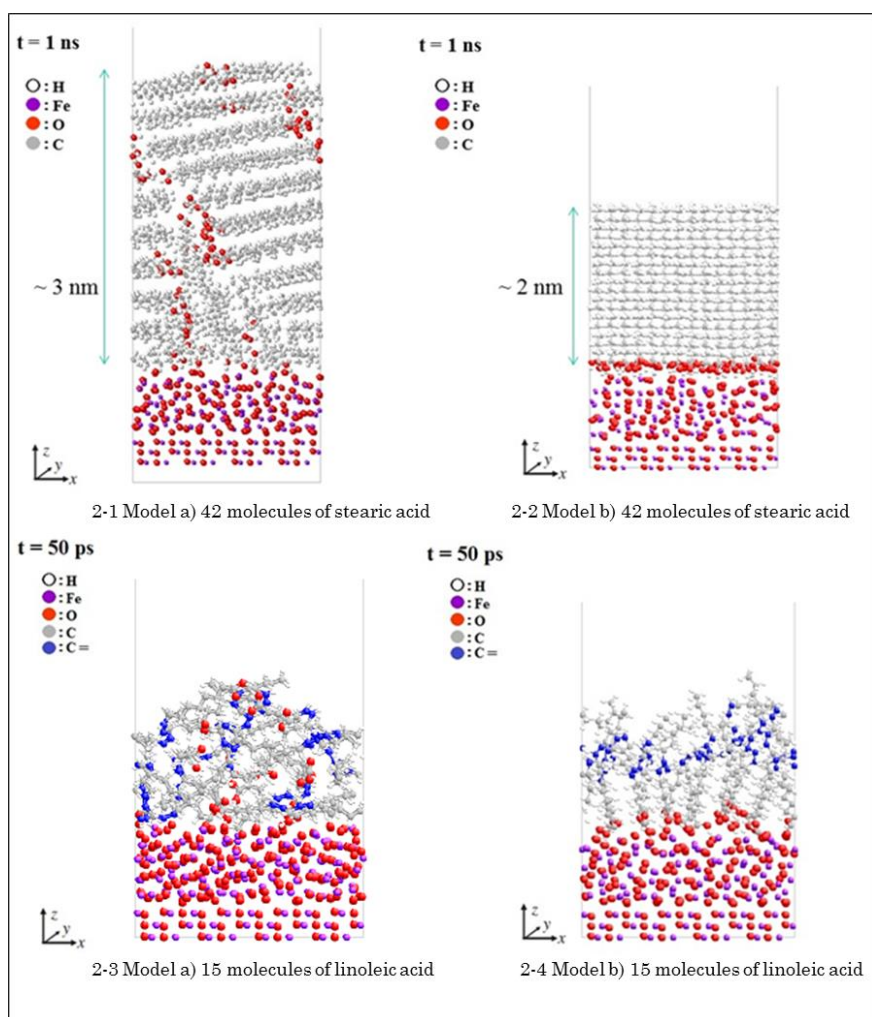


FIGURE 2: SNAPSHOTS OF MD SIMULATIONS AT 50 °C. 2-1: 42 MOLECULES OF STEARIC ACID ON IRON OXIDE AFTER 1 NS USING MODEL A)(RANDOM). 2-2: 42 MOLECULES OF STEARIC ACID ON IRON OXIDE AFTER 1 NS USING MODEL B)(SAM). 2-3: 15 MOLECULES OF LINOLEIC ACID ON IRON OXIDE AFTER 50 PS USING MODEL A). 2-4: 15 MOLECULES OF LINOLEIC ACID ON IRON OXIDE AFTER 50 PS USING MODEL B).

On iron oxide, a) and b) models of adsorption of stearic and linoleic acids molecules are compared. Figure 2 represents snapshots of MD simulations after 1 ns for stearic acid (figure 2-1 and 2-2) and 50 ps for linoleic acid (figure 2-3 and 2-4). It is not necessary to increase further the simulation time because the energy of the system is quite constant (see § 2.2.1.3). Probably, the SAM formation is kinetically very slow so MD simulation reaches its limit in terms of time scale to observe the SAM formation.

For model a), molecules lay down parallel to the surface due to Coulomb and van der Waals interactions (see figure 2-1 and 2-3). The layering is more obvious for stearic acid than for linoleic acid because double carbon bonds induce steric effects.

Results are completely different with model b) (see figure 2-2 and 2-4). When a SAM of stearic acid molecules is placed on iron oxide surface, the adsorption is effective through polar groups although it is not possible to distinguish whether the adsorption is symmetric or asymmetric. In model a) (figure 2-1), acid groups are localized at different “heights” in the whole contact whereas in model b) (figure 2-2), acid groups are localized only at the interface with the substrate.

In addition, the stearic acid film thickness for the same number of molecules is around 3 nm for model a) (figure 2-1) compared to 2 nm for model b) (figure 2-2).

Both models present some similarities with linoleic acid on iron-based surfaces in terms of organization and thickness of the film. The SAM is disordered and cannot be well-distinguished because of steric effect. The only difference between the two models is the localization of acid groups (all located at the interface substrate/additives vs. located at different “heights” in model b and a respectively).

MD simulation can give qualitative analysis of the orientation of molecules and can be used as a first screening procedure when designing new molecules. However MD cannot treat with chemical reactions. The following part will focus on the adsorption mechanism that occurs during the formation of the adsorbed film.

## 2.2 Quantitative approach: DFT, TB-QC, UA-QCMD simulations

### 2.2.1 Stearic acid: single molecule vs. single molecule included in SAM (50 °C, $\text{Fe}_2\text{O}_3$ )

#### 2.2.1.1 Adsorption mechanism of a single molecule

The interaction between a single stearic acid molecule and an iron oxide surface is here studied in detail. Initially, the fatty acid molecule is far enough from the iron oxide surface in order to avoid any interactions and an initial velocity is given to respect the Boltzmann law. When simulation time increases, the molecule moves randomly and at a certain time, it reaches the surface where it lies down. This position is kept until the end of the simulation time as presented in figure 3.

Figure 4 shows inter and intra-molecular interactions between the acid group (oxygen and hydrogen atoms) and the substrate (as iron atoms). Table 1 gives inter and intra-molecular interactions total energies of stearic acid at initial and final steps, e.g.  $t = 0$  ps and  $t = 15$  ps. Special attention is paid to atomic bond populations (BP) that can clarify whether the bond dissociates or not. The BP quantifies the presence (or absence) of electrons in the considered pair and also then the absence or presence of covalent bonding between the two atoms. Total energy ( $E_{\text{total}}$ ), is the sum of (i) interatomic energy caused by molecular orbital interaction, (ii) inter-atomic energy caused by Coulomb interaction and (iii) inter-atomic energy caused by atomic core repulsion.

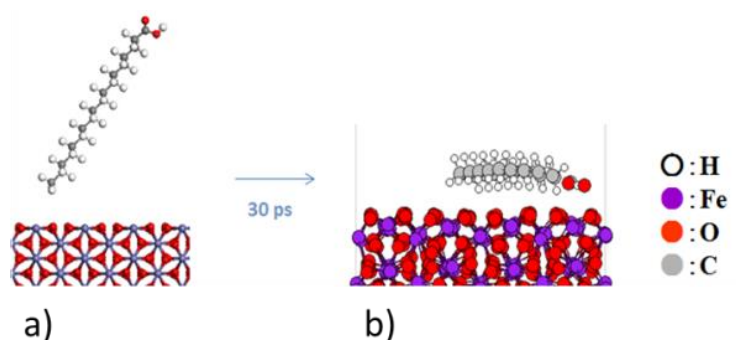
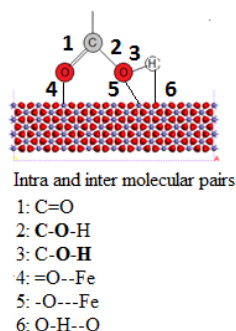


FIGURE 3: A SINGLE STEARIC ACID MOLECULE ON AN IRON OXIDE SURFACE DESIGNED WITH MATERIAL STUDIO® SNAPSHOTS A): AT INITIAL CONFIGURATION. B): AFTER 30 PS OF SIMULATION

FIGURE 4: REPRESENTATION OF DIFFERENT INTERACTIONS PAIRS BETWEEN A SINGLE STEARIC MOLECULE ACID AND A  $\text{Fe}_2\text{O}_3$  SURFACE

At initial step, BP is equal to 1.09, 0.69 and 0.63 for C=O, C-OH and O-H pairs, respectively. At the same time, total energy is -199.2, -134.0 and -115.4 kcal/mol for the same pairs. These results show that the molecule is not dissociated in the vacuum when it is far from the surface. In addition, there is no initial interaction with the substrate as BP and total energy are 0 for all inter-molecular pairs.

After 15 ps, both BP and total energy (the absolute value) of intra-molecular pairs decrease slightly. Inter-molecular BP is equal to 0 for all considered pairs between the molecule and the substrate. Nevertheless, final total energy of inter-molecular pair increases to 6.01, 9.81 and 7.32 kcal/mol for =O---Fe, H---O and HO---Fe, respectively. This indicates that the molecule of stearic acid lying on the surface interacts only weakly with the substrate. As a definition, the adsorption mechanism is said to be a physisorption through the acid group.

TABLE 1: BOND POPULATION (BP) AND TOTAL ENERGY ( $E_{\text{TOTAL}}$ ) OF DIFFERENT INTRA AND INTER-MOLECULAR PAIRS AT INITIAL AND FINAL STEP (15 PS) FOR A SINGLE STEARIC ACID MOLECULE ADSORPTION ON AN IRON OXIDE SURFACE AT 50°C BY UA-QCMD

Pair	Initial step		Final step	
	BP**	$E_{\text{total}}^*$ (kcal/mol)	BP**	$E_{\text{total}}^*$ (kcal/mol)
<i>Intra-molecular pairs</i>				
C=O	1.09	-199.2	1.07	-196.8
C-O-H	0.69	-134.0	0.58	-130.7
C-O-H	0.63	-115.4	0.62	-114.2
<i>Inter-molecular pairs</i>				
=O---Fe	0.00	0.00	0.00	-6.01
-O-H---O	0.00	0.00	0.01	-9.81
-O---Fe	0.00	0.00	0.00	-7.32

$$*E_{\text{total}} = E_{\text{mo}} + E_{\text{cl}} + E_{\text{er}}$$

$E_{\text{mo}}$ : interatomic energy caused by molecular orbital interaction

$E_{\text{cl}}$ : interatomic energy caused by coulomb interaction

$E_{\text{er}}$ : interatomic energy caused by atomic core repulsion

\*\*BP: Bond population

This UA-QCMD simulation was run three times with different initial position of the molecule far from the surface. The same final state was reached for the three simulations.

### 2.2.1.2 Adsorption mechanism of SAM

A SAM of 15 molecules (in a liquid-like state) was deposited above the flat iron oxide surface. To do so, molecules were first placed initially as close as possible to the surface but without any initial interactions with the surface. After 10 ps of UA-QCMD simulation, BP and energy values were recorded on all stearic acid molecules. A snapshot of the cell is shown as



shown in figure 5-c. Among the 15 molecules, 11 were chemisorbed through the carboxyl group, 1 molecule was chemisorbed through the hydroxyl group and 3 were physisorbed through the acid group. In the following, we are going to explain in detail the main adsorption mechanism, i.e. the chemisorption through the carboxyl group.

Table 2 gathers inter and intra-molecular interactions energies in the case of only one molecule of stearic acid chemisorbed through the carboxyl group. This molecule was chosen between the 11 which were chemisorbed and was inside the SAM at initial and final step, e.g.  $t = 0$  ps and  $t = 15$  ps. The analysis focuses on atomic bond population (BP), bond length, electric charges (see § 3.1.4) and total energy ( $E_{\text{total}}$ ).

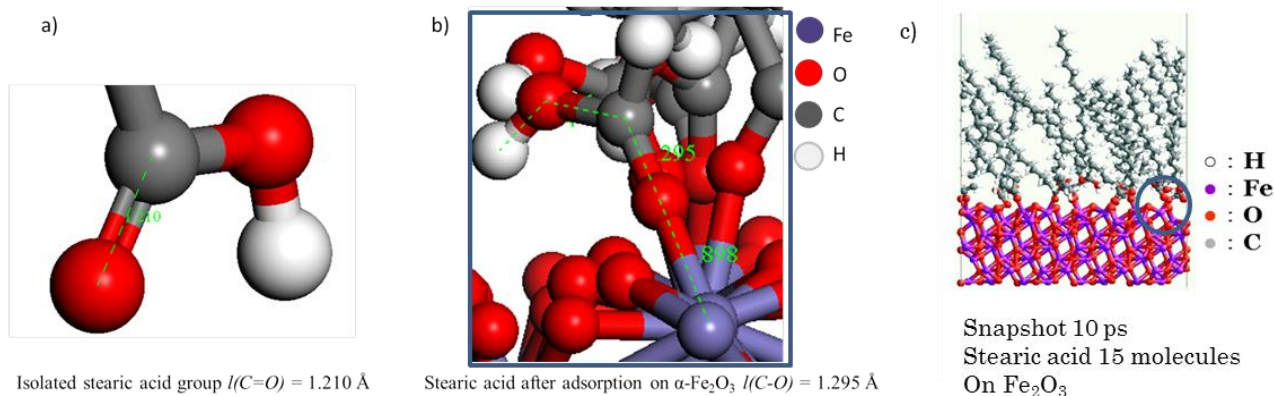


FIGURE 5: SNAPSHOT: A) ISOLATED STEARIC ACID ZOOMED ON THE ACID GROUP, B) ZOOMED ADSORPTION CONFIGURATION OF THE ACID GROUP, C) SAM 15 STEARIC ACID MOLECULES ON IRON OXIDE SURFACE AFTER 10 PS OF UA-QCMD SIMULATIONS AT 50 °C

At initial step, BP is equal to 1.03, 0.65 and 0.59 for C=O, C-OH and O-H intra-molecular pairs, respectively. Total energy is -188.5, -120.0 and -111.7 kcal/mol for the same considered pairs. These results are very similar to that obtained with a single molecule, suggesting that the presence of neighboring molecules in the SAM structure does not change significantly the mechanism. The slight difference comes from the cohesion force between the different alkyl chains. For  $=\text{O} \cdots \text{H}$ ,  $\text{O} \cdots \text{Fe}$  and  $\text{O}-\text{H} \cdots \text{O}$  bonds,  $\text{BP} = 0$ ,  $E_{\text{tot}} = 0$  kcal/mol showing that there is no interaction between the stearic acid molecules in the SAM and the substrate.

Between initial and final steps, there are slight differences of BP and total energy for the bonds inside the carboxyl group. The largest difference is for the C=O pair where the BP decreases from 1.03 to 0.92 and total energy decreases to 19.1 kcal/mol. The situation is very different for the bonds formed between the carboxylic group and the iron oxide: BP of  $=\text{O} \cdots \text{Fe}$  inter-molecular pair increases up to 0.45 and total energy reaches -86.5 kcal/mol. Other inter-molecular pairs have  $\text{BP} = 0.00$  and very small total energies. These results suggest that the  $\pi$  bond is strongly delocalized from intra to inter-molecular pairs. In fact, C=O bond is stronger than C-OH bond because it has two bonds:  $\sigma$  bond and  $\pi$  bond.  $\pi$  bond is weaker than  $\sigma$  bond and, therefore, it is easier to break. Final BP analysis indicates that there is a new chemical bond formed between the molecule (through the carboxyl C=O group) and the iron atoms of the substrate. The other part of the acid group also interacts but weakly and can be then neglected in a first approximation.

In addition, figure 5-b shows a zoomed adsorption configuration of the acid group on the surface. The stearic acid molecule is chemisorbed through the carboxyl group as we previously pointed out. The C=O bond length increases from 1.21 Å to 1.29 Å between the isolated state in vacuum (figure 5-a) and the chemisorbed state on the surface (figure 5-b). The increase of the C-O bond length confirms that the original C=O double bond is weakened. The formation of the C-O-Fe bonding is due to delocalization of  $\pi$  electrons from the carbonyl group

to this newly formed bond inducing a strong attachment of the fatty acid molecule on the surface.

TABLE 2: BP AND  $E_{\text{TOTAL}}$  OF DIFFERENT INTRA AND INTER-MOLECULAR PAIRS AT INITIAL AND FINAL STEPS FOR ADSORPTION OF A CHOSEN MOLECULE INSIDE THE SAM FOR 15 MOLECULES OF STEARIC ACID ON IRON OXIDE SURFACE AT 50 °C BY UA-QCMD

Pair	Initial step		Final step	
	BP**	$E_{\text{total}}^*$ (kcal/mol)	BP**	$E_{\text{total}}^*$ (kcal/mol)
<i>Intra-molecular pairs</i>				
C=O	1.03	-188.5	0.92	-169.4
C-O-H	0.65	-120.0	0.68	-121.6
C-O-H	0.59	-111.7	0.58	-106.5
<i>Inter-molecular pairs</i>				
=O---Fe	0.00	0.00	0.45	-86.5
-O-H---O	0.00	0.00	0.00	-3.19
-O---Fe	0.00	0.00	0.00	-4.67

$$*E_{\text{total}} = E_{\text{mo}} + E_{\text{cl}} + E_{\text{er}}$$

$E_{\text{mo}}$ : interatomic energy caused by molecular orbital interaction

$E_{\text{cl}}$ : interatomic energy caused by coulomb interaction

$E_{\text{er}}$ : interatomic energy caused by atomic core repulsion

\*\*BP: Bond population

In previous calculations, simulation of single molecule model was run for 15 ps and SAM model was run for 10 ps. Of course, this is very short compared with reality and we have to check if the equilibrium is achieved.

### 2.2.1.3 Influence of simulation time in the case of chemisorption

In order to study if stearic acid molecules achieve equilibrium once they reach the surface, the time of simulation was increased from 15 ps to 30 ps in the case of the chemisorbed single molecule. Figure 6 shows the evolution of the inter-molecular =O---Fe pair total energy as a function of time.

The plot is divided into three parts. For the first 5 ps, there is no interaction between the substrate and the molecule of stearic acid because the molecule is initially too far from the surface as we pointed out before. Then, a transition period occurs where electronic interactions between stearic acid and iron oxide atoms begin to appear. Eventually, after 15 ps, the system reaches an equilibrium and this explains why the molecule does not leave the surface.

It can be noticed that the energy value at equilibrium state is lower than the one during transition time. This is due to the effect of the velocity of the molecule when it arrives toward the surface.

From the figure 6, we deduced that it is better to run 20 ps simulation time in order to reach the equilibrium state. Then, the SAM model was also run for 20 ps and the same final state was reached after 10 ps. In addition to the evolution of pair energy with respect to time, the evolution of the mean square displacement is also performed to confirm the achievement of equilibrium state.



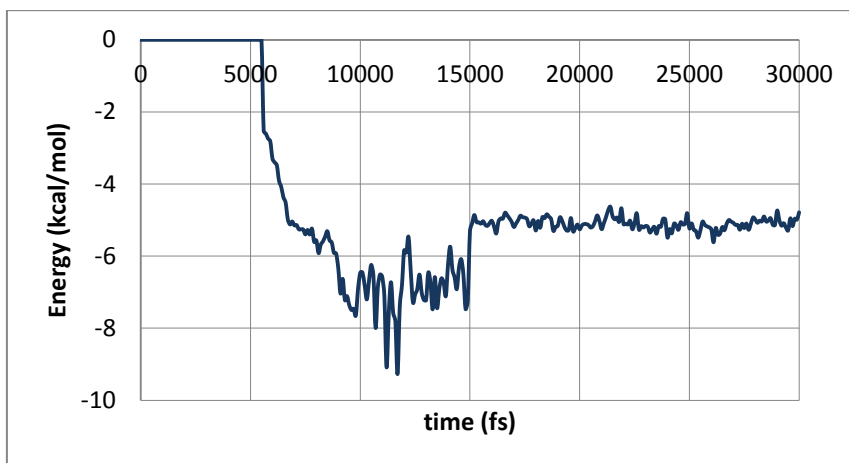


FIGURE 6: TOTAL ENERGY (EMO + ECL + EER) AS A FUNCTION OF TIME FOR THE INTRA-MOLECULAR PAIR C=O--FE OF STEARIC ACID MOLECULE ON IRON OXIDE SURFACE AT 50 °C CALCULATED BY UA-QCMD

Here we show that the adsorption kinetics of stearic acid on iron oxide surface can be very fast in the case of the chemisorption because only 20 ps is enough to reach equilibrium (figure 6). Afterwards, this molecule cannot leave its adsorption site. However, in the SAM situation with lower densities of molecules, the equilibrium state of the whole structure can change for much longer time because weakly physisorbed molecules can desorb and change adsorption sites continuously until they find a stable chemisorption state.

#### 2.2.1.4 Discussion on molecular models

As we stated before, it is important to notice that this analysis is only valid for short time (far less than one second of adsorption and in vacuum). In practical cases, during hours, some changes may occur. Unfortunately, this cannot be analyzed by our computational method. In practice, the formation of SAM on the surface is a long process as shown on the literature [1]. The formation of SAM from the “random” model cannot be observed at our time scale because it takes more than 12 hours to form the SAM naturally. This is why our MD simulations have been performed using two extreme models: the “random” model for one molecule (an initial state) and the SAM model (a final state). Between the two extreme cases, it has been also shown (using *in lubro* AFM studies) that the adsorbed film forms patchy and that the first molecules chemisorbed act certainly as a precursor for further chemisorbed molecules in forming SAM platelets [H. Spikes, private communication]. In the engine, the mechanical devices are in movement. Therefore, there is less time to form the thermal film. It is assumed that the real case is an intermediate state between the full SAM model and the “random” model.

The main result of this computer simulation study is that there is a clear difference between the adsorption mechanism on iron oxide surface of (i) an isolated molecule of stearic acid and (ii) one stearic acid molecule present in a SAM.

In the presence of an isolated molecule of stearic acid on iron oxide surface, results show (Table 1) that the chain does not break during the adsorption process. Regarding the slight difference in total energy  $E_{total}$  of intra-molecular pairs at initial and final steps, electrons from the acid group are delocalized to a different inter-molecular pair with the substrate, indicating only a physisorption of the acid group. Concerning the aliphatic chain lying on the surface, van der Waals interactions occur.

This fact was already highlighted by MD simulations performed by Greenfield and Ohtani [3]. In this case, the molecule is free to move in all directions like in vacuum. Physisorption of fatty acids in vacuum has already been studied by Ratoi et al. [4]. It is

important to emphasize that the computational work was done with no solvent whereas experimental analyses found in the literature were done in a liquid phase (with hexadecane or dodecane). Therefore, adding hydrocarbon molecules might prevent the molecule from laying down parallel to the surface, or may change the time necessary for the molecule to reach the surface.

On the other hand, the investigation of the adsorption mechanism of SAM model leads to a majority of chemisorbed molecules through the carboxyl group. It is obvious that it is energetically easier to break a  $\pi$  bond than a  $\sigma$  bond [5]. Nevertheless, many authors have mentioned that the adsorption mechanism is a chemisorption leading to the formation of metal carboxylate. Our results with molecular simulations show that no hydrogen dissociation has been observed during the adsorption process. In fact, it has been highlighted by Hsu et al. that the formation of carboxylate occurred in air without activation process but has a really slow kinetic rate [6]. This may explain why it cannot be observed with our UA-QCMD method working only a few ps.

In a SAM containing 15 molecules of stearic acid, it has been shown that only few molecules are physisorbed through the acid group or chemisorbed through the hydroxyl group. On the “liquid like” system, stearic acid seems to arrive on the surface with different orientation as suggested by observation of snapshot presented in figure 5-c. At this step, the question arising concerns the role of the orientation of stearic acid molecules regarding the surface on the adsorption mechanism.

### 2.2.2 Influence of orientation

The influence of the position was investigated in this work by imposing different orientations and studying the adsorption mechanism.

TB-QC calculations are run for nine different initial positions as shown in figure 7. The angle that is studied is defined as the angle between the alkyl chain and the horizontal surface. As TB-QC is a static computational method, different positions of the molecule of stearic acid on the iron oxide surface are imposed. Table 3 gathers final BP and final total energy of three different pairs: C=O—Fe, HO—Fe and C-OH—O for the different orientations of stearic acid.

In model 1, BP of HO—Fe is 0.20 and total energy is -38.4 kcal/mol corresponding to chemisorption, whereas the carboxyl group is only physisorbed with energy of -13.8 kcal/mol. In this case, the stearic acid molecule is physisorbed through the acid group and almost chemisorbed through the hydroxyl group.

In model 2 to 8, the molecule is chemisorbed through the carboxyl group with the delocalization of the  $\pi$  bond. BP is around 0.40 and total energy of C=O—Fe pair is around -79 kcal/mol. When the angle between the alkyl chain and the surface increases, the decrease of the BP and the energy for the C=O—Fe pair is observed. In fact, in model 5, there is almost a symmetric chemisorption as the BP and total energies of HO—Fe pairs are 0.17 and -34.3 kcal/mol, respectively.

In model 9, the BP and total energy decrease down to 0.22 and -45.4 kcal/mol that is the limit between chemisorption and physisorption. Regarding the C-OH—O pair, there is no influence of the angle between the alkyl chain and the surface as the BP and total energy of the pair remain almost constant.

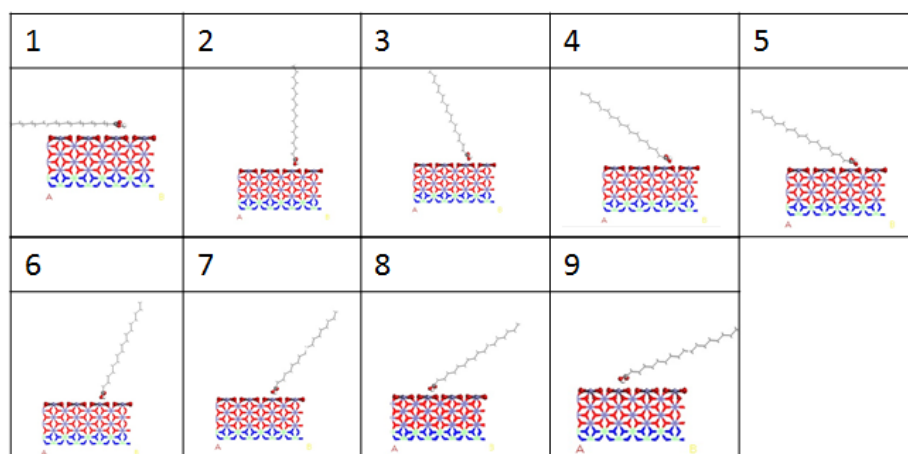


FIGURE 7: DIFFERENT POSITIONS OF STEARIC ACID MOLECULE TOWARD IRON OXIDE SURFACE FOR TB-QC CALCULATIONS.

TABLE 3: BOND POPULATION AND TOTAL ENERGY AFTER RUNNING STATIC TB-QC CALCULATIONS FOR THREE DIFFERENT PAIRS (C=O--Fe, HO--Fe AND C-OH---O) AND NINE DIFFERENT POSITIONS

Model number (Fig.8)	C=O---Fe		HO---Fe		C-OH---O		Adsorption
	Final BP**	Final $E_{total}^*$ (kcal/mol)	Final BP**	Final $E_{total}^*$ (kcal/mol)	Final BP**	Final $E_{total}^*$ (kcal/mol)	
1	0.04	-13.8	0.20	-38.4	0.00	-6.68	~Chemisorption C-OH
2	0.41	-79.9	0.00	-5.46	0.01	-9.71	Chemisorption C=O
3	0.45	-87.3	0.02	-8.81	0.01	-9.71	Chemisorption C=O
4	0.34	-67.2	0.08	-18.2	0.00	-8.33	Chemisorption C=O
5	0.37	-74.1	0.17	-34.3	0.00	-9.54	~Chemisorption symmetric
6	0.48	-92.5	0.00	-4.95	0.01	-10.5	Chemisorption C=O
7	0.42	-81.4	0.01	-5.39	0.01	-7.48	Chemisorption C=O
8	0.36	-70.4	0.01	-7.63	0.01	-5.91	Chemisorption C=O
9	0.22	-45.4	0.02	-9.11	0.01	-5.84	Chemisorption C=O

\* $E_{total} = E_{mo} + E_{cl} + E_{er}$  $E_{mo}$ : interatomic energy caused by molecular orbital interaction $E_{cl}$ : interatomic energy caused by coulomb interaction $E_{er}$ : interatomic energy caused by atomic core repulsion

\*\*BP: Bond population

In addition, rotation of the acid group position toward the surface (figure 8) was also investigated and leads to the same conclusion: depending on the position of the two oxygen atoms on the surface, different adsorption mechanisms can occur: symmetric (= through the two oxygens) or asymmetric (= through one of the oxygen) chemisorption or physisorption, while keeping the hydrogen of the hydroxyl group and, therefore, the acid function. Crowell et al. have defined mono-dentate, bridging and bi-dentate adsorption for aluminum substrate <sup>[7, 14]</sup> (see *chapter 1 § 2.2.1.1*). This definition is mainly used when a carboxylate is formed even though it is not always clear whether the hydrogen is dissociated or not from the hydroxyl group.

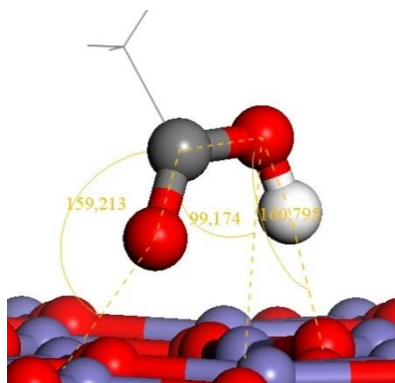


FIGURE 8: ANGLE MEASUREMENT BETWEEN THE ACID GROUP OF SA AND IRON OXIDE SURFACE

The adsorption of carboxylic acids on Zn-ZnO(0001) surface has been investigated by DFT calculations with dispersion forces [9]. Different position has been imposed in order to study different adsorption mechanisms. The most stable mechanism for carboxylic acid on the Zn-ZnO surface is a dissociative bridging adsorption with the carboxylate group attached to two Zn atoms and the proton transferred to the neighboring Zn atom to form Zn-H bond.

This study confirms that the orientation of molecules reaching the surface influences definitely the adsorption mechanism. This is true for hematite ( $\text{Fe}_2\text{O}_3$ ) in our case but depending on the environment, different oxides or hydroxides layers can cover the iron substrate and, therefore, the reactivity between stearic acid molecule and the substrate can be modified. This is examined in the following section.

### 2.2.3 Influence of the substrate

Simulations were performed by changing the nature of the substrate. Pure iron, iron oxide and an iron hydroxide were investigated.

#### 2.2.3.1 Adsorption mechanism of a single molecule

This section focuses on the interaction between a single molecule of stearic acid and an iron-based surface. At the beginning, the stearic acid molecule is far ( $\sim 10 \text{ \AA}$ ) from the surface in order to avoid any interactions between the substrate and the molecule. When simulation time increases, we have already shown that the molecule eventually reaches the pure iron and iron oxide surface and lies down. On another hand, the molecule bounces on the iron hydroxide surface. Table 4 gathered the most interesting inter and intra-molecular interactions energy values of stearic acid and iron based surfaces at initial and final steps, e.g.  $t = 0 \text{ ps}$  and at  $t = 15 \text{ ps}$ .

At initial step, in all cases, there is no interaction between the molecule and the substrate because BP and total energy are equal to 0 for all inter-molecular pairs.

On pure iron, between initial and final steps, there is a difference in the C=O pair because we find that the BP decreases from 1.2 to 1.0 and the total energy of the pair shows a 20.5 kcal/mol decrease. In the meantime, BP of C=O—Fe inter-molecular pair increases up to 0.5 and total energy up to -69.6 kcal/mol. The other considered inter-molecular pairs have a BP equal to 0 and very small total energy. Final BP analysis indicates that there is a chemical bond between the molecule and the iron atoms: the stearic acid molecule is always chemisorbed on the pure iron surface.

On iron oxide surface, it has already be shown previously that the stearic acid molecule is physisorbed because the molecule lays down parallel to the substrate (§ 2.2.1.1).

On iron hydroxide, BP and total energy do not change between initial and final steps for intra and inter-molecular pairs of stearic acid. There is no attachment of the molecule when the surface is saturated by O-H group.

It can be concluded that the reactivity between a single molecule of stearic acid and iron-based surfaces decreases when oxidation/hydroxylation of the surface increases.

TABLE 4: BP AND TOTAL ENERGY OF DIFFERENT INTRA AND INTER-MOLECULAR PAIRS AT INITIAL AND FINAL STEP (15 PS) FOR A SINGLE STEARIC ACID MOLECULE ADSORPTION ON AN PURE IRON, IRON OXIDE, IRON HYDROXIDE SURFACE RESPECTIVELY AT 50 °C BY UA-QCMD.

		Fe				Fe <sub>2</sub> O <sub>3</sub>				FeOOH			
Pair		Initial BP**		Final E (kcal/mol)*		Initial BP		Final E (kcal/mol)		Initial BP		Final E (kcal/mol)	
Stearic acid	<i>Intra-molecular interactions</i>												
	C-OH	0.7	-134.9	0.7	-133.1	0.7	-134.0	0.6	-130.7	0.7	-134.1	0.7	-134.6
	C=O	1.2	-210.1	1.0	-189.6	1.1	-199.2	1.1	-196.8	1.1	-209.4	1.1	-206.5
	O-H	0.6	-111.9	0.6	-112.1	0.6	-115.4	0.6	-114.2	0.6	-110.6	0.6	-111.4
	<i>Inter-molecular interactions</i>												
	Fe-OH	0	0	0.0	-8.81	0	0	0	-7.32	0	0	0	0
	Fe-O=	0	0	0.5	-69.6	0	0	0	-6.01	0	0	0	0
	O-HO	-	-	-	-	0	0	0	-9.81	0	0	0	0

$$*E = E_{mo} + E_{cl} + E_{er}$$

$E_{mo}$ : interatomic energy caused by molecular orbital interaction

$E_{cl}$ : interatomic energy caused by coulomb interaction

$E_{er}$ : interatomic energy caused by atomic core repulsion

\*\*BP: Bond population

### 2.2.3.2 Adsorption mechanism of SAM

A SAM of 15 molecules is deposited above the different iron-based surfaces. After 10 ps of UA-QCMD calculation, snapshots of the cell are taken and shown in figure 9. By visualization only, it is clear that pure iron surface is more reactive with stearic acid molecules than both iron oxide and hydroxide ones. On pure iron, all molecules have same orientation and are chemisorbed on the surface through the acid group. On iron hydroxide, molecules are not adsorbed on the surface and the well-arranged monolayer does not remain intact.

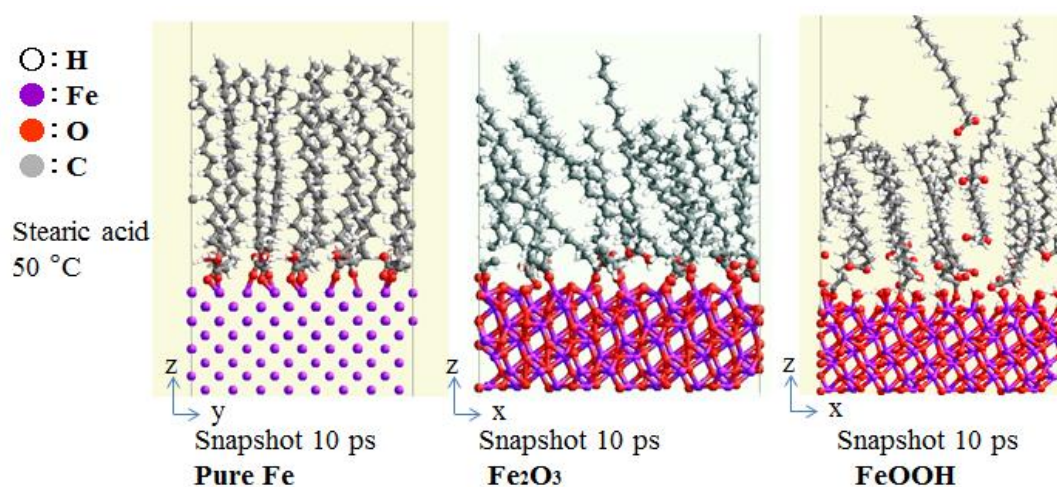


FIGURE 9: SNAPSHOT AFTER 10 PS OF UA-QCMD: SAM 15 MOLECULES OF STEARIC ACID ON PURE IRON, IRON OXIDE AND IRON HYDROXIDE RESPECTIVELY AT 50 °C

Table 5 summarizes the ratio of the different adsorption types that can occur as a function of the iron-based surfaces.

On pure iron surface, all acids molecules are chemisorbed through the carboxyl group with a mean binding energy of -54 kcal/mol. The influence of orientation has also been studied. Results show that whatever the position, the molecule always chemisorbs through the carboxyl group.

On iron hydroxide surface, most of the molecules are physisorbed through the acid group or even bounce on the surface, which is poorly reactive. Nevertheless, a few molecules can find an adsorption site and interact with iron.

As for the single molecule, reactivity between stearic acid in SAM configuration and iron-based surface decreases when oxidation/hydroxylation increases.

During the formation of the adsorbed film, hydrogen atom is not dissociated from the hydroxyl group. The acid function molecular architecture is then conserved.

TABLE 5: PROPORTION OF DIFFERENT POSSIBLE ADSORPTION MECHANISM FOR SAM OF STEARIC ACID ON IRON-BASED SURFACE AT 50 °C

SAM 15 molecules	substrate	Symmetric Physisorption acid group	Asymmetric Chemisorption carboxyl group	Asymmetric Chemisorption hydroxyl group	No adsorption
Stearic	Fe <sub>2</sub> O <sub>3</sub>	20%	70%	10%	0%
Stearic	Fe	0%	100%	0%	0%
Stearic	FeOOH	50%	13,3%	6,7%	30%

Steel surfaces that are exposed to ambient air and moisture are always partially covered with oxides and hydroxides where fatty acid molecules bind to the surface <sup>[12]</sup>. This is in contradiction with our results where we find that pure iron surface is more reactive than iron oxide or iron hydroxide surfaces toward fatty acids molecules. In our simulation, the surface is flat as it is at nano-scale but in a real case, the surface contains roughness and defects that can favor the chemisorption of molecules. In addition, the different surfaces are treated separately with molecular simulations whereas experimentally, different surface features are present simultaneously.

On another surface such as aluminum, it has been shown that different nature of surfaces lead to different types of adsorption sites and, therefore, different adsorption mechanisms. In fact, stearic acid binds to sapphire surface via bi-dentate interaction of carboxylate with two oxygen atoms while it binds to alumina surfaces via both bi-dentate and mono-dentate interactions <sup>[13]</sup>. In addition, the presence of water favors desorption of stearic acid from the aluminum surface <sup>[13]</sup>. This highlights the importance of having knowledge on the nature of the surface.

In the same way, one LB monolayer of stearic acid bonds to the polycrystalline copper surfaces both symmetrically and asymmetrically through the acid group with a tilt angle from 39° to 49° <sup>[10]</sup>. The tilt angle is in agreement with the one measure for the 'liquid like' model.

All presented data were obtained at 50 °C but it is interesting to focus now on the impact of temperature on adsorption and to study the possibility to observe, for instance, desorption at higher temperature.



### 2.2.4 Influence of temperature

Simulations are carried out under a constant volume and at temperatures of 50, 100 and 150 °C for a SAM of 15 stearic acid molecules and at 20, 50, 150 °C for single molecule of stearic acid in order to investigate potential desorption of molecules at higher temperatures.

TABLE 6: BP AND TOTAL ENERGY OF THE =O—Fe PAIR FOR STEARIC ACID ON IRON OXIDE SURFACE AT FINAL STATE, UA-QCMD SIMULATIONS AT 20, 50 AND 150 °C

Stearic acid pair	BP	Etotal (kcal/mol)	T (°C)	Time to reach equilibrium (ps)
C=O - Fe	0.0	-6.03	20	50
C=O - Fe	0.0	-6.01	50	15
C=O - Fe	0.0	-5.30	150	10

Table 6 displays UA-QCMD simulation results of single molecule of stearic acid on iron oxide surface. Results show only a kinetic effect of temperature on the adsorption mechanism. In fact, the total energy and bond population with respect to temperature does not change significantly as shown in table 6. No desorption is observed and the adsorption energy remains constant. For the same initial position, it takes about 50 ps to reach an equilibrium state at 20 °C, about 15-20 ps at 50 °C and about 10 ps at 150 °C. Of course, in practical cases, the activation of molecules of the base oil may desorb the fatty acid molecule.

In addition, Figure 10 shows snapshots after 100 ps of MD simulations at 50, 100 and 150 °C for the SAM model of stearic acid. Qualitatively, it is observed that the film remains attached on the surface after the simulation and that no molecule is desorbed even at the highest temperature. It seems that the film is adsorbed on the surface through interactions with the acid group.

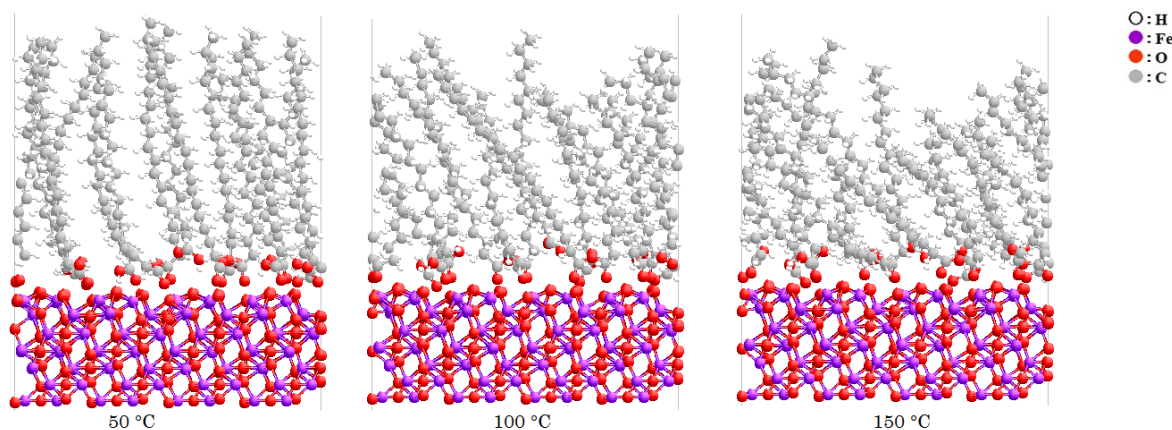


FIGURE 10: SNAPSHOTS AFTER 100 PS OF MD SIMULATIONS AT 50, 100 AND 150 °C OF A SAM CONTAINING 15 MOLECULES OF STEARIC ACID (LIQUID LIKE) ABOVE AN IRON OXIDE SURFACE.

Bowden and Tabor predicted desorption of fatty acids at high temperature as shown on table 7 [19]. In fact, as the temperature is raised, there is an increase in the thermal agitation of the molecules until a temperature where molecules are disoriented and they fade out all together. The desorption temperature was shown to be highly dependent on the substrate material. The transition temperature is much higher than the bulk melting-point (stearic acid melting point is 69 °C) of the fatty acid [20]. Therefore, it is likely that 150 °C is not yet the transition temperature of fatty acids on iron oxide surfaces.

TABLE 7: BREAKDOWN TEMPERATURE FOR DIFFERENT COUPLE LUBRICANT/SURFACE <sup>[19]</sup>

Surfaces	Lubricant	Desorption temperature (°C)
<b>Copper</b>	1% stearic acid	90
<b>Copper</b>	Smear copper stearate	94
<b>Platinum</b>	Smear copper stearate	110
<b>Cadmium</b>	1% stearic acid	130
<b>Cadmium</b>	Cadmium stearate	140
<b>Platinum</b>	Cadmium stearate	140
<b>Steel</b>	Smear sodium stearate	280

The adsorption mechanism quantitatively derived from the computer simulation gives strong evidence to the one proposed by Simic and Kalin at 25 °C and 80 °C which is symmetric or asymmetric adsorption through the acid group <sup>[21]</sup>.

Many parameters have been studied for the adsorption mechanism of stearic acid: the influence of the substrate, the orientation of the molecules, temperature of the system and the simulation time. The same study was applied for oleic and linoleic acids which are unsaturated fatty acids. Main results are presented in the following part.

### 2.2.5 Influence of unsaturation

Figure 11 represents snapshots after 100 ps of MD simulations at 50 °C and on an iron oxide surface, for a SAM model of 15 molecules of stearic, oleic and linoleic acids, respectively. At 100 °C and 150 °C, adsorbed films of oleic and linoleic acid are the same as the one at 50 °C. It is concluded that, like stearic acid, adsorbed films of unsaturated acids behave similarly and no desorption occurred at 150 °C. It is noticed that, like stearic acid, adsorption of oleic acid SAM and linoleic acid SAM occur through the acid group. However, the adsorbed film is more disordered when the number of double bonds in the backbone increases. In fact, steric effect becomes important with double carbon bonds and this prevents the formation of a close-packed monolayer. Then, the thickness of the film is significantly decreased.

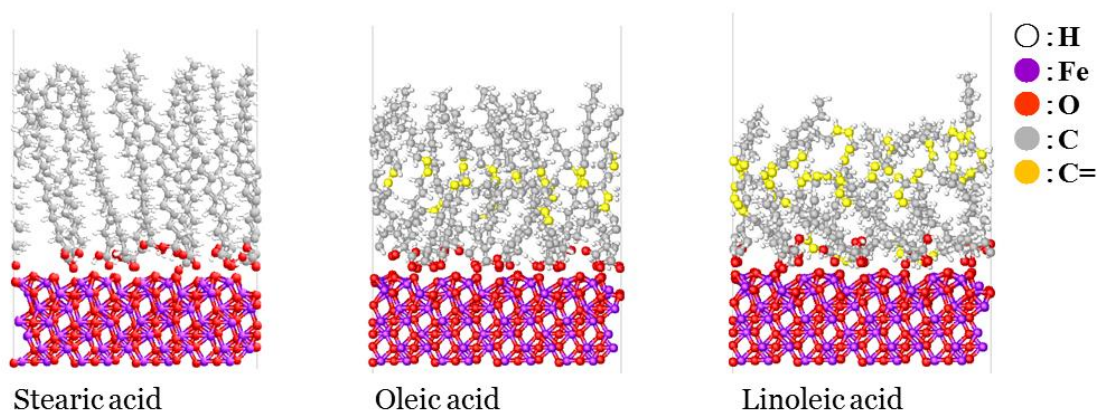


FIGURE 11: SNAPSHOTS AFTER 100 PS OF MD SIMULATIONS AT 50 °C FOR A SAM OF 15 MOLECULES OF STEARIC, OLEIC AND LINOLEIC ACID RESPECTIVELY.



In order to investigate quantitatively the adsorption mechanism on iron oxide surface, UA-QCMD simulations are run on a SAM model of 15 molecules of stearic, oleic and linoleic acids, respectively. Interactions between the fatty acid carboxylic group and the iron from the substrate are investigated at 50 °C. Table 8 gathers the ratio of different possible adsorption mechanisms that can occur for the different fatty acids.

TABLE 8: PROPORTION OF DIFFERENT POSSIBLE ADSORPTION MECHANISM OF STEARIC, OLEIC AND LINOLEIC ACID RESPECTIVELY ON IRON OXIDE SURFACE AT 50 °C

SAM 15 molecules	substrate	Symmetric Physisorption acid group	Asymmetric Chemisorption carboxyl group	Asymmetric Chemisorption hydroxyl group	Symmetric Chemisorption Acid group
Stearic	Fe <sub>2</sub> O <sub>3</sub>	20%	70%	10%	0%
Oleic	Fe <sub>2</sub> O <sub>3</sub>	6.7%	6.7%	26.7%	60%
Linoleic	Fe <sub>2</sub> O <sub>3</sub>	0%	86.7	6.7%	6.7%

On iron oxide surface, the three molecules do not adsorb in the same way but chemisorption is always predominant and is effective through the acid group. This chemisorption can be either symmetric or asymmetric, e.g. through one or the two oxygen atoms of the acid group. The double carbon bond does not have any impact on the adsorption mechanism. The interaction between the carbon from C=C and the surface is around 2 kcal/mol/pair whereas single carbon interaction with the surface is around 1 kcal/mol/pair.

For stearic and linoleic acids, the main adsorption mechanism is chemisorption through the carboxyl group. It is surprising that for oleic acid, the main adsorption mechanism is chemisorption through the two oxygen atoms.

To understand this difference between oleic, stearic, and linoleic acids, Figure 12 shows two snapshots of the models that were taken after geometry optimization of the molecules (oleic and linoleic acids). Stearic acid is not presented because the geometry of the molecule at the surface is exactly the same as linoleic acid. Results clearly show that, after geometry optimization, the hydrogen atom is oriented toward the surface for linoleic acid and parallel to the surface for oleic acid. This favors the adsorption of the hydroxyl group without hydrogen dissociation from the oxygen of the hydroxyl group. Otherwise, hydrogen atoms would have some repulsion with iron and this does not favor the adsorption through the hydroxyl group.

This set of results highlights again the importance of the orientation of the acid group toward the surface in order to understand the adsorption mechanism of fatty acids. Two geometries are possible for the three fatty acids and, therefore, symmetric and asymmetric chemisorptions are possible.

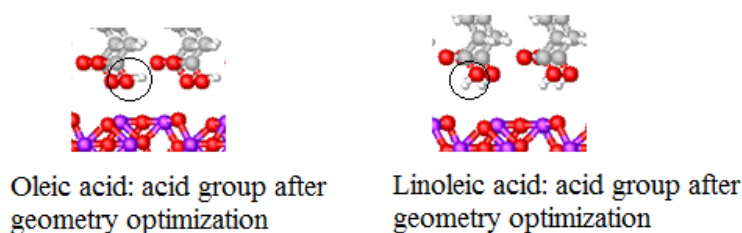


FIGURE 12: SNAPSHOT OF MODEL AFTER GEOMETRY OPTIMIZATION. LEFT: OLEIC ACID, RIGHT: LINOLEIC ACID

To compare the strength of adsorption of each fatty acid, we have selected the same adsorption mechanism type, which is the chemisorption of fatty acid molecules through the carboxylic group. Table 9 gathers the bond population and the total energy for pairs (i) oxygen from the carboxyl group of the molecule and (ii) iron from the iron oxide surface at final step (15 ps). The bond population is  $0.45 \pm 0.01$  for the three fatty acids. The binding energy is similar for the three considered fatty acids and lies between -85.4 kcal/mol and -87.7 kcal/mol.

TABLE 9: BOND POPULATION AND TOTAL ENERGY (SUM OF INTERATOMIC ENERGIES CAUSED BY MOLECULAR ORBITALS, COULOMB INTERACTIONS AND ATOMIC CORE REPULSIONS) CALCULATED BY QC FOR THE OXYGEN FROM CARBOXYL GROUP – IRON FROM SUBSTRATE PAIR AT 50 °C FOR AN ISOLATED MOLECULE EXTRACTED FROM SAM AFTER MD SIMULATIONS OF STEARIC, OLEIC AND LINOLEIC ACIDS

	Pair	BP	E <sub>total</sub> (kcal/mol)
<b>Stearic acid</b>	=O---Fe	0.45	-86.5
<b>Oleic acid</b>	=O---Fe	0.45	-85.4
<b>Linoleic acid</b>	=O---Fe	0.46	-87.7

Therefore, we can deduce that the three fatty acids have the same reactivity towards the iron oxide surface. This means that once a molecule reaches the surface and is chemisorbed, it stays definitely on the surface. Moreover, no desorption is observed at 150 °C. This information will be considered when the competition of OFMs will be investigated in chapter 5.

The difference in monolayer adsorption between stearic and oleic acids has been described as the bend in the hydrocarbon chain of oleic acid prevents the fatty acid from forming a close-packed monolayer <sup>[15]</sup> but it has been shown that the adsorption for stearic and oleic acids onto steel is similar <sup>[16]</sup> which is in agreement with our molecular simulations.

More recently, Lundgren has studied the adsorption of fatty acids in alkanes with Quartz Crystal Microbalance (QCM) technique <sup>[17, 18]</sup>. The adsorbed amount from hexadecane increased with increasing degree of unsaturation which suggests that linoleic acid adsorb in multilayers. Nevertheless, the number of double bonds does not influence the chemisorbed amount as the chemical binding on the surface depends only on the interaction between the fatty acid head group and the surface.

Depending on the number of unsaturation, it can be more or less easy to form a close-packed and well-arranged monolayer to protect the surface from wear and friction. The question that is now raised is how many molecules are on the surface? This is why the effect of different densities was studied by computational chemistry.

### 2.2.6 Influence of density of molecules in the SAM

Depending on the density of acid molecules in the SAM, the plot of surface pressure as a function of the specific area per molecule displays different slopes typically representing gas-like, liquid-like and solid-like states (see Chapter 1 figure 7) <sup>[8]</sup>. In this study, we choose two different densities for stearic, oleic and linoleic acids: 0.027 molecules/Å<sup>2</sup> (~ liquid-like) and 0.042 molecules/Å<sup>2</sup> (still liquid-like for stearic acid but solid-like for oleic and linoleic acids). For stearic acid, a higher density was studied but no comparison could be made with unsaturated molecules. In this last case, the SAM was very compact and perpendicular to the surface.

First MD simulations were run in order to see the arrangement of the monolayer and then UA-QCMD is run in order to study the impact of density on adsorption mechanism. Some snapshots are presented in figures 13 and 14.

Qualitatively, when the density is increased, the monolayer is better arranged. This is also true in the presence of unsaturation. For unsaturated molecules, a steric effect is also present with higher density and some molecules could not reach the surface.

For the liquid-like film, both stearic and oleic acids molecules show different orientations on the surface, leading to different adsorption mechanism as mentioned in the previous parts.

For the solid-like film, molecules have the same orientation towards the surface and quantitative analysis is needed to confirm this observation.

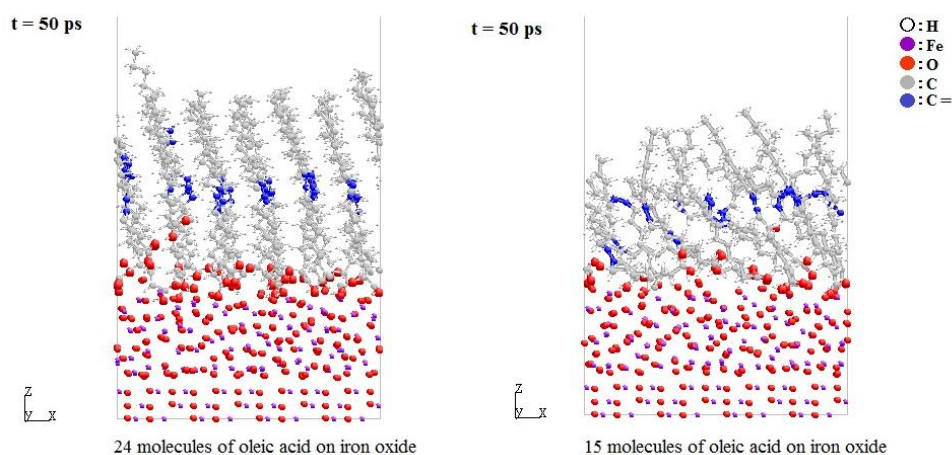


FIGURE 13: EFFECT OF DENSITY- LEFT: SOLID LIKE SAM OF OLEIC ACID ON IRON OXIDE SURFACE, RIGHT: LIQUID LIKE SAM OF OLEIC ACID ON IRON OXIDE SURFACE- SNAPSHOTS AFTER 50 PS OF MD SIMULATION

UA-QCMD simulations show that increasing the density makes the SAM to become more and more densely packed and all molecules are chemisorbed through the carboxyl group with the same range of energy and bond population. This strongly suggests that the SAM model itself imposes an orientation to the molecules and it is this orientation that governs the adsorption mechanism. In a close-packed SAM, molecules can only move through the z axis and are all oriented identically towards the surface. By reducing the density, freedom of molecules increases giving them the possibility to move in different directions and as a consequence, different adsorption mechanisms can result.

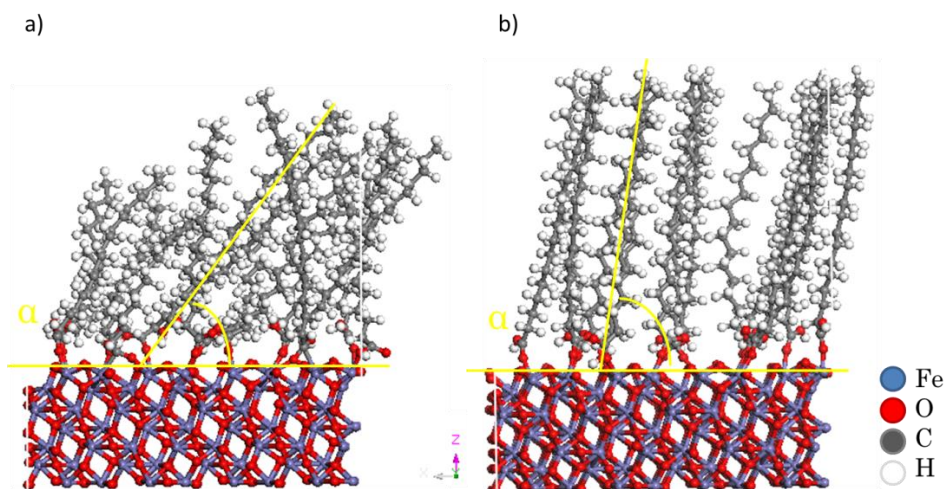


FIGURE 14: UA-QCMD SNAPSHOTS AFTER 15 PS AT 50 °C. EFFECT OF DENSITY WITH: A) 15 MOLECULES OF STEARIC ACID, B) 24 MOLECULES OF STEARIC ACID, ON IRON OXIDE SURFACE, DEFINITION OF THE TILT ANGLE (YELLOW)

It is also noticed in figure 14 that the SAM has naturally a tilt angle noted  $\alpha$  (see figure 14) toward the surface. Table 10 gathered tilt angles, e.g. angle between the alkyl chain and the surface plane as a function of density for (zy) and (zx) plan respectively. The tilt angle increases from about 40 ° to about 80 ° with increasing the density from ‘liquid-like’ to ‘solid-like’ model. In addition, the tilt angle is quite constant ( $\pm 5^\circ$ ) in a ‘solid-like’ SAM.

TABLE 10: TILT ANGLE FOR STEARIC ACID SAM IN DIFFERENT DENSITY PLAN ZY

Density	Min tilt angle	Max tilt angle	Mean tilt angle
<i>plane ZY</i>			
Liquid like	35 °	65 °	43 °
Solid like	83 °	97 °	85 °
<i>plane ZX</i>			
Liquid like	40 °	100 °	45 °
Solid like	75 °	85 °	80 °

Different tilt angles have been imposed to study the most stable position for carboxylic acid with a density of 0.026 molecules/Å<sup>2</sup> on the zinc surface, which is the same density as our ‘liquid like’ model (0.027 molecules/Å<sup>2</sup>) on iron oxide surface. It is shown that the most stable orientation is with a tilt angle of 35 ° in the (yz) plane and it is stable during one pico-second of ab initio MD simulations run at 700 K [9]. This is in agreement with our tilt angle found in the (yz) plane for the liquid like model that is a bit higher (main tilt angle 43 °) but some molecules have a tilt angle of 35 °.

Experimentally, the molecular orientation of a monolayer of stearic acid on copper surface has been quantified by X-ray absorption spectroscopy and the tilt angle is found to be 49 ° [10]. This is in agreement with a ‘liquid like’ model in our computational works.

The question that is raised is why molecules in a SAM configuration are naturally organized with a tilt angle? Ulman shows that the optimized distance between two acid groups in a SAM oriented perpendicular to the surface is between 4.45 and 4.6 Å [11]. In the liquid like model, the distance is 6.6 Å [9], which is larger than the optimized distance. To optimize lateral interactions between the alkyl chains, a tilt of the chains to the surface is therefore needed. Then, van der Waals interactions stabilized the tilted configuration for chain length bigger than 9 carbons [9].

When the surface coverage increases, the distance between two acid groups decreases and, therefore, molecules are close to be perpendicular to the surface as shown in figure 14-b.

In addition, temperature has an effect on the surface coverage. In fact, at 25 °C, when the concentration of fatty acid increases, the surface coverage also increases inducing the increase of bonding sites occupation on the surface and this confirms that fatty acids molecules have good adsorption ability on iron-based surfaces. Fatty acids are physisorbed at 25 °C at low coverage by forming hydrogen bonds with the oxide or hydroxide surface. At higher temperature (80 °C), the mobility of fatty acid molecules is better and a great increase in surface coverage at low concentration is observed in comparison with the surface coverage at 25 °C. The limit of the surface coverage is correlated with the availability of adsorption sites. At higher temperature, fatty acid can form mono-dentate or bi-dentate bonds between carboxyl group and iron-based surface or can also dissociate to lead to the formation of iron carboxylate in a mono-dentate form [21]. The adsorption mechanism type is determined by the nature of the surface.

With molecular simulations, temperature only has a kinetic effect. It seems that temperature in experimental study and density in computational study are correlated. At low

density, some molecules are physisorbed through the acid group with UA-QCMD simulation which is similar to what happened at 25 °C experimentally. On the other hand, at high surface coverage, all molecules are chemisorbed with UA-QCMD simulations which are in agreement to what happened at 80 °C experimentally. The link between temperature and arrangement of molecules is also highlighted by Campen *et al* [22]. She shows that at 35 °C, molecules are less close-packed and *trans* or *cis* molecules lead to the same friction behavior whereas at 100 °C *trans* molecules give a best tribological behavior than *cis* molecules due to the effect on film packing.

### 2.2.7 Synthesis

Both qualitative and quantitative analyses have been made on stearic acid in order to evaluate the impact of different parameters that can affect the adsorption mechanism. The different conclusions can be summarized as follows:

- ✦ A single molecule is found to be physisorbed through the acid group on iron oxide surface. At the opposite, the same molecule inserted in a SAM is mainly chemisorbed through the acid group (carboxyl oxygen) on iron oxide surface.
- ✦ The SAM does not form spontaneously according to preliminary MD simulations.
- ✦ The orientation of the acid function of the molecule, when it just arrives on the surface, is the main driving force for determining the adsorption mechanism
- ✦ Different adsorption mechanisms are possible on iron oxide surface but the main mechanism in the SAM structure is chemisorption through the carboxyl group
- ✦ Reactivity of stearic acid decreases when oxidation/hydroxylation of the surface increases
- ✦ Increasing the density of stearic acid molecules on iron oxide surface favors the same orientation of molecule and a unique adsorption mechanism (chemisorption); it also favors a well arrangement of molecules onto the surface and the formation of a close-packed monolayer
- ✦ Unsaturation has no significant effect on adsorption mechanism of the acid group
- ✦ Unsaturation induces steric effect that prevents the formation of a well arranged and close-packed monolayer
- ✦ Temperature has only a kinetic effect on the adsorption mechanism
- ✦ In all simulations, hydrogen is never dissociated from oxygen of the hydroxyl group; the architecture of the acid function remains intact. However, bond lengths and electric charges on atoms can vary.

These results can be confirmed by other computational methods such as DFT calculations and other analyses rather than only bond population and total energy. It is possible to improve the analysis by quantifying the contribution of long range interaction, molecular orbital, repulsion, etc. and thus, with respect of time. This information is available on output files from MD simulation as shown as an example in annex 2.

In order to build a realistic adsorption model, it is first necessary to start with a very simple model, e.g. one molecule in vacuum, and progressively to improve the model. Continuously, fitting of parameters was performed to improve input's data and this can still be improved in future works.

UA-QCMD seems to be a powerful tool to study the adsorption mechanism of some lubricant additives such as C18 fatty acid on some iron-based surfaces. It is now needed to validate our model and our conclusion extracted from computational work by doing some experimental analyses.

To better understand the performance of lubricant additives and to optimize their formulation, we need first of all to understand their adsorption mechanism. It is always better to combine two different techniques in order to validate our results and model. In this study, XPS analyses as well as PM-IRRAS analyses have been performed to understand the formation of the adsorbed film.

### 3. Analytical characterization of adsorbed fatty acids on different type of surfaces by XPS and PM-IRRAS analysis

#### 3.1 XPS analysis

##### 3.1.1 Adsorption of stearic acid on iron oxide surface

First of all, XPS analysis of stearic acid white crystalline powder is performed in order to get a reference position of the C1s peak for the carboxylic function. The carbon C1s XPS spectrum obtained on stearic acid powder is presented in figure 15-a. The C1s photo peak exhibits clearly two contributions: one peaking at 284.8 eV characteristic of the alkyl chain and another one shifted at 289.2 eV. This last binding energy is characteristic of the carboxylic group COOH, according to the database.

Then, *in situ* adsorption of stearic acid from the gas phase on iron oxide surface (as steel surface after ion etching for 10 seconds) is carried out after 30 minutes and after 2 hours of adsorption time. After adsorption, XPS is performed without any cleaning and in vacuum. The evolution of C1s peaks positions over adsorption time is studied as shown in figure 15-a.

If interactions are weak, the C1s peak should be located in the same position as for the molecule itself in the crystal with only hydrogen bonds. On the other hand, a shift is characteristic of strong interactions with the substrate or even chemical reaction.

After 30' and 2h of adsorption in presence of iron oxide surface (figure 15-b and 15-c), XPS analysis reveals a shift in the C1s carboxylic function from 289.2 eV to 288.9 eV. This shift is quite small but clearly visible and this suggests that the acid group has interacted with the metal oxide. According to the position of the peak, different reactions can be proposed: either chemisorption through the carboxyl and/or the hydroxyl group or chemical reaction with dissociation of hydrogen from the hydroxyl group and formation of iron carboxylate.

For example, the position of C1s peak in copper stearate has been measured in the literature and has been found to be located at the same binding energy as the shifted peak in our study. However, XPS analysis is not sensitive enough to identify the exact origin of this peak at 288.9 eV and to conclude if it is the soap which is formed. Other studies also show that the adsorption of stearic acid on sapphire leads to a shift for the carboxylate peak at 289.0 eV and the position of the aliphatic carbon's peak at 284.8 eV <sup>[13]</sup>. The authors could emphasize the absence of free fatty acid but could not determine the exact adsorption mechanism through the acid group <sup>[13]</sup>. Some C1s XPS spectra of unslide and slide track of stearic acid and linoleic acid show the methylene carbon peak at 284.1 eV, the methylene attached to carboxylic group peak at 285.6 eV, the symmetric COO- peak at 287.9 eV and the C=O asymmetric COO- or unreacted strong adsorption through carboxylic group peak at 290.2 eV <sup>[2]</sup>. The peak obtained in the present study is between the two mentioned peak so a mixture of different adsorption mechanisms can be expected.

Islam *et al.* presented experimental results regarding the energy difference between the C1s peak of carboxylate or carboxylic acid carbon atom and the aliphatic carbon atom <sup>[9]</sup>. For the isolated molecule, the variation is about 4.1-4.5 eV (4.4 eV in our study). For the



adsorbed molecule in bridging configuration, the variation is 3.3-3.8 eV that indicates that the two peaks are coming closer as in our experiment (from 4.4 eV to 4.1 eV). Nevertheless, no values are recorded for chemisorption through the carboxyl group experimentally [9]. DFT calculation enables to quantify the distance between the two peaks in case of adsorption through the carboxyl group and it was found equal to 3.3 eV [9] which is at the same range as the stearate bridging configuration. Therefore, the XPS technique has strong limitations to separate the two types of adsorption in our case (carboxylate versus chemisorption through carboxyl group).

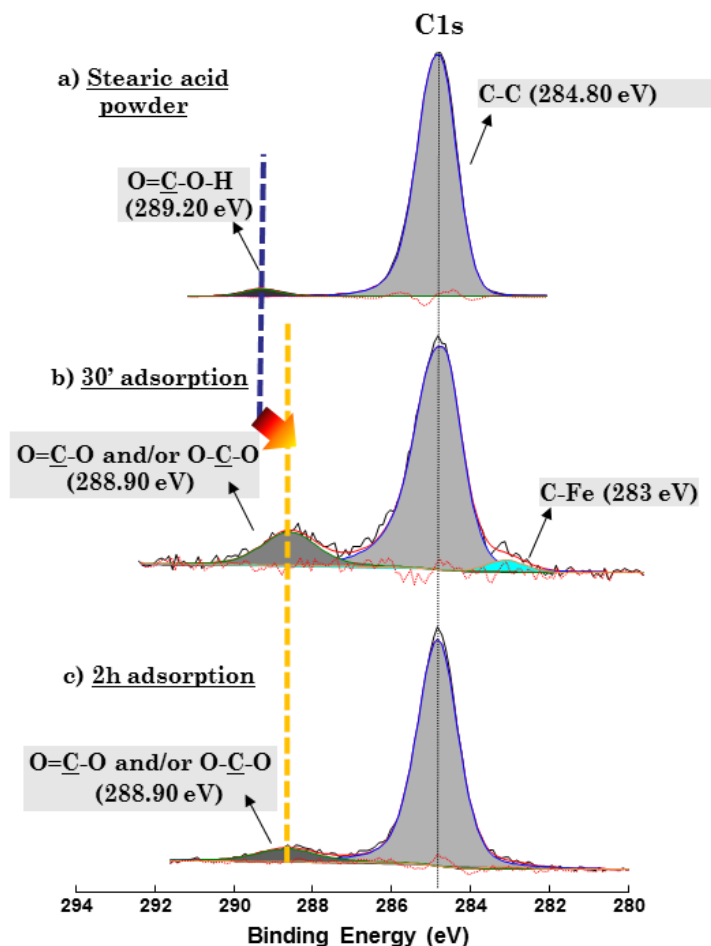


FIGURE 15: XPS ANALYSIS: *IN SITU* ADSORPTION OF STEARIC ACID ON IRON OXIDE SURFACE, CARBON 1S SPECTRA OF A) STEARIC ACID POWDER ALONE, B) ANALYSIS 30 MIN. AFTER ADSORPTION, C) ANALYSIS 2 HOURS AFTER ADSORPTION.

Coming back to our C1s XPS spectrum, the width of the carbon peak seems to reduce with increasing adsorption time. This suggests that the film is organizing over time. In fact, the intensity ratio C-C/C-O is not characteristic to one specific orientation (SAM, horizontal layering, anti-SAM, etc.) because the organization of the film is progressive. This method cannot indicate the orientation of molecules precisely.

On the other hand, the Tourgaard nanostructure analysis technique has been used elsewhere to determine the thickness of the stearic acid layer on oxidized flat steel that is about 20 Å, e.g. a monolayer with a tilt angle [24].

The presence of the shift and the width of the carbon peak are in agreement with UA-QCMD simulations which show that stearic acid molecules are chemisorbed on iron oxide surface with different adsorption mechanism depending on the orientation of the molecule

when it arrives to the surface. Computer simulations did not detect the formation of any stearate during the formation of the thermal film.

*In situ* preparation of sample and adsorption enable to control approximately the oxide/hydroxide layer by applying etching and to be in conditions that are very close to UA-QCMD simulation (section 2.2). Therefore, it is possible to study the adsorption of stearic acid on different iron-based surfaces.

### 3.1.2 Influence of the substrate

General XPS spectra are presented in figure 16 before and after 2h of adsorption of stearic acid with three different substrates: on metallic iron, iron oxide and native steel surface with no etching (called 'as is' in the following). In order to complete the observations based on general spectra, high resolution carbon 1s spectra are investigated and main results are gathered in table 11.

On metallic iron (figure 16-I), XPS analyses show increase in both carbon and oxygen quantity during the 2 hours of adsorption which show that stearic acid molecules have high reactivity with metallic iron. C1s spectra indicate a shift to lower energy of 0.7 eV after 30 minutes and 0.8 eV after 2 hours of adsorption which confirms chemisorption through the acid group.

On iron oxide surface (figure 16-II), the atomic percentage of carbon increases from 25.6% before adsorption to 47.1% after adsorption. On another hand, the atomic percentage of oxygen decreases from 56.1% to 41.1% after adsorption, indicating that stearic acid molecules are adsorbed on the iron oxide surface. In fact, the surface already contains many oxygen atoms before adsorption of fatty acids. C1s spectra indicated a shift of 0.3 eV after 30 minutes of adsorption and 0.6 eV after 2 hours of adsorption. This shift confirms the progressive chemisorption through the acid group.

On 'as is' steel surface (figure 16-III), the atomic percentage of carbon barely change before and after adsorption which suggests that there is no or weak interactions between stearic acid molecules and the surface. This is confirmed by the absence of shift with respect of time on the C1s spectra. Surface, contaminations, in addition to hydroxide/oxidized layer prevent the strong adsorption.

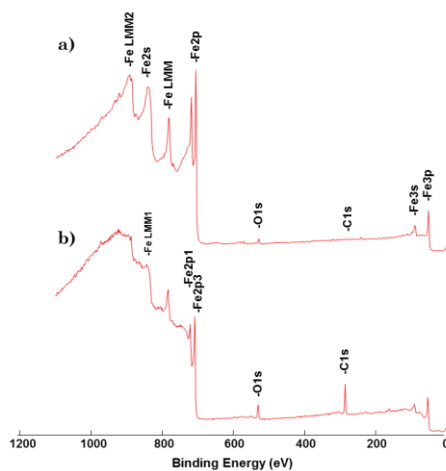
The shift of C1s is higher on metallic iron (0.8 eV) than on iron oxide surface (0.6 eV) confirming that when the oxidation increases, the reactivity of stearic acid molecules with the surface decreases.



**I)**

a) Metallic iron before adsorption

b) Metallic iron after adsorption for 2h



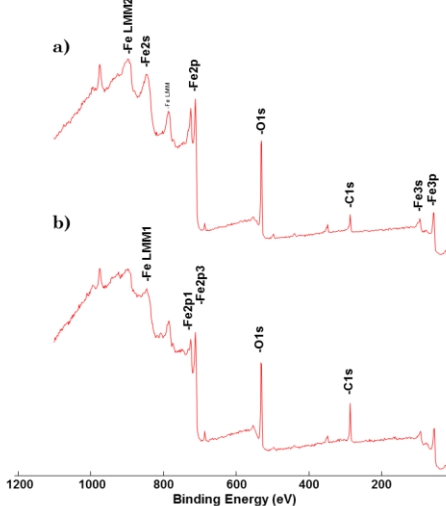
Metallic iron before adsorption	
Element	Atm %
C1s	4.2
O1s	5.4
Fe2p	90.4

Metallic iron after adsorption for 30'	
Element	Atm %
C1s	53.4
O1s	14.6
Fe2p	32

**II)**

a) Iron oxide before adsorption

b) Iron oxide after adsorption for 2h



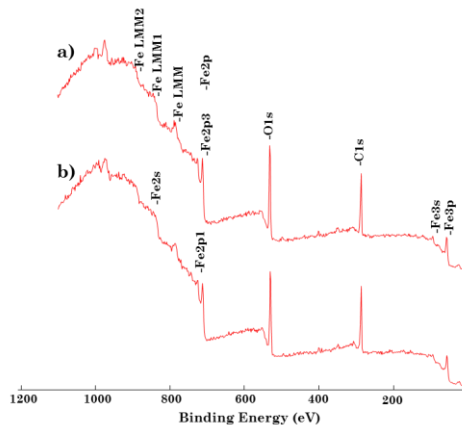
Iron Oxide before adsorption	
Element	Atm %
C1s	25.6
O1s	56.1
Fe2p	18.3

Iron Oxide after adsorption for 2h	
Element	Atm %
C1s	47.1
O1s	41.1
Fe2p	11.8

**III)**

a) As is before adsorption

b) As is after adsorption for 2h



As is before adsorption	
Element	Atm %
C1s	57.7
O1s	39.8
Fe2p	2.5

As is after adsorption for 2h	
Element	Atm %
C1s	61.7
O1s	35.9
Fe2p	2.3

FIGURE 16: GENERAL SPECTRA BEFORE ADSORPTION AND AFTER 2H OF ADSORPTION ON: I) METALLIC IRON, II) IRON OXIDE, III) AS IS AISI 52100

TABLE 11: SUMMARY OF C1S SPECTRA MAIN RESULTS FOR THE ADSORPTION OF STEARIC ACID VAPOR ON GOLD, METALLIC IRON, IRON OXIDE AND AS IS STEEL SURFACE AT DIFFERENT ADSORPTION TIME

Stearic acid adsorption (Binding Energy = BE)			
	Metallic Iron	Iron Oxide	AISI 52100
30'	BE of COOH shifted of 0.7 eV (Chemisorption)	BE of COOH shifted of 0.3 eV (Chemisorption)	Non reactive
2h	BE of COOH shifted of 0.8 eV (Chemisorption)	BE of COOH shifted of 0.6 eV (Chemisorption)	Non reactive

Stearic acid molecules present different adsorption mechanisms depending on the iron-based surface. The question that is raised now is if the same behavior is observed for unsaturated fatty acid?

### 3.1.3 Influence of unsaturation

The influence of unsaturation is investigated by studying the adsorption mechanism of stearic, oleic and linoleic acid respectively on metallic iron, iron oxide and 'as is' surfaces. XPS analyses are presented in the following.

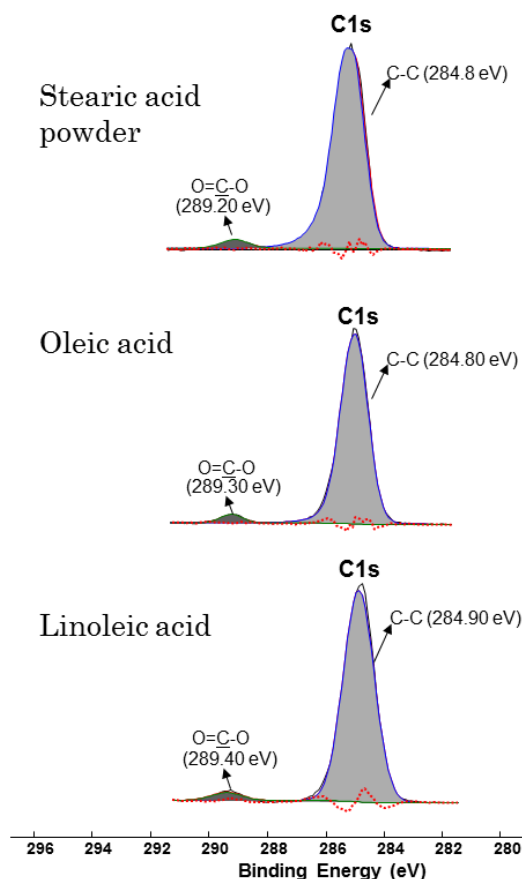


FIGURE 17: XPS ANALYSIS OF PURE MATERIALS - CARBON C1S OF STEARIC ACID POWDER, OLEIC ACID AND LINOLEIC ACID

Figure 17 shows the carbon C1s spectra of pure stearic acid powder, oleic acid and linoleic acid in order to have references of saturated and unsaturated fatty acids. The three

spectra look similar with two defined peaks. The first at 284.8 eV  $\pm$  0.1 eV for the alkyl chain carbon and the other are at 289.3 eV  $\pm$  0.1 eV characteristic of the carboxylic group.

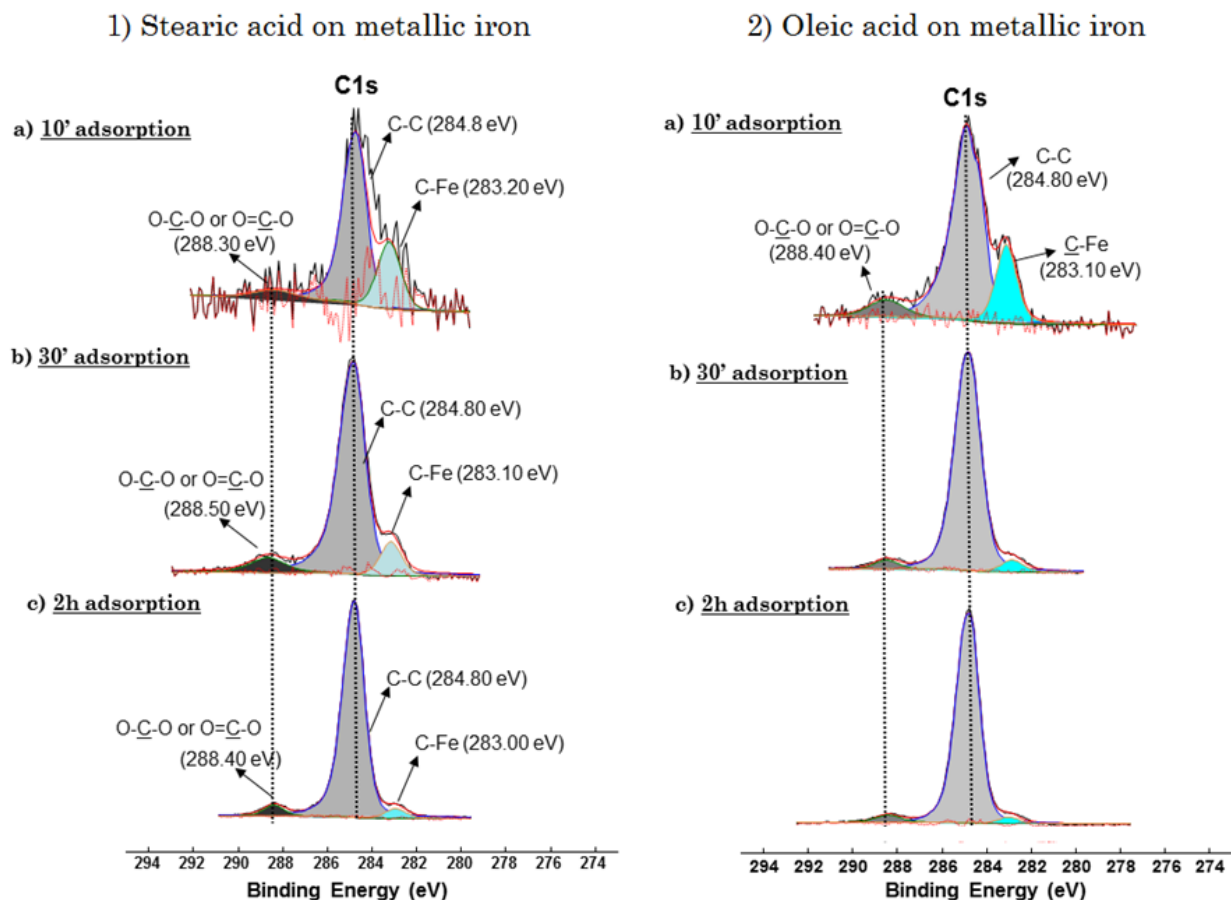


FIGURE 18: COMPARISON OF C1S SPECTRA AFTER 10', 30' AND 2H ADSORPTION OF STEARIC ACID (1) AND OLEIC ACID (2) RESPECTIVELY ON METALLIC IRON SUBSTRATE

Comparison of C1s spectra at different adsorption times for stearic and oleic acids on metallic iron is presented in figure 18. For both stearic and oleic acids, the shift in the C1s carboxylic peak is observed, even after 10 minutes of adsorption if it is compared with the corresponding peak of pure additives (Figure 17). Moreover, the width of the alkyl chain carbons seems to reduce with increasing adsorption time. Molecules are chemisorbed on the surface through the acid group but once again, XPS analysis cannot distinguish between the formation of chemisorbed carboxylic group and the iron soap (carboxylate).

The study of the influence of unsaturation, time of adsorption and different substrates are collected in tables 11, 12 and 13.

On metallic iron, a shift toward lower binding energy is observed for the three fatty acids. It is noticed that when the number of unsaturation increases, the shift increases slightly. In fact, after two hours of adsorption, the shift is about 0.8 eV, 0.9 eV and 1 eV for stearic, oleic and linoleic acid respectively. Nevertheless, metallic iron is reactive toward fatty acids and chemisorption occurred through the acid group.

On iron oxide, a shift toward lower binding energy is observed for the three fatty acids. Again, after two hours the shift is bigger for linoleic (0.8 eV) acid than for stearic acid (0.6 eV). In addition, the shift increases progressively with time for stearic acid as the shift goes from 0.3 eV after 30 minutes of adsorption to 0.6 eV after two hours of adsorption whereas with

unsaturated fatty acids, the shift remains constant right after 30 minutes of adsorption. It seems that the adsorption of stearic acid is slower than the adsorption of oleic and linoleic acid. Further investigations are needed to confirm this trend.

On 'as is' surface, there is no shift observed for the three fatty acids which means that molecules are weakly adsorbed on the surface.

TABLE 12: SUMMARY OF C1S SPECTRA MAIN RESULTS FOR THE ADSORPTION OF OLEIC ACID VAPOR ON GOLD, METALLIC IRON, IRON OXIDE AND AS IS STEEL SURFACE AT DIFFERENT ADSORPTION TIME

<b>Oleic acid adsorption (Binding Energy=BE)</b>			
	Metallic Iron	Iron Oxide	AISI 52100
30'	BE of COOH shifted of 0.9 eV (Chemisorption)	BE of COOH shifted of 0.7 eV (Chemisorption)	Non reactive
2h	BE of COOH shifted of 0.9 eV (Chemisorption)	BE of COOH shifted of 0.7 eV (Chemisorption)	Non reactive

TABLE 13: SUMMARY OF C1S SPECTRA MAIN RESULTS FOR THE ADSORPTION OF LINOLEIC ACID VAPOR ON GOLD, METALLIC IRON, IRON OXIDE AND AS IS STEEL SURFACE AT DIFFERENT ADSORPTION TIME

<b>Linoleic acid adsorption (Binding Energy=BE)</b>			
	Metallic Iron	Iron Oxide	AISI 52100
30'	BE of COOH shifted of 0.9 eV (Chemisorption)	BE of COOH shifted of 0.8 eV (Chemisorption)	Non reactive
2h	BE of COOH shifted of 1 eV (Chemisorption)	BE of COOH shifted of 0.8 eV (Chemisorption)	Non reactive

Both computational simulation and XPS analysis confirm that the adsorption mechanism is the same for saturated and unsaturated fatty acids. The double carbon bond does not interfere with the adsorption mechanism of fatty acids on iron-based surfaces.

Studies on SAM have been done previously and samples are prepared 12 to 24h before any analysis. UA-QCMD only represents few ps but molecules are initially placed close to the surface with the orientation that favor the formation of SAM in order to overcome the time needed to organize the film. XPS analyses were run after 30 minutes of adsorption and 2 hours of adsorption in order to check the influence of adsorption time.

### 3.1.4 Combination of experimental study and molecular simulations

Comparison of XPS analyses and TB-QC simulations can be done. With XPS, the core-electron binding energy of element is measured. For fatty acids, it is C1s or O1s peaks. Depending on the type of molecule (alcohol, carboxylic acid, alkane, etc.), valences of carbon differ. Our TB-QC method calculate only valence orbital and do not take into consideration core orbital. But, charge (amount of electrons in valence orbital) influences energy of core orbital. This is why binding energy and electrical charges on atoms can be related by a curve [25]. A correlation curve has been constructed for C1s spectrum by using QC methods with 'COLORS' and 'Material Studio©' software's in addition to experimental data (*XPS data from [www.techbd.podzzone.net/xpsstate/](http://www.techbd.podzzone.net/xpsstate/)*). Carbon atomic charge has been calculated by TB-QC and DFT methods for different model compounds: propane, propanol, propanone and propanoic acid. Then, these charges are plotted as a function of binding energy found in the literature for the model compounds and the correlation curve could be plotted as shown in figure 19.

Therefore, change of charge by UA-QCMD calculations correlates quite well with the shift in XPS binding energy. The correlation coefficient is  $R^2 = 0.98$ . Similar work has been done for the simulation of XPS C1s spectra of organic monolayers by quantum chemical methods [26].

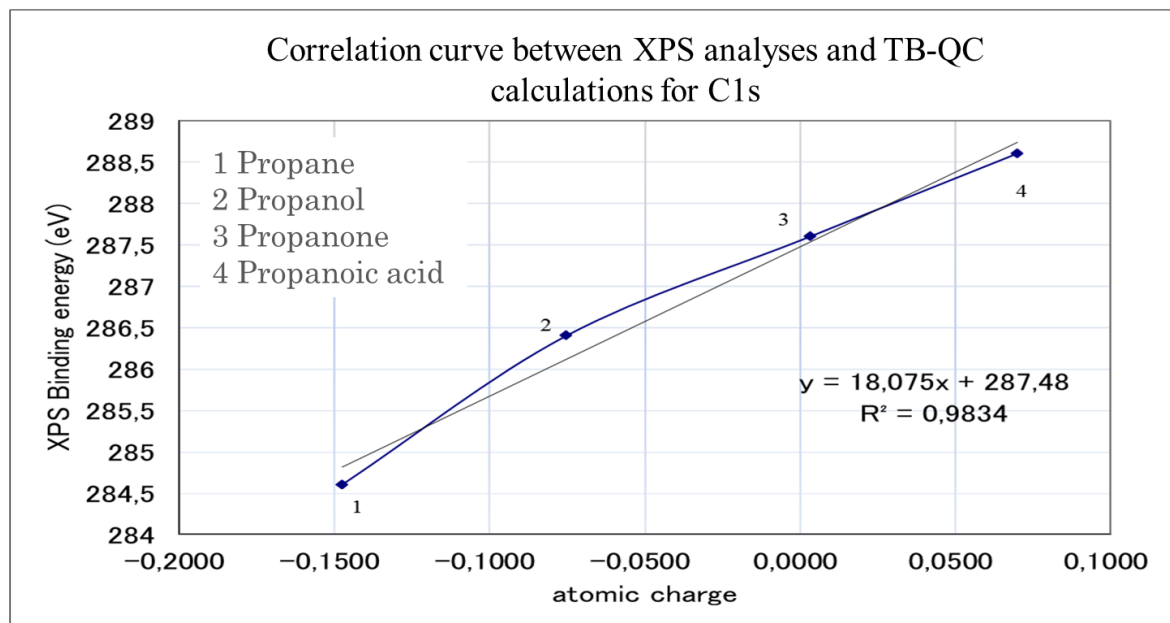


FIGURE 19: CORRELATION CURVE BETWEEN XPS ANALYSES AND QUANTUM CHEMICAL METHOD FOR C1S WITH MODEL COMPOUNDS: PROPANE, PROPANOL, PROPANONE, PROPANOIC ACID

Table 14 gathered initial and final charges (after 15 ps of UA-QCMD simulations) of some stearic acid molecule atoms and iron, oxygen atoms of the iron oxide surface in the case of chemisorption of stearic acid on iron oxide through the acid group. The biggest charge difference between initial and final charge is observed on the carbon atom of the acid group with a shift from charge equal to 0.21 to charge equal to 1.123. In our XPS analysis, the main shift also concerns the carbon of the acid group so the two methods are in agreement.

Iron atom (from  $\text{Fe}_2\text{O}_3$  substrate) seems to give electrons to the carbon of carboxylic group and also to oxygen of hydroxyl group as it loses electrons. This gain of electron for the carbon atoms induces a decrease of binding energy as it is observed with our XPS analysis (figure 15). On the other hand, the charge of the oxygen of carboxyl group does not change so the electrons exchange is directly between carbon and iron atoms. Surrounding oxygen atoms from the surface are also giving electrons but it is much smaller in comparison with the contribution of iron. It is important to note that neighboring iron and oxygen atoms from the surface also give electrons to the acid group in order to equilibrate the charge in the system. In addition, hydrogen gives electrons to oxygen of the hydroxyl group and additional interactions between surrounding molecules also occur (SAM model= cohesion forces).

By using our correlation curve (figure 19), a shift from 0.21 to 0.123 charge on the carbon of carboxyl group is equivalent to a binding energy shift from 291.3 eV to 289.7 eV, inducing a shift in lower energy of 1.6 eV. In our XPS analyses, the carboxylate/carboxylic carbon atom peak also shifted to lower energy but with a shift of 0.6-1 eV (depending of the fatty acid and the substrate types). Our XPS peak shift is in the same direction but a bit lower than the one expected by the correlation curve.

The difference in the shift value obtained by our XPS analysis and by our correlation curve can be explained by several hypotheses. It is possible that after 2h of adsorption, few carboxylate functions might have time to be formed as shown by PM-IRRAS study (*cf.* § 3.2).

The carboxylate carbon has probably a different charge and, therefore, a different binding energy. In addition, the surface used in XPS and UA-QCMD are not totally identical. Some defects on the real surface can have some impacts on the adsorption mechanism of fatty acid molecules on iron-based surfaces. Finally, initial carboxylic carbon's charge is correlated to a binding energy equal to 291.3 eV which is higher than initial carboxylic C1s peak at 289.2 eV. Therefore, the model should be improved in order to fit better with experimental value but it is a promising tool to help XPS analysis interpretation.

TABLE 14: EFFET OF CHARGE; INITIAL AND FINAL CHARGES OF SOME ATOMS OF ONE STEARIC ACID MOLECULE (CHEMISORBED THROUGH CARBOXYL GROUP ON THE SURFACE) FROM THE SAM WHICH INTERACT AND OXYGEN, IRON ATOMS FROM THE IRON OXIDE SURFACE, UA-QCMD 15 PS SAM 15 MOLECULES, 50 °C

Atom number	Initial charge	Final charge (15 ps)	difference	transfer	Binding energy
C (COOH)	0.21	0.123	0.087	e- gain	Decrease
O= (COOH)	-0.159	-0.158	0.001	-	-
Oh (COOH)	-0.142	-0.185	0.043	e- gain	Decrease
Ho (COOH)	0.210	0.197	0.013	e- loss	Increase
Fe	0.28	0.308	0.028	e- loss	Increase
O (Fe <sub>2</sub> O <sub>3</sub> )	-0.226	-0.218	0.008	e- loss	Increase
O (Fe <sub>2</sub> O <sub>3</sub> )	-0.175	-0.173	0.002	-	-
O (Fe <sub>2</sub> O <sub>3</sub> )	-0.189	-0.181	0.008	e- loss	Increase

In conclusion, XPS analysis is not able to distinguish between the chemisorption and the formation of carboxylate. This is why some PM-IRRAS analyses were performed as a complementary technique to tackle the adsorption mechanism and the arrangement of molecules on the surface. It is important to note that the PM-IRRAS analysis will be performed on surfaces obtained in a liquid phase system whereas simulations and XPS analysis were performed under a gas phase.

## 3.2 PM-IRRAS analysis

### 3.2.1 Characterization of adsorbed stearic acid film

Before any investigation of the adsorbed film, the ATR spectrum of pure stearic acid is carried out as a reference and is presented in figure 20. Several vibration modes are characteristic of the stearic acid molecule. The alkyl chain presents two main contributions at 2915 cm<sup>-1</sup> and 2848 cm<sup>-1</sup> characteristic of CH<sub>3</sub> and CH<sub>2</sub> stretching modes respectively. Additional peaks are characteristic of the *trans* conformation of CH<sub>2</sub> at 1300 cm<sup>-1</sup> and 1462 cm<sup>-1</sup>. The carboxylic function shows a stretching mode at 1700 cm<sup>-1</sup>. The characteristic peak of stearic acid reference model compound for Fourier transformed-infra-red (FTIR) spectrum and our ATR spectrum are at the same position [6]. In addition, FTIR spectrum of iron stearate reference model compound is also presented: the peak at 1700 cm<sup>-1</sup> disappears and a new peak grows at 1585 cm<sup>-1</sup> representing C-O-Fe bonds specific vibrations [6].

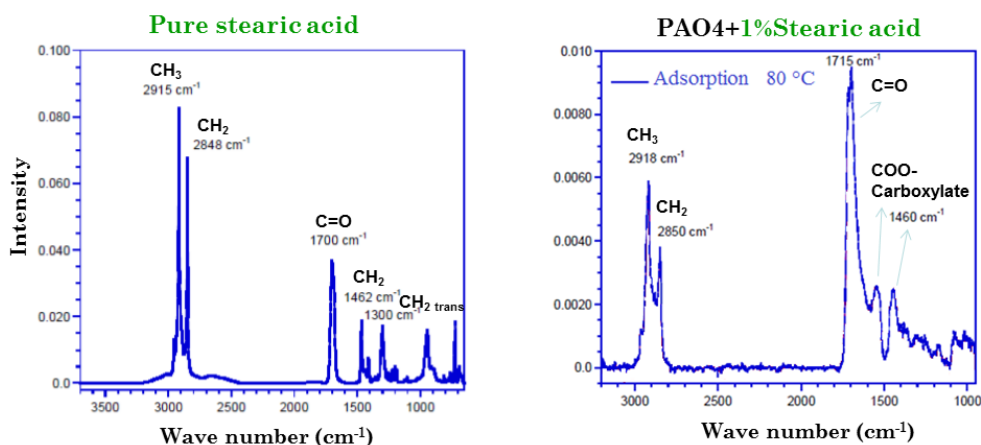


FIGURE 20: LEFT:ATR SPECTRUM OF PURE STEARIC ACID (REFERENCE), RIGHT: PM-IRRAS SPECTRUM OF ADSORPTION OF PAO4 + 1%W STEARIC ACID ON STEEL SURFACE AT 80 °C.

Figure 20 also shows PM-IRRAS spectrum but after adsorption of stearic acid on steel at 80 °C. The presence of the alkyl chain is confirmed by the presence of the two peaks at 2918  $\text{cm}^{-1}$  and 2850  $\text{cm}^{-1}$ . Even after two cleanings with pure heptane, the C=O band at 1715  $\text{cm}^{-1}$  still remains. Therefore, we can conclude that the stearic acid molecule is still present in majority on the sample. Molecules are both physisorbed (removed after washing) and chemisorbed through the acid group, strong enough to stay after washing. In addition, the PM-IRRAS spectrum indicates the presence of stearate function with two bands at 1460  $\text{cm}^{-1}$  and 1580  $\text{cm}^{-1}$ . Then, the adsorbed film is composed of stearic acid and iron stearate. However, the spectrum shows that the adsorbed film seems to contain much more acid functions than carboxylate ones. According to Crowell's definitions <sup>[14]</sup>, asymmetric and symmetric vibration modes distance is 120  $\text{cm}^{-1}$  *i.e.* between 80  $\text{cm}^{-1}$  and 200  $\text{cm}^{-1}$ . Therefore, both mono-dentate and bridging configurations are present in the film.

From PM-IRRAS, simulation can be done to predict the thickness of the film and organization of molecules on the substrate. The simulation indicates the presence of a compact and organized film with a film thickness estimated at about 25 Å. This is equivalent to a monolayer as shown in figure 21. The formation of a well-arranged and compact stearic acid monolayer has been highlighted by computational chemistry, especially when the density of molecules on the substrate is increased. From the PM-IRRAS analysis, the stearic acid film is composed of stearate and stearic acid chemisorbed on the surface through the acid group which formed a 'solid-like' close-packed and well-arranged monolayer.

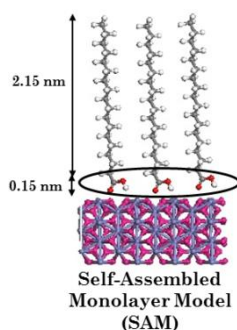


FIGURE 21: STEARIC ACID SELF-ASSEMBLED MONOLAYER ORGANISATION ON IRON OXIDE SURFACE

Material Studio© software, which contains CASTEP DFT calculations, is able to simulate the infra-red spectrum of compounds as shown in figure 22 for the example of stearic acid molecule. The spectrum is the same as the ATR spectrum of stearic acid (see figure 20). It



would have been interesting to compare simulated IR spectrum of chemisorbed molecule on iron oxide surface but the model could not converge and further investigations are needed. Nevertheless, computational chemistry seems to be a powerful tool to help the comprehension of complex system and complex experimental results.

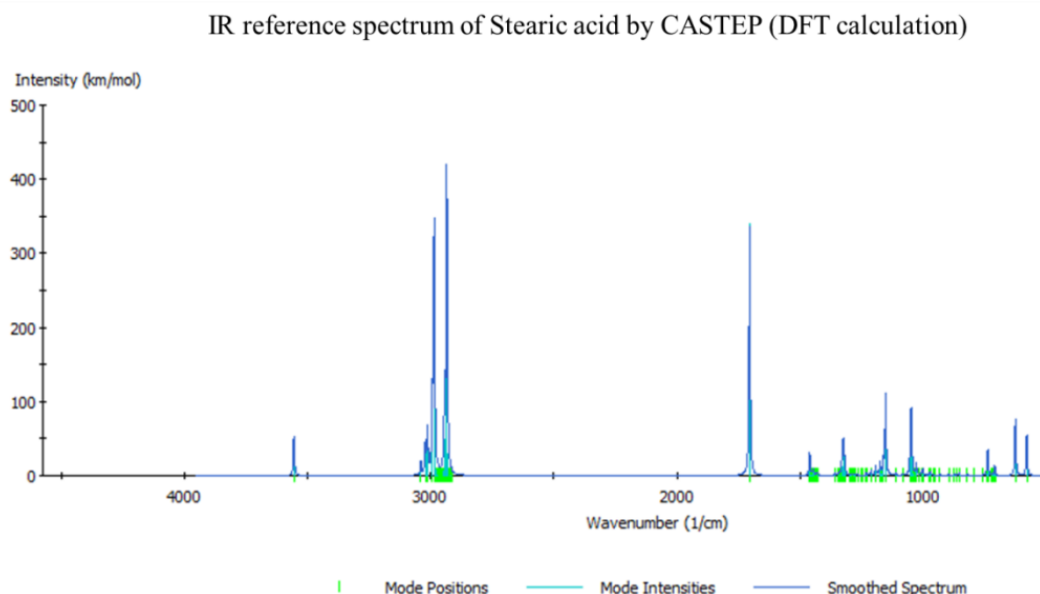


FIGURE 22: REFERENCE SPECTRUM FOR ISOLATED STEARIC ACID MOLECULE BY CASTEP CALCULATION FROM MATERIAL STUDIO® V6 SOFTWARE.

Our computer simulation is able to study the first nanoseconds of the adsorbed film formation. Surface analysis can analyze the final state of the adsorbed film, after a long time process, (several hours of contact with the molecules). This suggests that the stearate (if any) does not form at the beginning of the adsorption process but needs a much longer time to be produced.

The combination of XPS, PM-IRRAS and computational chemistry enable to better understand the formation of the thermal film for saturated fatty acids and results obtained by different techniques are in agreement. Is it also true for unsaturated molecules?

### 3.2.2 Influence of unsaturation

First, ATR spectrum is run for pure oleic acid as a reference (figure 23). The position of peaks are similar to those of stearic acid with a slight shift to higher wave number ( $\sim +9\text{ cm}^{-1}$ ). In addition, the C=C band is characterized by a very small band in  $3007\text{ cm}^{-1}$  and at  $1657\text{ cm}^{-1}$ .

Figure 23 also shows the PM-IRRAS spectra of liquid oleic acid (red curve) and PAO 4 + 1%w of oleic acid (blue curve) adsorbed on steel surface at  $150\text{ }^{\circ}\text{C}$ .

After adsorption on steel surface of both pure liquid oleic acid and oleic acid in PAO 4, bands characteristic of  $\text{CH}_3$  and  $\text{CH}_2$  are still remaining indicating the presence of the alkyl chain. It is noticed that the weak peak of C=C band seems to disappear after adsorption of oleic acid on steel surface. This does not mean that the double carbon bond is broken, it may be that the double carbon bond is orientated parallel to the surface and, therefore, is not sensitive with this vibrational technique. Even after heptane washing, the C=O band is still present at  $1696\text{ cm}^{-1}$  which confirms that the acid group is still present. These molecules are chemisorbed on the surface through the acid group. On the other hand, bands at  $1580\text{ cm}^{-1}$  (anti-symmetric mode) and  $1460\text{ cm}^{-1}$  (symmetric mode) indicate the presence of carboxylate form. Chemical reaction occurred through the acid group. As for stearic acid, there is more



acid form than carboxylate form. The composition of the adsorbed film is the same for liquid oleic acid and in presence of PAO 4. Saturated and unsaturated molecules have the same adsorption mechanism as shown by computational chemistry, XPS and PM-IRRAS analysis. This result is also confirmed by FTIR analysis on adsorbed stearic acid and linoleic acid on steel surface [2].

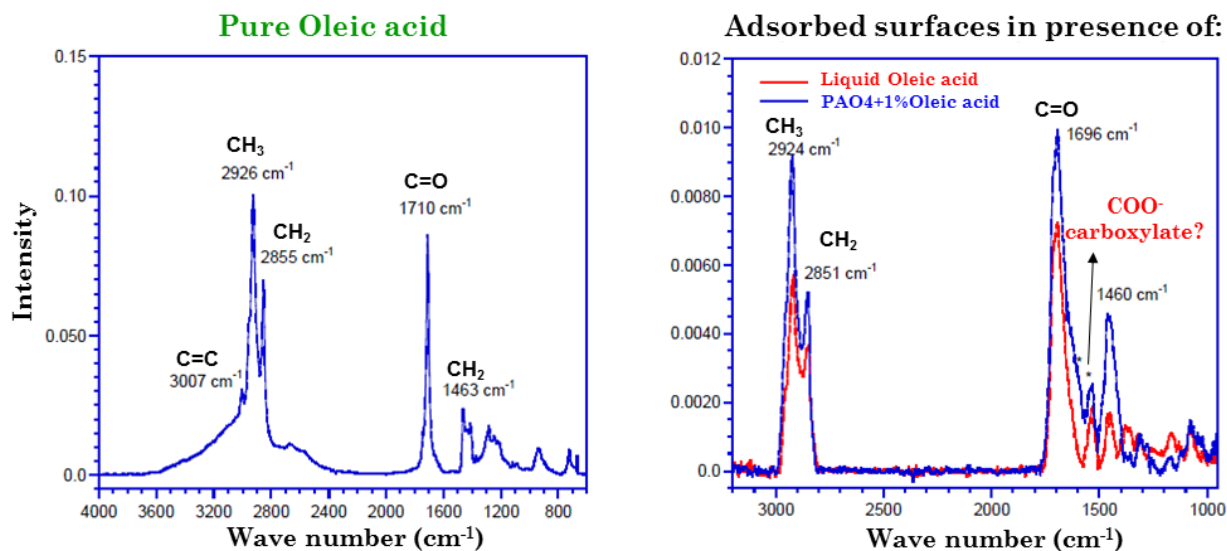


FIGURE 23: LEFT: ATR SPECTRUM OF PURE OLEIC ACID (REFERENCE), RIGHT: PM-IRRAS SPECTRUM OF ADSORPTION OF PAO4 + 1%W OLEIC ACID AND LIQUID OLEIC ACID ON STEEL SURFACE RESPECTIVELY AT 150 °C.

The simulation of the film thickness evaluates a 50 Å film thickness which is about two monolayers thick. Moreover, the simulation indicates that the film is not well organized. This is in agreement with the computer simulation and the literature [15-18].

### 3.2.3 Comparison XPS, PM-IRRAS analysis and UA-QCMD simulations

Experimental and computational results are in quite good agreement regarding the adsorption mechanism, influence of substrate and influence of unsaturation. The main difference is the detection of carboxylate functions with PM-IRRAS technique whereas no carboxylate functions have been observed after UA-QCMD simulations.

It is important to note that XPS analysis conditions (adsorption in vacuum from the gas phase) are similar to those used for UA-QCMD simulation, e.g pure additives with controlled surfaces whereas PM-IRRAS analyses are performed on a native steel surface. As already mentioned in the literature [13], real surface is heterogeneous so different adsorption mechanism can occur at the same time. The surface used for PM-IRRAS contains certainly both FeOOH and Fe<sub>2</sub>O<sub>3</sub> surfaces in addition to FeO [2].

Moreover, XPS analyses are made *in-situ* whereas PM-IRRAS analyses are made *ex-situ* and after a long time after the surface is introduced in the liquid additive. Hsu et al. show FTIR spectrum of stearic acid on copper just after dip-coating and after 24h. The ratio of C=O vibration mode/C-O vibration mode is equal to 2.99 right after dip-coating and 0.73 after 24h which indicate that when the exposure to air is increased, the C=O band becomes lower and C-O band becomes higher which confirm that the formation of carboxylate can occur in air without activation but its kinetic rate is slow [6].

## 4. Conclusion

In this part, we combined different techniques (including both computational chemistry and experimental analysis) to study the formation of the adsorbed film of fatty acids on steel

and we investigated the parameters having an impact on the adsorption mechanism. The following conclusion can be made:

- ✦ On steel surface, molecules are mainly chemisorbed through the acid group but there is a presence of some carboxylate function (PM-IRRAS) which indicates a chemical reaction that occurred during the formation of the thermal film (Low kinetic rate)
- ✦ Saturated and unsaturated fatty acid molecules present similar adsorption mechanisms
- ✦ When the oxidation/hydroxylation of the substrate increases, the reactivity of the surface with fatty acids decreases
- ✦ The film organized itself progressively with time
- ✦ Saturated molecules form a compact and well organized film whereas unsaturated molecules do not form a well-arranged film.

The environments, which have an impact on substrate composition, have a direct impact on the reactivity of the surface with fatty acids. For the same material, regarding the humidity or presence of oxygen, different adsorption mechanisms can occur with fatty acids so it is important to have an idea of the material composition and conditions in which it will be used before designing lubricant additives for specific applications.

At this step, we think that the adsorption mechanism of some C18 fatty acids on iron-based surfaces has been made clearer and this at the atomic scale. This result has been obtained by the combination of different techniques. Regarding the use of OFM, it is now interesting to study the tribological behavior of C18 fatty acid on iron-based surface in terms of friction and wear.

## 5. References

- [1] Schwartz D K, Mechanisms and kinetics of self-assembled monolayer formation, *Annual Review of Physical Chemistry*, 52 (2001) 107-137.
- [2] Sahoo R R, Biswas S K, Frictional response of fatty acids on steel, *Journal of Colloid and Interface Science*, 333 (2009) 707-718.
- [3] Greenfield M L, Ohtani H, Molecular dynamics simulation study of model friction modifier additives confined between two surfaces, *Tribology Letters* 7 (1999) 137-145.
- [4] Ratoi M, Anghel V, Bonvington C, Spikes H A, Mechanism of oiliness additives, *Tribology International* 33 (2000) 241-247.
- [5] Petrucci et al., General Chemistry: Principles and Modern Applications. 10th ed. *Upper Saddle River: Pearson Education, Inc.*, 2010
- [6] Hsu S M, Zhang J, Yin Z F, The nature and origin of tribochemistry, *Tribology Letters* 13 (2002) 131-139.
- [7] Przedlacki M and Kajdas C, Tribochemistry of fluorinated fluids hydroxyl groups on steel and aluminum surfaces, *Tribology Transactions*, 49 (2006) 202-214.
- [8] Petty M C, Langmuir-Blodgett films: an introduction, Chapter II, *Cambridge university press*, 1996.
- [9] Islam M M, Diawara B, Marcus P, Costa D, Synergy between ionic-covalent bonds and van der Waals interactions in SAMs formation: a first principles study of adsorption of carboxylic acids on the Zn-ZnO(0 0 0 1) surface, *Catalysis Today* 177 (2011) 39-49.
- [10] Fischer D A, Hu Z S, Hsu S M, Molecular orientation and bonding of monolayer stearic acid on a copper surface prepared in air, *Tribology Letters* 3 (1997) 41-45.
- [11] Ulman A, Formation and structure of self-assembled monolayer, *Chemical Review* 96 (1996) 1533.
- [12] Majzner M, Kajdas C, Reactions of carboxylic acids under boundary friction conditions, *Tribologia* 34 (2003) 63-80.
- [13] Lim M S et al., Adsorption and desorption of stearic self-assembled monolayers on aluminum oxide, *Langmuir* 23 (2007) 2444-2452.
- [14] Crowel J E, Chen J G, Yates Jr J T, A vibrational study of the adsorption and decomposition of formic acid and surface formate on Al(111), *Journal Chemical Physics* 85 (1986) 3111-3122.
- [15] Greenhill E B, Adsorption of long-chain polar compounds from solution on metal surfaces, *Transaction Faraday Society* 45 (1949) 625.
- [16] Daniel S G, Adsorption on metal surfaces of long-chain polar compounds from hydrocarbon solutions, *Transaction Faraday Society* 47 (1951) 1345.
- [17] Lundgren S M, Persson K, Kronberg B, Claesson P M, Adsorption of fatty acids from alkane solution studied with quartz crystal microbalance, *Tribology Letters* 22 (2006).
- [18] Lundgren S M et al., Unsaturated fatty acids in alkane solution: adsorption to steel surfaces, *Langmuir* 23 (2007) 10598-10602.

- [19] Bowden F P, Tabor D, The friction and lubrication of solids, *Oxford Classic Texts in the Physical Science*, Chapter X, **2001**.
- [20] Tabor D, The influence of temperature on lubricating films, *Nature*, 145 (**1940**) 308.
- [21] Simič R, Kalin M, Adsorption mechanisms for fatty acids on DLC and steel studied by AFM and tribological experiments, *Applied surface science*, (**2013**) dx.doi.org/10.1016/j.apsusc.2013.06.131
- [22] Campen S et al., On the increase in boundary friction with sliding speed, *Tribology Letters*, DOI 10.1007/s11249-012-0019-4 (**2012**).
- [23] Fischer D A, Hu Z S, Hsu S M, Tribochemical and thermochemical reactions of stearic acid on copper surfaces in air as measured by ultra-soft X-ray absorption spectroscopy, *Tribology letters* 3 (**1997**) 35-40.
- [24] Johansson E, Nyborg L, XPS study of carboxylic acid layers on oxidized metals with reference to particulate materials, *Surface Interface Analyses*, 35 (**2003**) 375-381.
- [25] Carlson T A, Photoelectron and Auger spectroscopy, Chapter 5 p 178 *Plenum Press* (**1975**).
- [26] Giesbers M, Antonius T M, Marcelis T M, Zuilhof H, Simulation of XPS C1s spectra of organic monolayers by quantum chemical methods, *Langmuir* 29 (**2013**) 4782-4788.
- [27] Chernyshova I V, Ponnurangam S, Somasundaran P, Adsorption of fatty acids on iron hydroxides from aqueous solutions, *Langmuir* 27 (**2011**) 10007-10018.

## 6. Summary chapter 3

The first step in the comprehension of tribological behaviors of C18 fatty acids on iron-based surfaces consists in studying adsorption mechanisms that can occur during the formation of the thermal film. Therefore, two adsorption models have been built for molecular simulation and mainly UA-QCMD method: a single molecule of fatty acid on an iron-based surface and a Self-Assembled Monolayer (SAM) of fatty acid molecules on an iron-based surface.

It is interesting to observe that a single molecule is physisorbed on iron oxide surface through the acid group whereas the prevailing adsorption mechanism of molecules in the SAM is a chemisorption through the carboxyl group. In fact, the orientation of the acid group and, therefore, the orientation of the alkyl chain, have an impact on the adsorption mechanism. According to the angle in which the molecule reaches the surface, different adsorption mechanisms can occur: symmetric or asymmetric. By increasing the density of the SAM, one orientation is favored which can explain the prevailing adsorption mechanism (chemisorption). The stearic acid monolayer is well-arranged with a tilt angle toward the surface in order to optimize the cohesion force between molecules in the SAM. During the formation of the adsorbed layer, no hydrogen dissociation from the hydroxyl group is observed. By changing the nature of the surface, the reactivity of the surface with fatty acids is also changed. In fact, when the oxidation or hydroxylation degree is increased, the reactivity of fatty acids toward the surface is decreased. Adsorption mechanisms of oleic and linoleic acids on iron-based surfaces are the same as those with stearic acid molecules. The double carbon-carbon bond in case of oleic and linoleic acids does not interact with the surface but it provides steric effects which inhibit the formation of a well-arranged monolayer like it is the case with stearic acid molecules. Finally, temperature has no effect on adsorption mechanisms of fatty acids on iron-based surfaces but it has a kinetic effect. Critical desorption temperature is not reached for the studied pure additives at 150 °C.

These results have been confirmed by surface analysis of adsorbed layer. XPS spectra show a shift in the C1s carbon peak of the acid group to lower binding energy which confirms chemisorption through the acid group. Nevertheless, this technique was not sensitive enough to confirm the type of adsorption: formation of carboxylate function or symmetric/asymmetric adsorption through the acid group. Therefore, PM-IRRAS analyses have been performed which could identify the presence of both acid function and carboxylate function. The carboxylate function has not been observed with molecular simulations because the kinetic of carboxylate formation might be very slow. Nevertheless, there are more acid functions than carboxylate functions in the adsorbed layer. Moreover, PM-IRRAS analyses show that stearic acid monolayer is well-arranged whereas oleic acid monolayer is divided into two parts: one that is well-arranged and one that is not because of the presence of double carbon-carbon bonds.

## 6. Résumé chapitre 3

La première étape dans la compréhension du comportement tribologique des acides gras C18 sur des surfaces à base de fer consiste à étudier les mécanismes d'adsorption ayant lieu lors de la formation du film thermique. Ainsi, deux modèles d'adsorption ont été construits pour la modélisation moléculaire, principalement par la technique UA-QCMD : un modèle comportant une seule molécule d'acide gras sur une surface à base de fer et le modèle de la monocouche auto-assemblée (SAM) sur une surface à base de fer.

Il est intéressant de constater qu'une molécule simple se physisorbe sur l'oxyde de fer par les deux oxygènes du groupement acide alors que le mécanisme prédominant dans un modèle SAM est la chimisorption par le groupement carboxyle. En effet, l'orientation du groupement acide, et donc a fortiori de la chaîne alkyle a un impact sur le mécanisme d'adsorption. Selon l'angle avec lequel la molécule arrive à la surface, plusieurs types d'adsorption sont possibles : symétrique ou asymétrique. En augmentant la densité du SAM, une orientation est privilégiée d'où le mécanisme d'adsorption prédominant (chimisorption). Cette monocouche est bien organisée et rangée avec un angle par rapport à la surface permettant d'optimiser les interactions intermoléculaires. En revanche, l'hydrogène du groupement hydroxyle ne se dissocie pas durant la formation du film adsorbé. En changeant la nature de la surface, la réactivité de la surface est également changée. En effet, lorsque le degré d'oxydation ou d'hydroxylation augmente, la réactivité des acides gras vis-à-vis de la surface est diminuée. Les mécanismes d'adsorption de l'acide oléique et linoléique sur les surfaces à base de fer sont identiques à celles de l'acide stéarique. Pourtant, ces dernières possèdent des doubles liaisons carbone-carbone. Celles-ci n'interagissent pas avec la surface. En revanche, elles génèrent des gênes stériques qui empêchent la formation d'une monocouche bien organisée comme pour l'acide stéarique. Enfin la température n'a pas d'effet sur le mécanisme d'adsorption mais sur la cinétique du phénomène. La température critique de désorption ne semble pas atteinte à 150 °C pour les additifs purs.

Ces résultats ont été confirmés par des analyses de surface des films adsorbés. Les spectres XPS montrent un déplacement du pic du carbone (C1s) de la fonction acide vers des énergies de liaison plus basses lors de l'adsorption, traduisant une chimisorption par le groupement acide. Cette technique ne nous a pas permis de trancher sur le type de chimisorption (formation carboxylate, adsorption symétrique ou asymétrique). C'est pourquoi nous avons effectué des analyses par PM-IRRAS qui nous ont permis d'identifier la fonction acide, traduisant l'adsorption de l'acide gras, et la présence de carboxylate traduisant une réaction chimique. Ceci n'a pas été observé en modélisation moléculaire car la cinétique du phénomène est sans doute très lente. Néanmoins, il y a plus de forme acide que de forme carboxylate dans les échantillons adsorbés étudiés. De plus, les analyses montrent que l'acide stéarique forme une monocouche bien organisée alors que le film adsorbé d'acide oléique est divisé entre une partie bien organisée et une autre partie désorganisée dû à la présence d'insaturations.

## **Chapter 4: Tribological behavior of pure C18 fatty acids**

---

## **Chapitre 4: Comportements tribologiques des acides gras C18 purs**

## Chapter 4: Tribological behavior of pure C18 fatty acid

---

### Table of contents

1. Introduction .....	124
2. Friction between adsorbed layers by MD simulation .....	125
2.1 Generalities on friction behavior by MD .....	125
2.2 Influence of selected parameters .....	127
3. Evolution of adsorption films during sliding process by UA-QCMD .....	139
3.1 Effect of pressure and sliding: into the formation of carboxylate .....	139
4. Friction behavior of pure additives by experimental study.....	140
4.1 Effect of unsaturation and temperature.....	140
4.2 Analyzis of the tribofilm by PM-IRRAS .....	142
5. Comparison of experimental and numerical results.....	144
5.1 Considerations concerning MD calculations before comparison with experimental study .....	144
5.2 Effect of Parameters.....	145
6. Conclusion.....	146
7. References.....	147
8. Summary chapter 4.....	150

### 1. Introduction

In the previous chapter, the formation of adsorbed film was investigated in terms of adsorption mechanism depending on different parameters. Regarding the nature of the surface, fatty acid molecules are physisorbed and/or chemisorbed on the substrate. Saturated and unsaturated fatty acids have the same adsorption mechanism through the acid group. However, only stearic acid molecules are well-organized in a close-packed monolayer. This can be explained by the fact that steric effects prevent the formation of a well-arranged monolayer for both oleic and linoleic acid.

Now, we are interested in submitting this film to “severe” mechanical conditions e.g. pressure and shear stress. Also we want to investigate the tribological behavior of 18 fatty acid adsorbed layers on iron-based surfaces under mixed and boundary lubrication regimes. This is the aim of this chapter with a study on pure additives, e.g. without any base oil.

Several tools will be used to study fatty acids behavior under friction. MD simulation is performed here to calculate the friction coefficient as well as the velocity profile inside the layer. UA-QCMD simulations are run in order to study possible chemical reactions that could be induced by mechanical shear stress. All simulation results will be presented in the paragraph 2. Then, in paragraph 3, friction tests are run to evaluate the tribological behavior of pure stearic, oleic and linoleic acid on steel surface. Different temperatures are investigated



from room temperature to 150 °C. In addition, in experimental part, surface characterization of the tribofilm is performed with PM-IRRAS analysis after friction test.

## 2. Friction between adsorbed layers by MD simulation

### 2.1 Generalities on friction behavior by MD

To study the tribological behavior of OFM on iron-based surfaces, MD simulation is performed by considering the sliding between two monolayers of fatty acid molecules deposited on iron oxide. First, the two monolayers are compressed against each other at a pressure of 300 MPa. Second, when equilibrium has been achieved, the upper iron oxide surface is forced to slide in the x direction at a sliding velocity of 100 m/s. Before detailing the impact of parameters such as unsaturation in fatty acids, density, or surface compositions, on the friction behavior of monolayers, general considerations regarding MD calculations are first considered. Does the tilt of molecules adsorbed on the surfaces is observed like in experimental works? Differences in temperature control and in sliding speed on both experimental and MD calculations are then discussed.

#### 2.1.1 Tilt Angle

In the previous chapter, we have shown that the stearic acid molecules in the SAM structure have a tilt angle on the substrate surface (*chapter3 § 2.2.6 Table 9*). This angle favored van der Waals interactions and this confers stability to the well-arranged monolayer. After applying a pressure on the two monolayers as shown in figure 1, the tilt angle value decreases from an average value of 80 ° for the adsorbed film to 65 ° for both top and bottom layer in the compressed state. It is interesting to note that all molecules have the same orientation when there are under high pressure. When shear stress is applied in the x directions during 1 ns of MD simulation while maintaining the pressure, the tilt angle further decreases from 65 ° to 60 ° for the bottom layer but strongly increases after orientation to 120 ° for the top layer (see figure 1). In fact, all molecules are oriented toward the sliding direction after about 40 ps which are in agreement with Tupper and Brenner's work [1]. Different initial models (fig. 1.a and 1.b) have been tested (against vs. toward the sliding direction) and final states are always the same.

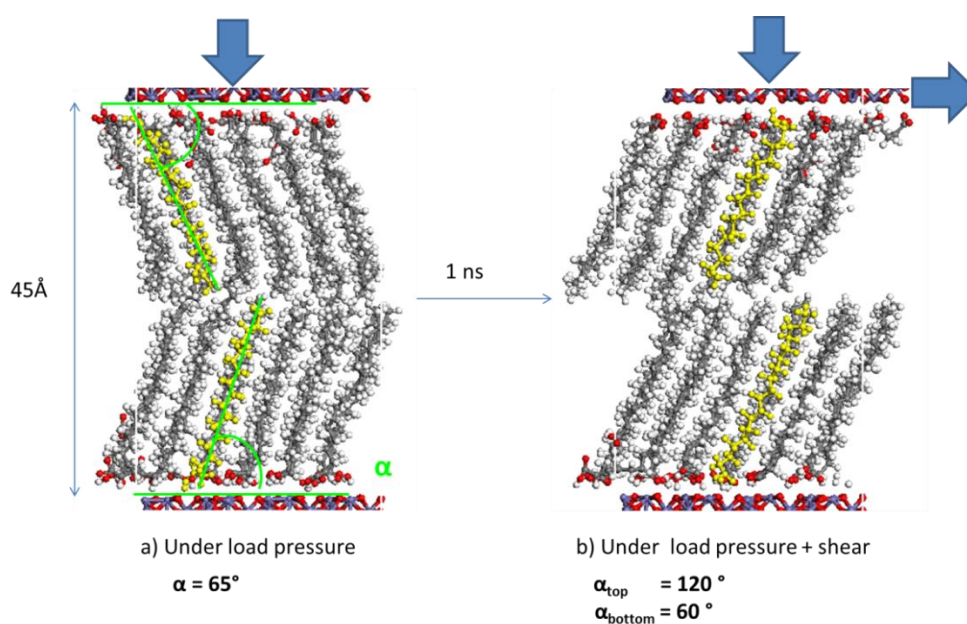


FIGURE 1: CHANGE IN TILT ANGLE OBSERVED DURING FRICTION MD SIMULATION OF TWO INTERACTING MONOLAYERS. SAM 24 STEARIC ACID MOLECULES ON EACH IRON OXIDE SURFACE 1 NS MD SIMULATION, 50 °C

Fisher et al. [2] have measured the tilt angle before and after friction tests. Tribological conditions applied on the stearic acid monolayer can reorient the alkyl chains by around  $12^\circ$  without substantial loss of surface coverage [2]. This average change observed on steel and copper surfaces are in agreement with our change from about  $15^\circ$  between the adsorbed layer and the layer under severe conditions. A stable chemically bonded molecular adsorbed layer persists on the surface after tribochemical treatments. In addition, the molecular orientation of the molecules is preserved after rubbing. Nevertheless, when sliding heights decrease, e.g. pressure increases, the tilt angle increases until a limit where disorder in the SAM appears with non-recovery of the original SAM structure [3].

### 2.1.2 Sliding speed and temperature control

Because of simulation cost, the sliding speed in MD simulation is always much higher than in experimental tests (100 m/s against 70 mm/s). It is shown that friction coefficient increases when sliding speed increases for saturated fatty acids but not with unsaturated fatty acids [4]. To overcome this high sliding speed, a thermostat is applied on the system by scaling the velocity (*cf. Chapter 2 § 2.2.6 for details*). First, the evolution of the temperature at the interface is checked as shown in figure 2. Figure 2 represents the evolution of temperature of -OH oxygen force field type with respect of time. It is seen that at both  $50^\circ\text{C}$  and  $150^\circ\text{C}$ , the temperature remains constant during the whole simulation.

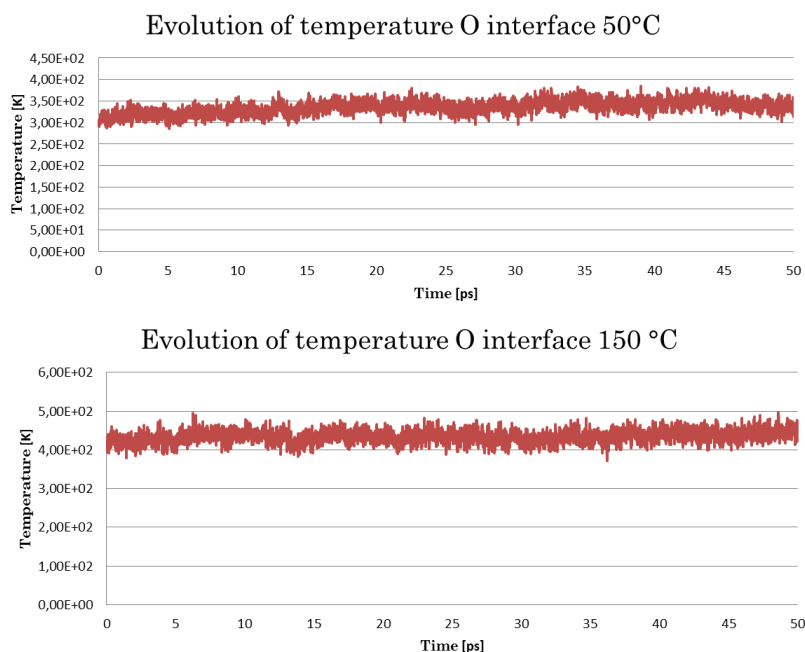


FIGURE 15: EVOLUTION OF TEMPERATURE OF THE HYDROXYL GROUP OXYGENS AT THE INTERFACE WITH THE SUBSTRATE, MD SIMULATIONS AT  $50^\circ\text{C}$  AND  $150^\circ\text{C}$  UNDER SHEAR CONDITION WITH A THERMOSTAT

Eventually, much attention is paid on the fact that friction coefficients calculated by MD simulations and the ones measured with experimental devices are not directly comparable. The reason is that size and time scales are completely different. The simulation box is a few nanometers large whereas experimental sample is several millimeters large as shown in figure 3. Typically, the MD simulation time step can hardly overpass a few nanoseconds duration because of the presence of hydrogen (*chapter 2 § 2.2.3*) whereas experimental test is run for several tens of minutes.

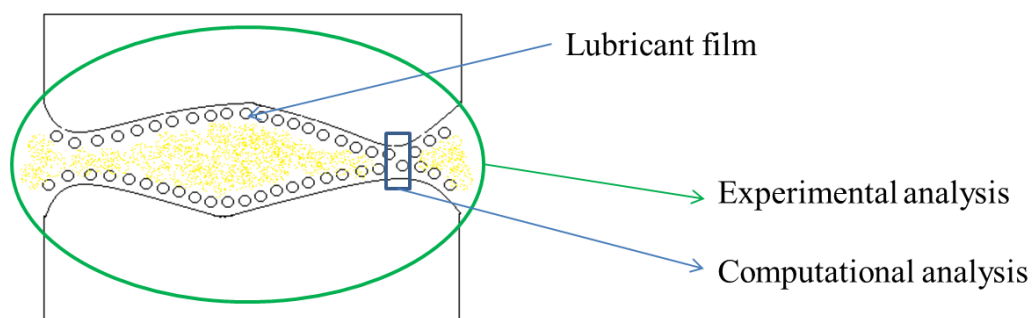


FIGURE 16: EXPERIMENTAL AND NUMERICAL SAMPLES: DIFFERENT CELL SIZE AND TEST TIME

In more recent works, MD simulations and experiments have been run at same sliding speed, and different friction coefficients were obtained [5]. In fact, materials, substrates, load, temperature, velocity among other factors have an impact on friction coefficient and are therefore considered in the model. When comparing experimental and simulation friction coefficient, it is more reasonable to compare variations rather than real values of friction coefficient.

## 2.2 Influence of selected parameters

In our study, many MD simulations were run while changing only one parameter at a time, in order to see its impact on friction coefficient and on the organization of the film (the type of molecule, the type of substrate, the density of OFM on iron-based surfaces, and the alkyl chain length). Each MD simulation has been run twice in order to check the reproducibility of our method. In this chapter, the chosen tribological system is composed of one SAM of fatty acid deposited on each iron-based substrate. Pressure has been chosen similar to that of the experimental study, e.g. 300 MPa. The temperature is fixed to 50 °C for all MD simulations.

### 2.2.1 Influence of unsaturation degree and density

#### 2.2.1.1 Qualitative and quantitative study

The quantitative study in chapter 3 (§ 2.2.5) has shown that the adsorption mechanism of saturated and unsaturated fatty acids in the SAM structure is a chemisorption through the acid group and more particularly, through the carboxyl group. The difference between stearic, oleic and linoleic acids concerns the arrangement of the film on the surface, not the chemical reaction with the oxide. As they do not arrange on the surface identically, different friction behaviors can be expected.

Basically, our model consists of two monolayers of stearic, oleic and linoleic acid, respectively, compressed between two iron oxide surfaces at a constant pressure of 300 MPa. Two identical densities of the molecules in the film were chosen on each surface inside the simulation box. The first is 15 molecules corresponding to 0.027 molecules/Å<sup>2</sup> and a liquid-like structure. The second is 24 molecules on each surface corresponding to 0.042 molecules/Å<sup>2</sup> generating a solid-like state. Temperature is fixed at 50 °C for all simulations. Figure 4 displays snapshots of the situation observed after 100 ps of sliding time.

In the liquid-like model (figure 4-1), the two monolayers can hardly be recognized when double bonds are present in the chain. This is the case for oleic (figure 4-b-1) and linoleic acid (figure 4-c-1). As a consequence, no sliding plane is observed for unsaturated fatty acids. It seems that some entanglement or interdigitation occurs between the two monolayers. On the other hand, the two stearic acid monolayers can be well distinguished after friction and they apparently slide between the extremities of the methyl group in the chain (figure 4-a-1).

In the solid like model (figure 4-2), the film thickness is much higher and the two monolayers are distinguished for both saturated (figure 4-a-2) and unsaturated (figure 4-b-2 and 4-c-2) fatty acids. However, the presence of double carbon bonds induces some steric effect and a non-linearity of the alkyl chain. The two monolayers slide on each other without any entanglement.

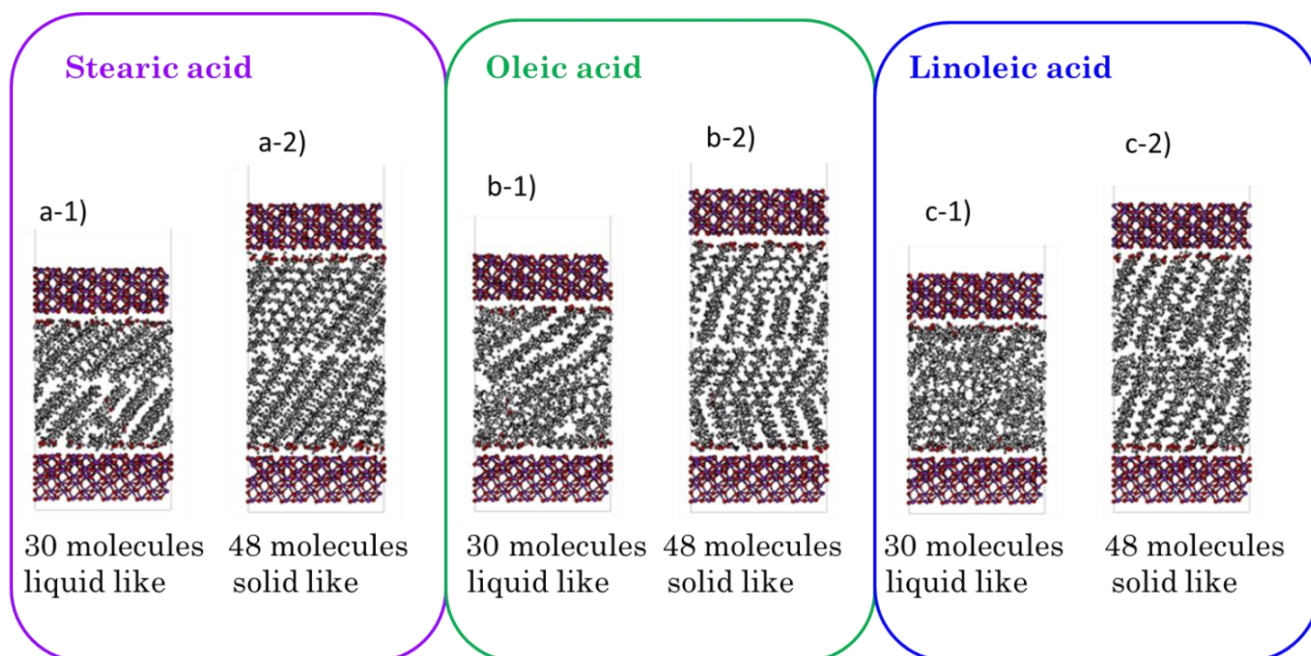


FIGURE 17: SNAPSHOTS AFTER 100 PS OF MD SIMULATION UNDER LOAD PRESSURE OF 300 MPA AND 100 M/S SHEAR FOR THE SAM MODEL OF A) STEARIC ACID, B) OLEIC ACID, C) LINOLEIC ACID BETWEEN IRON OXIDE SURFACE WITH A DENSITY OF 1) 0.027 MOLECULES/ $\text{\AA}^2$  AND 2) 0.042 MOLECULES/ $\text{\AA}^2$  AT 50 °C

Let us consider the case of stearic acid. Figure 5 presents the initial  $z$  position as a function of the  $x$  displacement for each atom after 100 ps of MD simulation for the following models: liquid-like and solid-like stearic acid SAM between iron oxide surfaces (figures 4-a-1 and 4-a-2). The idea is to follow the displacement in  $x$  direction of one atom, initially at a certain  $z$  position.

A sliding plane is clearly distinguished at the extremity of the alkyl chains between the two monolayers in both liquid and solid like cases (figure 5-1 and 5-2 red lines). For the liquid-like system (figure 5-1 green line), there is also a partial slip at the wall, meaning that the monolayer is not strongly adsorbed on the bottom surface. On the other hand, for the solid-like system (figure 5-2), there is a clear sliding plane between the two monolayers. Both the top and bottom monolayer are strongly adsorbed on the surface and molecules slide on each other with an expected tilt angle.

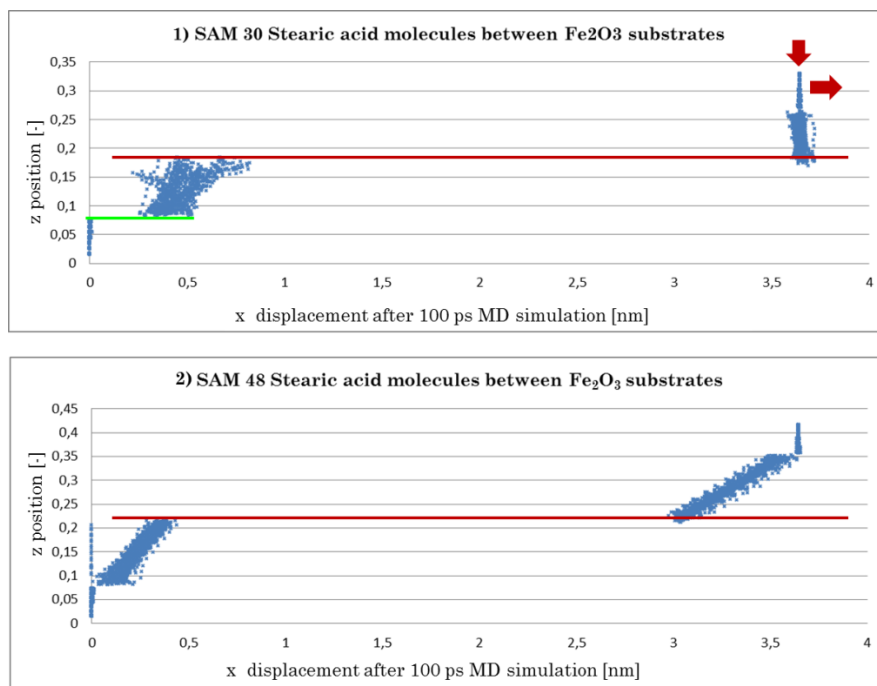


FIGURE 5: X DISPLACEMENT COORDINATION OF EACH ATOMS AFTER 100 PS OF MD SIMULATION AS A FUNCTION OF INITIAL Z COORDINATION: STEARIC ACID 1) LIQUID LIKE SAM AND 2) SOLID LIKE SAM BETWEEN IRON OXIDE SURFACES, 50 °C, 300 MPA NORMAL LOAD, 100 M/S SLIDING SPEED (RED NARROWS). SLIDING PLANES ARE INDICATED BY RED AND GREEN LINES

The friction coefficient is evaluated by MD simulations and results are presented in figure 6. The friction coefficient is calculated over a period of 100 ps for each model (see *chapter 2 § 2.2.8*).

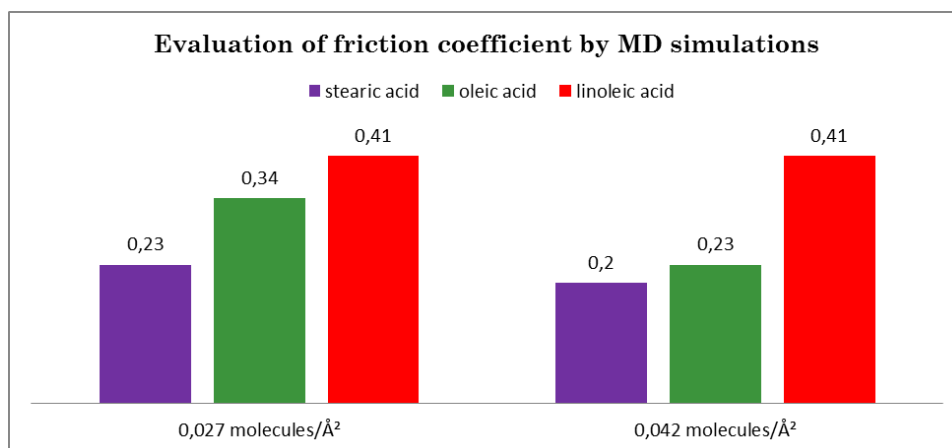


FIGURE 6: MD FRICTION COEFFICIENT (AFTER 1 NS UNDER 300 MPA LOAD AND 100 M/S SHEAR) OF STEARIC (VIOLET) OLEIC (GREEN) AND LINOLEIC (RED) ACID SAM BETWEEN IRON OXIDE SURFACE AT 50 °C: LEFT) LIQUID LIKE SAM, RIGHT) SOLID LIKE SAM

Figure 6 clearly shows that stearic acid provides the lowest friction coefficient, compared with unsaturated acids, and this whatever the density of the molecules. The friction coefficient of oleic acid SAM decreases from 0.34 to 0.23 when the density increases from 0.027 to 0.042 molecules/Å². On the other hand, the friction coefficient for linoleic acid SAM is not influenced by the density. By looking closely, it is seen that after the double carbon bonds, the remained alkyl chain is not organized at all and many entanglements appear which can explain why there is no difference in the evolution of friction coefficient.

The substrate separation was measured with Material Studio© V6 software and distances are gathered in table 1. The difference in stearic acid film thickness is 14 Å which is

traduced by a decrease of the tilt angle when the density increases (*see chapter 3 section 2.2.6*). The difference in film thickness is 16 Å and 14 Å for oleic and linoleic acid respectively, which is similar to stearic acid.

TABLE 1: FILM THICKNESS REGARDING THE NUMBER OF UNSATURATION (STEARIC, OLEIC AND LINOLEIC ACIDS) AND THE DENSITY (0.027 MOLECULES/Å<sup>2</sup> AND 0.042 MOLECULES/Å<sup>2</sup>) BETWEEN TWO IRON OXIDE SURFACES AFTER 100 PS OF MD SIMULATION UNDER 300 MPa LOAD PRESSURE AND 100 M/S SHEAR, 50 °C

Number of molecules	Distance between two surfaces with stearic acid (nm)	Distance between two surfaces with oleic acid (nm)	Distance between two surfaces with linoleic acid (nm)
30	3.1	3.2	2.9
48	4.5	4.8	4.3

### 2.2.1.2 Discussions

The tribological results obtained by MD have shown that two phenomena can occur in the contact when two monolayers of fatty acids in regards are sliding on each other: first slip at the interface between the two monolayers and second slip at the interface monolayer-substrate. As the nature of the surface plays a main role in the slip at the interface, this will be considered in the next section (§2.2.2). But let us discuss the sliding phenomenon between the two monolayers. Regarding the type of monolayers (well or not well organized), two cases are found in literature and lead to different friction behaviors.

First of all, it is clearly seen that the alkyl chains do not entangle under stress for stearic acid. The monolayers slide on each other, with the sliding plane between the two monolayers. Molecules are resistant to compression certainly due to osmotic pressure. In fact, entropic effects can also produce repulsive forces that may balance the attractive van der Waals forces and this prevents the two monolayers from interdigitation [6]. There are repulsion forces between opposing –CH<sub>3</sub> groups that provide low interfacial shear stress [7] as shown in figure 7-a. It should result in low friction coefficient.

On the other hand, especially with liquid-like model of unsaturated molecules, the sliding plane between the two monolayers is not clear. Unsaturated molecules can be compared to branched molecules because they both induce some steric effects. The unsaturated molecular shape results in the difficulty to achieve complete surface coverage so the probability of metallic contact is increased. As shown in figure 7-b, there are some area where molecules can interdigitate. It should result to a higher friction coefficient.

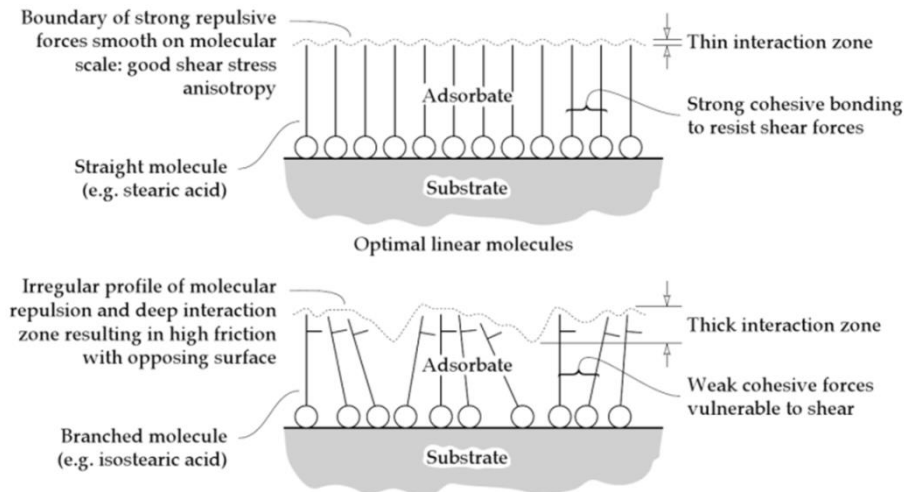


FIGURE 7: DISRUPTION OF ADSORBATE FILM STRUCTURE BY BRANCHED MOLECULE [7]



The difference of friction behavior of saturated and unsaturated molecules that we have obtained by MD can be explained by the different organization of adsorbed layers. In case of saturated molecule (stearic acid), the first model (figure 7a) is found, leading to lower friction than with unsaturated molecules (second model-figure 7b). In literature, several studies from both experimental <sup>[8]</sup> and simulation works <sup>[9]</sup> have shown the same relationship between monolayer organization and friction behavior.

But in our simulations, friction coefficient values are higher than those usually given in the literature. For example, the packing of fatty acids molecules adsorbed on mica from a solution of hexadecane has been previously estimated by using the Surface Force Apparatus (SFA). Results indicate that stearic and oleic acid molecules form a monolayer on each surface like in our simulation model <sup>[8]</sup>. Estimated film thicknesses are 46-54 Å and 50-55 Å for stearic and oleic acids, respectively. These values are not far from our calculation for the highest density (45 Å and 46 Å see table 1). The slight discrepancy can be attributed to the presence of some hexadecane molecule in the interface, increasing slightly the distance in the SFA. Friction coefficient is lower for stearic acid (0.055) than for oleic acid (0.1). Therefore, the values of friction coefficients for both acids are 3-4 times lower in the SFA than in our MD simulation.

Let us have a look in a zoom area of the interface of the two monolayers in our MD simulations. Figure 8 represents series of snapshot at different MD simulation times. It seems that molecules have some difficulty to slide on each other and that some impacts between hydrogen atoms cannot be avoided. The sliding between the two monolayers is therefore not smooth and this can increase the friction coefficient. This effect has been already observed <sup>[10, 11]</sup> where the friction between an amorphous carbon tip and two n-alkane monolayers has been examined. It is important to have in mind that in all these MD simulations, there is no solvent. The presence of solvent (which is the case in most experimental works) will probably modify interactions between the two monolayers and will have an effect also on friction. This will be discussed in the next chapter.

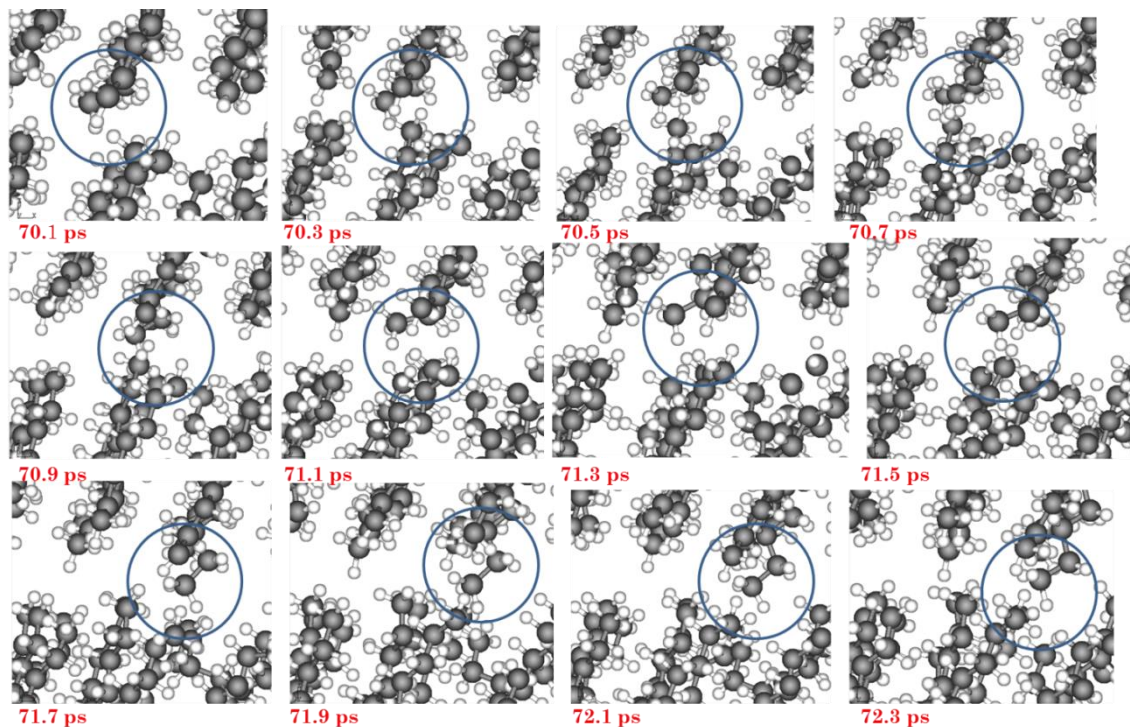


FIGURE 8: SNAPSHOTS OF INTER-MOLECULAR LAYERS, MD SIMULATION STEARIC ACID SOLID-LIKE SAM UNDER 300 MPA LOAD PRESSURE AND 100 M/S SLIDING SPEED, 50 °C.

As some slip at the interface monolayer-substrate is also found in our MD simulations, the nature of the substrate should be studied.

## 2.2.2 Influence of oxidized/hydroxide layer on iron-based surface

### 2.2.2.1 Qualitative and quantitative study

Similar MD simulations were run by replacing iron oxide surface by iron hydroxide one (in fact iron oxide saturated by water). All the other parameters of the simulation were identical (pressure 300 MPa, speed 100 m/s and temperature 50 °C). In chapter 3 § 2.2.3, iron hydroxide surface has been described as less reactive than iron oxide surface. Figure 9 shows snapshots after 100 ps of sliding time.

For the liquid-like models (figure 9-1) with molecules deposited on iron hydroxide, (figure 9-a-1 figure 9-b-1 and 9-c-1), the two monolayers are not easily distinguished whatever the unsaturation degree. Moreover, acid groups are detected in the middle of the bifilm confirming the fact that molecules have been detached from the surface.

For the solid like models (figure 9-2) with molecules deposited on iron hydroxide surfaces, the two monolayers can be distinguished even if some molecules perturb the well-arranged monolayer.

On iron hydroxide surface, it is more difficult to determine the existence of a well-defined sliding plane with the snapshots. Therefore, displacement profile (figure 10) is investigated with both iron oxide and iron hydroxide surfaces models.

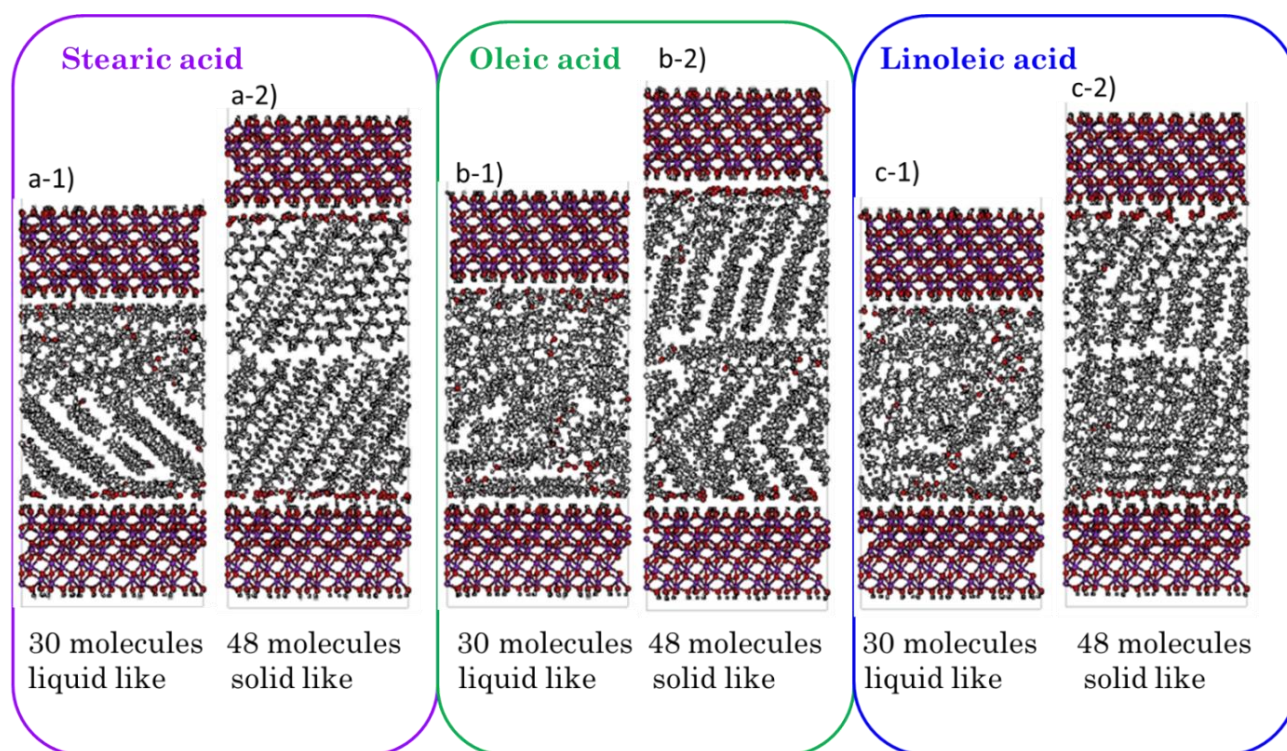


FIGURE 9: SNAPSHOTS AFTER 100 PS OF MD SIMULATION UNDER LOAD PRESSURE OF 300 MPa AND 100 M/S SHEAR FOR THE SAM MODEL OF A) STEARIC ACID, B) OLEIC ACID, C) LINOLEIC ACID BETWEEN IRON HYDROXIDE SURFACE WITH A DENSITY OF 1) 0.027 MOLECULES/Å<sup>2</sup> AND 2) 0.042 MOLECULES/Å<sup>2</sup> AT 50 °C

Let us consider the case of stearic acid. Figure 10 presents the x displacement for each atom after 100 ps of MD simulation as a function of initial z position for the following models:



liquid-like and solid-like stearic acid SAM between iron hydroxide surfaces (figures 9-a1 and 9-a-2).

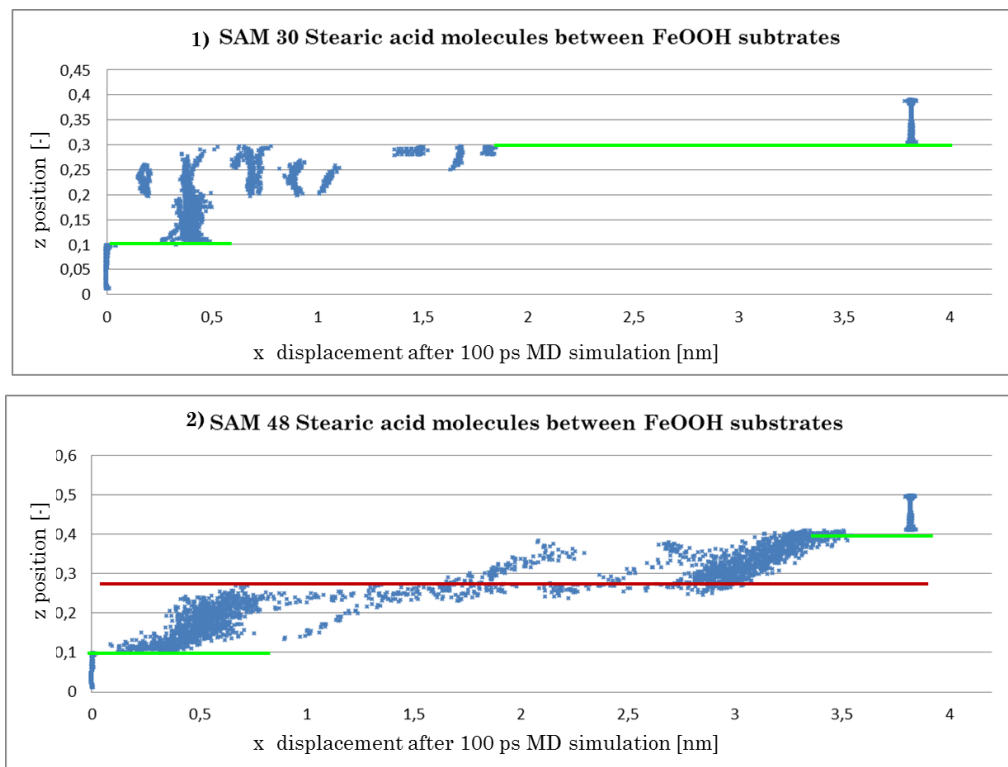


FIGURE 10: X DISPLACEMENT COORDINATION OF EACH ATOMS AFTER 100 PS OF MD SIMULATION AS A FUNCTION OF INITIAL Z COORDINATION: STEARIC ACID 1) LIQUID LIKE SAM AND 2) SOLID LIKE SAM BETWEEN IRON OXIDE SURFACES, STEARIC ACID 3) LIQUID LIKE SAM AND 4) SOLID LIKE SAM BETWEEN IRON OXIDE SURFACES, 50 °C, 300 MPA NORMAL LOAD, 100 M/S SLIDING SPEED. SLIDING PLANES ARE INDICATED BY GREEN AND RED LINES.

Using iron hydroxide surfaces, the behavior is drastically different (figure 10-1 and 10-2) from the one observed using iron oxide surfaces (figure 5). For the liquid-like system (figure 10-1), sliding planes are at the interface substrate/monolayer, meaning that additives are not strongly adsorbed on the surface. Sometime, molecules between the two substrates are dragged by the sliding substrate at different sliding speeds characterized by the different glitches seen in graph number 1. The organization of the film seems to be completely lost after sliding. In addition, there is also a sliding plane between the two monolayers for the solid-like system (figure 10-2) but it is much less visible than in the case of iron oxide (figure 5-2).

Comparison of calculated friction coefficients of stearic acid squeezed between iron oxide and iron hydroxide surfaces are presented in figure 11. Friction is slightly lower with iron hydroxide than with iron oxide at the two studied densities. Even in the absence of additives, iron hydroxide substrates originally exhibit lower friction than iron oxide substrates ( $\mu = 1.33$  and  $1.75$  respectively as shown in figure 11). Another difference observed is that friction decreases when density increases on iron oxide surface whereas the opposite behavior is seen with iron hydroxide. On iron oxide, this is explained by the good ordering in the molecules and a clear definition of a sliding plane between the two monolayers. On iron hydroxide, the sliding plan is partially located in the interface substrate/additives as well as between the two monolayers (figure 10-1 and 10-2) so the organization of the film does not impact greatly the friction behavior.

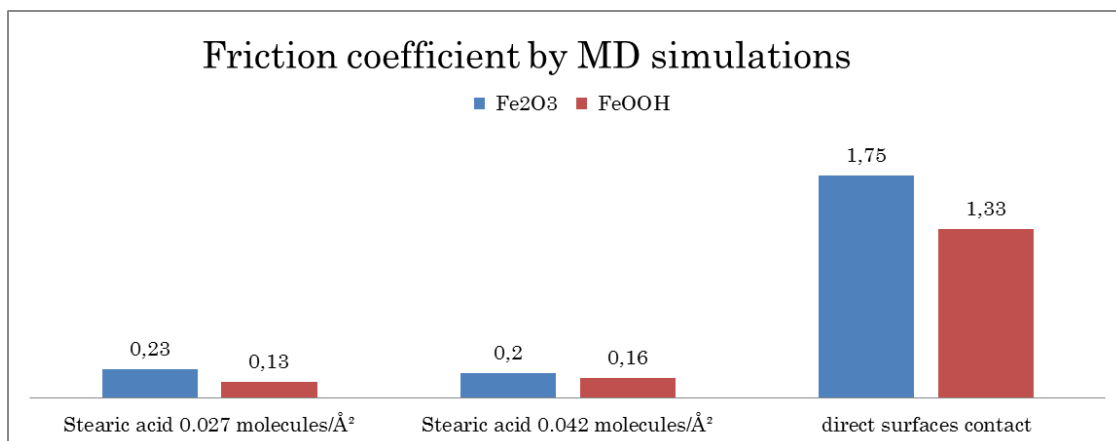


FIGURE 11: EVALUATION OF FRICTION COEFFICIENT BY MD SIMULATION FOR STEARIC ACID ON IRON OXIDE (BLUE COLOR) AND IRON HYDROXIDE (RED) SURFACES AT 50 °C AND TWO DIFFERENT DENSITIES: LEFT) LIQUID LIKE MODEL, RIGHT) SOLID LIKE MODEL AFTER 100 PS OF MD SIMULATION UNDER 300 MPA LOAD PRESSURE AND 100 M/S SHEAR IN X DIRECTION

In the case of hydroxide, the film thickness increases with increasing density (from liquid-like to solid-like monolayer) as shown in figure 9 and table 2. The film thickness between iron hydroxide surfaces is slightly thicker than between iron oxide surface (1-3 Å).

TABLE 2: FILM THICKNESS REGARDING THE NUMBER OF UNSATURATION (STEARIC, OLEIC AND LINOLEIC ACIDS) AND THE DENSITY (0.027 MOLECULES/Å² AND 0.042 MOLECULES/Å²) BETWEEN TWO IRON HYDROXIDE SURFACES AFTER 100 PS OF MD SIMULATION UNDER 300 MPA LOAD PRESSURE AND 100 M/S SHEAR, 50 °C

Number of molecules	Distance between two surfaces with stearic acid (nm)	Distance between two surfaces with oleic acid (nm)	Distance between two surfaces with linoleic acid (nm)
30	3.3	3.3	3.0
48	4.8	5.0	4.5

### 2.2.2.2 Discussions

First of all, friction of stearic acid in SAM model is lower with iron hydroxide than with iron oxide. It seems that slip at the wall is very easy on iron hydroxide. This situation is very similar to glycerol on Diamond-Like Carbon (DLC) in which there is slip at the wall with low friction coefficient due to very weak roughness of the interface [12].

Then friction is reduced with iron oxide when the density of molecules is increased. This is due to the organization of molecules in a close-packed monolayer with same adsorption mechanism to the surface and to a smoother sliding plane between the two monolayers. On the other hand, the friction coefficient increases when the density is increased on iron hydroxide surface. The appearance of a sliding plane between the two monolayers probably induces some friction as terminated methyl group slide one across another with different conformations (see section 2.1.1.2). In the liquid-like model, the two monolayers react like a fluid or a solvent so there is no impact at the interface.

MD simulations of alkylsilane and alkoxyasilane SAM on amorphous silica substrate have been particularly studied in the literature [13]. Alkylsilane molecules are hydrogen bonded or physisorbed to the substrate whereas alkoxyasilane molecules are covalently bonded or chemisorbed to the surface. It has been shown that in the presence of water monolayer, friction is reduced as a result of a slip plane that is formed between water layer and SAMs [13]. This behavior is very similar to the behavior observed with our iron oxide fully covered by –OH termination (and so-called FeOOH substrate). To conclude, both the nature of the surface

and the number of unsaturation in the fatty acid have an impact on the tribological behavior of OFMs on iron-based surfaces.

The present study has been performed with C18 fatty acids. Several authors have investigated the influence of alkyl chain length on tribological behavior <sup>[14-21]</sup>. In the next section, the influence of alkyl chain length will be investigated by our MD simulations.

### 2.2.3 Influence of chain length

#### 2.2.3.1 Results

First, one solid-like SAM (same density) of linear fatty acid molecules is deposited on iron oxide surface. Then, the system is let to relax. Eventually, sliding tests are performed with same procedure used in previous sections (300 MPa contact pressure, 100 m/s sliding speed and constant controlled temperature of 50 °C). Figure 12 shows snapshot of the simulation taken after 1 ns of MD simulation for C6 (figure 12-a) and C10 (Figure 12-b) fatty acids solid-like SAM on iron oxide surfaces. As can be seen, below 10 carbons in the chain, the SAM configuration cannot be maintained and molecules adopt the ‘random’ configuration as shown in chapter 3 section 2.1.1 and in figure 10-a. This is because the cohesion force between alkyl chains is not strong enough to keep the SAM configuration. At the opposite, from C10-C18 fatty acids, the SAM configuration is stable over time and the bottom and top SAMs are sliding on each other with the same tilt angle as shown in figure 12-b. The main result here is that stabilization of the SAM by van der Waals interactions between the chains is efficient for molecules with at least 9 carbons in the chain <sup>[14]</sup>. For information, cohesive interactions between neighboring chains increase by 0.8 kcal/mol per methylene unit in the alkyl chain <sup>[15]</sup>.

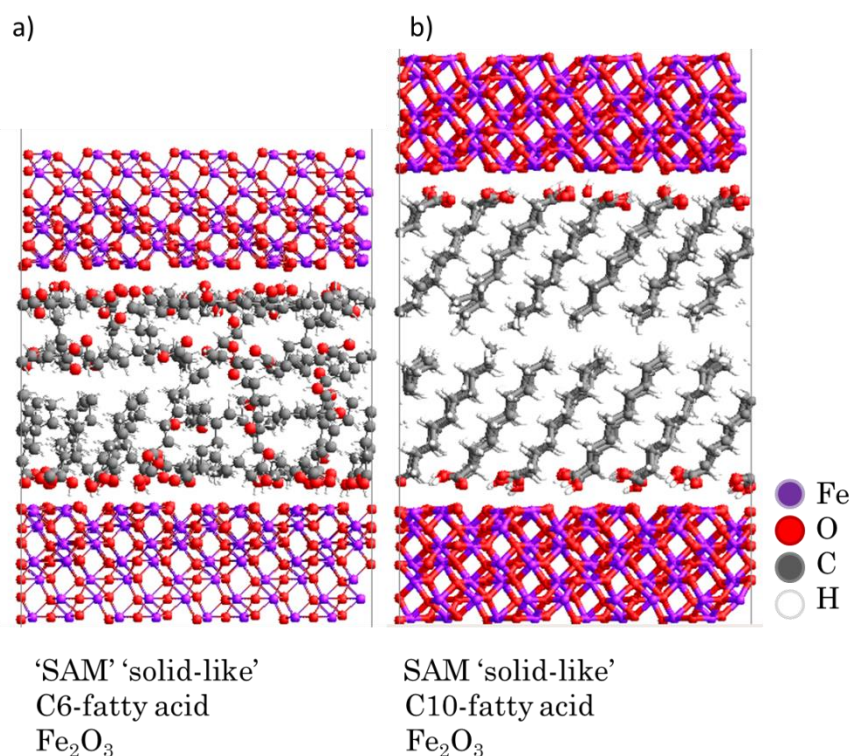


FIGURE 12: SNAPSHOTS AFTER 1 NS OF MD SIMULATION WITH 300 MPA NORMAL LOAD AND 100 M/S SLIDING SPEED IN X DIRECTION AT 50 °C WHEN INITIAL STATE IS ON SOLID LIKE SAM OF A) C6 FATTY ACID MOLECULES, B) C10 FATTY ACID MOLECULES ON EACH IRON OXIDE SURFACE

Many experiments have shown that friction coefficient decreases when the alkyl chain length increases until a given number of carbons (about 10) afterwards the friction coefficient remains constant [16]. As an example, friction coefficient in systems lubricated with 500 ppm solutions of C6-C22 fatty acids in a diesel fuel matrix is about 0.095 for C6 fatty acids, 0.085 for C8 fatty acid and 0.073 for C10 to C18 fatty acids [22].

Figure 13 shows friction coefficient in system with pure C6 to C18 fatty acids calculated by MD simulation over a period of 100 ps. Friction coefficient decreases from 0.32 (when the chain length of C6 fatty acids) to about 0.2 with C16 and C18 fatty acids. Decrease of friction coefficient with the increase of alkyl chain length has been observed many times in literature. But regarding parameters such as the solvent used, the “way” the decrease occurs could be different [23]. The solvent has also a significant impact on the effect of chain length in boundary lubrication and could explain the differences found in literature and with our results.

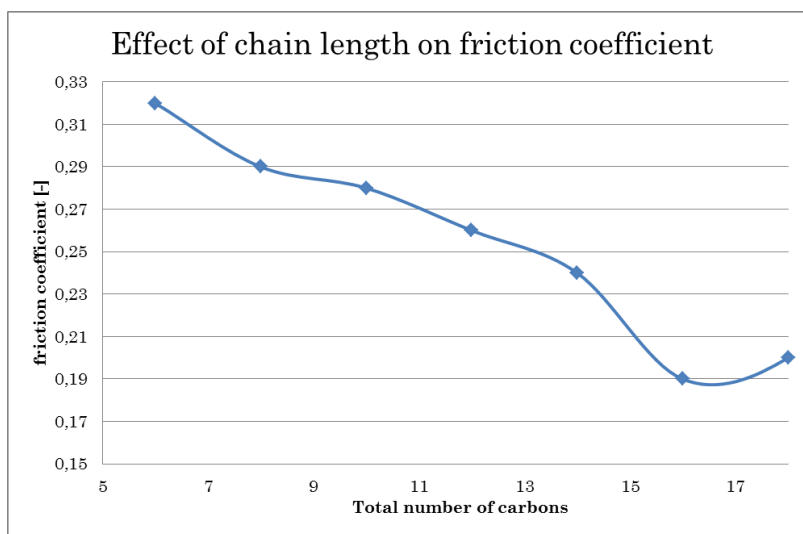


FIGURE 13: FRICTION COEFFICIENT CALCULATED BY MD SIMULATION (LAST 100 PS) FOR DIFFERENT LINEAR ALKYL CHAIN LENGTH FATTY ACIDS BETWEEN IRON OXIDE SURFACES WITH 300 MPA NORMAL LOAD AND 100 M/S SLIDING SPEED AT 50 °C.

Despite the difference that is observed in the molecules organization between short and long alkyl chain lengths, we found that the substrate separation after 1 ns sliding test is proportional to the alkyl chain length, as shown in figure 14. This is similar to results obtained for C8-C20 alkylsilane monolayer by Cheng *et al* [15].

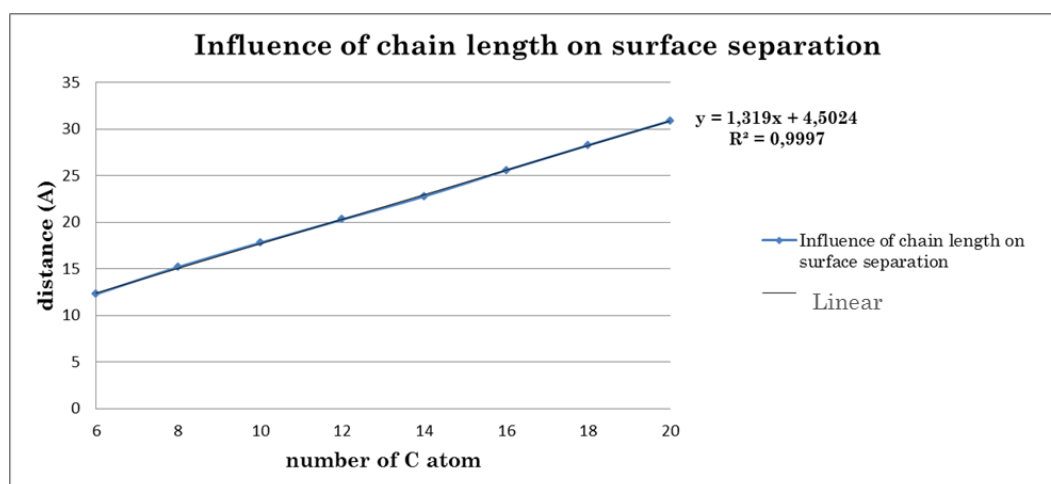


FIGURE 14: DISTANCE BETWEEN THE TWO IRON OXIDE SURFACES AS A FUNCTION OF FATTY ACID AKLYL CHAIN LENGTH

### 2.2.3.2 Discussions

From our MD results, the decrease of friction coefficient with the number of carbon atoms in the alkyl chain, already shown in literature, was confirmed. Different phenomena can explain this behavior.

First of all, in case of short chains, cohesion forces between alkyl chains are not strong enough to form a solid-like SAM configuration as it is for longer chains. When a less densely packed or disordered monolayers is found, the resulting friction coefficient is usually higher than for the SAM and this for further reasons: 1) more entanglements between the two adsorbed layers are found (cf. figure 7-b) and 2) as a greater number of defects is found, barriers to defect creation decrease under contact conditions [15].

When a SAM configuration is obtained (with more than C10), SAMs are sliding on each other exhibiting lower friction behavior like presented previously (figure 7-a).

In addition to disorganization of short alkyl chain SAM, another explanation for high friction coefficient with short alkyl chain length might be the presence of a non-contact friction forces due to electromagnetic interactions between the two metallic substrates. A quantitative interpretation of the Electrical Contact Resistance (ECR) in a tribological contact propose to establish that friction coefficient evolves as a power law of the tribologic interface thickness  $l$  resulting from the presence of organic molecules as shown in figure 15 [24, 25]. When  $l$  increases, the term  $K/l^n$  becomes negligible and  $\mu = \mu_0$ .

Evolution of  $\mu$  as a function of Log (Rc)

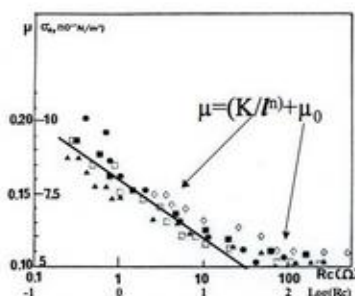


FIGURE 15: EVOLUTION OF FRICTION COEFFICIENT AS A FUNCTION OF ECR VARIATIONS [24]

Basically, this assumption proposes that significant friction forces can exist (in vacuum) between two metal surfaces separated by a very small gap, typically less than 1 nm. As a consequence, additional tangential forces with metal surfaces separated by two monomolecular polar acids layers may occur if the distance, and therefore the alkyl chain length, is not large enough to inhibit this effect. Moreover, the presence of the molecules in the gap could screen these forces. Experimentally, Mansot *et al.* verify that in the presence of an insulating polymer layer, friction drastically increases when the film thickness is below 1 nm and related this behavior to derive from Postnikov theory for energy dissipation in boundary with  $n = 4$  in equation presented on figure 15 [24, 25]. In these works, the gap between surfaces was measured by tunneling current. Recently, these non-contact forces have been evidenced by using a very sensitive oscillating AFM [26].

To check (or not) the presence of this phenomenon in our case, some DFT calculations were performed as preliminary results. The distance between two iron surfaces was fixed during the calculation as shown in the model schematic (figure 16). Total energy of the system was calculated for different x or y positions in order to mimic sliding conditions. Figure 16



presents, as an example, the evolution of the energy as a function of y displacement while fixing the surface separation at 1 nm. Then, the energy necessary to reach the maximum energy (slope: red arrow in figure 16) is evaluated and so the frictional force as shown in table 3.

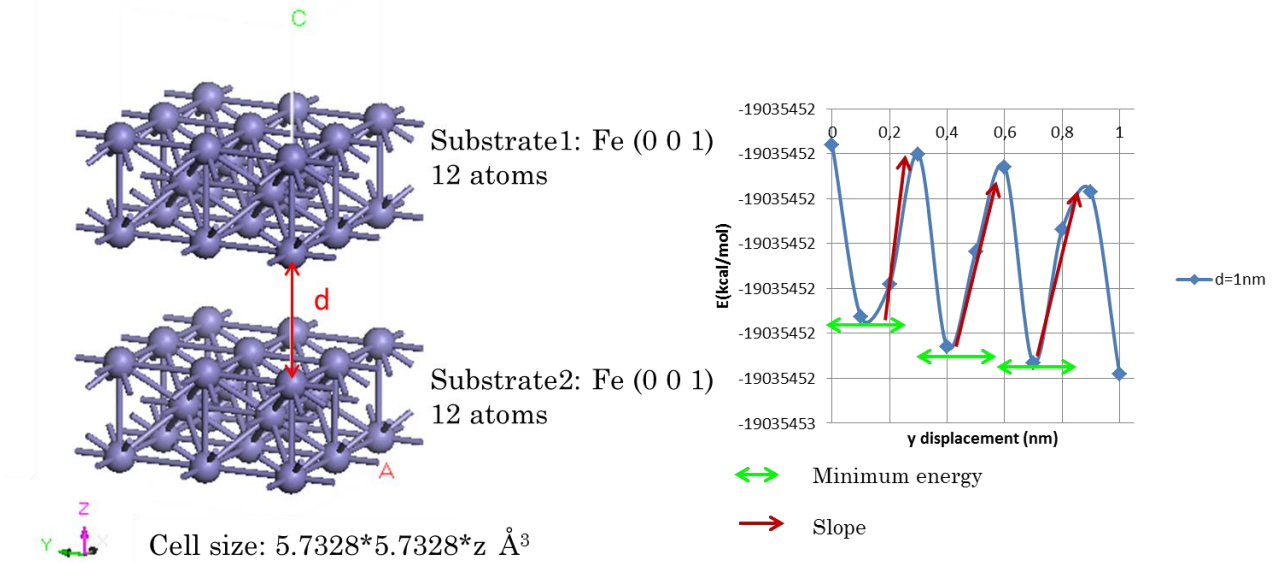


FIGURE 16: MODEL FOR NON CONTACT FRICTION EVALUATION: TWO IRON SUBSTRATES SEPERATED BY A FIXED DISTANCE D, ENERGY OPTIMIZATION IS PERFORMED WITH DIFFERENT Y POSITION OF THE UPPER SUBSTRATE IN ORDER TO EVEALUATE THE ENERGY AS A FUNCTION OF DISPLACEMENT BY DMOL3, EXAMPLE OF 1 NM SEPERATION LENGTH

The value 40 MPa (mean area force value from table 3) for the non-contact friction is equivalent to a friction coefficient of 0.1 under a normal load of 400 MPa. This means that the non-contact friction could contribute to the friction behavior of iron surface when the distance is very short, e.g. with short alkyl chain length. However, this effect is no longer observed for a distance greater than 1.5 nm that correspond, in our study, to fatty acid with more than 8 carbons (figure 14). Of course, this is only some preliminary results on pure iron. Further and deeper investigations are needed to check this behavior with iron oxide surface and with the presence of hydrocarbon or fatty acids monolayer instead of vacuum.

TABLE 3: EVALUATION OF FRICTION COEFFICIENT DURING NON CONTACT SLIDING OF TWO IRON SUBSTRATE SEPERATED BY 1 NM – ENERGY IS CALCULATED WITH MATERIAL STUDIO V6 DMOL3 DFT METHOD.

low energy point	(slope)kcal/mol.nm	kJ/mol.nm	kJ/m (=kN)	Area force (kN/m <sup>2</sup> )	Friction coefficient under 400 MPa
1	1.80	7.55	1.25E-12	38200	~ 0.1
2	1.99	8.35	1.39E-12	42200	
3	1.90	7.95	1.32E-12	40200	

Although long chain fatty acids have the same friction behavior in terms of friction coefficient, the choice of number of carbon atoms needed for good tribological behavior are based on the solubility of the fatty acids in the base oil as well as its performance in a large range of temperature. In fact, when the chain length increases, the desorption temperature increases. For stearic acid, the friction coefficient decreases slightly when the temperature is

increased until a transition temperature in which the friction coefficient increases drastically. The transitional temperature is linked to a disorientation of the film followed by its desorption. No transitional behavior was observed for C16 and C18 fatty acids when the temperature was raised up to 180 °C whereas for lower chain length, a transition temperature are observed at lower temperature (~100 °C for C12 fatty acid) at the studied conditions <sup>[16]</sup>. This is why C16 and C18 fatty acids are the best saturated fatty acids in terms of friction and wear <sup>[20]</sup> for a large range of temperature. The use of longer alkyl chains in fatty acids could be useful under higher pressure than the one experienced here (300 MPa).

It was reported in literature that under 500 MPa, C32-alkanes can avoid direct contact whereas C64-alkanes can avoid direct contact up to 1 GPa <sup>[21]</sup>.

MD simulation enables to quantify the friction behavior of fatty acids on iron-based surface. Nevertheless, the adsorbed film is analyzed qualitatively with MD simulation. At this step, the question that is raised is how the thermal film behaves when it is submitted to contact pressure and shear stress. To answer this question, MD simulation reaches its limit and quantum chemistry is needed to treat the problem using potential chemical reaction.

### 3. Evolution of adsorption films during sliding process by UA-QCMD

UA-QCMD applied on a system as large as two opposite SAM between iron oxide surfaces takes a long time to be simulated. Because of that, only sliding with stearic acid SAM on iron oxide surfaces was run with UA-QCMD simulation. The simulation is performed in three steps. First, the normal load was applied to study effect of pressure on the film. Then, MD simulation was run until the top substrate does not oscillate anymore which corresponds to equilibrium with a load pressure of 300 MPa. Finally, sliding speed of 100 m/s is applied on the system to investigate the influence of friction on the film.

#### 3.1 Effect of pressure and sliding: into the formation of carboxylate

Analysis of binding energy and bond population of selected pairs (intra and inter-molecular pair with carboxylic group) after applying normal load shows a change in the adsorption mechanism as shown in table 4. Normal load seems to favor the symmetric chemisorption, e.g. strong adsorption of the two oxygen atoms of the carboxylic function on iron oxide surface. In fact, the percentage of symmetrically adsorbed molecules rises from 0 to 43% after applying the normal load. This is in agreement with previous works by Fisher *et al.* who explained that the bidentate surface configuration was favored after the occurrence of the tribochemical reactions induced by surface rubbing <sup>[2]</sup>. The other major adsorption mechanism remains the asymmetric chemisorption through the carboxylic group but as mentioned in chapter 3, this is highly dependent on the orientation of molecules when they just reach the surface.

TABLE 4: COMPARISON OF ADSORPTION MECHANISM BEFORE AND AFTER NORMAL LOAD

Physisorption	Symmetric chemisorption through acid group	Asymmetric chemisorption through carboxyl group	Asymmetric chemisorption through hydroxyl group
<i>Adsorbed thermal film</i>			
20%	0%	70%	10%
<i>After press</i>			
7%	43%	50%	0%

An analysis of the bond population and bonding energy of target pairs (as in chapter 3), e.g. pairs between carboxylic group and the substrate, is performed after sliding test. We could not complete the whole simulation but some interesting results can already be observed after 5 ps. It appears that both the normal load and shear stress favor the formation of the carboxylate function. In fact, energetical study shows a large weakening of the hydroxyl group O-H from  $\sim -115$  kcal/mol to  $\sim -30$  kcal/mol. Moreover, interaction between oxygen of the hydroxyl group and iron of the surface is increased from  $\sim -7$  kcal/mol to  $\sim -27$  kcal/mol. This has been observed for 2 molecules over the 30 molecules present in the cell. The simulation time should be much longer to confirm the break of the O-H bond and definitely the formation of stearate at the surface.

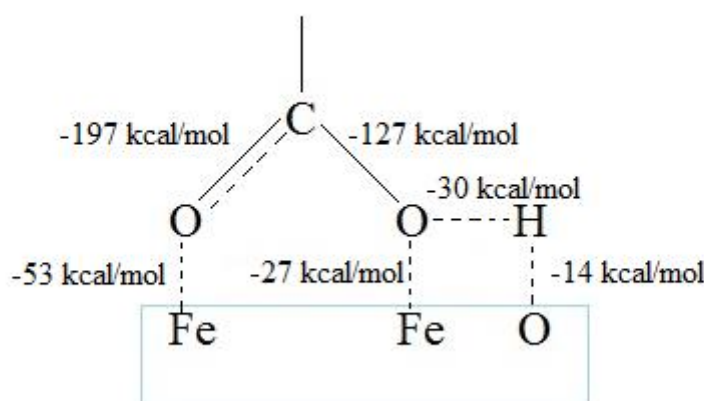


FIGURE 17: SCHEMA REPRESENTING BINDING ENERGY AFTER 5 PS OF UA-QCMD ON SOME STEARIC ACID MOLECULES INCLUDED IN A LIQUID LIKE SAM BETWEEN IRON OXIDE SURFACES SUBMIT TO 300 MPA PRESSURE AND 100 M/S SLIDING SPEED AT 50 °C

The presence of carboxylate is not new and was already highlighted in previous work where it seems that friction promotes the formation of carboxylate [2, 27-32]. This will be discussed in detailed after experimental results presentation.

## 4. Friction behavior of pure additives by experimental study

In this part, the friction and wear behaviors of pure additives on steel surface are investigated. After friction tests, surface characterization are performed in order to validate our computational models.

The tribological behavior of the three fatty acids is studied with the reciprocating linear tribometer at four different temperatures: 25 °C, 50 °C, 100 °C and 150 °C. Stearic acid is only tested at 100 °C and 150 °C as pure stearic acid is solid under 80 °C. Therefore both the effect of temperature and unsaturation can be investigated. Each test is performed three times to confirm reproducibility. Friction coefficient as a function of the number of cycles is then considered.

### 4.1 Effect of unsaturation and temperature

Figure 18 summarizes the friction behavior of saturated fatty acid, e.g. stearic acid and unsaturated fatty acids, e.g. oleic and linoleic acid at different temperatures.

At 25 °C, all pure additives have friction coefficient around 0.07-0.08. The same behavior is observed at 50 °C with a slight increase of friction coefficient ( $\sim 0.09$ ) for both oleic and linoleic acids. At 100 °C, friction coefficients decrease for stearic and oleic acid down to 0.06 and is slightly decreased for linoleic acid down to 0.08 in comparison with lower temperatures. Finally, at 150 °C, linoleic acid loses its lubricant properties with an increase of friction



coefficient up to about 0.12. Stearic and oleic acids maintain their good tribological behavior even at high temperature such as 150 °C. From the two molecules, stearic acid has the best tribological behavior in terms of friction coefficient at each temperature and especially at 150 °C (0.05-0.06).

In terms of wear, some optical pictures were taken with the microscope (see figure 19). In figure 19, it is noticed that at each temperature, wear tracks are difficult to see as very small wear is found on the flat sample for stearic and oleic acid. On the other hand, important wear tracks are observed for linoleic acid solution on steel surface at 150 °C.

In terms of friction and wear, stearic acid has the best tribological behavior. Pure oleic acid is also a good OFM at 50 °C, 100 °C and 150 °C. The advantage of oleic acid compared to stearic acid as lubricant additive is that stearic acid is liquid at all the studied temperatures.

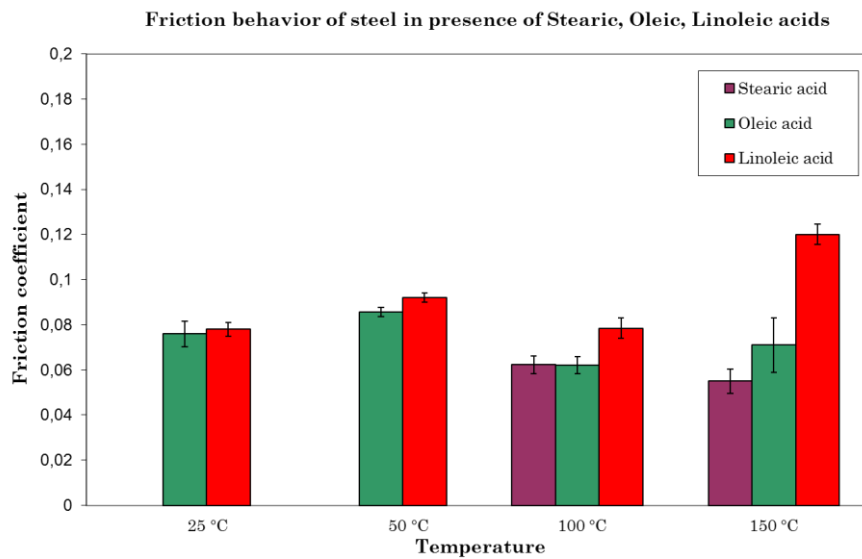


FIGURE 18: STEADY STATE FICTION COEFFICIENT VS PURE STEARIC, OLEIC AND LINOLEIC ACID AT 25 °C, 50 °C, 100 °C AND 150 °C. EXPERIMENTAL CONDITIONS: RECIPROCATING PIN-ON-FLAT TEST WITH AISI 52100 STEEL COUPLE RESPECTIVELY, WITH MAXIMUM SLIDING SPEED OF 56 MM/S, ATMAXIMUM HERTZIAN PRESSURE OF 320 MPA DURING 4000 CYCLES; TESTS ARE REPEATED 3 TIMES









Lubricant	50°C	100°C	150°C
Pure Stearic acid	-----	 $\mu = 0.06$	 $\mu = 0.053$
Pure Oleic acid	 $\mu = 0.085$	 $\mu = 0.065$	 $\mu = 0.058$
Pure Linoleic acid	 $\mu = 0.091$	 $\mu = 0.077$	 $\mu = 0.116$

FIGURE 19: OPTICAL IMAGES OF AISI 52100 STEEL FLAT WEAR SCARS OBTAINED AFTER TRIBOLOGICAL TESTS WITH PURE STEARIC ACID, PURE OLEIC ACID AND PURE LINOLEIC ACID AT 50, 100 AND 150 °C - EXPERIMENTAL CONDITIONS: RECIPROCATING PIN-ON-FLAT TEST WITH AISI 52100 STEEL COUPLE RESPECTIVELY, WITH MAXIMUM SLIDING SPEED OF 56 MM/S, ATMAXIMUM HERTZIAN PRESSURE OF 320 MPA DURING 4000 CYCLES; TESTS ARE REPEATED 3 TIMES

Nevertheless, values presented in figure 18 are mean values and it is interesting to follow the friction coefficient as a function of the number of cycles. In figure 20, the friction coefficient of pure stearic acid on steel surface at 100 °C and 150 °C as a function of the number of cycles is presented. The friction test is reproducible as the standard deviation of friction coefficient does not exceed 11 %. On the other hand, it takes about 500 cycles to reach a steady state value of friction coefficient at 100 °C and 150 °C. In fact, the friction coefficient goes from about 0.08 to 0.06 and from about 0.08 to 0.05 at 100 °C and 150 °C respectively. Once the steady state is reached, it remains constant over time, meaning that the protective film is not removed.

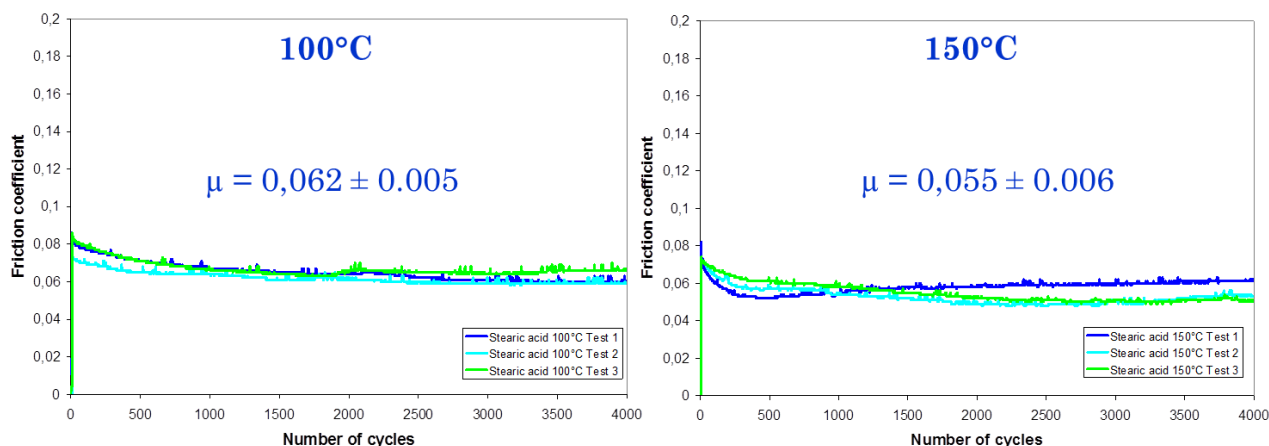


FIGURE 20: EVOLUTION OF FRICTION COEFFICIENT AS A FUNCTION OF CYCLES NUMBER FOR STEARIC ACID AT 100 °C AND 150 °C. LINEAR TRIBOMETER PIN ON FLAT CONTACT WITH MAXIMUM SLIDING SPEED OF 56 MM/S AND MAXIMUM HERTZIAN PRESSURE OF 320 MPA DURING 4000 CYCLES; TESTS ARE REPEATED 3 TIMES

The low friction coefficient of 0.08 for stearic acid blended at 1%w in hexadecane has been measured in another study with a ball-on-cylinder contact at 300 MPa of Hetzian contact pressure at 0.5 or 10 mm/s and at temperature of 100 °C which is more severe than in our study [16].

It seems that increasing the number of double carbon bonds inhibits the good tribological behavior of fatty acids at high temperature. These experimental results are relevant compared to MD simulations presented previously. In order to understand the tribological behavior observed with friction tests, physico-chemical characterization of tribofilms are needed. The tribofilms formed with pure additives are analyzed by PM-IRRAS.

#### 4.2 Analyzis of the tribofilm by PM-IRRAS

First, pure additives are analyzed by IR in order to have a reference. Figure 21 presents the IR spectra of stearic and oleic acid. They have been recorded by ATR in order to characterize the vibration mode of molecules. Details on this spectrum description are presented in chapter 3 §3.2. The alkyl chain presented two main contributions at 2915 cm<sup>-1</sup> and 2848 cm<sup>-1</sup> characteristic of CH<sub>3</sub> and CH<sub>2</sub> function respectively. The carboxylic function is presented by a stretching band at 1700 cm<sup>-1</sup>. For oleic acid, the C=C band is characterized by a very small band in 3007 cm<sup>-1</sup> and at 1657 cm<sup>-1</sup>.

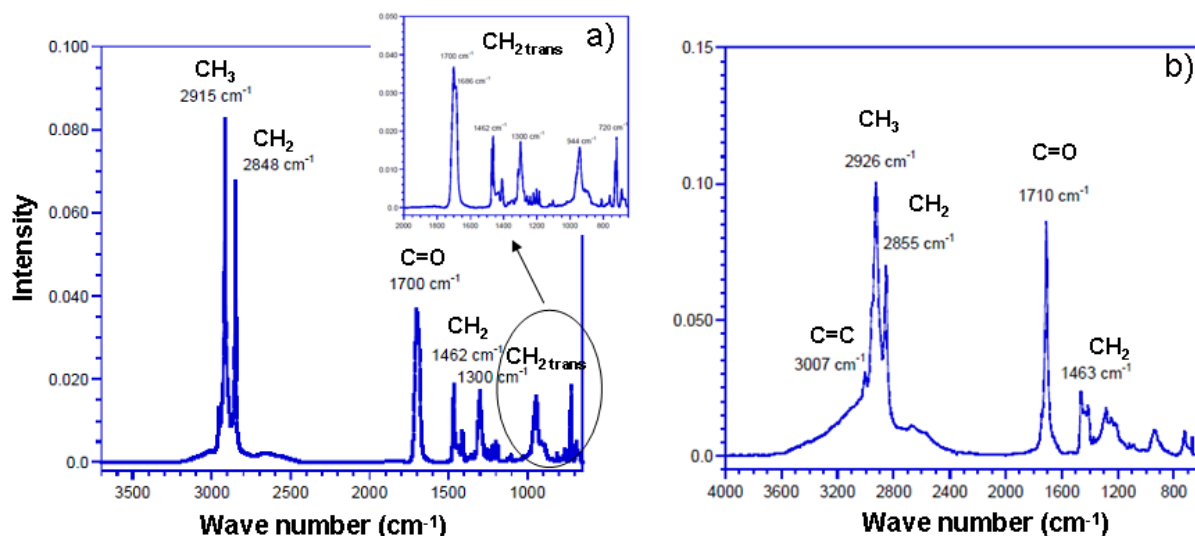


FIGURE 21: ATR SPECTRA WITH GERMANIUM (GE) POLARISATION S OF STANDARD MOLECULE: A) PURE STEARIC ACID, B) PURE OLEIC ACID

Analyzes of surfaces after friction test are presented in figure 22. It is important to note that the mean spectrum obtained by PM-IRRAS scans a surface of a few mm<sup>2</sup>. Because of the small size wear track, spectrums contain informations from area inside and outside the wear track.

For stearic acid, after a first wash, spectrum shows the presence of the stearic acid form with elongated vibration of C=O bond at 1715 cm<sup>-1</sup>, and the stearate form with elongated vibration of COO<sup>-</sup> symmetric group at 1460 cm<sup>-1</sup> and asymmetric group at 1570 cm<sup>-1</sup>. After a second wash, same species are present on the surface with a lower intensity. Regarding Crowell's definition (see *chapter 3 § 3.2.1*) [32], the wavenumber distance between asymmetric and symmetric COO<sup>-</sup> bands is 110 cm<sup>-1</sup> which is between bi-dentate and bridging configurations so the two configurations seems to be present in the sample.

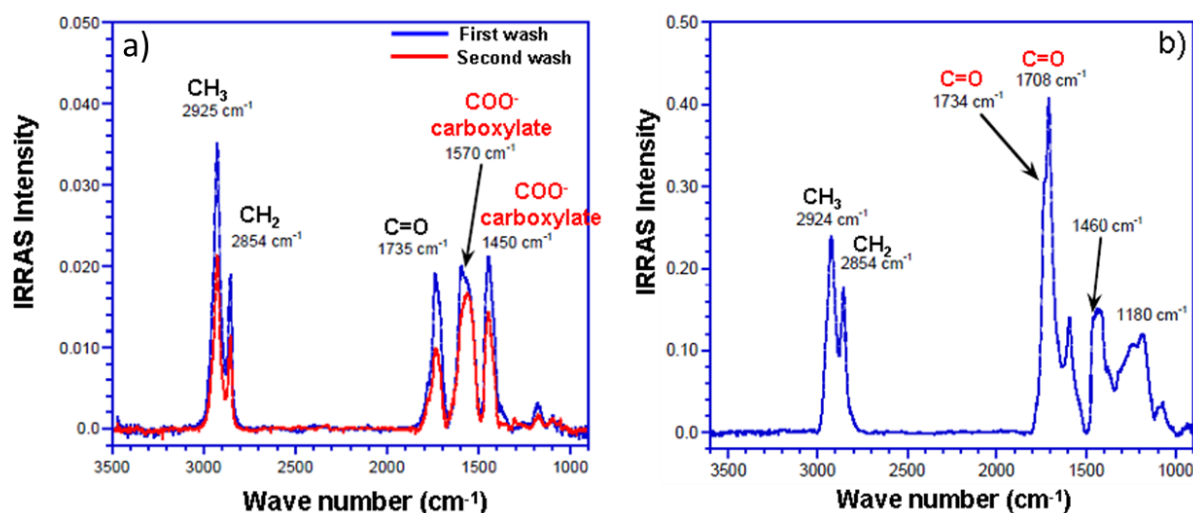


FIGURE 22: PM-IRRAS SPECTRA AT 150 °C OF SURFACE AFTER FRICTION WITH: A) PURE STEARIC ACID AFTER FIRST AND SECOND WASH WITH HEPTANE, B) PURE OLEIC ACID AFTER SECOND WASH WITH HEPTANE

In comparison with the adsorbed film (*chapter 3 § 3.2.1*), it seems that there are more stearate forms than stearic acid forms from which it can be deduced that friction favors the formation of stearate. This is in agreement with UA-QCMD simulation on stearic acid SAM

between iron oxide surfaces submitted to pressure and shear stress (see results and discussion in *section 3.1*).

The film thickness is estimated to 50 Å which can represent two monolayers. For pure oleic acid on steel surface at 150 °C after friction test, only the acid function which is characterized by vibration elongated bands of C=O at 1734 cm<sup>-1</sup> and 1708 cm<sup>-1</sup> are present. The peak characteristic of the C=C bond is not present at 3009 cm<sup>-1</sup>. It does not mean that the double carbon bond disappeared but it can be explained by the fact that the double carbon bond is parallel to the surface and, therefore, hard to detect.

The oleic acid film thickness is evaluated to be higher than 1000 Å so the interaction and characterization of species at the surface is not possible. In literature, QCM analysis suggests multilayer formation for the unsaturated fatty acids [8].

Both experimental and molecular simulations output many results. It is now time to compare them.

## 5. Comparison of experimental and numerical results

Before making comparison of the friction behavior of pure C18 fatty acids in presence of iron based surfaces by both experimental and numerical results (cf. § 5.2. and 5.3 and 5.4), it is important to have in mind certain limitations concerning MD simulations (§5.1).

### 5.1 Considerations concerning MD calculations before comparison with experimental study

The main difference between experimental friction tests and MD simulation is that MD simulations represent the first cycle whereas friction tests are performed during 4000 cycles. It has been shown from figure 15 that few cycles are needed to reach steady state. In the literature, boundary lubrication conditions applied on different saturated fatty acids on AISI 52100 steel substrates show that further cycles are needed to reach the steady state [16].

To design a physically representative MD simulation of atomic friction, many parameters should be improved. Martini *et al.* show a review on how friction is affected by many interrelated parameters [33]. Therefore, MD simulation requires a wide variety of interaction potentials to be able to accurately describe experimentally measured friction. In addition, real surface are rarely perfect crystal. Knowledge of real surface characteristics is really important for modelers, as they need to build, as much as they can, realistic surface. Moreover, matching surface shapes that are often found in MD calculations are not really representative of contact areas. Another question that is raised is how to apply a physically realistic thermostating scheme. All thermostats require that one or more parameters need to be specified in order to determine how fast energy is removed from the system. The best way to model sliding might be to allow temperature rise as local heating at the interface (due to asperity contacts) is typical in most sliding contacts. Finally, the velocity is an important factor as atomic friction generally increases with sliding speed and should not be neglected. The works of Martini *et al.* are limited by solid-solid contact in a vacuum environment so in our study, liquid lubrication, self-assembled monolayer, humidity effects and the presence of third bodies can be added to parameters that should interfere with friction response and should be improved in the model in order to make MD simulation a predictive and efficient tool.

## 5.2 Effect of Parameters

### 5.2.1 Effect of unsaturation

MD friction simulations of stearic, oleic, linoleic acids SAM with iron oxide surfaces and experimental friction tests on AISI52100 steel show the same trend: stearic acid has the best tribological behavior in terms of friction reduction up to 150 °C, followed by oleic acid and finally linoleic acid.

MD simulations enable to see the organization of the SAM and shows that the difference in friction behavior comes from the ability to form a close packed monolayer. It also could confirm that on iron oxide surface, SAM slide one across the other and the sliding plane is between the two monolayers. Sliding plane is less clear when the unsaturation number increases or when the density of the SAM decreases.

After friction tests, optical images of the samples show that important wear track is observed in presence of linoleic acid at 150 °C whereas no visible wear is observed for stearic and oleic acid.

The two methods are complementary to understand and observed the fatty acids behavior when they are submitted to severe conditions.

### 5.2.2 Effect of the hydroxylation of the surface

In case of MD calculations, different friction behaviors of C18 fatty acid monolayers were found regarding the surface nature ( $\text{Fe}_2\text{O}_3$  and  $\text{FeOOH}$ ). With stearic acid SAM on  $\text{Fe}_2\text{O}_3$ , a sliding plane is clearly found at the interface between the monolayers. But with  $\text{FeOOH}$ , some slip between acid functions of the monolayer and the substrate occurs, as the acid-surface interactions are much weaker in case of  $\text{FeOOH}$  than in presence of  $\text{Fe}_2\text{O}_3$ .

In the experimental case, it is more complicated as the surface composition cannot be controlled completely. The surface of AISI52100 steel is a native iron oxide which is a mixture of oxides and hydroxides. Regarding the environmental conditions (humidity for example), the exact composition might change. In the real case, both mechanisms could probably occur.

### 5.2.3 Effect of sliding process on chemical reaction at the interface monolayer-substrate

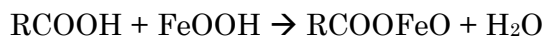
UA-QCMD simulations enable to see *in-situ* chemical mechanism that might occur during sliding process. Normal load promotes the chemisorption through the two oxygen atoms of the acid group. Preliminary results under sliding conditions show that the hydrogen atom will probably dissociate from the acid group, bond to the surface and promote the formation of carboxylate. In fact, PM-IRRAS analyses of the sample after friction tests confirm that after friction, there is more carboxylate form than acid forms. The two methods are therefore in agreement.

#### *Mechanism of stearate generation during friction*

Several works in literature reports the fact that friction promotes the generation of carboxylate when using fatty acids as lubricant additives [29, 30 and 34]. Our results, experimental and numerical, also follow this trend: 1) PM-IRRAS analyses of wear tracks shows more carboxylate function inside wear track than outside and 2) UA-QCMD suggest an -OH (from acid function) dissociation during friction. It is now interesting to discuss why.

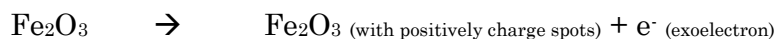
The shear in tribological contacts can cause the removal of oxide layers, providing some defects that can enhance chemisorption with the formation of iron carboxylate. In addition,

local temperature rise due to friction can also promote the formation of carboxylate [28]. It is proposed by Kajdas that the reaction mechanism is the negative ion radical action mechanism (NIRAM) [27, 31]. The NIRAM is based upon the ionization mechanism of fatty acids caused by action of exoelectrons. Exoelectrons are electrons of low energy (2-3 eV) spontaneously emitted from fresh surfaces such as aluminum and steel surfaces under tribological condition. This emission occurs when a material's surface is disturbed, for example, during friction process [27]. The existence of oxides is necessary for electron emission [35]. This is confirmed by other studies which say that the formation of carboxylate is favored by the presence of moisture and/or oxygen [36-38] in which the following reaction occurred:



Apart from the action of oxides or adsorbed organic films, the local temperature rise in the rubbing process promotes also the liberation of exoelectron [27]:

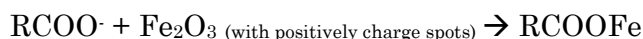
*friction process*



Energy of exoelectrons is sufficient to form ionization of fatty acids:



Finally the anions formed can easily react with positively charged surfaces:



Dissociated proton can be adsorbed on the surface or formed  $\text{H}_2\text{O}$  or  $\text{H}_2$ .

From our simulations, mechanism is different even if it leads to the same results that is to say the generation of carboxylates. But our UA-QCMD rather suggests an adsorption of the fatty acid molecule and then the dissociation of the OH rather than an action of the exoelectrons.

## 6. Conclusion

In this chapter, molecular simulation, friction test and surface characterization by PM-IRRAS are performed to study the tribological behavior of pure additives on steel surface. Effect of unsaturation, nature of the substrate, density and temperature were investigated. Table 5 summarizes main results obtained with the different techniques and the following conclusion can be made:

- ✦ Stearic acid has the best tribological behavior, even at 150 °C
- ✦ Friction increase with increasing number of unsaturation
- ✦ Saturated molecules are more densely packed and ordered than unsaturated molecules
- ✦ The nature of the substrate induces different friction behaviors (sliding planes between two SAMs, between SAM and substrate)
- ✦ Tribological conditions promote the formation of carboxylate

This study could confirm the formation of carboxylate induced by friction process. We could also make the link between the friction behavior and organization of films for the different fatty acids. It is now interesting to introduce these additives in a model base oil to study the tribological behavior of C18 fatty acids in a liquid system and to study the competition of the different OFMs toward the surface.

## 7. References

- [1] Tupper K J, Brenner D W, Molecular dynamics simulations of friction in self-assembled monolayers, *Thin Solid Films* 253 (1994) 185-189.
- [2] Fischer D A, Hu Z S, Hsu S M, Tribochemical and thermochemical reactions of stearic acid on copper surfaces in air as measured by ultra-soft X-ray absorption spectroscopy, *Tribology Letters* 3 (1997) 35-40.
- [3] Wu C D, Lin J F, Fang T H, Molecular dynamic simulation and characterization of self-assembled monolayer under sliding friction, *Computational Materials Science* 39 (2007) 808-816.
- [4] Campen S et al., On the increase in boundary friction with sliding speed, *Tribology Letters*, DOI 10.1007/s11249-012-0019-4 (2012).
- [5] Dong Y, Qunyang L, Martini A, Molecular dynamic simulation of atomic friction: a review and guide, *Journal of Vacuum Science & Technology* 31 (2013) 030801
- [6] Tabor D, Gases, liquids and solids and other states of matter, Chapter 12 The colloidal state of matter, 3<sup>rd</sup> edition, Cambridge (1991)
- [7] Stachowiak G W, Batchelor A W, Engineering Tribology, 3<sup>rd</sup> edition, *Elsevier*, Chapter VIII: Boundary and extreme pressure lubrication, 2005.
- [8] Lundgren S M, Ruths M, Danerlöv K, Persson K, Effects of unsaturation on film structure and friction of fatty acids in a model base oil, *Journal Colloid Interface Science* 326 (2008) 530-536.
- [9] Davidson J E, Hinchley S L, Harris S G, Parkin A, Parsons S, Tasker P A, Molecular dynamics simulations to aid the rational design of organic friction modifiers, *Journal of Molecular Graphics and Modelling* 25 (2006) 495-506.
- [10] Mikulski P T, Herman L, Harrison J A, Odd and Even model Self-Assembled Monolayers: Links between friction and structure, *Langmuir* 21 (2005) 12197-12206.
- [11] Harrison J A, Schall J D, Knippenberg M T, Gao G, Mikulski P T, Elucidating atomic-scale friction using molecular dynamics and specialized analysis techniques, *Journal of Physics Condensed Matter* 20 (2008) 354009.
- [12] Morita Y, Jinno S, Murikami M, Hatakeyama N, Miyamoto A, A computational chemistry approach for friction reduction of automotive engines, *International Journal of Engine Research (to be published)*
- [13] Lorenz C D, Chandross M, Grest GS, Stevens M J, Webb E B, Tribological properties of alkylsilane self-assembled monolayers, *Langmuir* 21 (2005) 11744-1174
- [14] Islam M M, Diawara B, Marcus P, Costa D, Synergy between iono-covalent bonds and van der Waals interactions in SAMs formation: a first principles study of adsorption of carboxylic acids on the Zn-ZnO(0 0 0 1) surface, *Catalysis Today* 177 (2011) 39-49.
- [15] Cheng H, Hu Y, Influence of chain ordering in frictional properties of self-assembled monolayers (SAMs) in nano-lubrication, *Advances in Colloid and Interface Science*, DOI 10.1016/j.cis.2012.01.003 (2012).
- [16] Jahamir S et al., Chain length effects in boundary lubrication, *Wear* 102 (1985) 331-349.

- [17] Murray S F, Burwell J T, Measurement of the incremental friction coefficient of several homologous series of straight-chain hydrocarbon compounds, *Symposium on Fundamentals of Lubrication, Annals of the New York acad. Sci.* 53 (1951) 906-918
- [18] Levine O, Zisman W A, Physical properties of monolayers adsorbed at the solid-air interface, *Journal of Physical Chemistry* 61 (1957) 1068-1077.
- [19] Sameshima J, Akamatu H, Isemura T, The friction coefficients of liquids, *Rev. Phys. Chem. Jpn* 14 (1940) 55.
- [20] Majzner M, Kajdas C, Reactions of carboxylic acids under boundary friction conditions, *Tribologia* 34 (2003) 63-80.
- [21] Zheng X, Zhu H, Kosasih B, Tieu A K, A molecular dynamics simulation of boundary lubrication: the effect of n-alkanes chain length and normal load, *Wear* 301 (2013) 62-69.
- [22] Kajdas C, Majzner M, Reactions of carboxylic acids under boundary friction conditions, *Lubrication Science* 14 (2003) 84-107.
- [23] Allen C M, Drauglis E, Boundary layer lubrication: monolayer or multilayer, *Wear* 14 (1969) 363-384.
- [24] Mansot J L, Aspects microscopiques de l'action des réducteurs de frottement en lubrification limite, *Thèse Docteur Ingénieur*, Ecole Centrale Lyon, 1982.
- [25] Postnikov S N, Electrophysical and electrochemical phenomena in friction cutting and lubrication, *Litton Educational Publishing, Inc.* New York, 1978.
- [26] She J H, Balatsky A V, Non-contact friction and relaxational dynamics of surface defects, *Physical Review Letters* 108 (2012) 136101.
- [27] Kajdas C, Importance of the triboemission process for tribochemical reaction, *Tribology International* 38 (2005) 337-353.
- [28] Simić R, Kalin M, Adsorption mechanisms for fatty acids on DLC and steel studied by AFM and tribological experiments, *Applied Surface Science* 283 (2013) 460-470.
- [29] Hsu S M, Zhang J, Yin Z F, The nature and origin of tribochemistry, *Tribology Letters* 13 (2002) 131-139.
- [30] Przedlacki M, Kajdas C, Tribochemistry of fluorinated fluids hydroxyl groups on steel and aluminum surfaces, *Tribology transactions* 49 (2006) 202-214.
- [31] Kajdas C, About an anionic radical concept of the lubrication mechanism of alcohols, *Wear* 116 (1987) 167-180.
- [32] Crowel J E, Chen J G, Yates Jr J T, A vibrational study of the adsorption and decomposition of formic acid and surface formate on Al(111), *Journal of Chemical Physics* 85 (1986) 3111-3122.
- [33] Dong Y, Li Q, Martini A, Molecular dynamics simulation of atomic friction: a review and guide, *Journal of Vacuum Science & Technology* A31 (2013) 030801.
- [34] Fischer D A, Hu Z S, Hsu S M, Molecular orientation and bonding of monolayer stearic acid on a copper surface prepared in air, *Tribology Letters* 3 (1997) 41-45.



- [35] Ramsey J A, The emission of electrons from aluminum abraded in atmospheres of air, oxygen, nitrogen and water vapor, *Surface Science* 8 **(1967)** 313-322.
- [36] Sahoo R R, Biswas S K, Frictional response of fatty acids on steel, *Journal of Colloid and Interface Science*, 333 **(2009)** 707-718.
- [37] Ratoi M, Anghel V, Bonvington C, Spikes H A, Mechanism of oiliness additives, *Tribology International* 33 **(2000)** 241-247.
- [38] Russel J A, Campbell W E, Burton R A, Ku P M, Boundary lubrication behavior of organic films at low temperature, *ASLE Transactions* 8 **(1965)** 48-58.

## 8. Summary chapter 4

After the formation of the adsorbed layer, we have placed the two surfaces covered by an adsorbed SAM under severe conditions, e.g. normal load and shear stress.

The evaluation of friction coefficient by MD simulation shows that stearic acid has the best tribological behavior on iron oxide surface followed by oleic acid and linoleic acid. This result is true for the two studied density: “liquid-like” and “solid-like”. In fact, saturated molecules are arranged in a close-packed monolayer with a sliding plan between the two monolayers, especially at higher density. On the other hand, unsaturated molecules have double carbon-carbon bonds which generate steric effect and, therefore, an irregular film. Those irregularities favor the interdigitation of layers which are responsible for friction increase. Same simulations applied with iron hydroxide surfaces show the presence of additional sliding plane which is a slip at the wall, inducing lower friction coefficient. Friction tests have confirmed the efficiency of stearic acid compared to oleic and linoleic acid with notable performance at 150 °C.

Preliminary UA-QCMD simulations show that a normal load favors the symmetric chemisorption of the acid group and the shear stress seems to promote the formation of carboxylate function with the dissociation of hydrogen from hydroxyl group. It confirms the importance of having an oxide layer on the surface to favor the adsorption of hydrogen on the oxygen of the surface. Moreover, PM-IRRAS analyses confirm the presence of both carboxylate functions and acid functions. And after the friction test, there are more carboxylate functions than acid functions which confirm the catalytic effect of friction process for the formation of carboxylate function.

Finally, MD simulations were used to show the effect of alkyl chain length on the friction behavior. In absence of solvent, the friction decreases when the chain length increases. This is linked to the fact that a minimum of methyl group number is needed to create enough cohesion force to maintain the SAM.

## 8. Résumé chapitre 4

Après avoir formé le film adsorbé, nous avons placé deux surfaces recouvertes d'une monocouche auto-assemblée en contact avec une pression normale et une vitesse de cisaillement définies.

L'évaluation du coefficient de frottement du système SAM adsorbé sur l'oxyde de fer par Dynamique Moléculaire montre que l'acide stéarique est le meilleur réducteur de frottement suivi de l'acide oléique et linoléique et ce, aux deux densités étudiées. En effet, les molécules saturées s'organisent selon un film compact avec un plan de glissement entre les deux monocouches, notamment lorsque l'on augmente la densité du film. En revanche, les molécules insaturées possèdent des doubles liaisons carbone-carbone qui créent des gênes stériques et donc un film irrégulier. Ces irrégularités offrent la possibilité d'interpénétration des couches, facteur augmentant le frottement. Les mêmes travaux sur l'hydroxyde de fer montrent l'ajout d'un nouveau plan de glissement à la surface (SAM-substrat) entraînant un frottement encore plus bas. Les tests de frottement confirment l'efficacité de l'acide stéarique devant l'acide oléique et l'acide linoléique avec des performances remarquables à 150 °C.

Des études préliminaires d'UA-QCMD montrent que l'application d'une pression normale favorise la chimisorption par les deux oxygènes du groupement acide et le frottement semble promouvoir la formation de carboxylate, l'hydrogène du groupement hydroxyle se dissociant de l'acide, confirmant l'importance d'avoir une couche d'oxyde pour former un carboxylate. De plus, les analyses PM-IRRAS confirment la présence de carboxylates. Après frottement, il y a plus de formes carboxylates que de formes acides en comparaison avec les films adsorbés ce qui valide l'effet du frottement en tant que catalyseur à la formation de carboxylates.

Enfin, des simulations MD montrent l'effet de la longueur de chaîne de l'acide gras sur le frottement. En l'absence de solvant, le frottement diminue lorsque la longueur des chaînes augmente. Ceci est lié au fait qu'un nombre de groupement méthyl minimum est nécessaire pour créer des forces de cohésion suffisantes au maintien de la monocouche auto-assemblée.



## **Chapter 5: Tribological behavior of C18 fatty acids blended in PAO 4**

---

## **Chapitre 5: Comportement tribologique des acides gras C18 dans la PAO 4**

## Chapter 5: Tribological behavior of C18 fatty acids blended in PAO4

---

### Table of contents

1. Introduction .....	154
2. Friction behavior of C18 fatty acids in PAO 4 by experimental approach .....	154
2.1 Friction test experiments .....	154
2.3 Characterization of the tribofilm .....	159
3. Competition of C18 fatty acids in PAO 4.....	162
3.1. Friction behavior of C18 fatty acids mixture in PAO 4 .....	162
3.2. Evaluation of diffusion coefficient of OFM in PAO 4 by MD simulation .....	163
3.3 Discussions: coupling experimental results and MD simulations .....	166
4. Conclusion.....	166
5. References.....	168
6. Summary chapter 5.....	169

### 1. Introduction

In previous chapters, the adsorption mechanism of some pure C18 fatty acids on iron-based surfaces and their tribological behavior were investigated. It has been highlighted that saturated and unsaturated fatty acids are both adsorbed on the surface through the acid group. Nevertheless, pure stearic acid presents the best tribological behavior up to 150 °C. In fact, stearic acid can form a well-arranged and close-packed monolayer where unsaturated fatty acids can't because of steric effects. In addition, it was shown by computational chemistry and confirmed by experimental surface characterization that the formation of carboxylate is promoted by friction conditions, e.g. normal load and shear stress.

Now, it will be interesting to introduce the C18 fatty acids in model base oil and to study its tribological behavior. To do so, 1%w of C18 fatty acids was blended in PAO 4 and the friction behavior of the different blends is then investigated. After tests, characterization of the friction surfaces is made by PM-IRRAS analysis. Temperature, concentration and the effect of unsaturation are investigated. The results are presented in part 2.

Then, mixtures of saturated and unsaturated fatty acids in PAO4 are studied to detect synergic or anti-synergic effects as it is the case in vegetable oils. Different temperatures are used to mimic the behavior of the thermal engine. To complete the experimental studies, MD simulations are performed to evaluate the diffusion coefficient of those additives in PAO 4 at different temperatures. The results will be developed in part 3.

### 2. Friction behavior of C18 fatty acids in PAO 4 by experimental approach

#### 2.1 Friction test experiments

Each additive is blended at 1%w in the PAO 4. Friction tests are performed by using a reciprocating linear tribometer with a maximum sliding speed of 56 mm/s, a maximum

Hertzian pressure of 320 MPa during 20 minutes (4000 cycles) as it was done previously for pure additives (*Chapter 4 § 4*). Three different temperatures (50 °C, 100 °C and 150 °C) are considered in order to simulate accurately conditions in the cam-tappet contact of a thermal engine. Each test is repeated three times to confirm reproducibility. Friction coefficient as a function of the number of cycles is then considered.

### 2.1.1 Influence of unsaturation and temperature

Figure 1 summarizes friction results obtained at 50 °C, 100 °C and 150 °C in presence of blends of PAO 4 with 1%w of stearic, oleic and linoleic acids, respectively. The friction coefficient is recorded at the steady state value at the end of the test (after 4000 cycles). In addition, figure 2 gathers optical micrograph pictures of samples after friction tests.

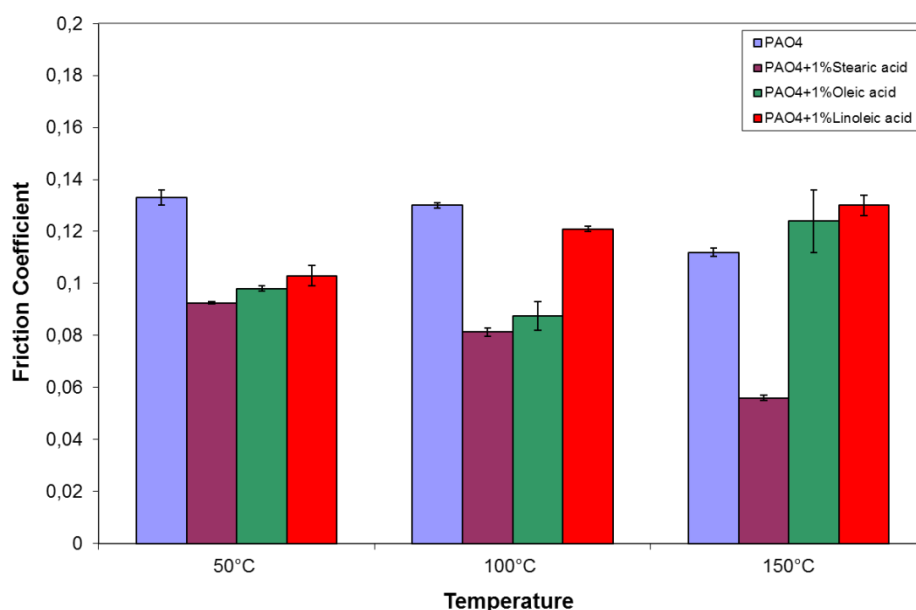


FIGURE 1: STEADY STATE FRICTION COEFFICIENT OF DIFFERENT BLENDS (PAO 4 BLENDED WITH 1%W STEARIC ACID, WITH 1%W OLEIC ACID AND WITH 1%W LINOLEIC ACID) AT 50, 100 AND 150 °C - EXPERIMENTAL CONDITIONS: RECIPROCATING PIN-ON-FLAT TEST WITH AISI 52100 STEEL COUPLE RESPECTIVELY, WITH MAXIMUM SLIDING SPEED OF 56 MM/S, AT MAXIMUM HERTZIAN PRESSURE OF 320 MPa DURING 4000 CYCLES; TESTS ARE REPEATED 3 TIMES

At 50 °C, results show that all studied blends of PAO 4 with fatty acids seem to be efficient in reducing both friction by 30-35 % and wear compared to PAO 4 alone (figures 1 and 2). In fact, figure 2 confirms that PAO 4 cannot ensure good tribological behavior by itself as wear track is observed at 50 °C but also at higher temperatures. Results at 50 °C are compared with those obtained at 100 °C and 150 °C. It appears that the increase of temperature leads to a drastic increase of friction and wear for linoleic acid and oleic acid. In fact, oleic acid loses its good tribological behavior (“high” friction and large wear) at 150 °C and linoleic acid loses its good tribological behavior even at 100 °C. On the other hand, in presence of stearic acid, a drastic decrease of friction by a factor of 2 ( $\mu$  is about 0.056) is observed at 150 °C associated with no visible wear (figure 2).

Comparing saturated versus unsaturated fatty acids, it seems that increasing the number of unsaturated bonds leads to a decrease of the lubricating properties of fatty acids at high temperature. Thus, stearic acid blended in the base oil gives the best tribological performance at the range of studied temperatures like it was already the case in the study of pure additives (*chapter 4 § 4*).


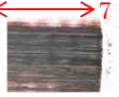
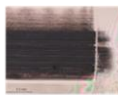





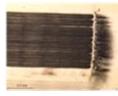



Lubricant	50°C	100°C	150°C
PAO4	 $\mu = 0.134$	 $\mu = 0.131$	 $\mu = 0.112$
PAO4+1%Stearic acid	 $\mu = 0.093$	 $\mu = 0.08$	 $\mu = 0.057$
PAO4+1%Oleic acid	 $\mu = 0.099$	 $\mu = 0.088$	 $\mu = 0.122$
PAO4+1%Linoleic acid	 $\mu = 0.099$	 $\mu = 0.121$	 $\mu = 0.134$

FIGURE 2: OPTICAL IMAGES OF AISI 52100 STEEL FLAT WEAR SCARS OBTAINED AFTER TRIBOLOGICAL TESTS WITH DIFFERENT BLENDS (PAO 4 BLENDED WITH 1%W STEARIC ACID, WITH 1%W OLEIC ACID AND WITH 1%W LINOLEIC ACID) AT 50, 100 AND 150 °C - EXPERIMENTAL CONDITIONS: RECIPROCATING PIN-ON-FLAT TEST WITH AISI 52100 STEEL COUPLE RESPECTIVELY, WITH MAXIMUM SLIDING SPEED OF 56 MM/S, AT MAXIMUM HERTZIAN PRESSURE OF 320 MPA DURING 4000 CYCLES; TESTS ARE REPEATED 3 TIMES

Moreover, it is interesting to compare the friction behavior of stearic, oleic and linoleic acids in presence or absence of PAO 4 as shown in figure 3. Steady state friction coefficient is a bit higher when additives are mixed in the PAO 4 than when they are used under pure form, with no solvent. Especially, pure oleic acid still has good tribological behavior at 150 °C but this behavior is lost when blended in PAO 4. On the other hand, at 150 °C, the mixture of stearic acid and PAO 4 has the same friction coefficient as pure stearic acid. In addition, there is no visible wear at 50, 100 and 150 °C for stearic acid blended in PAO4 at 1%w which is similar to pure stearic acid (*chapter 4 figures 18-19*).

It seems reasonable to conclude from our experimental results that friction coefficient is a bit higher in presence of PAO 4 than with pure additives. Some studies highlighted the fact that the couple base oil/additive is an important factor to take into account in the lubricant formulation [1-3]. The solvent could probably have an impact on the friction behavior by different ways. First of all, solvent could adsorb first on the surface in place of fatty acids as there are more PAO molecules than fatty acids molecules in the lubricant. A co-adsorption of base oil and fatty acids could be found, limiting so the formation of a well-ordered layer. Then, some interactions in the bulk of the lubricant could occur. Interaction between several fatty acids (ex: dimers generations) or interactions between fatty acids and solvent called matching in the following. Cameron and co-workers have reported that boundary lubrication can be affected by matching the chain length and shape of the additive with the carrier solution and this could lead to very good tribological behavior. As an example, even if oleic acid and stearic acid have the same number of carbon, oleic acid has better tribological behavior in tetradecane while stearic acid performs best in hexadecane [1]. In this study, PAO 4 is much heavier than C18 fatty acids and probably does not match or co-adsorb on the surface. Finally, in the contact, a flow of PAO 4 might be found between the adsorbed monolayers. Therefore, the sliding plane between monolayers is replaced by sliding plane between the monolayer and the base oil flow. If the branches are oriented toward the surface, some entanglements can occur with the adsorbed monolayer and will lead to higher friction while if the branches are oriented perpendicular to the adsorbed layer, the friction might decrease.



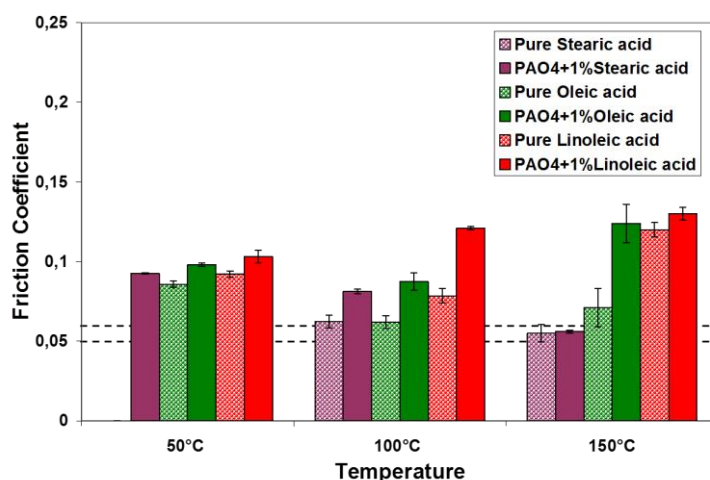


FIGURE 3: STEADY STATE FRICTION COEFFICIENT OF PURE STEARIC, OLEIC AND LINOLEIC ACIDS RESPECTIVELY AND DIFFERENT BLENDS (PAO4 BLENDED WITH 1%W STEARIC ACID, WITH 1%W OLEIC ACID AND WITH 1%W LINOLEIC ACID) COUPLE AT 50, 100 AND 150 °C. EXPERIMENTAL CONITIONS: RECIPROCATING PIN-ON-FLAT TEST WITH AISI 52100 STEEL COUPLE RESPECTIVELY, WITH MAXIMUM SLIDING SPEED OF 56 MM/S, AT MAXIMUM HERTZIAN PRESSURE OF 320 MPA DURING 4000 CYCLES; TESTS ARE REPEATED 3 TIMES

The most surprising result is the loss of good tribological behavior of oleic acid blended in PAO 4 at 150 °C in comparison with pure oleic acid at same conditions. Let's compare the evolution of friction for stearic and oleic acid respectively blended in PAO 4 at 150 °C (Figure 4). While friction coefficient decreases slightly during the 500 first cycles and then reaches an equilibrium value for stearic acid in PAO 4, for oleic acid in PAO 4 the friction decreases at the very first cycle followed by a drastic increase in friction coefficient up to around 500 to 1000 cycles and then it reach its steady state value. This drastic increase is correlated with the presence of wear as shown in figure 2. XPS analyses were performed inside and outside the wear track after the friction test with oleic acid blend. Table 1 shows that the same species are found inside and outside the track. The only difference is that we have more iron oxide inside the track (25.6%) than outside the track (9.6%) which confirms the presence of wear already observed on optical micrograph. As wear is important, the roughness inside the track is increased. It was already shown that the formation of a well-ordered layer is not easy with oleic acid because of steric effects with unsaturation. With increasing the roughness of the friction surfaces, the disorder of the monolayer is increased which lead to an increase of the friction coefficient. Then, less ordered layers leads to more entanglement of molecules of adsorbed layers as well, responsible for the increase of friction with unsaturated fatty acids [4].

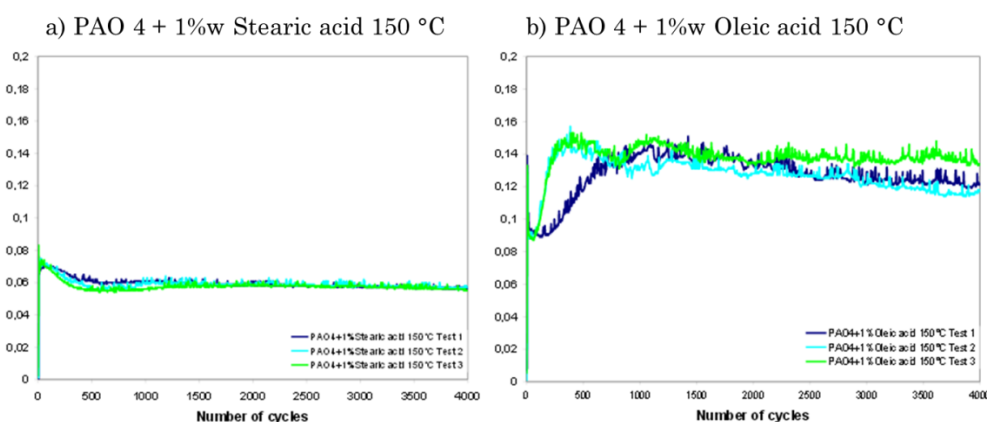


FIGURE 4: EVOLUTION OF FRICTION COEFFICIENT AS A FUNCTION OF CYCLES NUMBER FOR A) STEARIC ACID 1%W BLENDED IN PAO 4 AT 150 °C AND B) OLEIC ACID 1%W BLENDED IN PAO 4 AT 150 °C. EXPERIMENTAL CONDITIONS: RECIPROCATING PIN-ON-FLAT TEST WITH AISI 52100 STEEL COUPLE RESPECTIVELY, WITH MAXIMUM SLIDING SPEED OF 56 MM/S, AT MAXIMUM HERTZIAN PRESSURE OF 320 MPA DURING 4000 CYCLES; TESTS ARE REPEATED 3 TIMES

TABLE 1: XPS PEAK TABLE: BINDING ENERGY AND ATOMIC POURCENTAGE OF THE DIFFERENT ELEMENTS – XPS ANALYSES PERFORMED ON WEAR TRACK AFTER FRICTION TEST AT 150 °C. OLEIC ACID 1%W BLENDED IN PAO 4 ON AISI 52100 STEEL FLAT INSIDE AND OUTSIDE WEAR TRACK

Name	Peak Binding energy (eV)	At. %	Species
<b>Inside wear track</b>			
O1s	530.2	25.6	O-Fe
C1s	284.8	66.8	C-C
C1s	288.6	4.2	CO
O1s	531.9	21.6	O=C
O1s	533.2	7.6	O-C
<b>Outside wear track</b>			
O1s	530.0	9.6	O-Fe
C1s	284.8	69.3	C-C
C1s	288.7	5.1	CO
O1s	531.9	18.5	O=C
O1s	533.1	7.0	O-C

Another explanation could be related to the fact that PAO 4 molecules are agitated at high temperatures and therefore the kinetic energy of the molecules can be transferred to adsorbed oleic acid molecules and will favored their desorption. This phenomenon has not been studied with molecular simulation as the adsorption mechanism was studied in absence of base oil.

### 2.1.2 Influence of concentration

In this study, the C18 fatty acids were blended at a weight concentration of 1%. It can be wondered whether lower concentration is enough to obtain the same tribological behavior. Therefore, solution containing 0.5%w of stearic acid is compared to 1%w solutions.

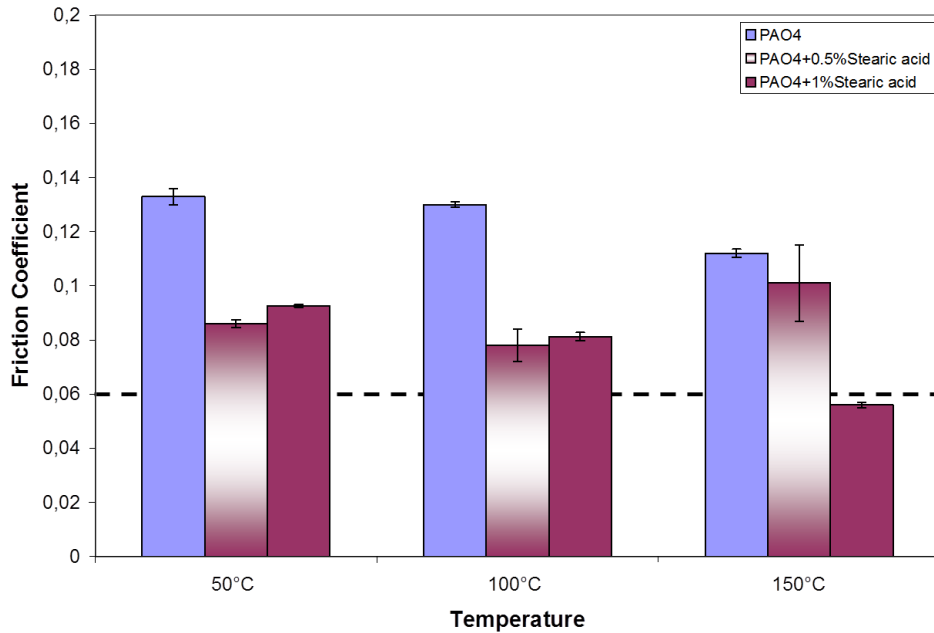


FIGURE 5: INFLUENCE OF CONCENTRATION ON THE STEADY STATE FRICTION COEFFICIENT OF DIFFERENT BLENDS (PURE PAO4, WITH 0.5%W OF STEARIC ACID AND WITH 1%W OF STEARIC ACID) AT 50, 100 AND 150 °C. EXPERIMENTAL CONDITIONS: RECIPROCATING PIN-ON-FLAT TEST WITH AISI 52100 STEEL COUPLE RESPECTIVELY, WITH MAXIMUM SLIDING SPEED OF 56 MM/S, AT MAXIMUM HERTZIAN PRESSURE OF 320 MPA DURING 4000 CYCLES; TESTS ARE REPEATED 3 TIMES

Figure 5 and 6 gathered respectively the steady state friction coefficient after 4000 cycles and the optical micrographs of AISI 52100 steel flat wear scars after friction tests with PAO4 alone and with blends containing 0.5%w and 1%w of stearic acid respectively. Until 100 °C, 0.5%w of stearic acid is enough to obtain good tribological behavior in terms of friction and wear as friction coefficient is around 0.09 and 0.08 at 50 and 100 °C respectively. Nevertheless, 0.5%w concentration is not enough to keep the good tribological behavior of stearic acid observed at 150 °C with blends containing 1%w of stearic acid. In fact, the friction coefficient is multiplied by two when the concentration is divided by two at 150 °C. In addition, wear scars are more important at 150 °C in PAO 4 at the lowest concentration and present heterogeneities: the alternation of “clear” and “dark” bands confirms that there are not enough stearic acid molecules to provide a full protective film.



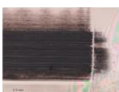


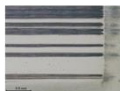



Lubricant	50°C	100°C	150°C
PAO4	 $\mu = 0.134$	 $\mu = 0.131$	 $\mu = 0.112$
PAO4+0.5%Stearic acid	 $\mu = 0.087$	 $\mu = 0.073$	 $\mu = 0.101$
PAO4+1%Stearic acid	 $\mu = 0.092$	 $\mu = 0.08$	 $\mu = 0.055$

FIGURE 6: OPTICAL IMAGES OF AISI 52100 STEEL FLAT WEAR SCARS LUBRICATED WITH PAO4 ALONE, PAO4+ 1%W STEARIC ACID AND PAO4+0.5%W STEARIC ACID TAKEN AFTER FRICTION TESTS. EXPERIMENTAL CONDITIONS: RECIPROCATING PIN-ON-FLAT TEST WITH AISI 52100 STEEL COUPLE RESPECTIVELY, WITH MAXIMUM SLIDING SPEED OF 56 MM/S, AT MAXIMUM HERTZIAN PRESSURE OF 320 MPA DURING 4000 CYCLES.

From our results, it can be concluded that the friction coefficient is reduced by increasing concentration. This trend was also found in literature as well as the fact that at higher concentrations, the friction coefficient remains constant <sup>[5]</sup>. The minimum concentration needed for the best friction behavior is dependent of the solvent. For example, in hexadecane, the minimum concentration of stearic acid for the friction reduction is 0.3%w <sup>[5]</sup>. As a conclusion, a minimum of 1%w of fatty acid in PAO 4 is needed to provide the good tribological behavior of the blends in a large range of temperature.

## 2.3 Characterization of the tribofilm

After friction tests, some samples are subjected to surface characterization in order to analyze the nature of the tribofilm. In fact, the previous chapter highlighted the presence of carboxylate promoted by friction (*chapter 4 § 3.1 and 4.2*). Carboxylates are strongly attached to the surface and, therefore, prevent the contact from adhesive wear. The present study focuses on the validity of the chemical reaction process induced by friction in presence of PAO 4 base oil.

### 2.2.1 PM-IRRAS analysis of the tribofilm

XPS analysis enables to detect the presence of a tribofilm but cannot differentiate chemisorbed carboxylic acid from carboxylate form (*chapter 3 § 3.1*); PM-IRRAS technique was

chosen to complete the characterization as it is much powerful to distinguish carboxylic and carboxylate chemical functions.

As already mentioned in chapter 3 and 4, ATR spectrum is first run in order to have reference band positions for stearic and oleic acids (figure 7). The alkyl chain presented two main contributions at  $2915\text{ cm}^{-1}$  and  $2848\text{ cm}^{-1}$  characteristic of  $\text{CH}_3$  and  $\text{CH}_2$  functions respectively. The carboxylic function is presented by a stretching band at  $1700\text{ cm}^{-1}$ . For oleic acid, the  $\text{C}=\text{C}$  band is characterized by a very small band in  $3007\text{ cm}^{-1}$  and at  $1657\text{ cm}^{-1}$ .

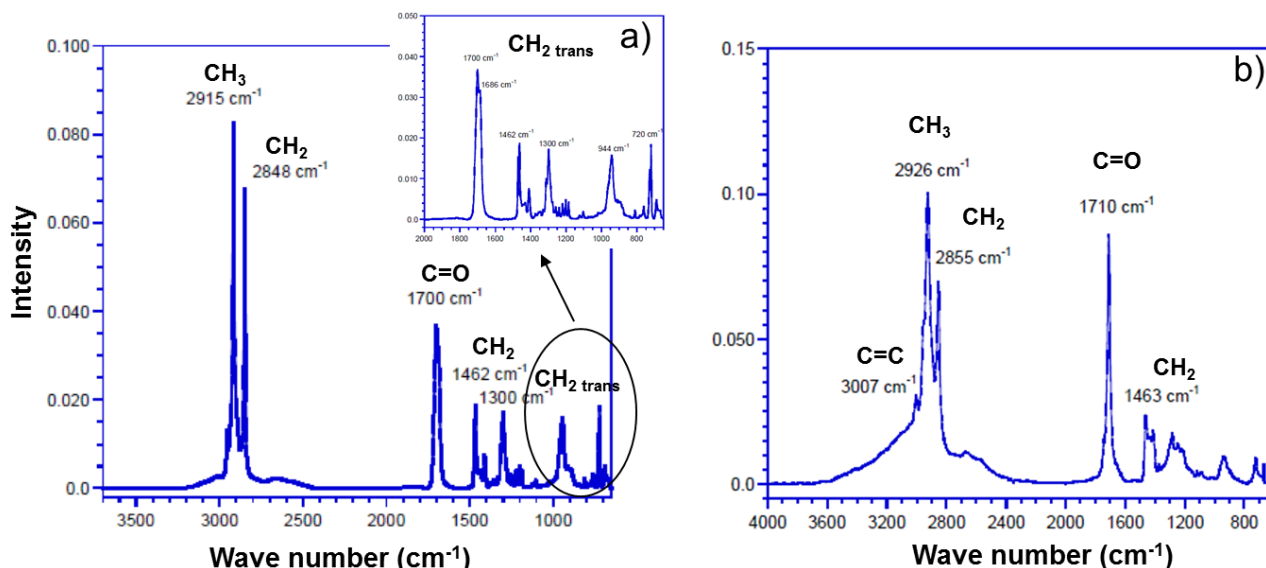


FIGURE 7: ATR SPECTRA OF STANDARD MOLECULES: A) STEARIC ACID, B) OLEIC ACID

Samples were selected for PM-IRRAS analyses in order to investigate the effect of the temperature on the tribological behavior. Samples presenting the best tribological behavior were chosen, e.g. PAO 4 blended with 1%w of stearic acid at  $50\text{ }^{\circ}\text{C}$  and  $150\text{ }^{\circ}\text{C}$ . An additional sample is selected to study the film composition when the good tribological behavior is lost, like for PAO 4 blended with 1% w of oleic acid at  $150\text{ }^{\circ}\text{C}$ . Unfortunately, the sample of steel surface with PAO4 blended with 1%w stearic acid at  $150\text{ }^{\circ}\text{C}$  was contaminated so PM-IRRAS results will not be presented.

It is important to remember that the lateral resolution with PM-IRRAS analyses is quite poor (analyzed area  $\approx$  few decades of  $\text{mm}^2$ ). Because of the small size of our samples (wear track length is  $4 \times 7\text{ mm}^2$ ), spectrums could contain both information from the inside and the outside of the wear track.

For stearic acid at  $50\text{ }^{\circ}\text{C}$ , after the first wash (red curve), the presence of the stearic acid, characterized by the  $\text{C}=\text{O}$  bond peak around  $1715\text{ cm}^{-1}$ , is found. Then, it is noted that additional peaks, characteristic of the stearate function at  $1570\text{ cm}^{-1}$  (anti-symmetric) and  $1460\text{ cm}^{-1}$  (symmetric), are also present. Regarding Crowell's definition (see chapter 3 § 3.2.1) [14], the wavenumber distance between asymmetric and symmetric  $\text{COO}^-$  bands is  $110\text{ cm}^{-1}$  which is between bidentate and bridging configurations. So, in our sample, the two configurations seem to be present. Finally, the position of  $\text{CH}_2$  group at  $2918$  and  $2850\text{ cm}^{-1}$  are characteristic of a close-packed and well-arranged layer with alkyl chains mainly under *trans* conformation. This is similar to results obtained with pure stearic acid (chapter 4 § 4.2). After the second wash (blue curve), the peak characteristic of stearic acid is not observed anymore. It means that the remaining stearic acid molecules are weakly adsorbed on the surface and can be removed with the solvent washing. On the other hand, the  $\text{CH}_2$  group

vibrations and carboxylate group vibrations confirm the presence of stearate on the surface. Simulation of film thickness has been estimated at 25 Å which is equivalent of a monolayer of stearic acid.

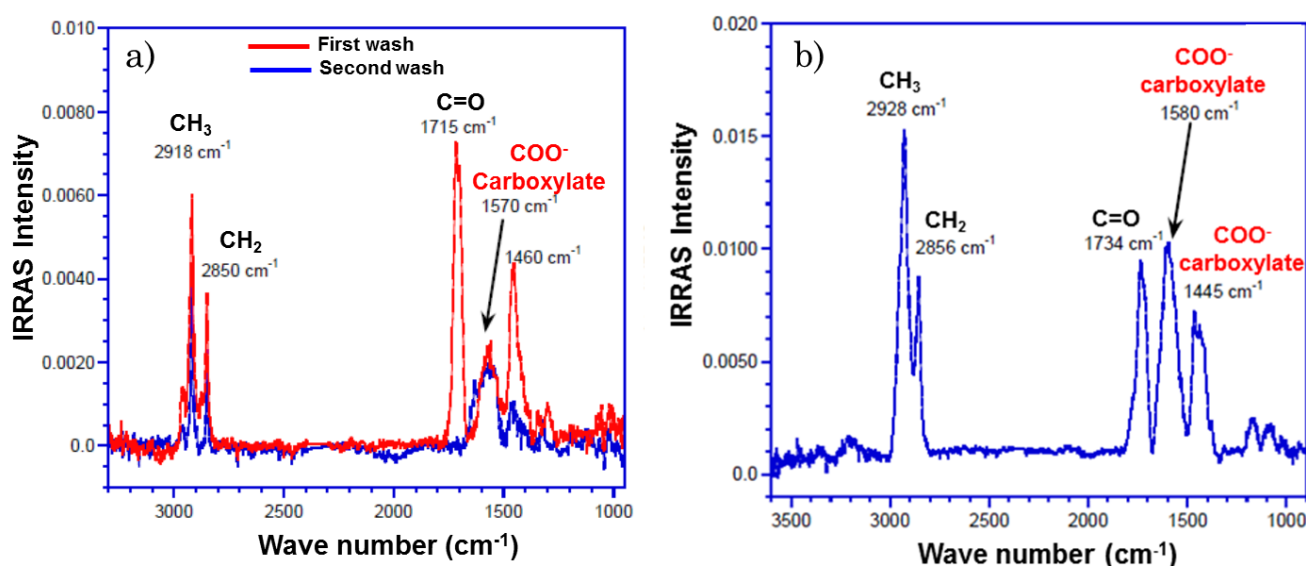


FIGURE 8: PM-IRRAS SPECTRA OF AN AISI 52100 STEEL FLAT SURFACE AFTER FRICTION TEST IN PRESENCE OF A) PAO4 + 1%W STEARIC ACID AT 50 °C, B) PAO4 + 1%W OLEIC ACID AT 150 °C, WASHED WITH HEPTANE

Finally, there is more stearate form in the tribofilm than in the adsorbed film as shown in figure 9. This is found here with blend of PAO and stearic acid but the trend was similar with pure stearic acid molecules (*c.f. Chapter 4 § 4.2*). This confirms again that tribological conditions, e.g. load and shear, are favoring the formation of stearate.

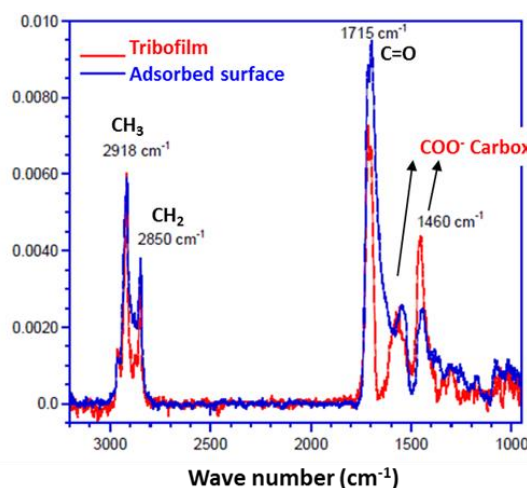


FIGURE 9: PM-IRRAS SPECTRUM OF ADSORBED SURFACE (BLUE CURVE) AND SURFACE AFTER FRICTION TEST (RED CURVE) FOR AISI 52100 STEEL FLAT SURFACE WITH PAO4 + 1%W STEARIC ACID AT 50 °C

Still the same trend is found with oleic acid. PM-IRRAS analysis of the wear track obtained with PAO4 at 150 °C, spectrum b) (figure 8-b) shows the presence of both carboxylate and acid forms. The acid form is characterized by a C=O band around 1734 cm<sup>-1</sup> and the carboxylate form is identified by COO<sup>-</sup> bands at 1580 and 1445 cm<sup>-1</sup>. The wavenumber distance between asymmetric and symmetric COO<sup>-</sup> bands is 135 cm<sup>-1</sup> which is between bidentate and bridging configurations so the two configurations seems to be present in the sample. The band that is characteristic of C=C bond around 3009 cm<sup>-1</sup> is not present in figure

7-b. It is important to note that if the C=C bond is orientated parallel to the surface, it will be not detected by PM-IRRAS so the absence of the band at  $3009\text{ cm}^{-1}$  does not mean that the double bond disappeared but can confirm that the layer is not well-arranged on the surface. In fact, the band intensity ratio and position of wavenumbers associated with  $\text{CH}_2$  group confirm that the structure is not well-arranged. In addition, the film thickness is estimated at  $50\text{ \AA}$  which represent two monolayers of oleic acid.

To conclude, it was shown here that with blends of fatty acid at 1%w in PAO (Chapter 5) and with pure molecules (Chapter 4), the same trend is found in tribofilm compositions: 1) in wear track both carboxylate and acid forms are found and 2) there is more carboxylates form in wear track rather than in adsorbed layers. These results are also confirmed by UA-QCMD simulations (*chapter 4 § 3*) which show a weakening of the OH bond in the acid function.

Among studied C18 fatty acid, stearic acid presents the best tribological behavior when blended with PAO 4 thanks to the formation of a well-ordered layer this for a large range of temperatures. Nevertheless, stearic acid presents disadvantages. One of them is that it is solid at room temperature and up to  $80\text{ }^{\circ}\text{C}$ . When blended with other fatty acids, as it is the case in vegetable oils [6-8], the solubility of stearic acid is increased. In fact, soybean and sunflower oils have similar amount of stearic acid. Differences in their unsaturated fatty acid may have been a controlling factor to induce lower friction and wear in soybean oils. It is not straightforward whether the stearic acid in the mixtures has the same efficiency as when it is alone. In fact, the chemical structure of fatty acids affects their diffusion toward the surface and, therefore, all the additives present in the base oil compete for the active surface sites. The final adsorption state depends on the different species initially present in the formulation. This is why the next section will focus on the friction behavior of mixture of different fatty acids and on their competition toward the surface (saturated versus unsaturated molecules).

### 3. Competition of C18 fatty acids in PAO 4

Mixtures of saturated and unsaturated fatty acids are studied to detect synergic or anti-synergic effects. Different temperatures are used to mimic the behavior of the thermal engine: from  $50\text{ }^{\circ}\text{C}$  up to  $150\text{ }^{\circ}\text{C}$ . To complete the experimental studies, Molecular Dynamic simulations are performed to evaluate the diffusion coefficient of those additives in PAO4 at different temperatures.

#### 3.1. Friction behavior of C18 fatty acids mixture in PAO 4

Mixtures of stearic with oleic acid and stearic with linoleic acids were prepared respectively in PAO4 up to 2% with an equal (1:1) ratio.

Figure 10 and 11 summarizes friction and wear results obtained at  $50\text{ }^{\circ}\text{C}$ ,  $100\text{ }^{\circ}\text{C}$  and  $150\text{ }^{\circ}\text{C}$  with these different mixtures. At the lowest temperature, the mixtures give almost the same range of friction coefficient and wear behavior as the fatty acids alone. However, at  $100\text{ }^{\circ}\text{C}$ , the mixtures give an intermediate friction and wear between the stearic acid and the unsaturated fatty acids especially in presence of linoleic acid. This result can be due to the fact that a strong competition occurs between the saturated and unsaturated fatty acids at  $100\text{ }^{\circ}\text{C}$  and it is likely that both of them adsorb on the surface. At the highest temperature, the mixtures give similar friction coefficient and wear behavior characteristic of the unsaturated fatty acid. This suggests that the presence of unsaturation in molecules help them to reach the steel surface more quickly. In order to study the diffusion of these fatty acids in presence of PAO4, we use MD simulation method.



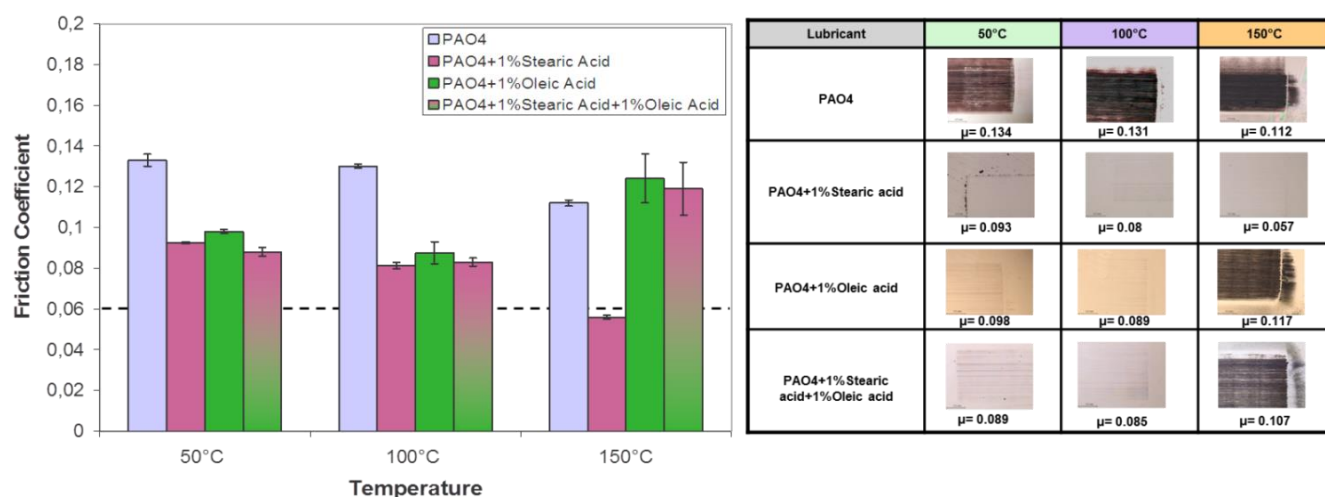


FIGURE 10: STEADY STATE FRICTION COEFFICIENT AND OPTICAL IMAGES OF AISI52100 STEEL FLAT WEAR SCARS LUBRICATED AT 50 °C, 100 °C AND 150 °C IN PRESENCE OF: PAO4, PAO4 + 1%W STEARIC ACID, PAO4 + 1%W OLEIC ACID, PAO4 + 2%W (1:1) STEARIC AND OLEIC ACIDS; EXPERIMENTAL CONDITIONS: RECIPROCATING PIN-ON-FLAT TEST WITH AISI 52100 STEEL COUPLE RESPECTIVELY, WITH MAXIMUM SLIDING SPEED OF 56 MM/S, AT MAXIMUM HERTZIAN PRESSURE OF 320 MPa DURING 4000 CYCLES; TESTS ARE REPEATED 3 TIMES

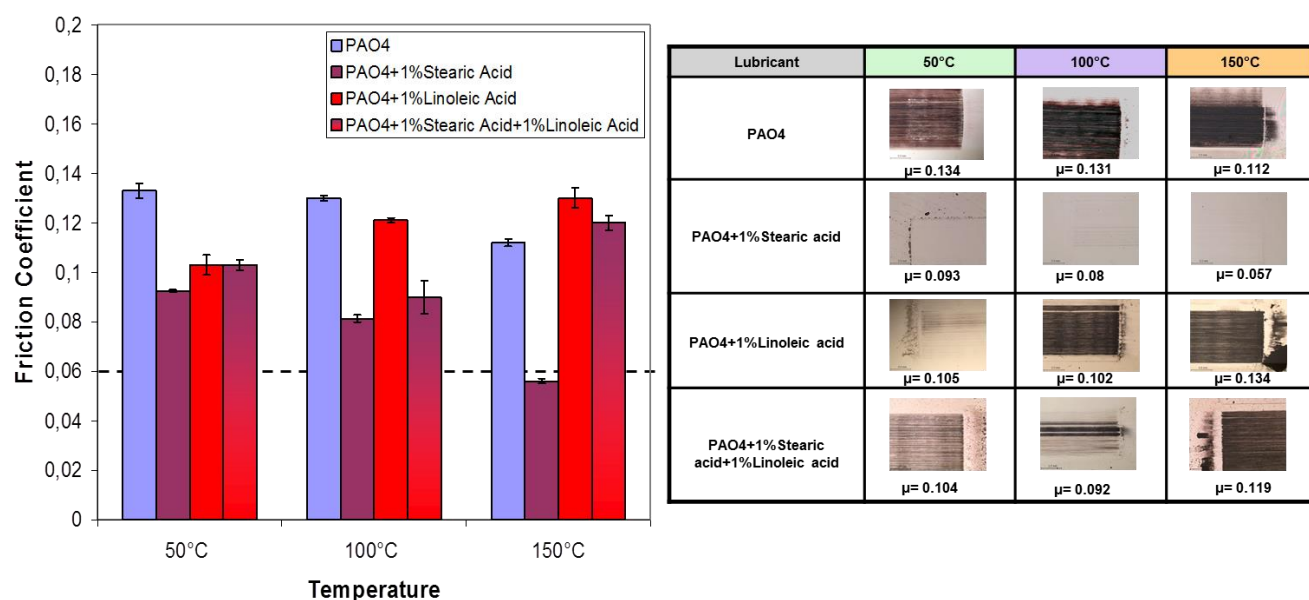


FIGURE 11: STEADY STATE FRICTION COEFFICIENT AND OPTICAL IMAGES OF AISI52100 STEEL FLAT WEAR SCARS LUBRICATED AT 50 °C, 100 °C AND 150 °C IN PRESENCE OF: PAO4, PAO4 + 1%W STEARIC ACID, PAO4 + 1%W LINOLEIC ACID, PAO4 + 2%W (1:1) STEARIC AND LINOLEIC ACIDS; EXPERIMENTAL CONDITIONS: RECIPROCATING PIN-ON-FLAT TEST WITH AISI 52100 STEEL COUPLE RESPECTIVELY, WITH MAXIMUM SLIDING SPEED OF 56 MM/S, AT MAXIMUM HERTZIAN PRESSURE OF 320 MPa DURING 4000 CYCLES; TESTS ARE REPEATED 3 TIMES

### 3.2. Evaluation of diffusion coefficient of OFM in PAO 4 by MD simulation

#### 3.2.1 C18 fatty acids blended at 1%w in PAO 4

The diffusion coefficient is calculated by MD as the mean square displacement (MSD) value of the sum of all atoms of the C18 fatty acid in x, y and z directions. Figure 12 gathers the diffusion coefficient obtained at 50 °C, 100 °C and 150 °C in presence of PAO 4 blended with 1%w of stearic, oleic and linoleic acids respectively.

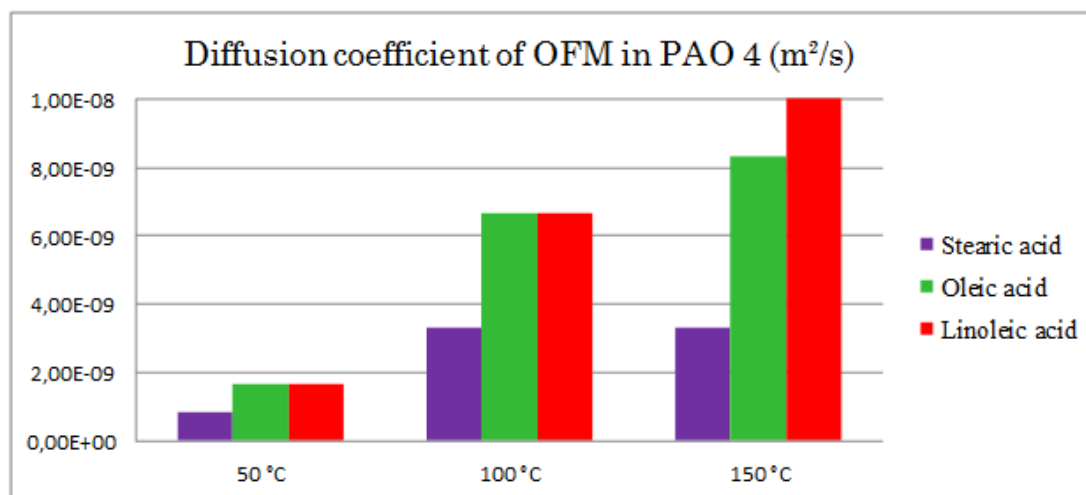


FIGURE 12: DIFFUSION COEFFICIENT OF 1%W STEARIC, OLEIC AND LINOLEIC ACIDS RESPECTIVELY IN PAO4 AT 50, 100 AND 150 °C CALCULATED BY MD SIMULATIONS (1 NS)

Results show that at each temperature, stearic acid diffuses slower than oleic acid which diffuses slower than linoleic acid. Values of diffusion coefficient are at the same range compared to literature [9-11]. The increase of temperature leads to an increase of the diffusion coefficient of stearic, oleic and linoleic acid, respectively. The difference between the diffusion coefficient of saturated and unsaturated molecules increases with the temperature. Comparing saturated versus unsaturated fatty acids, it seems that the double carbon bond induces bending of the molecule that facilitates the movement in the PAO4. These results suggest that when a mixture of stearic, oleic and linoleic acids is added in PAO4, linoleic acid will reach the surface at first, followed by oleic acid and finally by stearic acid. So there will be a depletion of stearic acid molecules in the final adsorbed film as no room is available anymore on the surface.

### 3.2.2 C18 fatty acids 1%w in PAO 4 submitted to pressure and shearing

Experimentally, friction tests are carried out with different mixtures of saturated and unsaturated molecules. It is therefore interesting to evaluate the diffusion coefficient of each studied fatty acids at a concentration of 1%w blended in PAO 4 when they are submitted to normal load and shear stress. Figure 13 shows snapshots taken at initial step and after 100 ps of MD simulation under 300 MPa load and 100 m/s sliding speed in x direction (blue arrows) for stearic acid (figure 13-a) and oleic acid (figure 13-b) in PAO 4. In addition, figure 14 shows the evolution of the fatty acid mean square displacement as a function of time.

Stearic acid is continuously moving in the PAO 4 base oil which is traduced by a linear curve presented in figure 14-a. The diffusion coefficient, which presents two contributions due to stearic acid diffusion in PAO 4 and to driving sliding speed, is  $1.1 \times 10^{-6} \text{ m}^2/\text{s}$ . On the other hand, oleic acid diffuses two times faster than stearic acid (Fig 14-b). From figure 13-b, it can be seen that oleic acid molecule is adsorbed on the surface during the simulation. This is traduced by a change in the curve slope indicated by the red arrow in figure 14-b after 50 ps of MD simulation. From 50 ps to 100 ps, the slope of the curve is progressively decreased. The molecule is adsorbed through the acid group but the remaining part is still moving in the base oil. With respect to time, the molecule progressively lays down along the surface until it is completely parallel (after 80 ps) as shown in figure 13-b. It is thought that the plateau will correspond to displacement due to the speed of the moving surface in x direction.



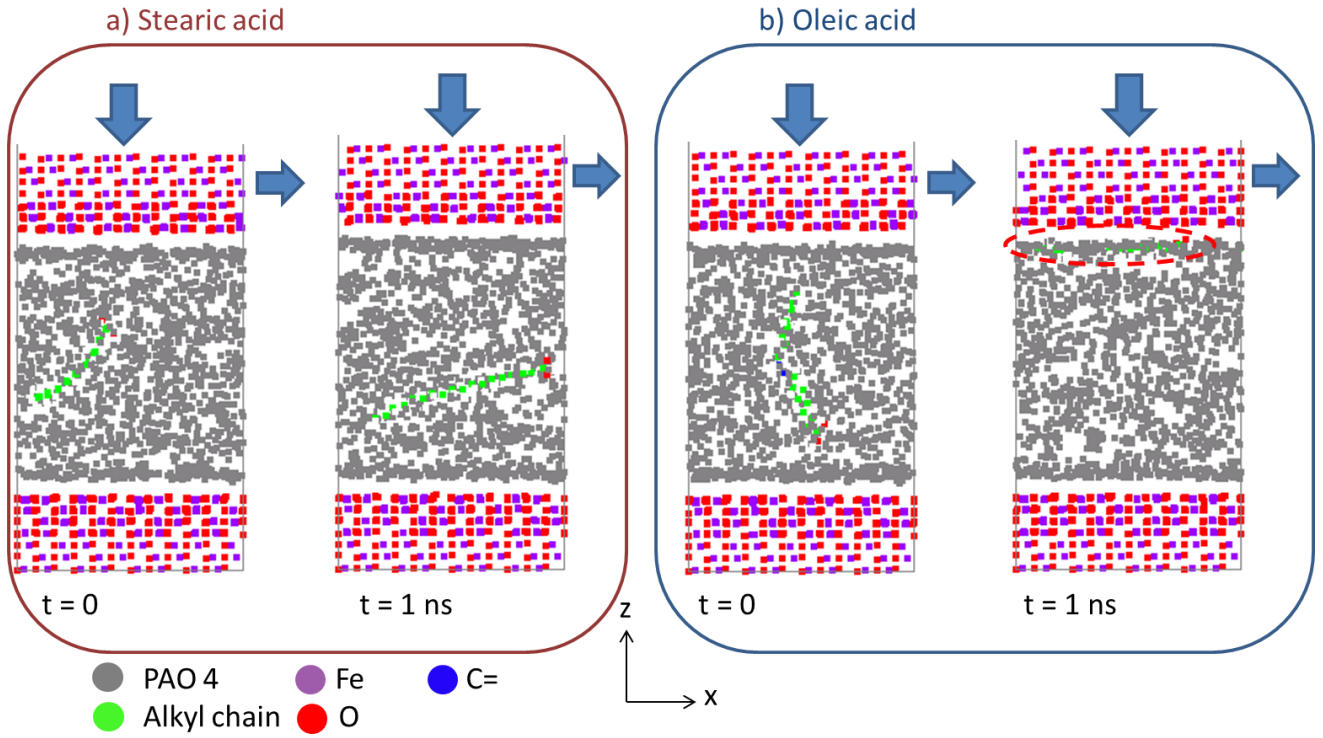
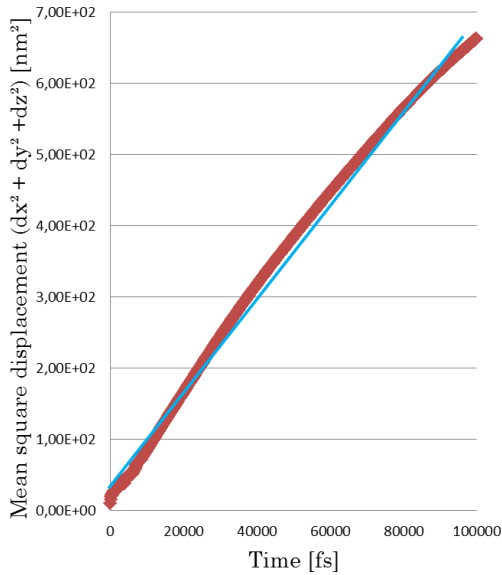


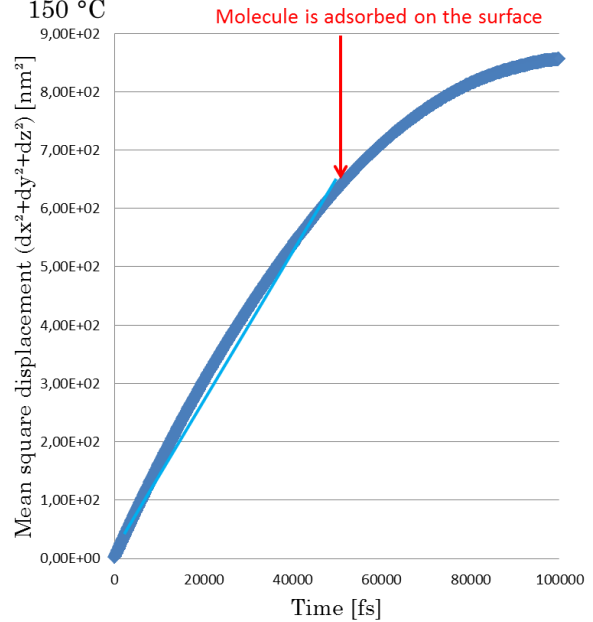
FIGURE 13: SNAPSHOTS OF MD SIMULATIONS AT INITIAL AND FINAL STEPS (100 PS), PAO 4 + 1%W OF A) STEARIC ACID AND B) OLEIC ACID BETWEEN IRON OXIDE SURFACES SUBMITTED TO 300 MPa NORMAL LOAD AND 100 M/S SLIDING SPEED IN X DIRECTION AT 150 °C

a) **Stearic acid** 1%w in PAO 4  
Between iron oxide surfaces  
150 °C



Diffusion coefficient:  $1.10 \cdot 10^{-6} m^2/s$

b) **Oleic acid** 1%w in PAO 4  
Between iron oxide surfaces  
150 °C



Diffusion coefficient (before adsorption):  $2.22 \cdot 10^{-6} m^2/s$

FIGURE 14: EVALUATION OF DIFFUSION COEFFICIENT WITH MEAN SQUARE DISPLACEMENT IN ALL DIRECTION AS A FUNCTION OF TIME FOR A) STEARIC ACID 1%W IN PAO4 AND B) OLEIC ACID 1%W IN PAO 4 BOTH SQUEEZED BETWEEN IRON OXIDE SURFACES WITH 300 MPa NORMAL LOAD ON TOP SURFACE AND 100 M/S SLIDING SPEED IN X DIRECTION FOR THE UPPER SUBSTRATE, 1 NS, 150 °C.

Finally, this additional study confirms that with tribological conditions, unsaturated molecules still diffuse faster than saturated molecules.

### 3.3 Discussions: coupling experimental results and MD simulations

When the mixture of unsaturated and saturated fatty acids is investigated by experimental analysis, anti-synergic effect is observed, e.g. the good tribological behavior of stearic acid is inhibited by the presence of oleic and linoleic acids at high temperature. Campen et al. already find this behavior when they mixed stearic acid and oleic acid with a 1:1 ratio in hexadecane at 100 °C <sup>[12]</sup>. Friction coefficient was 0.07, 0.11 and 0.10 for stearic, oleic and the mixture respectively. They suggest that oleic acid molecules are not able to pack effectively with stearic acid on the rubbing surfaces <sup>[12]</sup>.

In order to understand why the friction behavior of the fatty acids mixture is similar to the unsaturated fatty acid friction behavior, simulations were run to calculate diffusion coefficient of molecules in PAO4 (with and without pressure and shear stress). MD simulation results have shown that unsaturated molecules diffuse faster than stearic acid in PAO 4. In more practical words, in the mixture, linoleic acid and oleic acid molecules win the competition by reaching the surface before stearic acid molecules. The gap between the diffusion coefficient of unsaturated and saturated fatty acids increases with the temperature which suggest that the diffusion of molecules is an even more important factor at high temperature.

Then, the three fatty acids have the same reactivity towards the iron oxide surface (*chapter 3 § 2.2.5, 3.1.3, 3.2.2*) which means that once a molecule reach the surface and is chemisorbed, it stays definitely on the surface. That means that with mixture of saturated/unsaturated molecules, unsaturated fatty acid will adsorb first on the surface and will control then the friction behavior. Moreover, no desorption is observed at 150 °C (*Chapter 3 § 2.2.4*). The adsorption mechanism, quantitatively derived from our computer simulation, gives strong evidence of symmetric or asymmetric adsorption through the acid group <sup>[13]</sup> which was first qualitatively proposed by Simić and Kalin at 25 °C and 80 °C s. In presence of rubbing, they suggest a friction-induced formation of a carboxylate as discussed in chapter 4 section 3 <sup>[13]</sup>. The formation of carboxylate induced by friction is observed by UA-QCMD calculations (*chapter 4 § 3*) and PM-IRRAS analysis.

## 4. Conclusion

In this chapter, first, the tribological behavior of stearic, oleic and linoleic acid blended in PAO 4 is investigated at 50, 100 and 150 °C. As for pure additives, stearic acid presents the best tribological behavior, especially at 150 °C with no visible wear and a friction coefficient equal to 0.057. A minimum of 1%w of fatty acid is necessary in the PAO4 to conserve the good tribological behavior from 50 to 150 °C.

Characterization by PM-IRRAS of tribofilms obtained after tribotests with blend of PAO4 and fatty acids confirms results obtained with pure fatty acids. It shows the presence of both carboxylate and acid forms with more carboxylate form in the tribofilm than in the thermal film. It confirms the fact that friction promotes the formation of carboxylate. Furthermore, the tribofilm in presence of saturated fatty acid is thin and well-organized whereas in presence of unsaturated fatty acids, the formation of a well-organized thin film is inhibited by steric effect which explain the difference in tribological behavior of saturated/unsaturated fatty acids.

Then, the competition of C18 fatty acids is investigated by mixing saturated and unsaturated fatty acids in PAO 4 at different temperatures to study their tribological behavior on iron oxide surface. It is proposed that oleic and linoleic acids reach the surface first, before stearic acid, and adsorb on iron oxide surface at high temperature. In such case (mixture sample), the diffusion coefficient of molecule in the PAO 4 is an important factor to consider as it determines which molecule arrive first at the surface. Once the molecules arrive on the surface, it adsorbs chemically. In the case of stearic acid alone, molecules form close-packed monolayer which leads to low friction coefficient, especially at 150 °C. In the case of mixture,

mainly oleic and linoleic acid adsorb on the surface and prevent the formation of a close-packed monolayer due to steric effects which induce high friction coefficient, especially at 150 °C. This explains why the good tribological property of stearic acid is inhibited by unsaturated molecules.

## 5. References

- [1] Askwith T C, Cameron A, Crouch R F, Chain length of additives in relation to lubricants in thin film and boundary lubrication, *Proceeding Royal Society* 1 291 (1966) 500.
- [2] Cameron A., Day R.S., Sharma J.P., Smith A.J., Studies in interaction of additive and base stock, *ASLE Transactions* 19 (1976) 195 – 200
- [3] Hirano F, Sakai T, Kuwano N, Ohno N, Chain matching between hydrocarbon and fatty acid as interfacial phenomena, *Tribology International* 20 (1987) 186-204.
- [4] Lundgren S M, Ruths M, Danerlöv K, Persson K, Effects of unsaturation on film structure and friction of fatty acids in a model base oil, *Journal of Colloid Interface Science* 326 (2008) 530-536.
- [5] Jahanmir S et al., Chain length effects in boundary lubrication, *Wear* 102 (1985) 331-349.
- [6] Fox N J, Tyrer B, Stachowiak G W, Boundary Lubrication Performance of Free Fatty Acids in Sunflower Oil, *Tribology Letters*, 16 275-281 (2004).
- [7] Castro W, Weller D E, Cheenkachorn K, Perez J M, The effect of chemical structure of basefluids on antiwear effectiveness of additives, *Tribology International*, 38 321-326 (2005).
- [8] Siniawski M T, Saniei N, Adhikari B, Doezema L A, Tribological degradation of two vegetable-based lubricants at elevated temperatures, *Journal of Synthetic Lubrication*, 24 101-110 (2007).
- [9] G. Smits, Measurement of the Diffusion Coefficient of Free Fatty Acid in Groundnut Oil by the Capillary-Cell Method, *J. American Oil Chemists Society*, Vol 53 issue 4 112-124 (1976).
- [10] Mansfield W.W, The spontaneous emulsification of mixture of oleic acid and paraffin oil in alkaline solution, *Australian Journal of Scientific Research, series A: Phys. Sci.*, vol 5 331(1953).
- [11] Toshitaka F et al., Diffusion coefficients of linoleic acid methyl ester, Vitamin K<sub>3</sub> and indole in mixtures of carbon dioxide and *n*-hexane at 313.2 K, and 16.0 MPa and 25.0 MPa, *Fluid phase equilibria*, vol 164, issue 1(1993) 117-129
- [12] Campen S et al., On the increase in boundary friction with sliding speed, *Tribology Letters*, DOI 10.1007/s11249-012-0019-4 (2012).
- [13] Simič R, Kalin M, Adsorption mechanisms for fatty acids on DLC and steel studied by AFM and tribological experiments, *Applied Surface Science* 283 (2013) 460-470.
- [14] Crowel J E, Chen J G, Yates Jr J T, A vibrational study of the adsorption and decomposition of formic acid and surface formate on Al(111), *J. Chem. Phys.* 85 (1986) 3111-3122.

## 6. Summary chapter 5

After the study of tribological behavior of pure C18 fatty acids, we have blended 1%w of fatty acids in PAO 4. Friction tests show that, as for pure fatty acids, stearic acid has the best tribological behavior, even at 150 °C, followed by oleic acid which loses its good tribological behaviors at 150 °C and finally linoleic acid which loses them at 100 °C. The difference observed between pure unsaturated fatty acids and blended unsaturated fatty acids in PAO 4 traduces the impact of the solvent. A minimal concentration of 1%w of stearic acid in PAO 4 is necessary to provide tribological behavior that is as good as pure additives at high temperature. PM-IRRAS analyses have confirmed the presence of fatty acids on the surface, mainly under the carboxylate form.

It is clear that stearic acid has the best tribological behavior, even at 150 °C but its use is compromised because it is solid at room temperature. Mixing stearic acid with other fatty acids might improve its solubility in the base oil. Different fatty acid mixtures have been tested. Friction tests show that stearic acid loses its good tribological behavior at high temperature when it is mixed (ratio 1:1) with oleic acid or linoleic acid in PAO 4. This anti-synergic effect is due to the competition of fatty acids at the surface. It has been shown that adsorption mechanism of saturated and unsaturated fatty acids are the same so it seems that oleic and linoleic acids diffuse faster than stearic acid in PAO 4. The evaluation of diffusion coefficient by MD simulation could confirm this hypothesis and results obtained by experimental study.

## 6. Résumé chapitre 5

Après avoir étudié le comportement tribologique des acides gras C18 purs, nous les avons mélangés à 1% massique dans la PAO 4. Les tests de frottement montrent que, tout comme sous sa forme pure, l'acide stéarique présente le meilleur comportement tribologique, même à 150 °C, suivi de l'acide oléique qui perd ses propriétés tribologiques intéressantes à 150 °C et enfin de l'acide linoléique qui les perd à 100 °C. La différence observée entre les résultats obtenus pour les acides gras insaturés sous forme purs et dans la PAO 4 traduit de l'influence du solvant. Une concentration minimale de 1 % d'acide stéarique dans la PAO 4 est nécessaire pour obtenir un comportement tribologique similaire à sa forme pure à haute température. Les analyses des films frottés par PM-IRRAS confirment la présence des acides gras à la surface mais principalement sous forme de carboxylate.

Certes l'acide stéarique présente les meilleurs comportements tribologiques, même à 150 °C mais son utilisation est compromise car il est solide à température ambiante. Le mélanger à d'autres acides gras permet d'améliorer sa solubilité dans l'huile de base. Des mélanges de différents acides gras ont donc été testés. Les tests de frottement montrent que l'acide stéarique perd ses propriétés tribologiques à haute température lorsqu'il est mélangé de façon équimolaire à de l'acide oléique ou linoléique dans la PAO 4. Cet effet anti-synergique pour l'acide stéarique est dû à la compétition des acides gras à la surface. Le mécanisme d'adsorption étant le même pour les trois acides gras, il semblerait que les acides oléique et linoléique diffusent plus vite dans la PAO 4 que l'acide stéarique. L'évaluation du coefficient de diffusion par Dynamique Moléculaire confirme cette hypothèse et les résultats obtenus expérimentalement.

## **Chapter 6 : Synthesis**

---

## **Chapitre 6 : Synthèse**

## Chapter 6: Synthesis

---

### 1. Main results

A synthesis of the main results is presented here as well as a proposal mechanism of fatty acids behavior generalized for real case application.

#### 1.1 Adsorption mechanisms

Adsorption mechanisms of C18 fatty acids on iron-based surfaces have been investigated regarding the influence of several parameters.

On iron oxide, C18 fatty acids are mainly chemisorbed through the acid group. This is true for saturated and unsaturated molecules which have same adsorption mechanism. Nevertheless, saturated molecules are forming progressively a compact and well-organized film whereas unsaturated molecules do not form a well arranged film because of steric effects caused by double carbon-carbon bonds. No desorption has been observed at the studied temperatures, e.g. 50 °C, 100 °C and 150 °C, but the increase of temperature has a kinetic effect on adsorption mechanisms. Then, it has been highlighted that the orientation of the acid function of the molecule toward the surface determines the adsorption mechanism. And finally, reactivity of fatty acids decreases when oxidation/hydroxylation of the surface increases. In fact, the presence of humidity or oxygen have a direct impact on the nature of the substrate and therefore, on the adsorption mechanism.

#### 1.2 Friction behavior

Friction behavior of C18 fatty acids on iron-based surfaces have been investigated in presence or absence of base oil (PAO4) regarding the influence of several parameters.

##### 1.2.1 Pure additives

Among all studied fatty acids, stearic acid has the best tribological behavior, even at 150 °C. As for adsorption study, saturated molecules are more densely packed and well-ordered than unsaturated molecules, which is the reason why it provides lower friction coefficient. It has been also shown that friction promotes the formation of carboxylate function e.g. favors the breaking of OH bond of the acid function. This tribochemical reaction is modifying the interaction between the SAM and the substrate which has then an effect on friction. Modifying the nature of the surface has also an impact on SAM/substrate interactions and lead therefore to different friction coefficients. Finally, regarding considered systems, two “typical” friction behaviors leading to relatively “low” friction were found : 1) the first case is when a localized sliding plane is found between the two adsorbed SAM and 2) the second case when slip at the wall, between the SAM and the substrate, is observed as shown in figure 1. Finally, among all the different cases in simulation, an infinitely flat fully passivated surface exhibits the lowest friction coefficient with a slip at the wall.



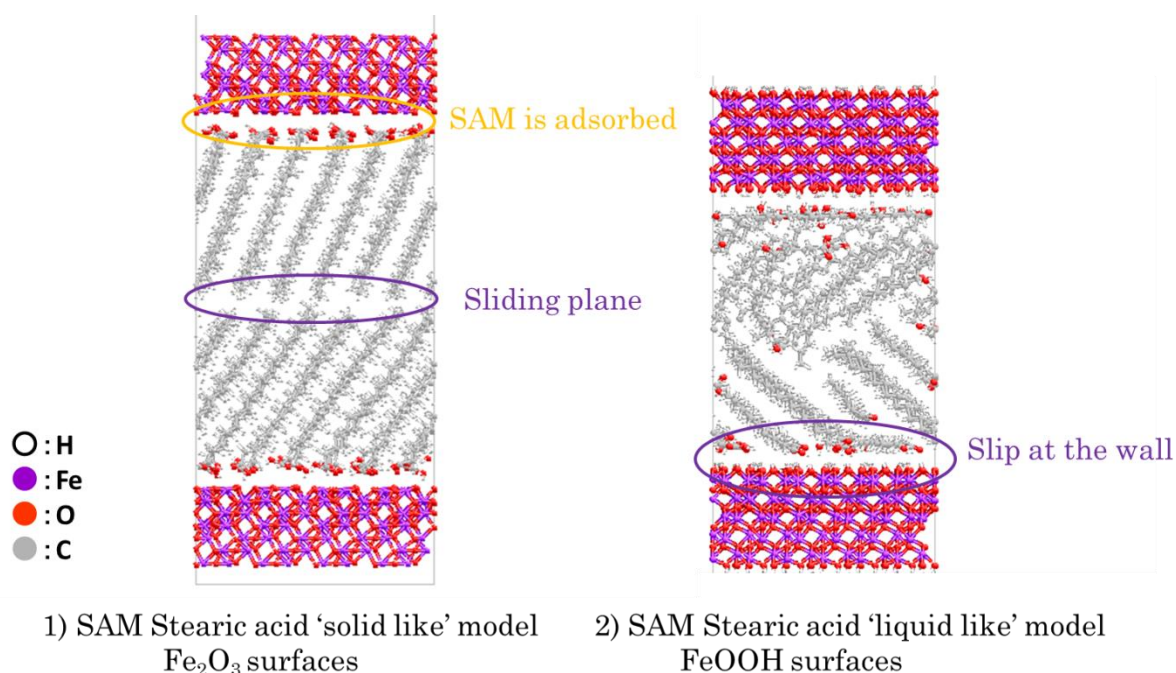


FIGURE 1: SNAPSHOT OF 1) SAM OF STEARIC ACID MOLECULES SOLID LIKE MODEL ON IRON OXIDE SURFACES, 2) SAM OF STEARIC ACID MOLECULES LIQUID LIKE MODEL ON IRON HYDROXIDE SURFACES DURING MD SIMULATION 300 MPA NORMAL LOAD, 100 M/S IN X DIRECTION, 1 NS, 50 °C.

### 1.2.2 Additives in the solvent

As for pure additives, stearic acid blended at 1%w in PAO 4 gives the best tribological behavior, even at 150 °C. Even if the solvent will not modify the intrinsic friction reduction properties of additives, it could have an impact on the friction behavior of the whole system. First, regarding the chemistry of additives (unsaturations or not) the diffusion behavior of molecules will not be the same in the solvent. Then, interactions between additives and solvent e.g. additives-additives or additives-solvent could occurred. Once the adsorbed layer is formed, PAO molecules could interact also with the monolayer with interdigitation or not. All this possible features have an impact on the friction coefficient of the system.

### 1.2.3 Mixture of additives

The good tribological behavior of stearic acid is inhibited by unsaturated fatty acids at high temperature when it is blended (1%w saturated molecules, 1%w unsaturated molecules) in PAO 4. In fact, unsaturated fatty acids diffuse faster in PAO 4 than stearic acid molecules. In this case, mainly oleic and linoleic acids adsorb on the surface first and prevent the formation of a close-packed monolayer of stearic acids. The adsorbed film of unsaturated molecules induces high friction coefficient, especially at 150 °C, due to steric effects.

## 2. Generalization to a real case application

### 2.1 Adsorption model

Our adsorption models were ideal models and now that we have identified adsorption mechanisms and parameters influencing adsorption mechanisms, a real case application model can be proposed. A schematic of a proposed 'realistic' model is presented in figure 2. First of all, the surface is not infinitely flat and do not contain only one 'type' of chemical composition. The surface contains some defects and is partially passivated as shown in figure 2. Moreover, the 'realistic' model must contain some oxygen, hydrogen and/ or water in the

system to mimic humidity of the environment on the substrate composition. Therefore, it has been shown that different adsorption mechanisms can occur.

Therefore, the adsorbed layer is not completely homogeneous as shown in figure 2. Some adsorption sites are iron oxides sites so the adsorbed layer is a close-packed monolayer of chemically adsorbed acid or carboxylate functions. Some others sites are iron hydroxides sites with some molecules that are physisorbed or chemisorbed on the surface with different tilt angles. Moreover, few molecules are present in the bulk. Finally, stearic acid molecules are blended in PAO 4. It is therefore possible to have some PAO 4 molecules that are physisorbed on the surface and present over the monolayer. Same adsorption models can be built for oleic and linoleic acids with less well-arranged monolayers parts because of some steric effects due to double carbon-carbon bonds.

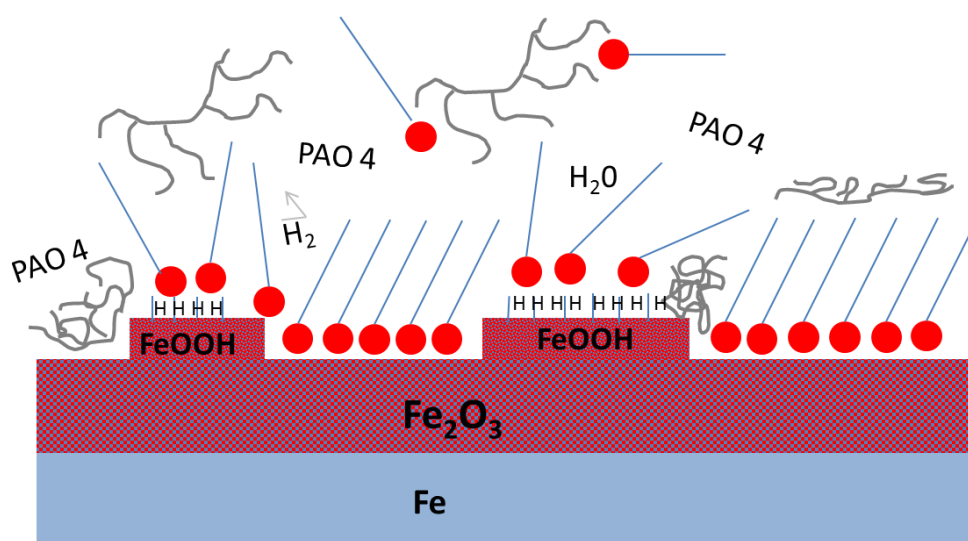


FIGURE 2: PROPOSITION OF SCHEMATIC ADSORBED LAYER OF STEARIC ACID IN PRESENCE OF PAO 4 IN THE THERMAL ENGINE

## 2.2 Friction model

Regarding surface compositions, two models have been studied in this work: monolayers between iron oxide surfaces (figure 1-1) and monolayers between iron hydroxide surfaces (figure 1-2). In a 'realistic' model, it should be in between the two studied models. Therefore, both sliding plane at the tail group of molecules interface and slip at the wall phenomenon could occur. In addition, PAO 4 molecules can co-adsorb on the surface, can be at the sliding interfaces or can prevent metal to metal direct contact in area where fatty acids molecules are, for example, desorbed or not strongly adsorbed on the surface. Non-homogeneity in the sliding plane location has a direct impact on friction coefficient so it is important to control as much as possible parameters that affect the friction coefficient.

In fact, in the thermal engine, the unsaturation degree is controlled by knowing additives and their concentration in the formulated oil. Moreover, temperature and pressure are imposed by the application (cam-tappet contact). On the other hand, the exact nature of the surface is harder to define as it depends on the environment. It seems that passivation of the surfaces is a good way to reduce the friction coefficient with slip at the wall phenomena. Therefore, it is important to control the nature of the surface. A DLC coating might be a good alternative.

## **General conclusion and perspectives**

---

## **Conclusion générale et perspectives**

## General conclusion and perspectives

---

In order to develop lubricants that are both respectful toward the environment and as efficient as actual ones, it is necessary to better understand lubricant additives adsorption mechanisms and their interactions with each other to better optimize their actions. To answer those questions, molecular simulation seems to be a pertinent tool.

In fact, our study is based on the understanding of adsorption mechanisms and tribological behavior of C18 fatty acids on iron-based surfaces by an original approach which consists in coupling molecular simulation approach and experimental approach. The coupling of molecular dynamics and quantum chemistry methods enables us to quantify adsorption mechanisms that occur during the formation of the thermal film but also to identify parameters that play a key role in organic friction modifiers tribological properties. Moreover, this method enables us to follow *in-situ* fatty acids behavior during the friction process. Finally, molecular dynamics method enables us to evaluate the friction coefficient and the diffusion coefficient of molecules in the solvent. Our models have been confirmed by experimental analysis. This study has been performed on model's molecules but it is also possible to apply the same procedure to a variety of systems.

### *Adsorption mechanisms*

We have shown that different adsorption mechanisms can co-exist in a same system. Those mechanisms, mainly physisorption or chemisorption of fatty acids on the surface, will vary according to the orientation of the molecules when they arrive on the surface, the film density, but most of it, the nature of the substrate (chapter 3). Once the fatty acid film is adsorbed on the surface (as Self-Assembled Monolayer (SAM)), the effect on friction on the evolution of fatty acids/surface interactions have been studied. It was shown that the friction process favors the formation of the carboxylate function (chapter 4).

To go further regarding the understanding of adsorption mechanism for the couple fatty acids and substrate, it would be interesting with UA-QCMD method, to impose the carboxylate function in order to check if a SAM with carboxylate functions is more efficient in friction reduction than a SAM with acid functions. By following the same procedure, it would be interesting to study adsorption mechanisms of other additives. Finally, to build a more physically realistic model, defects in the substrate should be added. In fact, real surfaces are partially amorphous and present some irregularity (roughness). Moreover, according to the environment in where the system is evolving, the presence of humidity or oxygen will modify the nature of the surface. A partial passivation of the surface should be investigated.

### *Help to read into experimental analysis*

Molecular simulation can also be used as a help to interpretation of experimental analysis results. We have shown that it is possible to simulate IR spectrum but also to correlate charges obtained with quantum chemistry calculation to binding energies measured with XPS analysis. It would be interesting to build other correlation curves like for example oxygen (O1s peak) or iron (Fe2p3/2 peak) in order to better understand chemical shifts during the adsorption of molecules on a substrate.

### *Tribological behavior*

Molecular dynamics simulations enable us to identify stearic acid as the best organic friction modifier among studied fatty acids, results that have been confirmed by friction tests

(chapter 4). In addition, UA-QCMD simulations and PM-IRRAS analysis have confirmed that friction has a catalytic effect on the formation of carboxylate function.

As for simulations applied for adsorption mechanisms, models should be built with imposing carboxylate function but also with adding some defects on the surface and see the impact on friction coefficient, organization of the film and atoms displacement profiles.

Understanding all factors that affect atomic friction is the first step toward being able to create a physically realistic model. It is therefore possible to considerably improve results obtained by MD simulations and make this tool very powerful in the selection of new additives. In a first step, the model should be improved by working on a bigger system. We should also work in lower sliding speed to study its impact, even in presence of a thermostat. In the meantime, results sensitivity as a function of different thermostat should be investigated. Finally, the effect of normal load should be studied as it is not impossible to have some local pressure raised over 300 MPa.

### *The effect of solvent*

To finish, the solvent (e.g. base oil) is the main component of a lubricant so its effect on additives properties should be controlled. We have studied the diffusion coefficient of fatty acids on PAO 4 and have compared the diffusion coefficient of the different studied fatty acids in order to study the competition among them to reach the surface (chapter 5). It is essential to study in more details the impact of PAO 4 (and generally speaking of solvent) on interactions between additives in the bulk system, on adsorption mechanisms of those additives but also on their tribological behavior. To illustrate this, here are some questions that it would be interesting to answer:

- ⊕ Is there any interaction between fatty acids (dimer formation) in the bulk?,
- ⊕ Is there any co-adsorption PAO 4/ fatty acids on the surface?,
- ⊕ Is there any desorption of fatty acids in presence of PAO 4?,
- ⊕ How is the film organization in presence of PAO 4?,
- ⊕ Does the presence of PAO 4 between adsorbed monolayers reduce friction?,
- ⊕ Etc.

After answering those questions, the same procedure should be applied on different type of solvent.

Technically speaking, the “unit atom” method for MD simulations applied in the calculation of diffusion coefficient seems to be an appropriate method to study the tribological behavior of fatty acids blended in PAO 4. In fact, it enables to work with a larger system than classical MD in term of atoms number and it is therefore more realistic.

This PhD work has enabled to show the potential of molecular simulation (MD, QC, UA-QCMD) in the study of issues link to friction by proposing the study of molecules adsorption mechanisms on the surface, their interactions in the bulk and their frictional behavior. As usual, hypotheses are made in order to run the calculation with reasonable time. In MD simulations, sliding speed is high in comparison with experimental conditions and the control of the temperature through the use of a thermostat are some examples. Even if models are constantly improved, it is essential to perform experimental study in order to check the accuracy of these hypotheses. This was our approach in this study. Experimental part will stay essential, particularly to have the knowledge of some results. But molecular simulation will enabled to understand details on observed phenomenon. It is also a potential tool toward the choice of new molecules. In fact, once phenomenon is well understood and once parameters influencing properties are well identified, it seems interesting to modify molecules with

molecular simulation in order to find one molecule which best complete the fixed specifications. Of course, it will be necessary to validate experimentally obtained results but the time safe in the selection of molecules can be considerable.

## Conclusion générale et perspectives

---

Dans le but de développer des lubrifiants respectueux de l'environnement et tout aussi performant que ceux actuellement sur le marché, il est nécessaire de mieux comprendre les mécanismes d'action des additifs de lubrification et leurs interactions afin d'optimiser leurs actions. Pour répondre à ces questions, la modélisation moléculaire semble être un outil pertinent.

En effet, notre étude est basée sur la compréhension des mécanismes d'adsorption et du comportement tribologique des acides gras sur des surfaces à base de fer par une approche originale visant à coupler une approche par modélisation moléculaire à une autre expérimentale. Le couplage de la dynamique moléculaire et de la chimie quantique nous a permis de quantifier les mécanismes d'adsorption qui ont lieu durant la formation du film thermique mais également d'identifier les paramètres qui jouent un rôle dans les propriétés tribologiques des modificateurs de frottement organiques. De plus, cette méthode nous a permis de suivre le comportement *in situ* des acides gras durant le processus de frottement. Enfin, les méthodes de dynamique moléculaire nous ont permis d'évaluer le coefficient de frottement et le coefficient de diffusion des molécules dans le solvant. Nos modèles ont pu être validés par des analyses expérimentales. Cette étude a été réalisée sur des molécules modèles mais il serait possible d'appliquer la même approche à une grande variété de système.

### *Les mécanismes d'adsorption*

Nous avons montré que différents mécanismes d'adsorption peuvent coexister dans un même système. Ces mécanismes, principalement la physisorption ou la chimisorption de l'acide gras sur la surface, vont varier selon l'angle avec laquelle les molécules arrivent à la surface, selon la densité des films, mais surtout selon la nature du substrat (chapitre 3). Une fois le film d'acide gras adsorbé à la surface (Monocouche Auto-Assemblée (SAM)), l'effet du frottement sur l'évolution des interactions acides gras/surface ont été étudiées. Il a été montré que le frottement favorise la formation de la fonction carboxylate (chapitre 4).

Pour aller plus loin concernant la compréhension des mécanismes d'adsorption acide gras-substrat, il serait intéressant en simulation (UA-QCMD) d'imposer la fonction carboxylate afin de voir si une SAM avec des fonctions carboxylates est plus efficace dans la réduction du frottement qu'une SAM d'acide gras. En suivant la même démarche, il serait intéressant d'étudier les mécanismes d'adsorption d'autres additifs. Enfin, pour construire un modèle physiquement plus réaliste, il faudrait ajouter des défauts de surface. En effet, les surfaces réelles sont partiellement amorphes et présentent des irrégularités (rugosité). De plus, selon l'environnement dans lequel le système évolue, la présence d'humidité et d'oxygène modifient la nature de la surface. Une passivation partielle de la surface serait à étudier.

### *Aide à l'interprétation des analyses expérimentales*

La modélisation moléculaire peut être également utilisée comme aide à l'interprétation des résultats d'analyse expérimentale. Nous avons montré qu'il était possible de simuler des spectres infra-rouge mais également de corrélérer les charges obtenues en chimie quantique aux énergies de liaison mesurées avec l'XPS. Il serait intéressant de construire des courbes de corrélation pour d'autres éléments comme par exemple l'oxygène (pic O1s) ou le fer (pic Fe2p3/2) afin de mieux comprendre les déplacements chimiques lors de l'adsorption des molécules sur une surface.

### *Le comportement tribologique*

Les simulations de dynamique moléculaire nous ont permis d'identifier l'acide stéarique comme étant le meilleur modificateur de frottement organique parmi les acides gras étudiés, résultat confirmé par les tests de frottement (chapitre 4). De plus, les analyses UA-QCMD et PM-IRRAS ont montré que le frottement agissait comme catalyseur à la formation de la fonction carboxylate.

Tout comme pour les simulations d'adsorption, il faudrait construire un modèle avec des fonctions carboxylates mais également ajouter des défauts et voir l'impact que cela entraîne sur le coefficient de frottement, l'organisation des films et les profils de déplacements des atomes.

Construire des modèles de simulation physiquement réalistes requiert la compréhension de tous les facteurs pouvant affecter le frottement atomique. Il serait possible d'améliorer considérablement les résultats obtenus par Dynamique Moléculaire et rendre cet outil très puissant dans la sélection de nouveaux additifs. Dans un premier temps, le modèle pourrait être amélioré en travaillant sur un système plus gros. Il faudrait également travailler à des vitesses de frottement plus faibles pour mesurer l'impact de la vitesse, même en présence de thermostat. Par la même occasion, la sensibilité des résultats en fonction de différents thermostats devrait être étudiée. Enfin, l'effet de la pression normale pourrait être étudiée car il est fort possible d'avoir des pressions locales plus élevées que 300 MPa.

### *L'influence du solvant*

Pour finir, le solvant est le composé principal d'un lubrifiant, son effet sur les propriétés des additifs doit être maîtrisé. Nous avons étudié la diffusion des acides gras dans la PAO 4 et comparé cette diffusion entre les différents acides gras étudiés afin d'étudier la compétition entre eux pour accéder à la surface (chapitre 5). Il est indispensable d'étudier plus en détail l'influence de la PAO 4 (et plus généralement du solvant) sur les interactions entre additifs dans le lubrifiant, sur les mécanismes d'adsorption de ces additifs mais également sur leur comportement en frottement. Pour illustrer cela, voici plusieurs questions auxquelles il serait intéressant de répondre :

- ✦ il y a-t-il des interactions entre acides gras (formation de dimère) dans le lubrifiant ?
- ✦ y-a-t-il co-adsorption PAO 4/Acide gras sur la surface ?,
- ✦ y-a-t-il désorption des acides gras en présence de PAO 4 ?,
- ✦ comment le film s'organise-t-il en présence de PAO 4 ?,
- ✦ la présence de la PAO 4 entre les monocouches adsorbées réduit-elle le frottement?
- ✦ etc.

Après avoir répondu à toutes ces questions, il serait intéressant de reproduire la même étude avec différents solvants.

D'un point de vue technique, la méthode « d'unité d'atome » par dynamique moléculaire appliquée au calcul du coefficient de diffusion semble être une méthode particulièrement appropriée à l'étude du comportement en frottement des acides gras en présence de la PAO 4. Elle permet de travailler sur des systèmes plus conséquents que la MD classique en terme de nombres d'atomes et est donc plus réaliste.

Ce travail de thèse a donc permis de montrer le potentiel de la modélisation moléculaire (MD, QD, UA-QCMD) à l'étude de problèmes liés au frottement en proposant d'étudier l'adsorption des molécules sur les surfaces, leurs interactions dans le solvant et leurs comportements en frottement. Comme souvent dans tout modèle, des hypothèses sont faites



afin de pouvoir mener les calculs dans des temps raisonnables. En MD, les vitesses de glissement élevées par rapport à l'expérience et le contrôle de la température par l'intermédiaire d'un thermostat en sont des exemples. Même si les modèles s'améliorent constamment, il paraît essentiel de réaliser en parallèle aux calculs des études expérimentales de manière à vérifier que ces hypothèses restent réalistes. C'est ce que nous avons tenté de faire dans ce travail. L'expérience est et restera essentielle ne serait-ce que pour connaître les résultats. Mais la modélisation moléculaire permet de comprendre le détail des phénomènes observés. Il y a aussi un très gros potentiel de l'approche sur le choix de nouvelles molécules. En effet, une fois les phénomènes bien compris et les paramètres importants identifiés, il semble aisé en modélisation moléculaire de modifier un peu les molécules de manière à trouver celle qui remplit au mieux le cahier des charges fixé. Il faudra valider expérimentalement les résultats obtenus mais le gain de temps sur la période de sélection des molécules peut-être conséquent.



# **Annex**

---

# **Annexes**

## Annex 1: Example of input file for MD or UA-QCMD simulations with all considered forcefields

## Annexe 1: Exemple de fichier d'entrée pour les simulations MD et UA-QCMD avec les champs de force pris en compte

index

1	COOH	40	8	0
2	CH2	40	8	0
3	CH3	40	8	0
4	H	20	7	0
5	HO	20	7	0
6	O=	40	2	0
7	OH	40	2	0
8	c1pao 4	40	8	0
9	c2pao 4	40	8	0
10	c3pao 4	40	8	0
11	Fetopmobile	40	3	0
12	Fetop	40	3	0
13	Otopmobile	40	2	0
14	Otop	40	2	0
15	Febas	40	3	0
16	Febasfixe	40	3	0
17	Obas	40	2	0
18	Obasfixe	40	2	0

nature

```

1 12.011 (C) 0.1960 (charge) ? LJ 2968753.3590[kcalA^12/mol]
1325.70810[kcalA^6/mol]
2 12.011 -0.0416 ? LJ 1790340.7240[kcalA^12/mol]
528.48190[kcalA^6/mol]
3 12.011 -0.0840 ? LJ 1790340.7240[kcalA^12/mol]
528.48190[kcalA^6/mol]
4 1.008 free ? LJ 7108.4660[kcalA^12/mol]
32.87076[kcalA^6/mol]
5 1.008 0.1710 ? LJ 1.0e-8[kcalA^12/mol]
0.00000[kcalA^6/mol]
6 15.999 -0.2860 ? LJ 272894.7846[kcalA^12/mol]
498.87880[kcalA^6/mol]
7 15.999 -0.1570 ? LJ 272894.7846[kcalA^12/mol]
498.87880[kcalA^6/mol]
8 13.021 0.0000 ? LJ 8123402.7649[kcalA^12/mol]
803.56360[kcalA^6/mol]
9 14.031 0.0000 ? LJ 5275037.2522[kcalA^12/mol]
1388.81040[kcalA^6/mol]
10 15.041 0.0000 ? LJ 6024261.8442[kcalA^12/mol]
2166.28820[kcalA^6/mol]
11 (Fe surface) 55.847 0.2550 ? LJ 1186612.1982[kcalA^12/mol]
7590.28296[kcalA^6/mol] Busing 1.280[A] 0.080[A]
12 (O surface) 15.999 -0.1700 ? LJ 272894.7846[kcalA^12/mol]
498.87880[kcalA^6/mol] Busing 1.520[A] 0.080[A]

```

pair table

```

0 0 - LJ : all pair
0 0 012 Busing (repulsive term)

```

<b>1</b>	<b>6</b>	<b>b</b>	<b>Morse</b>	<b>145.000000[kcal/mol]</b>	<b>2.060000[1/A]</b>		
<b>1.2300[A]</b>							
1	7	b	Morse	100.000000[kcal/mol]	2.000000[1/A]		
1.3700[A]							
1	2	b	Morse	76.000000[kcal/mol]	1.930000[1/A]		
1.5200[A]							
2	4	b	Morse	108.600000[kcal/mol]	1.771000[1/A]		
1.1050[A]							
2	2	b	Morse	88.000000[kcal/mol]	1.915000[1/A]		
1.5260[A]							
2	3	b	Morse	88.000000[kcal/mol]	1.915000[1/A]		
1.5260[A]							
3	4	b	Morse	108.600000[kcal/mol]	1.771000[1/A]		
1.1050[A]							
5	7	b	Morse	104.000000[kcal/mol]	2.280000[1/A]		
0.9600[A]							
8	9	b	Morse	88.000000[kcal/mol]	1.915000[1/A]		
1.5260[A]							
8	10	b	Morse	88.000000[kcal/mol]	1.915000[1/A]		
1.5260[A]							
9	9	b	Morse	88.000000[kcal/mol]	1.915000[1/A]		
1.5260[A]							
9	10	b	Morse	88.000000[kcal/mol]	1.915000[1/A]		
1.5260[A]							
11	12	b	Morse	76.0[kcal/mol]	2.00[1/A]	1.96[A]	
<b>trio</b>							
<b>1</b>	<b>7</b>	<b>5</b>	<b>b</b>	<b>Angle</b>	<b>50.000000[kcal/mol]</b>	<b>112.0000</b>	
1	2	4	b	Angle	45.000000[kcal/mol]	109.5000	
1	2	2	b	Angle	46.600000[kcal/mol]	110.5000	
2	1	7	b	Angle	122.800000[kcal/mol]	110.0000	
2	1	6	b	Angle	68.000000[kcal/mol]	120.0000	
2	2	4	b	Angle	44.400000[kcal/mol]	110.0000	
2	2	2	b	Angle	46.600000[kcal/mol]	110.5000	
2	2	3	b	Angle	46.600000[kcal/mol]	110.5000	
2	3	4	b	Angle	44.400000[kcal/mol]	110.0000	
3	2	4	b	Angle	44.400000[kcal/mol]	110.0000	
4	2	4	b	Angle	39.500000[kcal/mol]	106.4000	
4	3	4	b	Angle	39.500000[kcal/mol]	106.4000	
6	1	7	b	Angle	145.000000[kcal/mol]	123.0000	
<b>:PAO</b>							
8	9	8	b	Angle	46.600000[kcal/mol]	110.5000	
8	9	9	b	Angle	46.600000[kcal/mol]	110.5000	
9	8	9	b	Angle	46.600000[kcal/mol]	110.5000	
9	8	10	b	Angle	46.600000[kcal/mol]	110.5000	
9	9	9	b	Angle	46.600000[kcal/mol]	110.5000	
9	9	10	b	Angle	46.600000[kcal/mol]	110.5000	
<b>quad</b>							
<b>1</b>	<b>2</b>	<b>2</b>	<b>4</b>	<b>b</b>	<b>Torsion</b>	<b>1.422500[kcal/mol]</b>	<b>1.00 3.00</b>
<b>0.0000</b>							
1	2	2	2	b	Torsion	1.422500[kcal/mol]	1.00 3.00
0.0000							
2	1	7	5	b	Torsion	4.500000[kcal/mol]	1.00 2.00
180.0000							
2	2	2	4	b	Torsion	1.422500[kcal/mol]	1.00 3.00
0.0000							

0.0000	2	2	2	2	b	Torsion	1.422500[kcal/mol]	1.00	3.00
0.0000	7	1	2	2	b	Torsion	0.000000[kcal/mol]	1.00	0.00
0.0000	6	1	2	2	b	Torsion	0.000000[kcal/mol]	1.00	0.00
0.0000	2	2	2	3	b	Torsion	1.422500[kcal/mol]	1.00	3.00
0.0000	2	2	3	4	b	Torsion	1.422500[kcal/mol]	1.00	3.00
0.0000	3	2	2	4	b	Torsion	1.422500[kcal/mol]	1.00	3.00
0.0000	7	1	2	4	b	Torsion	0.000000[kcal/mol]	1.00	0.00
0.0000	6	1	2	4	b	Torsion	0.000000[kcal/mol]	1.00	0.00
0.0000	4	2	2	4	b	Torsion	1.422500[kcal/mol]	1.00	3.00
0.0000	4	2	3	4	b	Torsion	1.422500[kcal/mol]	1.00	3.00
180.0000	6	1	7	5	b	Torsion	4.500000[kcal/mol]	1.00	2.00
:PAO									
0.0000	9	8	9	8	b	Torsion	1.422500[kcal/mol]	1.00	3.00
0.0000	10	8	9	8	b	Torsion	1.422500[kcal/mol]	1.00	3.00
0.0000	8	9	9	9	b	Torsion	1.422500[kcal/mol]	1.00	3.00
0.0000	9	8	9	9	b	Torsion	1.422500[kcal/mol]	1.00	3.00
0.0000	9	9	9	10	b	Torsion	1.422500[kcal/mol]	1.00	3.00
0.0000	10	8	9	9	b	Torsion	1.422500[kcal/mol]	1.00	3.00
0.0000	9	9	9	9	b	Torsion	1.422500[kcal/mol]	1.00	3.00

**Annex 2:** Example of output file from UA-QCMD calculation**Annexe 2:** Exemple de fichier de sortie après des calculs d'UA-QCMD

Atom number Distance atom i-atom j [Å]

Atom type Bond population charge

Interatomic energy [kcal/mol]  
mo: molecular orbital interaction  
cl: coulomb interaction  
er: atomic core repulsion

Considered pair →

j	i	BP	Rij	q <sub>j</sub>	q <sub>i</sub>	Emo	Ecl	Eer	Emo+Eer	Emo+Eer+Ecl
FE 1	FE 2	0.000	5.244	0.331	0.326	0.0281	6.8390	0.0000	0.0281	6.8670
FE 1	FE 3	0.000	10.027	0.331	0.325	0.0000	3.5685	0.0000	0.0000	3.5685
FE 2	FE 3	-0.002	4.879	0.326	0.325	0.1511	7.2160	0.0000	0.1511	7.3671
FE 1	FE 4	-0.001	4.894	0.331	0.323	0.1242	7.2626	0.0000	0.1242	7.3868
FE 2	FE 4	0.000	10.009	0.326	0.323	0.0000	3.4938	0.0000	0.0000	3.4939
FE 3	FE 4	0.000	5.139	0.325	0.323	0.0469	6.7900	0.0000	0.0469	6.8369
FE 1	FE 5	0.199	2.277	0.331	0.315	-23.9789	15.2010	49.9414	25.9624	41.1635
FE 2	FE 5	0.000	5.490	0.326	0.315	0.0128	6.2012	0.0000	0.0128	6.2141
FE 3	FE 5	0.000	10.210	0.325	0.315	0.0000	0.0000	0.0000	0.0000	0.0000
FE 4	FE 5	0.000	5.550	0.323	0.315	0.0208	6.0805	0.0000	0.0208	6.1014
FE 1	FE 6	0.000	5.974	0.331	0.318	-0.0061	5.8516	0.0000	-0.0061	5.8455
FE 2	FE 6	0.337	2.111	0.326	0.318	-40.8686	16.2945	794.3190	753.4504	769.7448
FE 3	FE 6	-0.002	5.125	0.325	0.318	0.1453	6.6955	0.0000	0.1453	6.8409
FE 4	FE 6	0.000	9.939	0.323	0.318	0.0000	3.4294	0.0000	0.0000	3.4295
FE 5	FE 6	-0.001	5.366	0.315	0.318	0.1323	6.1844	0.0000	0.1323	6.3167
FE 1	FE 7	0.000	10.195	0.331	0.312	0.0000	0.0000	0.0000	0.0000	0.0000
FE 2	FE 7	0.000	5.428	0.326	0.312	0.0452	6.2128	0.0000	0.0452	6.2580
FE 3	FE 7	0.134	2.439	0.325	0.312	-15.7357	13.7948	3.3062	-12.4295	1.3653

## AUTORISATION DE SOUTENANCE

Vu les dispositions de l'arrêté du 7 août 2006,

Vu la demande du Directeur de Thèse

Monsieur J-M. MARTIN

et les rapports de

Monsieur P. MONTMITONNET

Professeur - MINES Paris Tech Centre de Mise en Forme des matériaux (CEMEF) bureau 09c  
1 rue Claude Daunesse - 06904 SOPHIA ANTIPOLIS

Et de

Monsieur N. FILLOT

Docteur - Laboratoire de Mécanique des Contacts et des Structures - Institut National des Sciences  
Appliquées de Lyon - Bâtiment Jean d'Alembert Bureau 113005X - 18-20 rue des Sciences  
69621 Villeurbanne

**Mademoiselle LOEHLE Sophie**

est autorisée à soutenir une thèse pour l'obtention du grade de **DOCTEUR**

**Ecole doctorale MATERIAUX**

Fait à Ecully, le 17 janvier 2014

P/Le directeur de l'E.C.L.  
La directrice des Etudes

